

Pilot Tube Microtunneling:  
Instrumentation and Monitoring for  
Jacking Force and Productivity Analysis

by

Matthew P. Olson

A Thesis Presented in Partial Fulfillment  
of the Requirements for the Degree  
Master of Science

Approved April 2013 by the  
Graduate Supervisory Committee:

Samuel T. Ariaratnam, Chair  
Jason S. Lueke  
Claudia E. Zapata  
Pingbo Tang

ARIZONA STATE UNIVERSITY

May 2013

© 2013 Matthew Peter Olson  
All Rights Reserved

## ABSTRACT

Trenchless technology is a group of techniques whose utilization allows for the installation, rehabilitation, and repair of underground infrastructure with minimal excavation from the ground surface. As the built environment becomes more congested, projects are trending towards using trenchless technologies for their ability to quickly produce a quality product with minimal environmental and social costs. Pilot tube microtunneling (PTMT) is a trenchless technology where new pipelines may be installed at accurate and precise line and grade over manhole to manhole distances. The PTMT process can vary to a certain degree, but typically involves the following three phases: jacking of the pilot tube string to achieve line and grade, jacking of casing along the pilot bore and rotation of augers to excavate the borehole to a diameter slightly larger than the product pipe, and jacking of product pipe directly behind the last casing. Knowledge of the expected productivity rates and jacking forces during a PTMT installation are valuable tools that can be used for properly weighing its usefulness versus competing technologies and minimizing risks associated with PTMT.

This thesis outlines the instrumentation and monitoring process used to record jacking frame hydraulic pressures from seven PTMT installations. Cyclic patterns in the data can be detected, indicating the installation of a single pipe segment, and enabling productivity rates for each PTMT phase to be determined. Furthermore, specific operations within a cycle, such as pushing a pipe or retracting the machine, can be observed, allowing for identification of the critical tasks associated with each phase. By identifying the critical tasks and developing more efficient means for their completion, PTMT productivity can be increased and costs can be reduced. Additionally, variations in

depth of cover, drive length, pipe diameter, and localized ground conditions allowed for trends in jacking forces to be identified. To date, jacking force predictive models for PTMT are non-existent. Thus, jacking force data was compared to existing predictive models developed for the closely related pipe jacking and microtunneling methodologies, and the applicability of their adoption for PTMT jacking force prediction was explored.

To my Mother and Father, your support and encouragement along the way provided me  
with the will to persevere.

## ACKNOWLEDGMENTS

I would like to thank Dr. Samuel T. Ariaratnam for taking me under his wing and aiding me with completing my thesis in an organized and professional manner. Additionally, I am very grateful for all of the opportunities you have given me to promote my research, whether it was through technical papers, attending industry conferences, or professional networking.

My research would not have been feasible without the guidance of Dr. Jason S. Lueke. Thank you for giving me the opportunity to conduct this research, providing me with the data logging equipment and assisting me with the recording process, and meeting with me on a regular basis to discuss preliminary results and directions for further analysis. You have opened my eyes to the trenchless technology industry, and I am forever indebted to you for this.

I also would like to pay tribute to my other committee members, Dr. Claudia E. Zapata and Dr. Pingbo Tang, for their support and guidance throughout my studies. Dr. Zapata, your passion for geotechnical engineering has greatly influenced my desire to learn, and I have found great benefit from what you have taught me. Dr. Tang, thank you for introducing me to automatic data recognition processes and their usefulness in dissecting field data from pilot tube microtunneling (PTMT) projects.

Deep gratitude is owed to Ray Olson, Bob Olson, Dan Olson, Mike Gauger, Terry Johnson, and many other employees of Globe Contractors, Inc. and Bore Master, Inc. for providing me with the incredible opportunity to learn the ins and outs of the PTMT methodology as a laborer on the Reid Drive Interceptor Project. Thank you for allowing me to record jacking force data from your project. Being able to be onsite during the data

recording process was extremely valuable, as I was able to link field observations with data trends. Thank you, Dan and Terry, for answering numerous phone calls and emails regarding PTMT methodology and equipment.

I would like to thank Jeff Boschert from the National Clay Pipe Institute for assisting me with the data recording process. Your guidance and friendship throughout the last two years is highly appreciated.

Thank you to everyone I have worked closely with in the Center for Research in Underground Systems and Technology for making my time at Arizona State University more pleasurable. Long days in the office would not have been the same without you. I wish you all the best of luck.

Many thanks are also due to all of the graduate students and faculty members at the School of Sustainable Engineering and the Built Environment who have become my friends. I value the good times and the experiences we have shared.

# TABLE OF CONTENTS

	Page
LIST OF TABLES .....	ix
LIST OF FIGURES .....	xi
CHAPTER	
1 INTRODUCTION .....	1
1.1 Trenchless Technology Overview.....	2
1.2 Pilot Tube Microtunneling .....	3
1.2.1 Methodology and Equipment .....	4
1.2.2 Advantages and Limitations .....	10
1.3 Scope of Study .....	12
2 LITERATURE REVIEW .....	15
2.1 Data Collection of Trenchless Technology Projects .....	15
2.1.1 Physical Observational Methods .....	16
2.1.2 Automatic Data Logging .....	20
2.2 Jacking Force Studies and Theory .....	26
3 FIELD DATA COLLECTION .....	42
3.1 Reid Drive Interceptor Project .....	42
3.1.1 Monitored Installations.....	47
3.2 Prepping the Data Logger .....	49
3.2.1 Pressure Transducer Calibration.....	49
3.2.2 Programming the Data Logger .....	50
3.2.3 Connecting the Data Logger to Machines .....	52



CHAPTER	Page
4 PRODUCTIVITY ANALYSIS .....	57
4.1 Cycle Identification .....	58
4.1.1 Typical Cycle – Phase One.....	60
4.1.2 Typical Cycle – Phase Two .....	62
4.1.3 Typical Cycle – Phase Three .....	65
4.2 Installation Productivity .....	66
4.2.1 Phase One Productivity .....	68
4.2.2 Phase Two Productivity.....	72
4.2.3 Phase Three Productivity.....	76
4.3 Automatic Pattern Recognition .....	79
4.3.1 Methodology.....	80
4.3.2 Results .....	84
4.3.3 Advantages and Limitations .....	87
4.4 Summary .....	88
5 COMPARISON OF EMPIRICAL MODELS TO CASE STUDY .....	90
5.1 Hydraulic Pressure Correlations.....	91
5.1.1 Jacking Force.....	91
5.1.2 Pull-Back Force .....	95
5.1.3 Rotational Torque .....	96
5.2 General Trends .....	97
5.2.1 Installation Depth .....	99
5.2.2 Soil Type.....	100

CHAPTER	Page
5.2.3 Stoppages.....	108
5.2.4 Lubrication.....	111
5.2.5 Operator Technique .....	119
5.3 Application of Jacking Force Predictive Models .....	121
5.3.1 Comparison of Select Jacking Force Predictive Models to Collected Data ...	133
6 CONCLUSIONS AND RECOMMENDATIONS .....	141
6.1 Productivity Conclusions .....	141
6.2 Jacking Force Conclusions.....	145
6.2.1 General Trends .....	146
6.2.2 Applicability of Existing Jacking Force Predictive Models.....	149
6.3 Recommendations for Further Research .....	151
REFERENCES .....	154
APPENDIX	
A SUPPLEMENTAL FIGURES .....	160
B SUPPLEMENTAL TABLES .....	200
C SUPPLEMENTAL EQUATIONS .....	206
D L1 PRESSURE TRANSDUCER COMPLICATIONS.....	209

## LIST OF TABLES

Table	Page
Table 2.1 Interface Friction Coefficients for Numerous Pipe Materials and Residual Friction Angles (Staheli 2006).....	35
Table 2.2 Scherle’s Interface Friction Coefficients (Stein et al. 1989) .....	36
Table 2.3 Frictional Jacking Stress for Various Soil Types (Weber 1981) .....	37
Table 2.4 Friction and Arching Reduction Factors (Bennett 1998).....	40
Table 2.5 Jacking Force Reduction Factors (Osumi 2000).....	41
Table 3.1 Soil Characteristics Corresponding to Drives with Collected Data.....	46
Table 3.2 Monitored Installation Drive Characteristics.....	47
Table 5.1 Jacking Ram Characteristics for all Reid Drive Interceptor Jacking Frames ...	93
Table 5.2 Minimum and Maximum GBM Pressures and Torques .....	97
Table 5.3 Rankings of Force and Torque Magnitudes for PTMT and PT/HDD Phases ..	98
Table 5.4 Lubricant Volume and Concentration throughout the Reid Drive Interceptor Project .....	115
Table 5.5 Application of Jacking Force Equations for PTMT in Clay Soil (based on Chapman and Ichioka 1999).....	125
Table 5.6 Most Applicable Models for Each PTMT Phase .....	133
Table 6.1 Cycle Duration Characteristics for PTMT Installations .....	142
Table 6.2 Comparison of Average and Median Installation Rates .....	143
B.1 Existing Models for Predicting the Frictional Component of Jacking Force (Modified from Staheli 2006) .....	201
B.2 Overview of Forces and Torques Present on Each Drive .....	203

Table	Page
B.3 PTMT and PT/HDD Phase Specific Force and Torque Behavior .....	204
B.4 Drives Inclusive of Maximum and Minimum Forces and Torques .....	204
B.5 Reid Drive Interceptor Project Pipe Dimensions .....	205
D.1 List of 21” Installations and Transducer Operational Results .....	210

## LIST OF FIGURES

Figure	Page
1.1 Pilot Tube Installation during Phase One .....	5
1.2 Auger-Casing Installation and Pilot Tube Removal during Phase Two .....	6
1.3 Upsizing Reamer to Fit 25.5-Inch OD Casings, Casings in Background .....	6
1.4 Product Pipe Installation and Auger-Casing Removal during Phase Three .....	7
1.5 Akkerman PCH 22.5 (Akkerman 2013) .....	8
1.6 Akkerman PRH (Akkerman 2013) .....	8
1.7 Product VCP with Casing/Auger Inside (Gottipati 2011) .....	9
2.1 TensiTrak™ Load and Pressure Monitors (Finnsson 2004) .....	22
2.2 Instrumented Pipe (Norris and Milligan 1991) .....	24
2.3 WES Test Bed (Bennett 1998) .....	26
2.4 Analogy of Terzaghi's Trap Door Experiment (Bennett 1998) .....	30
2.5 Distribution of Normal Stress (Auld 1982) .....	31
2.6 Terzaghi's and Various Authors' Arching Theory (Stein et al. 1989) .....	31
2.7 Predicted Failure Envelope, Cavity Collapse Model (Atkinson and Potts 1977) .....	32
3.1 Exit Pit Installation for PT/HDD Procedure .....	45
3.2 Photograph of the Data Logger and Battery Inside Containment Box .....	53
3.3 Quick Coupler Connection Used for Pressure Transducer Connection to GBM Hydraulics (Lueke and Olson 2012) .....	54
3.4 Data Dolphin Containment Unit Strapped to the AA During Phase 2 (Lueke and Olson 2012) .....	55

Figure	Page
3.5 Power Pack & Data Dolphin Containment Unit Configuration for the BM Pusher	
During Phase 3.....	56
4.1 Typical Pilot Tube Installation Cycle .....	60
4.2 Typical Casing Installation Cycle.....	63
4.3 Typical VCP Installation Cycle .....	65
4.4 Ranking of Factors Affecting PTMT Productivity (Gottipati 2011) .....	67
4.5 Pilot Tube Installation Cycle Duration Frequencies.....	68
4.6 Cumulative Pilot Tube Installation Distance vs Time .....	70
4.7 21-Inch Nominal ID Casing Installation Cycle Duration Frequencies.....	73
4.8 8-Inch Nominal ID Casing Installation Cycle Duration Frequencies.....	75
4.9 Cumulative Casing Installation Distance vs Time.....	76
4.10 VCP Installation Cycle Duration Frequencies .....	77
4.11 Cumulative VCP Installation Distance vs Time .....	79
4.12 Time Series Data for Phase Three: a) Entire Time Series, b) Typical Installation Cycle, c) and d) Installation Cycles with Long Durations (Tang et al. 2013) .....	82
4.13 Scatter Plot of Voltage Time Series Data from All Transducers from Each PTMT Phase: a) L1, b) L2, and c) L3 Transducers (Tang et al. 2013) .....	85
4.14 Detected Cycles and their Duration (Tang et al. 2013) .....	86
5.1 Jacking Ram General Detail .....	92
5.2 Non-Adjusted Thrust Force vs. Time for a Pilot Tube Installation Cycle.....	94
5.3 Adjusted Thrust Force vs. Time for the Figure 5.2 Pilot Tube Installation Cycle .....	94
5.4 Broken HDPE Pipe from Drive Six.....	105

Figure	Page
5.5 Thrust Force for Casing Numbers 7, 8, 9, and 10 for Drive One .....	118
5.6 Illustration of the Dependency of Thrust Force on Operator Technique .....	121
A.1 Plan View of Reid Drive Interceptor Project .....	161
A.2 Photograph of Make-Up Tool Used in Phase One Operations .....	162
A.3 Thrust Force vs. Time for Phase One of Drive One .....	162
A.4 Rotational Torque vs. Time for Phase One of Drive One.....	163
A.5 Thrust Force vs. Length of Drive for Phase One of Drive One .....	163
A.6 Rotational Torque vs. Length of Drive for Phase One of Drive One .....	164
A.7 Thrust Force vs. Time for Phase Two of Drive One: a) Day One, b) Day Two, c) Day Three .....	165
A.8 Thrust Force vs. Length of Drive for Phase Two of Drive One .....	166
A.9 Thrust Force vs. Time for Phase Three of Drive One.....	166
A.10 Thrust Force vs. Length for Phase Three of Drive One.....	167
A.11 Thrust Force vs. Time for Phase One of Drive Two.....	167
A.12 Rotational Torque vs. Time for Phase One of Drive Two.....	168
A.13 Thrust Force vs. Length of Drive for Phase One of Drive Two .....	168
A.14 Rotational Torque vs. Length of Drive for Phase One of Drive Two.....	169
A.15 Thrust Force vs. Time for Phase Two of Drive Two: a) Day One, b) Day Two, c) Day Three, b) Day Four .....	171
A.16 Thrust Force vs. Length of Drive for Phase Two of Drive Two.....	171
A.17 Thrust Force vs. Time for Phase Three of Drive Two .....	172
A.18 Thrust Force vs. Length of Drive for Phase Three of Drive Two.....	172

Figure	Page
A.19 Thrust Force vs. Time for Phase One of Drive Three.....	173
A.20 Rotational Torque vs. Time for Phase One of Drive Three .....	173
A.21 Thrust Force vs. Length of Drive for Phase One of Drive Three .....	174
A.22 Rotational Torque vs. Length of Drive for Phase One of Drive Three.....	174
A.23 Thrust Force vs. Time for Phase Two of Drive Three: a) Day One, b) Day Two .	175
A.24 Thrust Force vs. Length of Drive for Phase Two of Drive Three.....	176
A.25 Thrust Force vs. Time for Phase One of Drive Four .....	176
A.26 Rotational Torque vs. Time for Phase One of Drive Four.....	177
A.27 Thrust Force vs. Length of Drive for Phase One of Drive Four .....	177
A.28 Rotational Torque vs. Length of Drive for Phase One of Drive Four .....	178
A.29 Thrust Force vs. Time for Phase Two of Drive Four: a) Day One, b) Day Two, c) Day Three .....	179
A.30 Thrust Force vs. Length of Drive for Phase Two of Drive Four .....	180
A.31 Thrust Force vs. Time for Phase One of Drive Five.....	180
A.32 Rotational Torque vs. Time for Phase One of Drive Five .....	181
A.33 Thrust Force vs. Length of Drive for Phase One of Drive Five.....	181
A.34 Rotational Torque vs. Length of Drive for Phase One of Drive Five .....	182
A.35 Thrust Force vs. Time for Phase Two of Drive Five .....	182
A.36 Rotational Torque vs. Time for Phase Two of Drive Five.....	183
A.37 Thrust Force vs. Length of Drive for Phase Two of Drive Five .....	183
A.38 Rotational Torque vs. Length of Drive for Phase Two of Drive Five .....	184
A.39 Thrust Force vs. Time for Phase Three of Drive Five .....	184



Figure	Page
A.40 Thrust Force vs. Length of Drive for Phase Three of Drive Five .....	185
A.41 July 8 <sup>th</sup> Thrust and Pull Force vs. Time for Drive Six .....	185
A.42 July 8 <sup>th</sup> Rotational Torque during PT Jacking and HDPE Pull-back vs. Time for Drive Six .....	186
A.43 July 12 <sup>th</sup> Thrust and Pull Force vs. Time for Drive Six .....	186
A.44 July 12 <sup>th</sup> Rotational Torque During PT Jacking and HDPE Pull-back vs. Time for Drive Six .....	187
A.45 July 8 <sup>th</sup> Thrust and Pull Force vs. Length of Drive for Drive Six .....	187
A.46 July 8 <sup>th</sup> Rotational Torque During PT Jacking and HDPE Pull-back vs. Length of Drive for Drive Six .....	188
A.47 July 12 <sup>th</sup> Thrust and Pull Force vs. Length of Drive for Drive Six .....	188
A.48 July 12 <sup>th</sup> Rotational Torque During PT Jacking and HDPE Pull-back vs. Length of Drive for Drive Six .....	189
A.49 July 19 <sup>th</sup> Thrust and Pull Force vs. Time for Drive Seven .....	189
A.50 July 19 <sup>th</sup> Rotational Torque During PT Jacking and Pre-reaming vs. Time for Drive Seven .....	190
A.51 July 20 <sup>th</sup> HDPE Pull-back Force vs. Time for Drive Seven .....	190
A.52 July 20 <sup>th</sup> Rotational Torque During HDPE Pull-back vs. Time for Drive Seven ..	191
A.53 Thrust Force vs. Length of Drive for Drive Seven .....	191
A.54 Rotational Torque During PT Jacking vs. Length of Drive for Drive Seven .....	192
A.55 Pull Force During Pre-ream and HDPE Pull-back vs. Length of Drive for Drive Seven .....	190

Figure	Page
A.56 Rotational Torque During Pre-ream and HDPE Pull-back vs. Length of Drive for Drive Seven.....	193
A.57 Jacking Force Predictive Model Comparison: Pilot Tube, Drive One .....	193
A.58 Jacking Force Predictive Model Comparison: Pilot Tube, Drive Two.....	194
A.59 Jacking Force Predictive Model Comparison: Pilot Tube, Drive Three.....	194
A.60 Jacking Force Predictive Model Comparison: Pilot Tube, Drive Four.....	195
A.61 Jacking Force Predictive Model Comparison: Pilot Tube, Drive Five .....	195
A.62 Jacking Force Predictive Model Comparison: 21-Inch Casing, Drive One.....	196
A.63 Jacking Force Predictive Model Comparison: 21-Inch Casing, Drive Two.....	196
A.64 Jacking Force Predictive Model Comparison: 21-Inch Casing, Drive Three .....	197
A.65 Jacking Force Predictive Model Comparison: 21-Inch Casing, Drive Four.....	197
A.66 Jacking Force Predictive Model Comparison: 8-Inch Casing, Drive Five .....	198
A.67 Jacking Force Predictive Model Comparison: 21-Inch VCP, Drive One .....	198
A.68 Jacking Force Predictive Model Comparison: 21-Inch VCP, Drive Two .....	199
A.69 Jacking Force Predictive Model Comparison: 8-Inch VCP, Drive Five.....	199
D.1 Voltage vs. Time for the June 20 <sup>th</sup> Installation .....	211
D.2 Voltage vs. Time for the June 30 <sup>th</sup> Installation .....	212
D.3 Voltage Outputs for the L1 Transducer Throughout Summer.....	213
D.4 Voltage Outputs for the L3 Transducer Throughout Summer.....	214

## **CHAPTER 1: INTRODUCTION**

Maintaining adequate water and wastewater infrastructure is paramount to providing the means for modern societies to flourish economically and to preserve the health of the society as a whole. Businesses depend on reliable supplies of treated water to cool equipment, manufacture goods, and operate in a way that conforms to contemporary sanitary regulations. Additionally, the abundant generation of water waste needs to be efficiently and effectively removed from their site to prevent production delays or shutdowns. As cities continue to grow and place an ever increasing demand on underground infrastructure systems, the importance of repairing, rehabilitating, and replacing current underground infrastructure systems in a cost effective and sustainable manner is well apparent. To complicate the matter, many of the existing underground infrastructure systems are failing or in poor condition.

The American Society of Civil Engineering's Report Card for America's Infrastructure (2013) rated the U.S. water and wastewater infrastructure with a grade of D. Combined sewer overflows (CSOs), in which the combined flow of storm and wastewater exceeds system capacity and is discharged untreated to local waterways, and outbreaks of water-borne pathogens, such as cryptosporidium or giardia, are incidental to such poor infrastructure. Environmental and health effects due to poor infrastructure are severe; Lake Michigan beach closures in Milwaukee are frequent as the yearly CSO volume has been as high as 8,000 million gallons within the last ten years (MMSD 2013), and waterborne disease is responsible for more than 3 million deaths and innumerable cases of sicknesses every year worldwide (WRF 2013). Bringing the underground water and wastewater infrastructure in the U.S. up to par is no easy task. It is estimated that

there is a need for \$335 billion and \$298 billion in drinking water and wastewater infrastructure investment, respectively (USGAO 2013). With limited funding, alternative methods must be employed to repair, rehabilitate, and replace existing infrastructure and install new infrastructure in a sustainable and economical manner. Trenchless technologies are a family of innovative construction methods that may be called upon to achieve said tasks.

### **1.1 Trenchless Technology Overview**

Trenchless Technology refers to a group of construction methodologies used to install, rehabilitate, and replace underground infrastructure while minimizing ground excavation, construction site footprint, and other social and environmental costs. Traditional open trench practices for installing and repairing underground infrastructure require a substantial amount of ground restoration, which tends to inflate direct project costs along with social and environmental costs. Although open trench installation has its place, namely in rural areas with limited congestion, trenchless technologies have proven to be highly effective in urban and environmentally sensitive areas.

In a paper written by Jung and Sinha (2007), a methodology for comparing direct, social, and environmental costs associated with underground pipeline construction was described. The above costs were specifically evaluated based on data from six traditional open trench and two trenchless technology, pipe bursting, projects. It was found that social and environmental costs were almost always higher with open trench techniques, as these methods negatively impact vehicular/pedestrian traffic, worker safety, local businesses, and pollution, to name a few. Direct installation costs for the pipe bursting methods were higher than that of open trench, due to the more specialized equipment

required, however, when comparing the total cost of the projects (e.g. direct, social, environmental, and other factors) pipe bursting proved to be the cheaper method. Lower total costs are common ground with many of the trenchless technologies when compared to open trench, a key component to creating an underground infrastructure system of good quality and function in a sustainable manner. Selecting the optimal trenchless technology for a given project depends on the project goals and site characteristics.

Trenchless technologies may be subdivided into those used for repair and new installations. Of the new installation methods, there are guided and unguided techniques. Many of the guided techniques are ideal for installation of gravity fed sewers or in congested underground space. Microtunneling provides the means to install pipelines with high degrees of accuracy, plus or minus one inch, in both line and grade through a laser guidance and remotely-controlled steering system (Gottipati 2011). Microtunneling requires a large capital investment, or rental fee, to acquire the slurry tanks, lubrication unit, control cabin, power pack, and microtunneling boring machine. A cheaper alternative to microtunneling is a variation termed pilot tube microtunneling (PTMT), also known as guided auger boring or the guided boring method.

## **1.2 Pilot Tube Microtunneling**

PTMT originated in Japan and Europe two decades ago as a way to install 4 to 6-inch laterals to connect residences to main sewer lines (Boschert 2007). Since its introduction in the United States in 1995, its niche has expanded to the installation of 48-inch mainlines for distances up to 580 feet (Gottipati 2011). Procedures required to conduct PTMT installations are adopted from the microtunneling, auger boring, and

horizontal directional drilling (HDD) methodologies. The following section outlines the methodology, equipment, advantages, and limitations of PTMT.

### **1.2.1 Methodology and Equipment**

PTMT is a hybrid technology which adopts techniques from three other trenchless technologies: microtunneling, auger boring, and HDD. HDD involves installation of a pilot bore to obtain line and grade followed by reaming and product pipe pull-back. The pilot bore is directionally controlled through the use of a slant faced steering head on the lead rod. This pilot bore, reaming, and product installation process is mimicked by the PTMT methodology in either two or three distinct phases. Akin to traditional microtunneling, PTMT uses a guidance system to install pipelines at high levels of accuracy in line and grade, plus or minus 0.25 inches per a 400-foot drive (Akkerman 2013). However, guidance is accomplished through the use of an LED target, digital theodolite, and a “real time” camera with PTMT, as opposed to a laser guided system with microtunneling. The auger boring methodology is adopted during jacking of the casing and product pipe and removal of the spoil material with auger flights. There are three common variants to the PTMT installation process: the two phase method, the three phase method, and the modified three phase method.

The common phase to all PTMT variations includes jacking of the pilot tubes to obtain proper line and grade (Figure 1.1). With this phase, pilot tubes are jacked from the jacking shaft to the reception shaft. A steering head with a slanted face is attached to the lead pilot tube. If pilot tubes are advanced without rotation, the tubes will proceed in the direction of the slant. An LED illuminated target, with two concentric circles and a line indicating the orientation of the slant, rests within the steering head. A camera is mounted

on a digital theodolite positioned in the jacking shaft, which views down the center of the hollow pilot tubes towards the LED target and displays an image in “real time” to a monitor located on the jacking frame. If the operator notices that the pilot tubes are drifting off of line or grade, the pilot tubes are rotated to orientate the slant on the steering head to the preferred direction and pilot tube jacking proceeds to bring the lead tube back on alignment. Lubrication of the pilot tube string is possible when dual walled pilot tubes are used. In this scenario, lubrication flows between the outer and inner walls to the steering head, where it is expelled, and the camera’s optical path is maintained within the inner wall.

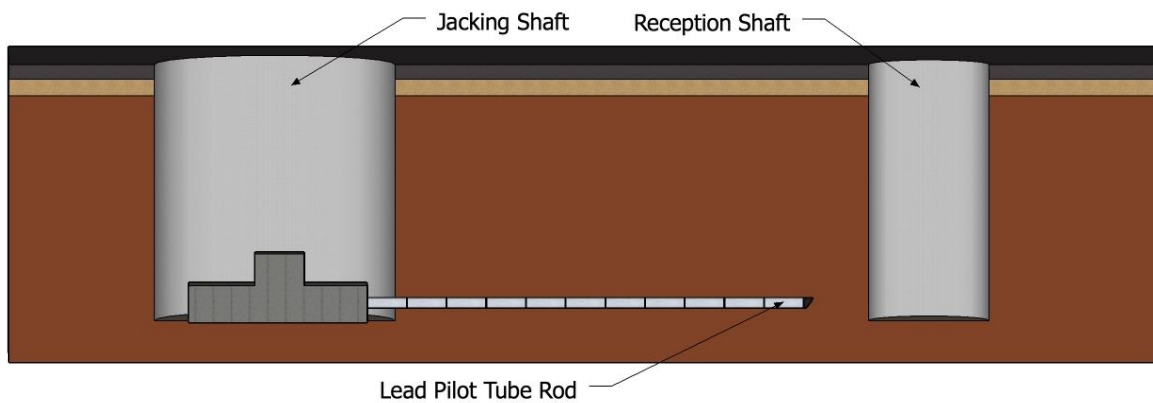


Figure 1.1 Pilot Tube Installation during Phase One

Deviation between the three PTMT installation processes occurs once the lead pilot tube reaches the reception shaft, at the onset of phase two. The remaining methodology for the three PTMT variations will first be described for the three phase method, then the modified three phase method, and finally the two phase method.

Phase two of the three phase method involves replacing the smaller diameter pilot tubes with larger diameter casings to increase the size of the borehole (Figure 1.2). Augers are used to excavate the soil at the face and transfer spoil back to the jacking shaft

where it may be removed. A reaming head (Figure 1.3), which transitions from the outside diameter (OD) of the pilot tubes to slightly larger than the OD of the casings, is used to link the pilot tubes to the casings. The purpose of the reaming head is threefold: 1) to upsize from the pilot tubes to the casings, 2) to break up the soil before it enters the casing, and 3) to transfer thrust force from the casings to the pilot tubes. Additionally, lubricant can be applied to the casing outside surface or to the auger flights through ports located in the reamer. As casings are jacked forwards along the pilot tube trajectory, pilot tubes are disassembled and removed once they enter the reception shaft.

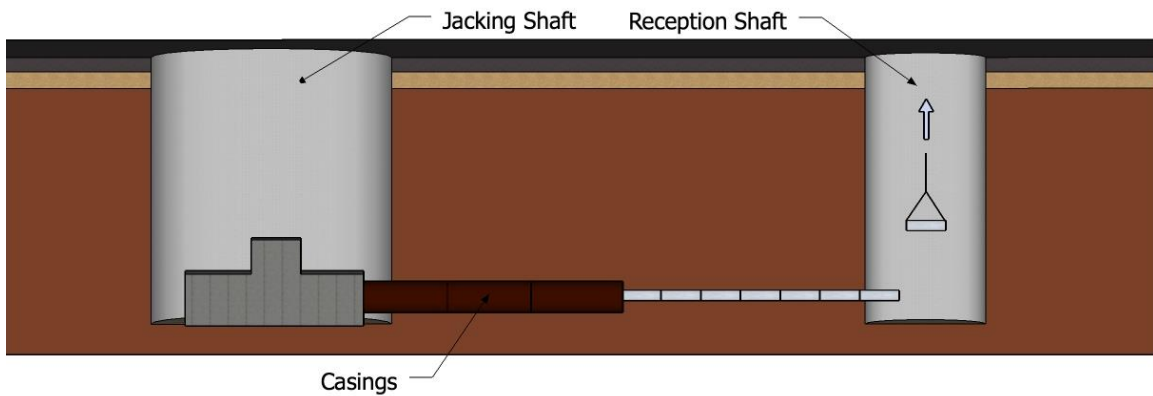


Figure 1.2 Auger-Casing Installation and Pilot Tube Removal during Phase Two



Figure 1.3 Upsizing Reamer to Fit 25.5-Inch OD Casings, Casings in Background



Phase three of the three phase method involves replacing the casings with the final product pipe (Figure 1.4). There is an adapter that links the casings to the product pipe which minimizes the contact pressure on the front product pipe and allows for a secure connection. All spoil material was removed in phase two, so the only operations taking place in this phase are jacking of the product pipe and removal of the casings. Furthermore, lubrication is not applied during this phase.

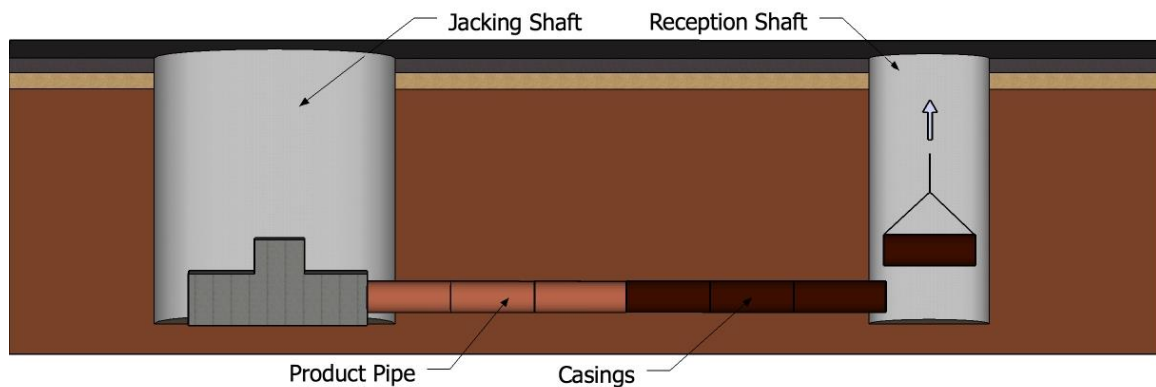


Figure 1.4 Product Pipe Installation and Auger-Casing Removal during Phase Three

The modified three phase method involves using a hydraulically powered cutting head (PCH) (Figure 1.5) or powered reaming head (PRH) (Figure 1.6). The main difference between the two heads is that cutting heads are fitted with cutting bits on their face and reaming heads have a cutting ring. Regardless of the excavation tools fitted to the powered heads, the heads are used to further upsize the borehole diameter from that of the casings installed in phase two. The units are positioned between the last casing installed in phase two and the first product pipe installed in phase three. Powered heads are directly linked to the auger flights within the casings and are capable of rotating these augers in the reverse direction. As a powered head advances, excavated material is channeled through to the auger flights inside the casings and transferred to the reception

shaft where it is removed. Hydraulic hoses powering the powered heads run through the inside of the product pipes. As such, the product pipes are often staged on the ground surface with the hoses already running through them. Lubrication is able to be applied at the face and rear of the powered heads. Face lubrication softens the soil, making it easier to excavate and remove, while rear lubrication aids in reducing frictional forces associated with jacking the product pipe.



Figure 1.5 Akkerman PCH 22.5 (Akkerman 2013)



Figure 1.6 Akkerman PRH (Akkerman 2013)

The two phase method of PTMT combines the second and third phases of the three phase PTMT methodologies. After the installation of the pilot tubes during phase one, a specialized reaming head is attached to the last pilot tube. This reaming head links

the pilot tubes to the product pipe and is advanced along the pilot bore as the product pipes are jacked from the jacking shaft. As the reamer advances, soil is funneled from the reamer to auger flights coupled within the product pipe, where it is transferred back to the jacking shaft. Figure 1.7 shows vitrified clay pipes (VCPs) with casings and augers inside. Benefits of the two phase method include the ability to install a variety of product pipe diameters with the same set of casings and augers and the ability to eliminate one of the phases necessary to complete a PTMT installation. However, the installation rate during the second phase is often slow when installing larger diameter product pipes, as a lot of soil needs to be removed through a casing of limited size.



Figure 1.7 Product VCP with Casing/Auger Inside (Gottipati 2011)

In addition to the two phase method, three phase method, and modified three phase method, there are hybrid methodologies which incorporate PTMT and other trenchless technologies to tailor the installation procedures to best suit project characteristics. PTMT may be used in conjunction with auger boring equipment. In this scenario, pilot tubes are installed with a traditional PTMT guided boring machine (GBM). After pilot tubes are installed, the GBM is removed and a conventional auger boring drill rig is used to complete the second and third phases. By adopting this hybrid

technique the benefits of using an auger boring drill rig (namely larger pipe diameters installed at quicker rates and a higher available thrust force) may be realized while maintaining the high degree of accuracy associated with PTMT. Pipe ramming can also substitute for the second phase of the PTMT process. In this scenario, a pipe is rammed following the pilot tube trajectory. This hybrid technology may be advantageous when crossing under railroads where settlement and heave requirements are stringent, yet the desire to maintain an accurate installation is still present. PTMT and HDD methodologies can be combined to birth a method in which line and grade can be held within fine tolerances and product pipe can be pulled from the reception shaft to the jacking shaft. With this hybrid method, the pilot tubes are installed as normal and a reamer and swivel are used to attach the lead pilot tube to a continuous string of pipe. Typical pipe types used for this method include high density polyethylene (HDPE) and fusible polyvinyl chloride (PVC) due to their ability to be fused together to form a highly tensile resistant pipe string with little variation in OD.

### **1.2.2 Advantages and Limitations**

There are many advantages of using PTMT for installation of new underground pipelines. The main advantage includes its ability to install pipelines with extreme accuracy in congested urban settings. Accuracy is on par with that of traditional microtunneling; however, the construction footprint associated with PTMT is smaller. Furthermore, PTMT is less expensive and less technology intensive than the microtunneling alternative (Abbott 2005). Another advantage of pilot tube technology is the ability to use the pilot tube jacking process in exploratory processes. Pilot tubes may be jacked through a proposed alignment to determine the soil suitability for installation of

subsequent casings and augers. If difficult ground conditions are encountered, pilot tubes may be retracted and an alternative alignment may be proposed.

PTMT is not without its limitations, however, and is not as versatile as traditional microtunneling when it comes to the soil conditions it can be used in. Soils with blow counts exceeding an N-value of 50 tend to be too hard for the standard penetration and displacement method and require the use of an air hammer to perform the installation. Cobbles and boulders exceeding 4 inches in diameter also add difficulty to advancement as well as problems with maintaining an accurate installation. Stability problems may be encountered when advancing through loose sands, but with adequate lubrication to reduce friction development and to maintain a stable borehole, installation in loose sands is possible. Sands below the water table also pose difficulties. As the second phase of PTMT involves open faced casing advancement with an auger spoil removal process, sand and water flowing into the casings may result in stability problems and excessive ground settlement above the bore alignment.

With the wide variety of upsizing and reaming tools available, larger diameter installations are possible. However, the production rate of installing products with diameters exceeding 48 inches decreases to a point where the implementation of alternative trenchless technologies is more cost effective. Drive length for PTMT installations is mostly controlled by the ability to accurately view the target in the lead pilot tube. The target becomes smaller and harder to see as installation length increases. Zooming in with the camera is possible; however, decreased resolution accompanies excessive zoom. Furthermore, longer drive lengths increase the probability of condensation forming in the inner walls of the tubes or lubricant leaking in and ponding

along the bottom. Both of these conditions make it more difficult for the operator to view the target and keep the pilot tubes on line and grade.

### **1.3 Scope of Study**

Being able to accurately predict jacking forces during PTMT operations based on project conditions such as depth of cover, soil type, and product pipe diameter is fundamental towards design of the thrust reaction wall in the jacking shaft, selection of the main jacking frame, selection of pipe, and determining the location of jacking and reception shafts. Previous research has been conducted to understand how jacking forces develop throughout an installation during other technologies (Stein et al. 1989, Bennett 1998, Chapman and Ichioka 1999, Milligan and Norris 1999, Osumi 2000, Baumert and Allouche (2002), and Staheli 1996 and 2006, among others), but jacking force research has yet to be completed on jacking loads from PTMT installations. Understanding the factors that affect jacking loads during PTMT will reduce risks associated with uncertain jacking forces, unnecessary factors of safety, and excessive contingency planning. Lower project costs associated with these factors can benefit contractors, engineers, and owners as well as aid with reducing underground infrastructure budget deficits (Lueke and Olson 2012).

In addition to dialing in uncertainties with regards to jacking force, productivity analysis of PTMT installations can provide insight to the factors that affect installation rates. Factors with a large influence on PTMT productivity may be identified and proactive control to reduce their hindrance on installation rate may be taken. Critical tasks associated with each PTMT phase may also be identified. Contractors may pinpoint these critical tasks and brainstorm or develop new techniques for maximizing

productivity during these tasks. Results from in depth productivity analysis may be used to develop PTMT simulations aiding engineers and contractors with predicting project schedules, benefitting project stakeholders.

With a need to further understand jacking forces and productivity during PTMT installations, this study was conducted in an attempt to reduce these uncertainties. To do so, PTMT jacking frames were instrumented with hydraulic pressure transducers to capture the hydraulic pressure during seven PTMT installations from the Reid Drive Interceptor Project in Appleton, WI throughout the summer of 2011. Four of the installations were of the three phase PTMT/Auger Boring methodology, one of the installations incorporated the traditional three phase PTMT method, and two of the installations were of the PT/HDD methodology. Recorded hydraulic pressures were time stamped, allowing for PTMT installation behavior to be correlated with time, and thus paving the way for productivity analysis. From the recorded hydraulic pressures and knowledge of the jacking frames' dimensional and hydraulic specifications, the jacking force necessary to install pipes during each phase of the PTMT methodology was able to be determined.

A comprehensive literature review of monitoring of trenchless technologies and existing jacking force predictive models was conducted to shed light on the means and methods for recording real-time data and predicting jacking force based on site, project, and ground conditions. Data analysis was conducted to decipher installation patterns within the data, indicating installation of segmental pilot tubes, casings, or product pipes. Expected installation rates during each phase of the PTMT process could be obtained from this analysis. Changes in productivity were linked to field notes collected during

installation, in an attempt to determine factors that influence production rates. The benefits and limitations of automatic computer recognition in deciphering installation patterns and performing productivity analysis are discussed in brief. Upon identifying cyclic patterns indicative of sectional pipe installation, thrust force with respect to length of drive could be observed and trends in thrust force variation could be identified. Select predictive models from the literature review were adopted and compared to the collected PTMT data. The applicability of the models, which were developed for alternative trenchless construction methods, for use in PTMT jacking force prediction was evaluated.



## **CHAPTER 2: LITERATURE REVIEW**

Monitoring of construction equipment is becoming increasingly important during trenchless installation of underground infrastructure, as equipment becomes more complex and proper equipment operation becomes an integral component to completing projects on time, with high quality, and under budget. Traditionally, monitoring has been accomplished through physical means, either by note taking and observations from equipment operators or project inspectors or through observing recorded video. Automated techniques, such as using data logging devices, have since been developed and allow for a more accurate and comprehensive understanding of installation behavior. Data from automated monitoring of pipeline installations can be correlated with time and may include pressure readings from equipment hydraulics, pull or push forces developed in the system, strains within the installed infrastructure, or drilling fluid usage. The following sections review literature on incorporating physical observational methods and data logging devices to collect data and current practices for predicting jacking forces during trenchless pipeline installation projects.

### **2.1 Data Collection of Trenchless Technology Projects**

Data collection serves a variety of purposes in trenchless technology. One of such applications includes the ability to perform detailed productivity analysis. Depending on the data collection method, productivity analysis may be as simple as determining average installation rates or as complex as revealing which operational tasks are most dependent on smooth and efficient workmanship and which tasks are, for the most part, independent of operator skill. Detailed productivity data enables contractors and engineers to pinpoint critical tasks within the construction workflow, enabling them to

brainstorm innovative techniques to improve efficiency, overall productivity, and consequently, save time and money for vested parties (Tang et al. 2013). Another facet of data collection is its ability to assist in achieving high levels of quality control and quality assurance through tracking installation loads.

Due to the vast majority of products installed through trenchless means being hidden beneath the surface, traditional on-site inspection is unsuited to provide sufficient quality control and quality assurance. Real-time data collection and transmittal to equipment operators can prevent operators from exceeding maximum tensile or compressive product pipe force ratings or improperly applying drilling fluids. Preventing excessive loading is critical in controlling the quality of the finished product, particularly because the final product cannot be easily accessed for direct inspection without defeating the purpose of using trenchless technology in the first place (Allouche 2002). Upon installation of a pipeline, the owner may desire assurance that the pipeline has not been damaged. In HDD, the product pipe is often pulled through the borehole an extra 1% or 2 meters, whichever is less, to inspect for damage and a mandrel is pulled through the pipeline to check for geometrical irregularities (Baumert and Allouche 2003). These techniques, however, lack the ability to detect reductions in the pipe's structural integrity due to excessive loading, a characteristic that could be predicted upon comparing allowable loads specified by the manufacturer to the installation loads generated during installation.

### **2.1.1 Physical Observational Methods**

Physical observational methods are a common way to collect installation specific information. These methods include those such as watching pressure gauges of

equipment hydraulics, observing signs of excessive force, detecting malfunctions with drilling fluid application, or noticing a decrease in installation rate under the same applied force. Even though these methods are rudimentary, may be subjective, and require experience to interpret correctly, they are still a valuable tool in providing useful information about a trenchless installation. Limited literature is available documenting the use of physical observations, attributable to their subjective and largely qualitative aspects. Nevertheless, a strong understanding of how these techniques are used during trenchless installations can be ascertained through speaking with experienced industry professionals. Terry Johnson, a foreman from Bore Master Inc., was interviewed to gain insight on how he uses these techniques to aid with his trenchless projects (Johnson 2013).

Johnson has over 25 years of experience in the tunneling industry and specializes in pipe jacking, pipe ramming, PTMT, and auger boring. An observational technique he utilizes throughout all projects includes tallying the sections of pipe installed throughout the day, allowing him to know the exact distance the drive has proceeded at any given time. Knowing the location of the cutter head or lead pipe section is critical towards being able to deal with unexpected problems at the cutter head or lead pipe section. Additionally, with technologies that consist of more than one pass along the alignment, such as PTMT or HDD, if equipment hydraulic pressures increase beyond expected values, note of the high pressure location may be taken, enabling the operator to make precautionary measures when passing this location in subsequent phases to mitigate potential difficulties that may arise. Mitigation techniques may include pumping additional drilling fluid to help lubricate and stabilize the borehole, advancing at a slower

rate, or upsizing in smaller increments during reaming processes. Besides correlating tunnel advancement with observed jacking resistance, Johnson monitors drilling fluid returns and consistency. In PTMT, Johnson checks to see that fluid is being expelled from the borehole surrounding the pilot tube, suggesting that drilling fluid is present along the entire borehole, and that the fluid is of the appropriate consistency, thick enough to remain in the borehole upon adding a new pilot tube and thin enough to prevent clogging in the pump and hoses.

If geotechnical investigations or previous installation experience in an area indicates soils that may result in high jacking forces, intermediate jacking stations may be utilized. Intermediate jacking stations are used to advance the installation in an ‘inchworm’ like fashion to avoid excessive forces. Friction resistance increases with drive length due to the increased soil-pipe contact area. Consequently, installing an intermediate jacking station halfway throughout a drive will essentially halve the soil-pipe interface area and the resulting friction resistance. This procedure is especially advantageous with installations of great length, large outside diameter, or problematic soils.

In 2003, common methods for providing quality control in terms of load monitoring during HDD installations included monitoring drill rig pull on display gauges and the use of weak links, or break away swivels (Baumert and Allouche 2003). Dial gauges on drill rigs typically read thrust/pull pressure, rotation pressure, and mud pressure. It is extremely important for an operator to monitor these gauges to ensure the pipe is not being overstressed, the advancement rate is appropriate, and that mud pressures are within an acceptable range. The pull load measured by the drill rig,

unfortunately, provides only an upper bound measurement of the actual load transferred to the pipe, as the pull load measured by the rig measures a combination of the loads necessary to pull the pilot rod string, reamer, and the pipe. Thus, dial gauge readings do not provide the operator with much insight of the actual pipe loading (Baumert and Allouche 2002).

Use of weak links, or breakaway swivels, provide insurance during HDD operations that pipe loadings will not be overstressed by breaking before loading approaches an unacceptable level. With this technology, an owner can be assured that the pipeline has not been overstressed, although, this practice often results in the loss of the pipeline in the borehole and costly pipe recovery and reinstallation operations. Not only are remedial operations costly and time consuming, but the pipe may also be damaged in the retrieval process. Furthermore, brief periods of pull loads exceeding specified pipe load capacity by small percentages are not likely to damage thermoplastic pipe; however, it will result in breakage of the weak link (Baumert and Allouche 2003).

Although physical observational methods enable the operator to gain an understanding of the soil's resistance and to alter operational procedures to ease installation, these methods do not provide the means to record data in an accurate and precise manner for use in quality control, quality assurance, and research tasks aimed at increasing efficiency, predicting jacking forces for feasibility and design purposes, and reducing jacking forces to expand capabilities of existing technologies. To capture data detailed enough to provide these benefits an automated data logging approach is advised.

### **2.1.2 Automatic Data Logging**

Automatic data logging has been employed through numerous trenchless technology projects for a vast assortment of reasons. Development of data logging technologies for purposes of leak detection in oil and gas pipelines is documented in Ariaratnam and Chandrasekaran (2010) and in wastewater force mains in Laven et al. (2007). In both of these instances, sensors pick up acoustic variations as they travel through pipelines to identify severity and location of leaks, providing a cost effective method for inspecting the integrity existing pipelines. Lueke et al. (2011) introduces the application of photogrammetric methods towards monitoring ground displacement due to trenchless installations and developing three-dimensional mapping for accurate as built documents. Data generated from photogrammetry can aid contractors with providing quality control for their trenchless installations and assist owners with maintaining an accurate and easy to use database of their utility locations. Maintaining a quality record of existing underground utility locations is paramount towards reducing the probability of striking utilities during future trenchless installations and allows for proper management of underground space. Besides using data logging for inspection and mapping purposes, a plethora of projects have utilized data logging to monitor and record installation loads.

Work by Ariaratnam and Colwell (2002) includes the field monitoring of three HDD installations in July, 2000 at the Sil Silica sand pit near Bruderheim, Alberta. Monitoring devices included a load cell, pressure transducers, and linear potentiometers attached to the interior of the product pipe. The load cell housed eight strain gauges and the data collection unit. By positioning the load cell between the product line and the reamer, the actual load transferred to the product line may be captured. This measurement

is unattainable by solely monitoring drill rig gauges due to the uncertainty of the force split between the reamer and product line (Ariaratnam and Colwell 2002). The pressure transducers used in the project measured the hydraulic fluid pressures experienced by the drill rig. By employing multiple transducers thrust/pull-back, rotational torque, and drilling fluid hydraulics were able to be measured and recorded. The linear potentiometers fitted to the inside of the product line measured the strain induced on the product line by monitoring changes in electrical current from one point to the next. Advantages of using the linear potentiometers to capture strain data included the relative ease of installation and the fact that they do not reinforce the pipeline in any way (Ariaratnam and Colwell 2002). The extensive monitoring of these installations allowed for monitoring of drill rig pullback pressures, drill rig rotational pressures, loading on the product pipe, and strain experienced by the product pipe, allowing for an in-depth understanding of the installation behavior.

In 2001, the Belgian National Gas Association mandated the use of a load and pressure monitoring device for all HDD installations under their jurisdiction (Finnsson 2004). In response, Digital Control Incorporated began development of TensiTrak™ (Figure 2.1), a load and pressure monitoring device. TensiTrak™ utilizes a strain gauge and pressure measuring device connected to a transmitter to transmit the recorded data in real time to the drill rig operator. The transmission device also has a locating function incorporated in its design, making it possible to obtain accurate depth and direction readings. Similar to the load cell utilized by Ariaratnam and Colwell (2002), the device is positioned between the reamer and product line.



Figure 2.1 TensiTrak™ Load and Pressure Monitors (Finnsson 2004)

The maiden voyage for TensiTrak™ was in Kirchheim/Nabern in Germany. Throughout the HDD installation of 80 meters of 160-mm PE gas pipe at a maximum depth of 1.2 meters, a maximum recorded load of 50 kN was observed. Irregular patterns in the recorded pull forces were observed, leading the technician to believe the transmitter was receiving interference when large vehicles passed over the transmitter. Thus, a second field trial in New York was conducted.

The NY field trial incorporated the use of two receivers to capture the data transmitted from the TensiTrak™. It was found that the errors present in the first field trial were due to problems with the receiver, not the TensiTrak™ device. Complications regarding the receivers have currently been worked out and more sophisticated signal processing and data transfer methods have been incorporated (Finnsson 2004).

Ariaratnam and Allouche (2003) conducted full-scaled field testing to evaluate the performance of seventeen segments of 100-mm diameter DR14 Class 200 bell-and-spigot C-900 PVC pipe joined with a new restrained joint system during HDD installations. In



these tests, the pull-head and the first two leading joints were equipped with twelve strain gauges to measure the tensile, bending, and shear strains induced on the pipe throughout the installation. Additionally, a load cell was fitted between the pull-head and the reamer to measure and record the actual pull forces transferred from the drilling machine to the leading pipe section. From the collected data, they were able to gain valuable information about the joint behavior and performance during installation and conclude that the maximum pulling length of the PVC pipe is a function of both borehole geometry and pulling load (Ariaratnam and Allouche 2003).

Sofianos et al. (2004) comment on how field monitoring of jacking resistance during a series of microtunneling installations in Athens, Greece was completed as a learning tool to aid future owners and designers with predicting jacking loads under similar installation parameters. Monitoring was accomplished by utilizing analogue piezometers which measured the pressure in the jacking frame's hydraulic jacks. Two to three measurements were taken per monitored pipe, yet for logistical reasons, pressures were not monitored for every pipe installed. Upon capturing the pressure readings, the pressures were converted to thrust force.

Ripley (1989) performed laboratory tests on model pipes at the University of Oxford to address specific issues raised by the tunneling community. In his experiments changes in soil pressures, pipe geometry, and strains experienced by the pipes were recorded. Data was used to investigate pipe deformation, deflection at pipe joints, stress distribution at pipe joints, and the effects of using joint packing materials on the magnitude of stress induced on the pipeline. He supports fieldwork monitoring of pipe

jacking installations to promote industry advancement and understanding of the soil structure interaction with regard to jacking pipe.

At Oxford University, Norris and Milligan (1991) instrumented pipe sections (Figure 2.2) and monitored them during numerous pipe jacking installations to investigate the performance of pipe joints and the interaction between pipes and the surrounding soil. Pipe instrumentation enabled measurement of the joint articulation, longitudinal strains, joint stress distribution, pore pressure, and normal and shear stresses at the soil-pipe interface. Furthermore, jacking loads were monitored at the jacking pit with load cells. The contact stress cells instrumented on the pipe sidewall gave the magnitude of radial and shear stresses, allowing for determination of the extent to which the pipe is in contact with the ground and a measure of the soil-pipe interface friction.

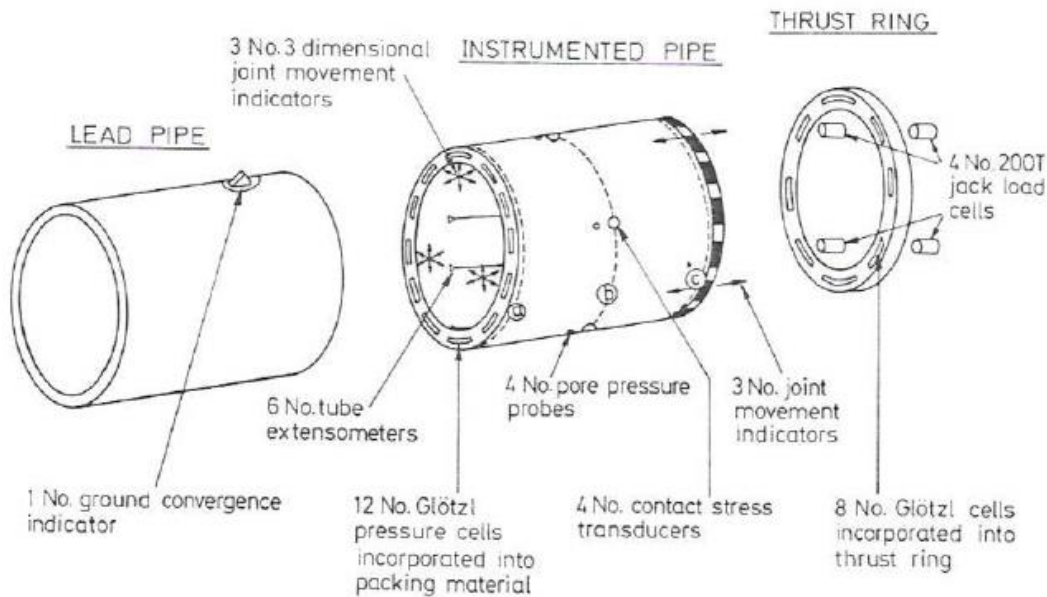


Figure 2.2 Instrumented Pipe (Norris and Milligan 1991)

One of the most extensive examples of field measurement and data collection in trenchless technology is that of the microtunneling tests performed at the Waterways Experiment Station (WES) facility in Vicksburg, MS (Bennett 1998). Detailed

descriptions of the testing that took place may be found in Bennett (1998); however, a short summary of the test facility construction and collected data is presented herein. A brief overview of the study's findings follows, in Section 2.2.

The WES testing facility included a specially designed trench 340-ft long, 16-ft wide, and 13-ft deep consisting of six different soil types placed in 60-ft long sections (Bennett 1998). Interfaces between soil type transitions were sloped to capture tunneling behavior during mixed face conditions. Two separate microtunnels, one with an auger removal process and the other with a slurry system, were conducted side by side in the test bed. A retrievable microtunnel test was performed in the test bed following the first two tests and reconstruction of the bed. Horizontal inclinometers and settlement plates were installed 2-ft and 4-ft above the crown of each intended tunnel alignment. Figure 2.3 depicts the testing bed, instrumentation, and microtunnel alignments for the first two tests. Strain gauges were fitted in eight of the 24-inch diameter Hobas pipe sections to capture strain behavior during the installation. Furthermore, jacking thrust loads, steering jack loads, and cutterhead torque were measured.

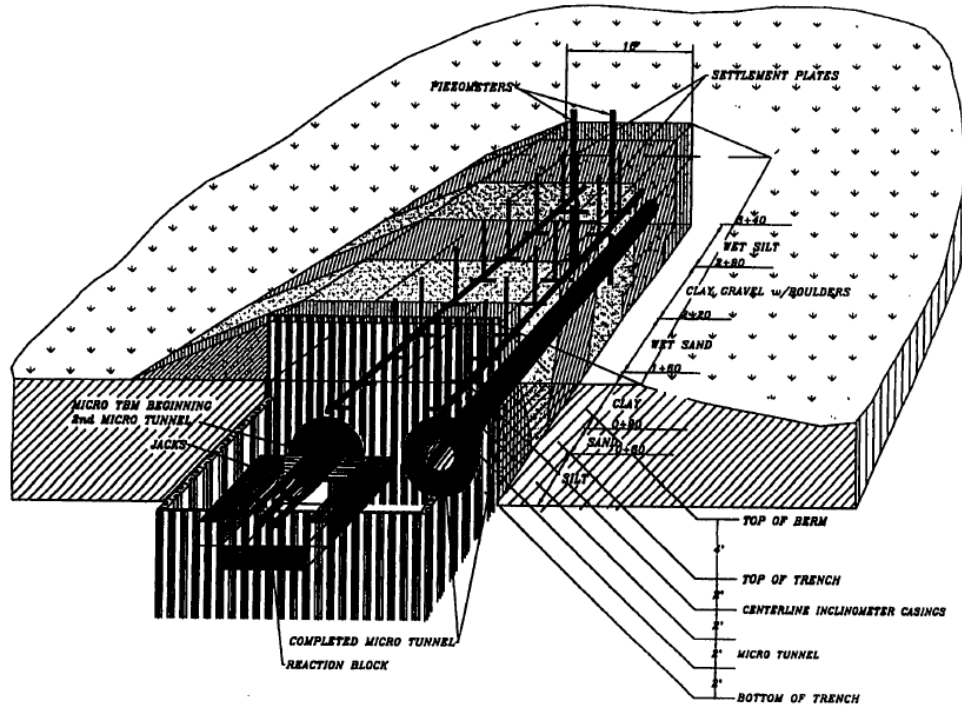


Figure 2.3 WES Test Bed (Bennett 1998)

## 2.2 Jacking Force Studies and Theory

The use of jacking systems to propel pipe segments along a tunnel alignment is a common core for trenchless technologies such as microtunneling, pipe jacking, PTMT, and other tunnel boring methods. At this time, research regarding jacking forces for PTMT has yet to be conducted. The fundamental ideology of computing jacking forces for technologies utilizing jacking systems is akin, and only slight deviations are necessary to capture the influence of differences in construction operations and sequences. Thus, it is advantageous to explore literature related to jacking forces for other trenchless technologies utilizing jacking frames to supply a basis of understanding of the jacking forces involved with PTMT.

The earliest works regarding monitoring of microtunneling installations for the purposes of recording installation loads began in the 1970's, and for the most part in

Japan and Germany. Stein et al. (1989) summarizes much of the early work completed by Salomo (1979), Scherle (1977), Weber (1981), and Herzog (1985) and provides empirical relationships for the determination of skin friction between various pipe materials and soil types with and without lubrication.

Jacking forces required for tunnel advancement are the result of two components, the penetration resistance of the jacking shield and the skin friction resistance developed along the pipe-soil interface (Pecora III and Sheahan 2004). As such, required jacking thrust for tunnel advancement is proportional to the length of the drive, as the pipe-soil interface surface area increases with drive length. Many studies have been completed to gain insight to the friction resistance. Reviews by Craig (1983) indicate that clays in France, Australia, UK, and Germany exhibit friction resistance between 5 and 20 kPa. The UK pipe jacking association (1995) suggests that one may expect average shear resistance to be between 5 and 15 kPa. The French Society for Trenchless Technology (FSTT) expresses average dynamic shear resistances for sandy, sandy-gravelly, and clayey ground of 5.4, 7.4, and 7.4 kPa, respectively, based on 14 microtunnelling installations conducted under the French National Research Project (FSTT 2004).

To put things in perspective, an installation in Athens, Greece analyzed by Sofianos et al. (2004) consisted of a 200-m drive using 1.49-m diameter pipes and a jacking frame with a capacity of 6000 kN. Such installation is only possible if the average shear resistance is limited to 6.4 kPa (Sofianos et al. 2004). Accordingly, particular attention must be given towards minimizing the degree and quantity of alignment deviations and corrections, providing adequate overcut, and properly injecting lubricant

into the annular space between the borehole and the pipe walls to allow for successful completion of this drive.

Due to the stable nature of the stiff to hard sandy clay (CL) present along the intended alignment in the Athens installation, it was decided that an open face articulated micro-backacter double shield would be successful advancing the tunnel. Consequence to the stable face and use of the open shield, the recorded thrust forces were believed to be only due to the shear resistance along the soil-pipe interface (Sofianos et al. 2004). They compared collected thrust force data to theoretical trust forces derived from two hypothesis: one, that the ground is in full contact with the pipe and causes loading on the entire outside surface area, and two, that the borehole remains intact and frictional resistance is solely based on the weight of the pipe and the soil-pipe interface at the bottom of the borehole.

Frictional resistance ( $F_s$ ) generated at the soil-pipe interface is related to the effective stress normal to the pipe ( $\sigma'$ ) and a friction coefficient ( $\mu$ ).

$$F_s = \sigma' \times \mu \quad (2.1)$$

Although Equation 2.1 is rather simple, determining the effective normal stress and friction coefficient is rather problematic. Both parameters can vary significantly throughout the length of a drive due to changing soil conditions, corrections in alignments, or simply with time, which can cause overcut and lubrication benefits to diminish as soil begins to relax. Terzaghi's Arching Theory (1943) is a widely accepted model for calculating the ground pressure, or effective normal stress, induced on the pipe walls (Bennett 1998, Bennett and Cording 1999, Pellet-Beaucour and Kastner 2002, Staheli 2006, and Shou et al. 2010).

Terzaghi developed his arching theory through performing an experiment where he filled a box with layers of sand and measured the vertical stresses as he incrementally lowered a trap door in the middle of the box. It was found that when the trap door was lowered, the trap door experienced decreases in vertical stress equal to the vertical component of the shear stress developed in the sand. He then proposed the following equation for the vertical stress in sand with zero cohesion at various heights above the trap door centerline:

$$\sigma_v = \frac{\gamma B}{K \tan \phi} \quad (2.2)$$

where  $\gamma$  = unit weight of the soil

$B$  = half of the trap door width

$\phi$  = angle of soil internal friction

$K = 1$  at the trap door centerline, 1.5 at  $2B$  above the centerline, and  $\frac{B}{z \tan \phi}$  at  $5B$

above the centerline (where  $z$  is the depth below ground surface)

The Terzaghi Arching Theory as modeled by the trap door experiment, as depicted in Figure 2.4 (Bennett 1998), does not however, directly apply to the vertical stress imposed on pipes, as alterations need to be made to take into account the cylindrical shape of a pipe's outer dimensions. Regardless, analysis of frictional resistance versus earth cover and standard penetration test  $N$  values do support the arching theory, as frictional resistance tends to decrease with deeper and stronger soils (Chapman and Ichioka 1999).

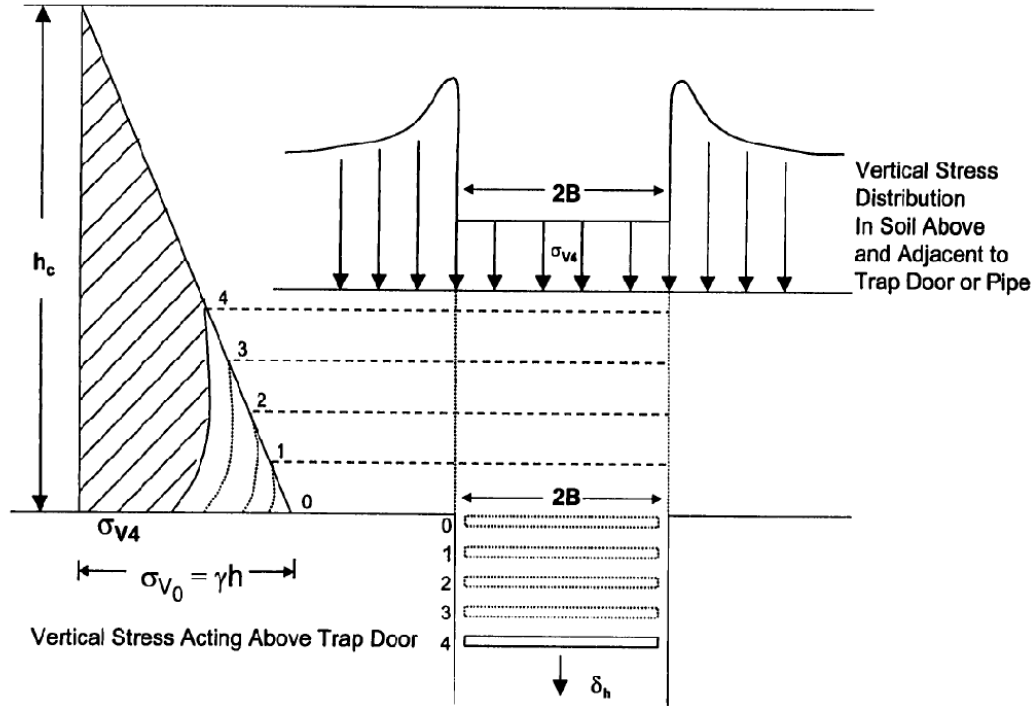


Figure 2.4 Analogy of Terzaghi's Trap Door Experiment (Bennett 1998)

There are a number of methods for applying the arching theory to cylindrical pipes. Variations in the methods account for differences in what to use as the trap door width, as the trap door width should be converted to pipe diameter in order to use the arching theory for pipe jacking purposes (Staheli 2006). Auld (1982) adopted the Terzaghi Arching Theory for this application and derived the following equations referring to Figure 2.5:

$$\sigma_v = \frac{\gamma B}{k \tan \phi} \left( 1 - e^{-k \tan \phi H/b} \right) \quad (2.3)$$

$$\sigma_H = 0.3 \gamma (0.5D + D \sigma_v) \quad (2.4)$$

$$\text{Total Pressure} = \frac{\pi D}{2} (\sigma_v + \sigma_H) \quad (2.5)$$



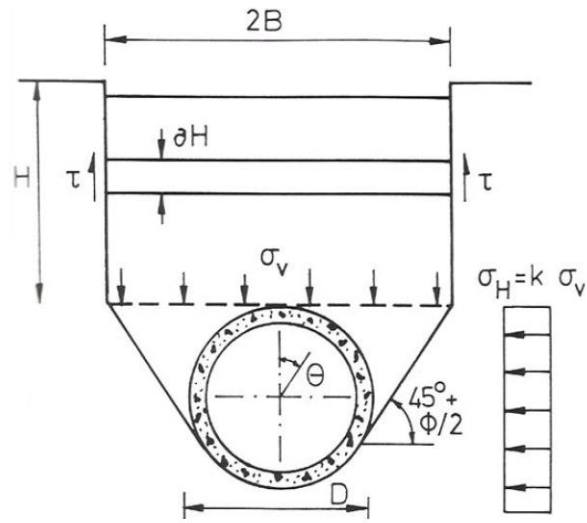


Figure 2.5 Distribution of Normal Stress (Auld 1982)

German Standards regarding normal stresses imposed on pipes during microtunneling using arching theory can be found in ATV A 161 (Stein et al. 1989). Figure 2.6 (Stein et al. 1989) summarizes work done by others, who have adopted Terzaghi's Arching Theory.

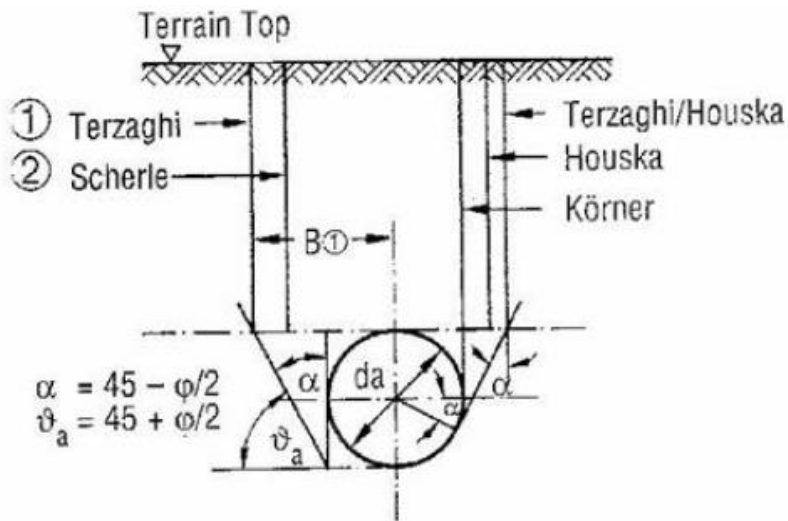


Figure 2.6 Terzaghi's and Various Authors' Arching Theory (Stein et al. 1989)

McNulty (1965) performed numerous tests evaluating Terzaghi's Arching Theory in sands using a 36-inch diameter cylindrical pressure cell. Trap doors of 3-inch and 6-

inch diameter were constructed in a way where upward and downward expansion from the pressure cell was possible. McNulty found that even in shallow depth of cover with respect to pipe diameter scenarios, slight deformations resulted in noteworthy decreases in stresses. Jester (1970) also conducted arching experiments, although he used Buckshot clay. He found that Terzaghi's Arching Theory under predicted stresses when the depth of cover equaled the diameter of the pipe and over predicted when the pipe diameter was three times greater than depth of cover.

Alternative to Terzaghi's Arching Theory, the cavity contraction model (Atkinson and Potts 1977) details the failure envelope above tunnels in sandy soil (Figure 2.7). The failure envelope is defined by the angle  $2\psi$ , where  $\psi$  is the dilation angle of the soil. Jacobsz et al. (2004) developed a centrifuge model based on the cavity contraction model. It was concluded that the cavity contraction model adequately represented actual ground conditions in granular material due to the predicted failure envelope being the location where the stress path at the tunnel crown reached failure (as summarized in Staheli 2006).

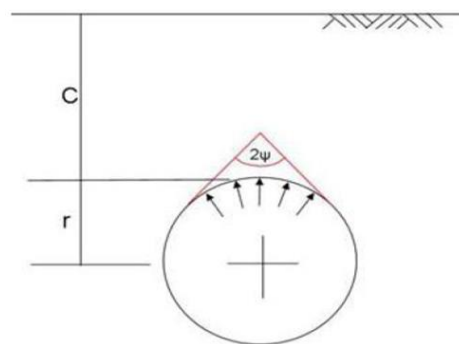


Figure 2.7 Predicted Failure Envelope, Cavity Collapse Model (Atkinson and Potts 1977)

Other work on cohesive soils includes that of Haslem (1986). He developed a predictive model (Equation 2.6) that accounts for adhesion between the soil-pipe

interface to determine the jacking forces in stable clay installations (Bennett 1998). Use of Haslem's predictive model requires accurate prediction of the adhesion factors and the contact width and pressure between the soil and pipe. Additional required parameters can be determined through laboratory testing. Contact force in stable clay bores may be estimated using the weight of the pipe, however, in soft or swelling clays, the contact force would be expected to be significantly greater and would require knowledge of the soil vertical stresses and swelling pressures to compute (Bennett 1998).

$$F_r = \alpha s_u b' \quad (2.6)$$

where  $\alpha$  = Adhesion factor

$s_u$  = Undrained shear strength

$b'$  = Soil-pipe contact width

and

$$b' = 1.6\sqrt{(P_u K_d C_e)} \quad (2.7)$$

where  $P_u$  = Contact force per unit length of pipe

and

$$K_d = \frac{d_b d_p}{d_b - d_p} \quad (2.8)$$

where  $d_b$  = Bore diameter

$d_p$  = Outer diameter of pipe

and

$$C_e = \frac{1 - \nu_s^2}{E_s} + \frac{1 - \nu_p^2}{E_p} \quad (2.9)$$

where  $E_S$  and  $E_P$  = Soil and pipe elastic modulus, respectively

$\nu_s$  and  $\nu_p$  = Soil and pipe Poisson's Ratios, respectively

Through the numerous installations monitored by Milligan and Norris (1999), they concluded that the overcut provided by tunneling shields typically remains stable with cohesive soils, with the exception of very soft clays. Moist fine or silty sand soils also tend to be stable due to capillary suction. Dry or fully saturated cohesionless soils tend to collapse and fill the annular space (Milligan and Norris, 1993). In order to fully understand the jacking forces expected during an installation, accurate prediction of the borehole conditions must be made. To complicate things further, heavily overconsolidated plastic clays have a tendency to swell upon pressure relief from the overcut. This characteristic, in combination injected drilling fluid, which provides a water source for increased swelling, can result in shrinkage of the borehole and particle to pipe contact, significantly increasing frictional resistance (Milligan and Norris, 1999). Additional components to their research include explanations for increased jacking forces due to misalignments and time effects.

In Staheli's doctoral work (2006), she focused on identifying the mechanisms controlling soil-pipe interface shearing for cohesionless soils from which she was able to develop a jacking force prediction model. Staheli ran a series of interface shear tests to determine the effects of surface roughness, normal stress, relative density, and particle angularity on shear behavior. Various pipe materials were tested under normal loads of 40, 80, 120, 160, and 200 kPa against two types of sand: Ottawa 20/30, a sub-rounded quartz sand, and Atlanta blasting sand, an angular blasting quartz sand. Additional specifics regarding the testing program can be found in Staheli (2006) and Iscimen

(2004). Based on the results, the interface friction coefficient between each soil and pipe combination could be determined. Extrapolation and interpolation was used to create Table 2.1 (Staheli 2006), which outlines interface friction coefficients for cohesionless soils with residual friction angles ranging from 25 to 40 degrees.

Table 2.1 Interface Friction Coefficients for Numerous Pipe Materials and Residual Friction Angles (Staheli 2006)

Soil at Interface	Soil-Pipe Interface Friction Coefficient					
Residual Angle of Friction	Hobas	Polycrete	Permalok Steel	Wet Cast Concrete	Vitrified Clay Pipe	Packerhead Concrete
25	0.37	0.40	0.38	0.43	0.42	0.49
26	0.39	0.41	0.40	0.45	0.44	0.50
27	0.41	0.42	0.42	0.47	0.46	0.52
<b>27.9 Ottawa 20/30</b>	<b>0.43</b>	<b>0.43</b>	<b>0.44</b>	<b>0.48</b>	<b>0.48</b>	<b>0.53</b>
28	0.43	0.43	0.44	0.48	0.48	0.53
29	0.45	0.44	0.46	0.50	0.50	0.55
30	0.47	0.45	0.48	0.51	0.52	0.56
31	0.49	0.46	0.51	0.53	0.54	0.57
32	0.51	0.47	0.53	0.55	0.56	0.59
33	0.53	0.48	0.55	0.56	0.58	0.60
34	0.55	0.49	0.57	0.58	0.60	0.61
<b>34.6 Atlanta Blasting</b>	<b>0.56</b>	<b>0.49</b>	<b>0.58</b>	<b>0.59</b>	<b>0.61</b>	<b>0.62</b>
35	0.57	0.49	0.59	0.60	0.62	0.63
36	0.59	0.50	0.61	0.61	0.64	0.64
37	0.61	0.51	0.63	0.63	0.66	0.65
38	0.62	0.52	0.65	0.65	0.68	0.67
39	0.64	0.53	0.67	0.66	0.70	0.68
40	0.66	0.54	0.69	0.68	0.72	0.69

Staheli developed her jacking force prediction model (Equation 2.10) based on the interface friction coefficients listed in Table 2.1 and normal forces derived from

Terzaghi's Arching Theory. She also outlined many of the relationships developed by other authors, as detailed by Stein et al. (1989), in Table B.1.

$$JF_{frict} = \mu_{int} \frac{\gamma \cdot r \cdot \cos\left(45 + \frac{\phi_r}{2}\right)}{\tan\phi_r} \cdot \pi \cdot d \cdot l \quad (2.10)$$

where  $JF_{frict}$  = Frictional component of jacking force (tons)

$\mu_{int}$  = Pipe-Soil residual interface friction coefficient (Table 2.1)

$\gamma$  = Total unit weight of the soil (tons/ft<sup>3</sup>)

$\phi_r$  = Residual friction angle of the soil (degrees)

$d$  = Pipe outside diameter (ft)

$r$  = Pipe radius (ft)

$l$  = Length of pipe (ft)

Scherle's work (1977) involved determining interface friction coefficients between concrete and asbestos pipe and gravely, sandy, and clayey soils. Due to variances in friction coefficients in the static, kinetic, and lubricated scenarios, Scherle established values for each (Table 2.2).

Table 2.2 Scherle's Interface Friction Coefficients (Stein et al. 1989)

Pipe-Soil Interface	Static Interface Friction Coefficient ( $\mu$ )	Sliding Interface Friction Coefficient ( $\mu$ )	Fluid Interface Friction Coefficient ( $\mu$ )
Concrete Pipe, Gravel or Sand	0.5 to 0.36	0.3 to 0.4	0.1 to 0.3
Concrete Pipe, Clay	0.3 to 0.4	0.2 to 0.3	0.1 to 0.3
Asbestos Cement Pipe, Gravel or Sand	0.3 to 0.4	0.2 to 0.3	0.1 to 0.3
Asbestos Cement Pipe, Clay	0.2 to 0.3	0.1 to 0.2	0.1 to 0.3

Weber (1981) established an upper bound for the interface friction coefficient, 0.46, or a soil friction angle of 24.7 degrees, based on the investigation of jacking forces of microtunneling installations (as summarized in Stein et al. 1989 and Staheli 2006). Utilizing his upper bound interface friction coefficient yields a conservative estimate, not necessarily the most accurate or precise. He included with his work tabulated values (Table 2.3) of the jacking stresses due to skin friction from the various microtunneling installations he used in his study.

Table 2.3 Frictional Jacking Stress for Various Soil Types (Weber 1981)

Soil Type	Jacking Stress due to Skin Friction (kPa)
Gravel, Sand	8.4 ± 2
Loamy Sand	9.3 ± 1
Loam	7.3 ± 1
Loam, Stones	5.7 ± 4

Chapman and Ichioka (1999) expanded on data collected from ISTT’s Working Group No. 3 (1994) on 398 microtunneling operations. They separated the case histories by soil type and installation method (i.e. slurry shield, auger, and push-in machines) and utilized a probability based method to develop a model to predict the jacking force for these scenarios. During analysis of the slurry shield machines, a total of 47 data sets were removed due to data abnormalities, such as localized thrust force irregularities due to boulders or unexpected ground conditions or machine or pipe damage (Chapman and Ichioka 1999). By eliminating erroneous data, variability in their scatter plots relating frictional resistance to pipe diameter and other parameters decreased significantly. Resultantly, their predictive models are based off of typical installations and do not capture the “worst case” scenario, which may be an issue when applying this model to projects with insufficient geotechnical investigation.

The predictive model developed by Chapman and Ichioka (1999) for slurry shield machines can be expressed with the following equation:

$$F = f_o + \pi DPL \quad (2.11)$$

where  $F$  = Total jacking force (T)

$f_o$  = Primary resistance (T)

$D$  = Outside pipe diameter (m)

$L$  = Jacking distance (m)

$P$  = Frictional resistance ( $T/m^2$ ), see Table B.1

And

$$f_o = D_o^2 \frac{\pi}{4} P_o \quad (2.12)$$

where  $D_o$  = Machine outside diameter (m)

$P_o$  = Face resistance ( $T/m^2$ )

Little correlation between outside diameter and face and frictional resistance was noticed in the analysis of 69 auger boring installations (Chapman and Ichioka 1999). Due to the variability in the results, they chose to use constant values for face and frictional resistance to achieve designated levels of coverage of the data. These constants designating 80% coverage were 50 and 70  $T/m^2$  for face resistance in clay and sand/gravel, respectively, and 0.7 and 0.75  $T/m^2$  for frictional resistance in clay and sand/gravel, respectively. Applying these constants to Equation 2.11 enables the prediction of jacking resistance for 80% of auger boring installations (Chapman and Ichioka 1999).



Data from push-in operations posed similar difficulties as the auger boring operations. Thus, an analogous approach was taken towards determining the face resistance. It was determined that 60 and 90% data coverage yields a face resistance of 200 and 400 T/m<sup>2</sup>, respectively (soil type not specified) (Chapman and Ichioka 1999). A linear relationship was able to be seen regarding friction resistance and pipe outside diameter and can be expressed through Equations 2.13 and 2.14. It should be noted that these equations are to be used with pipe outside diameters in the range of 100 to 250-mm.

$$\text{Clay: } P = -2.3D + 1.7 \quad (2.13)$$

$$\text{Sand: } P = -2.5D + 1.9 \quad (2.14)$$

Bennett (1998) reviewed case studies in sands, clay, and silts from 39 microtunneling projects totaling over 15,000 feet and conducted field tests in a 340-ft long testing facility, the Waterways Experiment Station, with a horizontal alignment consisting of six different soil types (Bennett 1998). Goals of his research were to evaluate ground deformations due to varying advancement rates and overcuts, to develop a model to accurately predict jacking forces, and to look at time effects, steering corrections, misalignment, and dewatering and their influence on jacking resistance. The model he developed, as outlined in Table B.1, predicts jacking force as a function of the pipe's surface area, normal stresses imposed on the pipe wall, and a coefficient of friction.

He concludes that normal stress is dependent on the effective soil unit weight and the outside diameter of the pipe and independent of the depth of cover. A reduction factor,  $C_a$ , is introduced to account for arching effects. A friction reduction factor,  $C_f$ , is

also implemented to properly establish the friction coefficient representing the soil-pipe interface behavior. As consequence to the well-designed experimental field tests and the high quality and abundance of the recorded data, Bennett was able to distinguish between “initial dewatered, non-lubricated” and “non-dewatered, lubricated” segments of the installations, providing insight to the effects of dewatering and lubrication on friction development. A summary of the arching and friction reduction factors found to be representative of his study can be viewed in Table 2.4.

Table 2.4 Friction and Arching Reduction Factors (Bennett 1998)

<b>Bennett's Friction and Arching Reduction Factors</b>				
Model	Dewatered, Non-Lubricated		Non-Dewatered, Lubricated	
	Arching Reduction Factor $C_a$	Friction Reduction Factor $C_f$	Arching Reduction Factor $C_a$	Friction Reduction Factor $C_f$
<b>Sand</b>				
Upper Bound	1.5	1.0	1.0	0.66
Best Fit	1.0	1.0	0.66	0.66
Lower Bound	0.75	1.0	0.5	0.5
<b>Stiff to Hard Clay</b>				
Upper Bound	1.0	1.0	0.66	0.66
Best Fit	0.66	1.0	0.5	0.5
Lower Bound	0.33	0.66	0.5	0.5
<b>Soft to Medium Clay</b>				
Upper Bound	1.0	1.0	3.0	1.0
Best Fit	0.66	1.0	1.5	1.0
Lower Bound	0.5	1.0	1.0	0.5

Another predictive model for determining the jacking resistance during pipe jacking includes that of Osumi (2000), from the Japan Microtunneling Association. Osumi reviewed 49 pipe jacking installations and developed his model empirically (Osumi 2000). His model incorporates interface friction and adhesion parameters, thus making it a valid predictor for jacking forces in cohesionless and cohesive soils. The

interface friction component incorporated the friction coefficient,  $\mu'$ , determined as the tangent of half of the soil internal friction angle, and a normal force dependent on the depth of cover and pipe weight. He applied a jacking force reduction factor,  $\beta$ , to reduce the calculated jacking forces to appropriately represent the studied microtunneling projects. Table 2.5 outlines the reduction factor for four soil types. Osumi does not provide explanation for the atypical soil classification “solid soil”, however, it is reasonable to assume he is referring to extremely hard soil or rock.

Table 2.5 Jacking Force Reduction Factors (Osumi 2000)

Soil Category	Jacking Force Reduction Factor ( $\beta$ )
Cohesive Soil	0.35
Sandy Soil	0.45
Gravel	0.60
Solid Soil	0.35

## **CHAPTER 3: FIELD DATA COLLECTION**

In order to develop a strong understanding of the PTMT process, it was advantageous to collect field data from numerous PTMT installations. Instrumenting PTMT machinery with hydraulic pressure transducers to intercept hydraulic pressures in thrust and rotational torque components provides insight to the methodological installation process and induced installation loads. Knowledge in these areas enables the means to perform productivity and jacking force analysis of all three phases of the PTMT process. It was beneficial to locate multiple PTMT installations in the same general area to simplify logistics of mobilizing data collection equipment, minimize the quantity of equipment needed for the study, and to make it possible for data collection procedures to be conducted by a sole individual in a timely manner. As such, the Reid Drive Interceptor Project in Appleton, WI was a prime candidate for field data collection of PTMT processes.

### **3.1 Reid Drive Interceptor Project**

The Reid Drive Interceptor Project was located in Appleton, WI on the north side of the Fox River (Figure A.1) and completed in the summer of 2011. The existing interceptor sewer (purple) was aging and concern was growing about sewer leakage into the Fox River. Consequently, a new interceptor located an average of 250-ft north of the river was proposed to alleviate the pollution risks. Proposed pipeline quantities for the project included approximately 2,400 lineal feet of 21-in nominal inside diameter (ID) sanitary sewer (red), 400 lineal feet of 8-in nominal ID sanitary sewer (yellow), and 1500 lineal feet of 4-in nominal ID sanitary lateral (blue). However, not all installations were

monitored with data logging devices due to the inability to procure and calibrate data logging instruments prior to the project start date.

Alignment for the sanitary sewer main was to run along Reid Drive, connecting to an existing sewer line just west of South Orchard Drive and East of Alicia Park near the bottom of the river bank. Steep northern river banks, two horizontal to one vertical, complicated the proposed design. To make the eastern connection feasible, while maintaining the specified slope of 0.2%, 35 to 40-ft installation depths were required for the sanitary sewer main. Such a deep installation and the close proximity of the houses adjacent to the proposed alignment caused project designers to shy away from using traditional open trench techniques. Open trench installation would have been possible in Alicia Park; however, due to the mature trees located in the park trenchless operations were preferred to minimize potential damages. Furthermore, the park is highly valued by the local residents and closing of the park would have unnecessarily increased social costs of the project. Additional difficulties regarding working around and relocating existing utilities within the proposed alignment would have surfaced if open trench methods were employed. The conglomeration of installation complications associated with open trench techniques lead designers to specify trenchless installation methods for the project.

The trenchless technique to be utilized for the installation of the sanitary sewer mains was not specified in project plans; yet, sanitary laterals were to be installed by HDD practices. The awarded contractor, Globe Contractors, Inc., subcontracted Bore Master, Inc. to perform the trenchless installations. Upon evaluating the site conditions, the geotechnical report, and their machinery inventory, Bore Master elected to use a three

phase PTMT/Auger Boring method to install the 21-in nominal ID mains and a traditional three phase PTMT method to install the 8-in nominal ID services. Steel pilot tubes and steel casings were used in the first and second phases. The product pipe material used in phase three was chosen to be Mission Clay's No-Dig VCP. No-Dig VCP is used on more PTMT projects than any other pipe material and is ideal for jacking installations due to its high 7,000 psi axial compressive strength, its compression gasket joint seal system, and its consistent outside dimensions (Mission Clay Products 2013).

A PT/HDD technique was used to install the 4-in nominal ID laterals. The PT/HDD procedure incorporates the guided protrusion of pilot tubes to provide the proper line and grade, attachment of a reaming head to create a borehole slightly larger than the product pipe, and pull back of the product pipe attached with a swivel to isolate the product line from the rotation necessary for the reaming process. Contrary to traditional HDD procedures, installation of a larger exit pit (Figure 3.1) to facilitate attachment of the reamer, swivel, and product pipe was necessary in most instances due to the inability to accurately steer the pilot tubes towards the ground surface upon successful completion of the pilot bore. As with many pull back operations (Carpenter 2007), HDPE pipe was utilized as the product pipe material due to its high tensile stress ratings.



Figure 3.1 Exit Pit Installation for PT/HDD Procedure

Utilizing the three phase PTMT, PTMT/Auger Boring, PT/HDD methods proved advantageous for this project for a variety of reasons. Deep installations are quite feasible with these technologies, as access to great depths is provided by the jacking and reception shafts required for the jacking machinery and pilot tube/casing removal. The only excavation necessary for these methods is that of the shafts. Thus, the decreased construction footprint enabled the residential streets to remain open, trucking traffic to be reduced, and surface restoration to be as minute as possible. Furthermore, the proximity of Alicia Park results in the presence of numerous children and other pedestrians. This increases the importance of having a safe construction site with minimal hazardous excavations.

Besides the ease of deep installations and significant societal benefits, PTMT technology allows for the installation of a product line at a high degree of accuracy in line and grade. By utilizing the theodolite, camera, and an LED target guidance system, design accuracy in line and grade of 0.25 inches in a 400 foot installation could be

maintained (Akkerman 2013). Accuracy of this caliber was necessary for this project due to the near flat grade of 0.2% and due to the fact that the sanitary sewer is to operate under gravity flow. Utilizing installation methods unable to provide such high accuracy standards may lead to back pitch in localized areas, which can cause severe operational problems in critical grade infrastructure systems such as this gravity flow sewer.

PTMT also was an ideal candidate for the type of soils documented throughout the alignment. Borings indicated fairly consistent soil at the depths of the proposed sewer, consisting mostly of red-brownish-gray silty clay with trace amounts of moist sand. Table 3.1 describes the soil characteristics expected to be encountered, based on the project’s geotechnical report, for the installation drives with collected data. Obstructions were not expected to be encountered during directional drilling procedures, as obstructions during the soil boring operation did not occur.

Table 3.1 Soil Characteristics Corresponding to Drives with Collected Data

Drive #	Estimated Depth Below Water Table (ft)	Stiffness	N	q <sub>u</sub> (tsf)	q <sub>p</sub> (tsf)	q <sub>s</sub> (tsf)	w (%)	γ <sub>d</sub> (pcf)
1	25	Medium Stiff	4	0.9	0.4	0.4	22	107.5
2	17	Medium Stiff	5	0.7	0.4	0.4	22	107.0
3	19	Medium Stiff	5	0.6	0.3	0.4	23	106.9
4	14	Medium Stiff	4	0.7	0.2	0.4	23	106.7
5	4	Stiff	9	1.6	1.2	0.7	17	107.1
6	3	Stiff	9	1.6	1.2	0.7	17	107.1
7	3	Stiff	8	1.8	1.4	0.5	21	107.1

where N = Standard penetration resistance N value (ASTM D-1586)

q<sub>u</sub> = Unconfined compressive strength

q<sub>p</sub> = Calibrated penetrometer resistance

q<sub>s</sub> = Vane-shear strength



$w$  = Moisture content

$\gamma_d$  = Unit weight of dry soil

### 3.1.1 Monitored Installations

All phases of seven installations, or drives, were monitored with data logging equipment throughout the duration of the project. The drive numbers and their corresponding characteristics may be viewed in Table 3.2. Jacking shafts were constructed at the locations of manholes 26.100, 26.102, and 26.106. Other manhole locations were the site of the reception shafts. Data collection during drives three and four adequately captured jacking behavior during phases one and two, although, jacking behavior for phase three of both drives was not. Upon downloading the phase three data for drive three, it became evident that pressure transducer outputs were constant and did not represent actual field conditions. Phase three data for drives one and two appeared to represent field conditions, but required some modification (see section 5.1.1). Further descriptions of the complications associated with this pressure transducer are detailed in Appendix D.

Table 3.2 Monitored Installation Drive Characteristics

Drive #	Manholes	Length (ft)	Depth (ft)	Nominal I.D. (in)	Product Pipe	Boring #
1	26.100 to 26.99B	405	38	21	VCP	B3 to B4
2	26.100 to 26.101	385	36	21	VCP	B3 to B3/B2
3	26.102 to 26.101	200	35	21	VCP	B2 to B2/B3
4	26.102 to 27.3	407	34	21	VCP	B2 to B1
5	26.106 to 26.100	123	26	8	VCP	B3
6	26.106 to NA*	230	25	4	HDPE	B3
7	26.100 to NA*	260	35 to 16	4	HDPE	B3

\*The exit locations for lateral installations were not at proposed manhole locations.

PT/HDD was utilized in drives six and seven to install 4-inch HDPE laterals. During each of these installations, deviations from the traditional methodology of a single pilot run to establish line and grade and one ream/pull-back of the HDPE product pipe existed. In drive number six, stresses induced throughout the installation caused the product pipe to yield, and eventually snap, about 40 feet from completion. The following day, a rescue shaft was constructed to access the location of the snapped HDPE pipe. Pilot tubes were then jacked to this location and the reaming assembly and swivel attachment were connected to link the HDPE pipe to the pilot tubes. Pull-back operations followed and were successful in pulling the product pipe back into the jacking shaft.

Due to the experience with the sixth drive, it was decided that an alternative approach would be used to install the HDPE lateral for drive seven. This approach involved jacking the pilot tubes to establish the line and grade, hooking up the reamer at the exit location, and pulling back the reamer without the product pipe attached. Once the reamer exited the pilot bore, pilot tubes were then jacked through the reamed borehole to the exit location. The reamer and swivel were then used to link the pilot tubes to the HDPE product line, and the product line was pulled through the borehole to the jacking shaft to complete the drive. It was thought that by pre-reaming the borehole, the forces experienced by the HDPE product line would be reduced and the chances of the product pipe failing would be minimized. The effect of pre-reaming is further described in Chapter 5. To differentiate between initial and subsequent pilot tube jacking and pull-back operations terminology such as “PT 1”, “PT 2”, “pull-back 1”, and “pull-back 2”, respectively, are utilized.

## **3.2 Prepping the Data Logger**

The data logger utilized to record the hydraulic pressures from the Akkerman GBM-240A guided boring machine (GBM) used in phase one, the American Auger 36-600 NG Auger Boring Machine (AA) used in phase three, and a custom built pipe pusher (BM pusher) used in phase three was the Data Dolphin DD-400 from Optimum Instruments, Inc. This data logger was used due to its extreme versatility, ability to store data on a flash memory to prevent data loss in the event of dead batteries, and its allowance for sample rates to be adjusted without being restarted. Voltage outputs transmitted from three pressure transducers (Econoline 10,000 psi, 0.5-4.5 VDC) to the data logger are correlated with the time and date of their occurrence, aiding with productivity analysis and for linking data with operational field notes. Before being able to begin recording field data with the device, the following procedures must be performed: calibration of the pressure transducers, programming of the data logger, and proper connection to the PTMT machinery.

### **3.2.1 Pressure Transducer Calibration**

Three pressure transducers, denoted as “L1”, “L2”, and “L3”, were used to output voltage values to the data logger from the hydraulic pressures in the GBM, AA, and BM pusher during installation. The first transducer, L1, was used to collect the thrust hydraulic pressure for the BM pusher. Transducer L2 was responsible for capturing the thrust hydraulics in the GBM. Transducer L3 output voltage from thrust hydraulics from the AA and rotational hydraulics from the GBM. It should be noted that the BM pusher is capable of producing 10,000 psi pressures, yet the AA and GBM are only capable of 5,000 psi pressures. A 10,000 psi hydraulic pressure is the maximum pressure the

transducers can read, resulting in a maximum voltage output of 4.5 volts. The Data Dolphin data logger is only able to record voltage inputs less than or equal to 2.5 volts. Consequently, a reducer was fixed between the L1 transducer and the data dolphin to scale down the voltages to a recordable level. L1 was not used to collect data for the other machines as it was thought the reducer may have a negative effect on the resolution of the collected data. Thus, utilizing three transducers was necessary to be able to capture both the thrust and rotational torque hydraulics during phase one and the operations of the BM pusher in phase three.

In order to ensure proper identification of machine hydraulic pressures during the installations, the pressure transducers needed to be calibrated in a controlled laboratory setting. Each transducer was individually hooked up to intercept hydraulic pressure from a hydraulic line that could be held at constant pressure. The transducers were then exposed to constant pressures of 500, 1000, and 2000 psi for between 30 to 60 seconds. The mean voltage value from a pressure transducer recorded by the data logger during a period of exposed hydraulic pressure was noted to be representative of the respective hydraulic pressure. The increase in voltage resulting from an increase in hydraulic pressure was linear for all three transducers, with fitted  $R^2$  values greater than 0.998 for all three lineal fits. Thus, linear extrapolation was used to determine voltage outputs resulting from each machine's maximum hydraulic pressure.

### **3.2.2 Programming the Data Logger**

In order to program the Data Dolphin to perform desired tasks, communication must be established through one of the following methods (Optimum Instruments 2004):

1. Direct connection via a RS-232 cable

2. Land line dial-up modem
3. Spread spectrum radio (2 to 20 mile range)
4. Wireless IP (via Data Dolphin's internal cellular modem) to the internet or an intranet
5. Ethernet

The ease of establishing a connection between the user and the Data Dolphin adds to versatility of the data logging system. One may connect wirelessly, or directly, to a Data Dolphin with an advanced communication module and have that Data Dolphin be the “hub” for a network of Data Dolphins, effectively enabling the user to communicate with all data loggers through the hub. A connection such as this would be advantageous for collecting data on a large project, where multiple installations are being completed at once and there is a need for using and accessing multiple Data Dolphins at one time. However enticing a wireless communication method may be, a direct connection using a RS-232 cable and a USB adapter was used for this study. The data logger containment box was taken away from the jobsite each night to monitor its condition and charge its battery if need be, making the simple direct connection the preferred method.

Once a connection between the Data Dolphin and the user has been established, communication is initiated by opening the Data Dolphin software and clicking the “load from Data Dolphin” button in the “dolphin setup” window. Upon doing so, Data Dolphin's current operating parameters should be displayed on the user's computer in the “status” window. To change any of the current operating parameters, the “dolphin setup” window needs to be used. From here, the Data Dolphin's internal clock time may be set so data is time stamped correctly with the time of day. Conditions regarding the sampling

rate may also be specified. For this study the sample rate was set to one sample every three seconds, to ensure that most operational procedures during the installation would be captured. A delayed start was often used so that recording would begin at the beginning of the work day in an attempt to optimize battery life. Other setup parameters were rarely used and are not worth mentioning. Additional setup parameters and Data Dolphin capabilities may be found in the Optimum Instrument's Data Dolphin Data Logger Series Operators Manual (2004).

After a period of data collection the data may be retrieved from the data logger by establishing a communication session with the unit as previously described. Afterwards, the "download" button should be clicked in the "status" window. The project site database on the user's computer will then be updated with the most recent Data Dolphin input capture. Alternatively, a specific date and time window may be selected to download data that has already been downloaded or to download data within a specific time frame. Upon filling the flash memory used to store data in the Data Dolphin, the software will direct the Data Dolphin to either stop recording new data or to record new data while simultaneously deleting the oldest data. For this case study, the Data Dolphin was programmed to stop recording once full. As such, it was important to clear the data from the flash memory as soon as it was downloaded and verified on the user's computer. Clearing the Data Dolphin's memory may be accomplished through selecting the "erase all data" button from the "tools" drop down menu.

### **3.2.3 Connecting the Data Logger to Machines**

The data logger, along with an external battery source, was housed in a containment box to keep it secure and in good condition while exposed to construction

site hazards (Figure 3.2). To facilitate connections to machine hydraulics, the pressure transducers were connected to the data logger with 25-ft cables. Quick coupler connections were installed immediately behind machine pressure gauges to present an efficient and easy way to attach the pressure transducers. Figure 3.3 illustrates the quick coupler system employed for phase one operations with the GBM. Utilization of quick coupler connections, as opposed a standard rotational attachment system, made the transducer hook up procedure simple and imposed minimal infringements upon the productivity of the installation process, a key factor in maintaining a good relationship with the contractor. Once the transducers were in place to intercept hydraulic pressures, the storage location of the Data Dolphin containment box needed to be evaluated on a phase by phase basis.



Figure 3.2 Photograph of the Data Logger and Battery Inside Containment Box

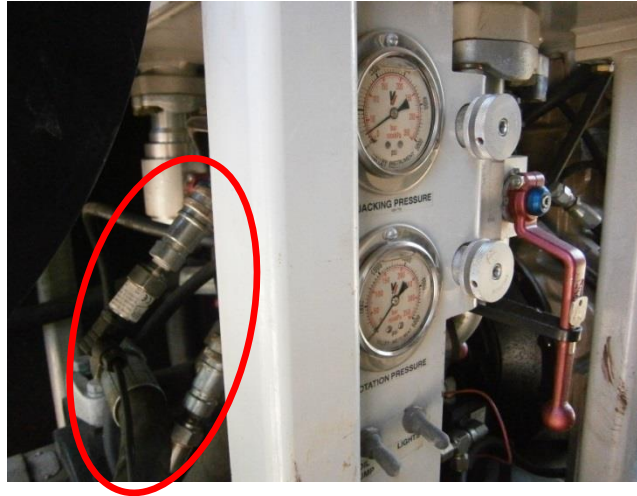


Figure 3.3 Quick Coupler Connection Used for Pressure Transducer Connection to GBM Hydraulics (Lueke and Olson 2012)

It was crucial to ensure the Data Dolphin would be safe from on-site hazards, that the 25-ft cables could span the distance from the containment box to the hydraulic lines, and that the containment box would be in a location where it did not interfere with phase specific operations or procedures. The power pack for the GBM, which contained the engine and pressure gauges and was enclosed in a steel 6 x 6 x 12 cubic foot containment box, was located beside the jacking shaft during installations. Inside the containment box proved to be the ideal location for the Data Dolphin due to the available storage space inside the unit, the close proximity of the dolphin and the pressure gauges, and the provided protection from the outside environment. Storage locations for the Data Dolphin while using the AA and the BM pusher were down in the jacking shafts.

When the AA was in use, the Data Dolphin was fastened on top of the machine's hydraulic fluid tank with two straps (Figure 3.4). Although the data dolphin was exposed to vibrations, the straps were sufficient in securing the device to the machine. The BM pusher was powered hydraulically by a large external power pack that would sit beside the pusher during installation. The hydraulic lines traveled up from the power pack to a



boom, across the boom, and down to the pusher (Figure 3.5). This boom was attached to the power pack with a swivel joint, enabling the boom to neatly guide the hydraulic lines forward as the pusher proceeded with pipe installation. As shown in Figure 3.5, the Data Dolphin rested securely on top of the power pack and the cable for the L1 transducer ran across the ground to the BM pusher's hydraulics. This configuration proved to be bothersome for the workers, as they would need to ensure the cable didn't snag on anything as the pusher moved back and forth. A later configuration of running the cable along the boom, following the other hydraulic lines, turned out to work the best.

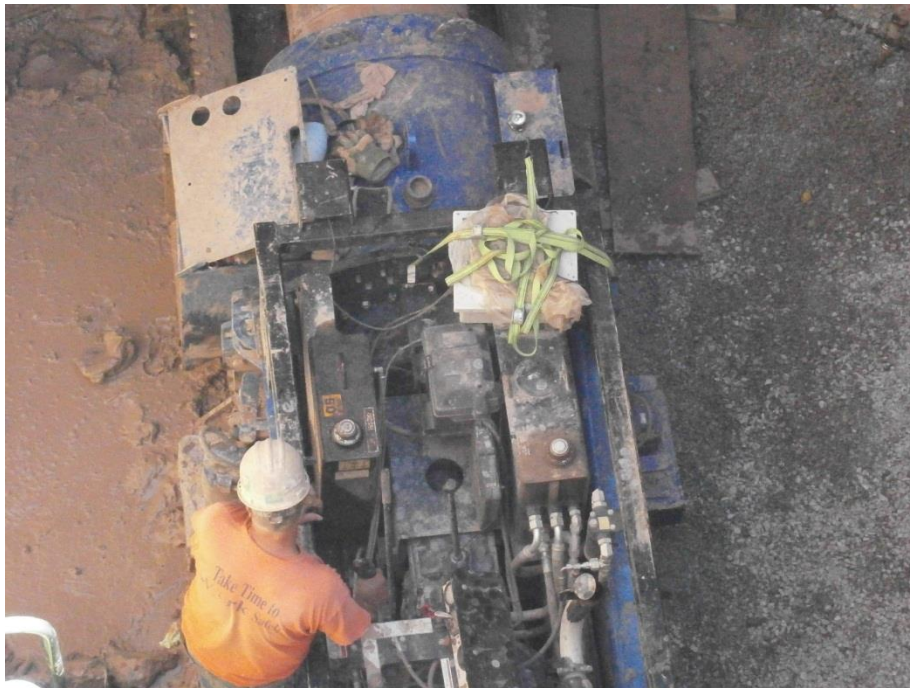


Figure 3.4 Data Dolphin Containment Unit Strapped to the AA During Phase 2 (Lueke and Olson 2012)



Figure 3.5 Power Pack & Data Dolphin Containment Unit Configuration for the BM Pusher During Phase 3

## **CHAPTER 4: PRODUCTIVITY ANALYSIS**

Instrumenting jacking frames with pressure transducers and logging the voltage outputs during all three phases of the PTMT process provides detailed construction workflow data, ideal for detailed productivity analysis. Insight into the factors affecting productivity can assist engineers and contractors with estimating accurate construction schedules and project costs (Olson and Lueke 2013). These factors may include, but are not limited to, installation depth, crew experience, utilities or other obstacles, pipe diameter, drive length, and site or ground conditions. Being able to predict installation rate based on these factors provides value to project stakeholders, as it aids evaluation of viable construction methodologies proposed for a project, increases contractor efficiency by providing a greater understanding of the critical tasks associated with PTMT installations, and supplies a framework for the development of PTMT simulation models to strengthen project schedules, cost estimates, and further academic studies. Data from instrumenting and monitoring jacking frames provides the means to attain such benefits.

Voltage output from pressure transducers fitted to the jacking frames correlates to distinct hydraulic pressure values, which may be linked to thrust force behavior generated by the hydraulic jacking rams. Since the Data Dolphin data logger time stamps the voltage outputs received from the pressure transducers, fluctuations in voltage versus time describe the operational behavior of the jacking frames, in terms of jacking force trends as well as installation productivity. Before trends in jacking force may be fully explored, it is necessary to be able to identify cyclic patterns in the recorded data. Cyclic patterns indicate operations that occur over and over again, akin to the installation of the numerous pipe sections required to complete a PTMT installation. By identifying the

cyclic patterns within each PTMT phase, data representative of each pilot tube, casing, or product pipe installation may be isolated. Once the data pertaining to each pipe is known, data may be analyzed with respect to the length of drive completed, or “chainage”, given that the length of a pilot tube, casing, and product pipe is known. From here, detailed analysis regarding jacking force trends, described in Chapter 5, and productivity analysis, discussed in this chapter, may be completed. Factors influencing productivity may be identified through in depth understanding of the elements, or operations, within typical installation cycles. Resultantly, methodology for identification of typical cycles and descriptions of their operational components are outlined in this chapter. Organization of this chapter proceeds as follows: identifying typical cycles within each phase and classifying their operations, productivity trends and observations, and the benefits of utilizing an automatic neuro network (ANN) for pattern recognition and productivity analysis.

#### **4.1 Cycle Identification**

Cyclic patterns representing particular operations required to complete installation of a single pipe section (i.e. pilot tube, casing, or product pipe) may be observed in the recorded voltage outputs from the pressure transducers fitted to the jacking frames’ hydraulics. Each of these operations, such as hooking up a pipe, jacking the pipe, pausing, or retracting the jacking rams, constitutes distinct behavior that may be identified within the recorded time series data. For example, voltage outputs are likely to be higher during jacking of a pipe section than during periods of pausing or readying a pipe section for installation. Recurring patterns of said operations indicate installation of a single pipe section. Isolating the installation of each pipe section allows for comparison

of jacking forces with respect to chainage, as well as productivity information such as installed length versus time. Time variability in a cycle's operations provides insight towards the dependency of each operation on factors such as crew experience and difficult soil conditions.

The following sections describe the operations that make up the cyclic patterns for phase one, two, and three (i.e. jacking of pilot tubes, casings, and product pipes). Cyclic patterns, and the operations within, are described in terms of voltage output from the hydraulic pressure detected from the pressure transducers. In doing so, analysis is based on the raw data collected by the Data Dolphin data logger. Furthermore, comparing voltage outputs allows for conjunctive comparison between thrust and rotational torque fluctuations representative of phase one operations.

Depending on the characteristic of an observed operation, its behavior, in terms of voltage fluctuations, may be easier or harder to identify. Most commonly, instances between operations resulting in high and low voltage outputs are easily identifiable and were chosen as the starting and end points of pipe section installation. Only after careful and prolonged observation and analysis of multiple cycles of each phase were the operational tasks within each cycle able to be identified. Consequence to predetermining the cycle start and end points, in order to complete preliminary work on jacking force versus chainage and installation rates, the start and end operations for each PTMT phase are not necessarily the same. The effect of defining differing start and end points for installation cycles of each phase is purely aesthetic and the consequences are insignificant. To provide consistency between this thesis and previously published works (Olson and Lueke 2013 and Tang et al. 2013), the start and end points for the installation

cycles remain unchanged. Start and end points for typical cycles for each phase are thus identified at the beginning of the corresponding section in this thesis.

#### 4.1.1 Typical Cycle – Phase One

A phase one cycle has been defined to start once the GBM has been disconnected from the pilot tube recently installed and the GBM has been retracted to its starting position. Throughout a phase one cycle five distinct operations may be seen, as depicted in the typical phase one cycle shown in Figure 4.1.

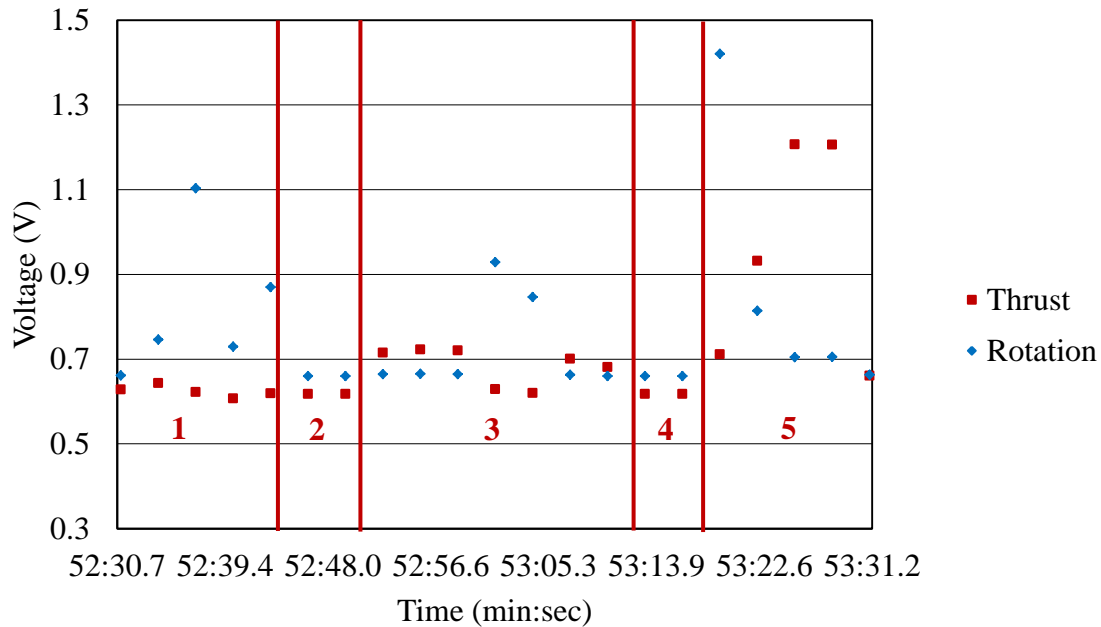


Figure 4.1 Typical Pilot Tube Installation Cycle

The majority of operation one includes hooking up a pilot tube to the previously installed tube and to the GBM. There is mainly only rotation during this operation. The rotation pulls the machine towards the borehole, so there shouldn't be any spikes in thrust voltages. There may be small deviations above the ambient thrust voltage observed in the beginning of this operation due to the operator moving the machine towards the incoming

pilot tube. Additionally, there may be a significant pause during this operation as the operator may be waiting for another crew member to bring in another pilot tube.

Operation two is relatively short and includes lowering the “make-up tool”, as termed by Akkerman (2013), to allow for installation of the recently hooked up pilot tube. The purpose of the make-up tool is to allow for tightening of pilot tubes prior to jacking operations and for separating the pilot tubes during pull-back operations. Figure A.2 shows the make-up tool and the slot on the pilot tube that allows for the make-up tool to grasp the pilot tube.

Jacking of the pilot tubes makes up the third operation in a phase one cycle. Rotation is infrequent during this operation, as rotation may be paused to correct alignment. In Figure 4.1, it may be seen that thrust decreased to the ambient level while rotation voltages increased. Rotation without thrust may have occurred to orient the bias on the lead pilot tube to steer the tubes back onto alignment upon further jacking.

Once the pilot tube has been pushed into the soil, operation four begins, in which the make-up tool is raised to grasp the slots on the installed pilot tube. Rotation may be observed as the tubes are rotated to align the pilot tube slots with the make-up tool.

Determining the task at hand during operation five proved rather difficult, as the high thrust force pressures may mislead one to believe that this operation dictates jacking of the pilot tubes. However, upon gaining familiarity with the thrust and rotational torque behavior of this operation in comparison to that of operation three, it became evident that expected trends in thrust forces occur in operation three, and not operation five. For example, in drive number two, thrust forces from operation three increased at the locations where high thrust pressures were described in the field notes, and fell upon

exiting those locations. On the contrary, high thrust values during operation five were relatively constant, except at a chainage of 125 feet, where they rose when second gear was initiated to ease jacking operations.

After much thought as to why thrust voltage output was higher during operation five than during operation three, where the pilot tube is being installed, it became evident that the high pressures in the thrust hydraulic lines were actually a result of the GBM rotating off of the installed pilot tube and retracting towards the starting position. The GBM uses rotational torque to disconnect from the pilot tube, and with the pilot tube location fixed in the make-up tool, the GBM is forced backwards creating high pressures in the jacking rams, even though the machine is not moving forwards. It is believed that these high pressures are maintained throughout retraction of the machine to its starting position. The instantaneous thrust voltage increase observed upon switching from first to second gear, provides support to the hypothesis that operation five includes disconnecting the pilot tube and retracting the GBM. Second gear supplies greater hydraulic pressure to thrust and rotational lines, as such the thrust voltage during this operation is likely to increase to a higher level, regardless of the location of the lead pilot tube and the soils of which it is advancing through.

#### **4.1.2 Typical Cycle – Phase Two**

The beginning of phase two typical installation cycles has been defined to start once the AA has traveled back to its starting position, farthest away from the borehole. A typical casing installation cycle may be seen in Figure 4.2. Casing cycle operations are in essence quite similar to that of the pilot tubes, although the operations have longer durations and exhibit different thrust voltage fluctuation behavior.



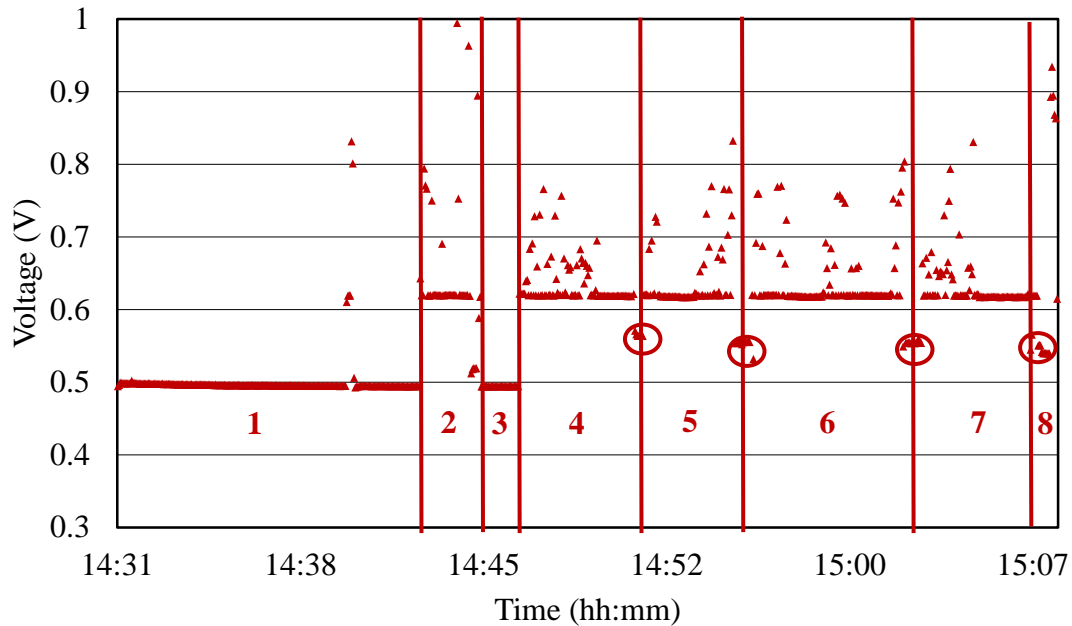


Figure 4.2 Typical Casing Installation Cycle

Operation one begins with cleaning up spoil returns around the borehole, adjacent to the AA tracks, and inside the barrel of the AA. Afterwards, the new casing is lowered onto the tracks to be prepped. To ready the casing for installation, the new auger flight is first fitted to the auger inside the previously installed casing. After that, the spigot end of the new casing is slid inside the bell of the casing previously installed, and pins are pushed into slots in the joint to secure the two casings together. This entire process takes some time and is the cause for the long duration of operation one.

Connecting the auger string to the rotational drive of the AA and sliding the casing into the AA barrel makes up operation two. High thrust voltage outputs may be observed if the AA is misaligned with the casing as it proceeds forward.

Operation three represents a short pause in which communication between the jacking shaft and reception shaft crew takes place to ensure all parties are ready to begin.

There may also be some readying or setup of equipment used to remove spoil material generated during excavation.

Jacking rams on the AA have a 35-inch stroke. Consequently, once the full stroke length has been reached, the rams have to be retracted back into their housing and reset before jacking may proceed. The reset process includes retracting the “dogs”, as termed by American Augers (2013), from the slots in the track with a hydraulic push bar cylinder, retracting the jacking rams back into their housing, and extending the dogs into slots in the track at a position 2.5-ft closer to the borehole. To completely push an 8-ft casing, three resets and four jacking periods are necessary. Each of the jacking periods corresponds to operations four through seven, as indicated in Figure 4.2. The reset sub-operations are circled in red. A full 35-inch stroke during the first and last push was not utilized due to the positioning of the casing at the start and end of operations four and seven, respectively.

The eighth operation begins once the casing has been completely advanced. The dogs are then retracted from the track and the AA is geared back to its starting position. When quick movement of the AA is desired and high thrust or pull power is not required, a “Quick Tran” rack and pinion system is used to gear the machine forwards and backwards at a fast rate. This system allows for increased productivity as it eliminates the need to move the machine through action of its jacking rams and resetting of the dogs. The system is independent of the thrust hydraulics and therefore its use does not directly cause fluctuations of the thrust voltage recorded by the Data Dolphin data logger. However, as the machine is retracted pressure in the thrust cylinders increases, akin to the behavior observed in phase one operation five.

### 4.1.3 Typical Cycle – Phase Three

Phase three installation cycles are defined to start once a VCP has just been installed and the machine is in its most forward position (closest to the borehole). A typical cycle depicting installation of a VCP can be seen in Figure 4.3.

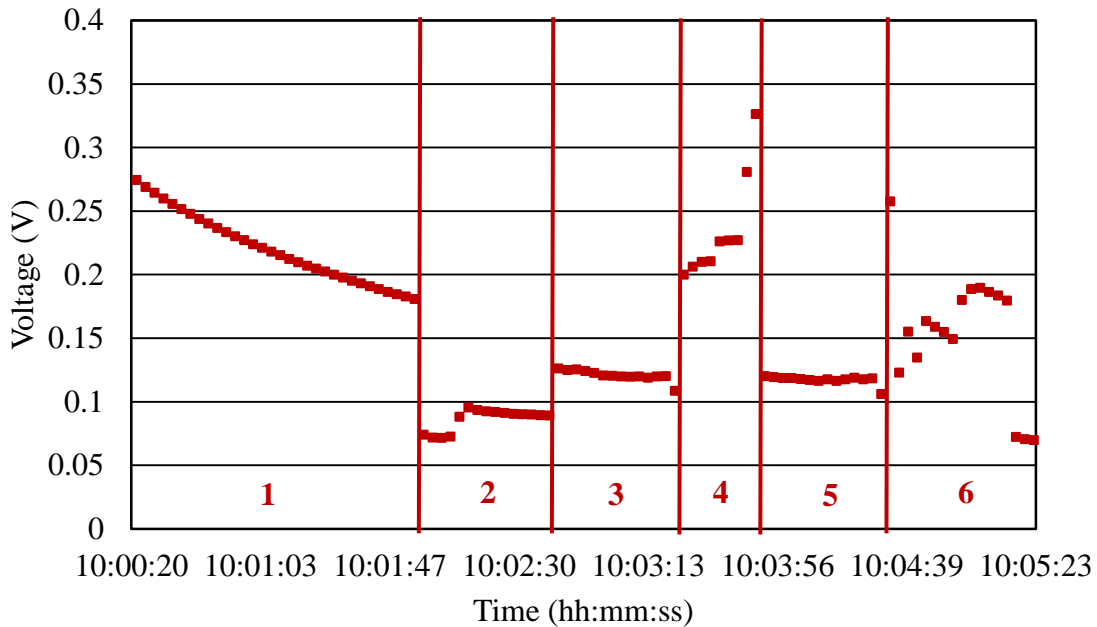


Figure 4.3 Typical VCP Installation Cycle

Phase one begins with retracting the hydraulic jacking rams inside their housing while simultaneously retracting the BM Pusher to its starting position with a battery powered winch. It is believed that there are high pressures in the hydraulic rams due to the combination of pressure left over from jacking the previous VCP and the resistance generated from winching the machine back to its starting position. This pressure gradually drains as the rams retract.

Operation two represents a pause in all tasks. The BM Pusher is turned off as the operator waits for the new VCP to be lowered into the jacking shaft.

The third operation consists of readying the next VCP for installation. Small fluctuations in thrust voltage output may be seen during this operation as the BM Pusher is moved back and forth by small amounts. Occasionally, the duration of this operation may be extended while the crew in the reception shaft works on disassembling and removing the casing. Disassembling casings is the critical task for phase three operations and requires an experienced crew to perform these tasks in an efficient manner.

As with phase two operations, the entire 8-ft pipe section cannot be installed without resetting the hydraulic rams. The rams for the BM Pusher have a 4-ft extension and thus require two separate pushes to complete installation of a VCP section. Operations four and six indicate pushing the first and last four feet of the VCP, respectively. The fifth operation includes retracting the dogs out of the track, retracting the hydraulic rams back inside the housing, and extending the dogs back into the track to complete the remainder of the installation.

#### **4.2 Installation Productivity**

In 2011, Arizona State University surveyed 22 North American PTMT contractors to evaluate the industry state of practice with regard to PTMT (Gottipati 2011). The survey asked respondents about their company profile, completed PTMT project information, and PTMT planning and risks. Figure 4.4 presents the results from the survey regarding factors affecting productivity. Productivity factors are listed on the vertical axis and the percentage of contractors of whom identified the factor as having an impact on PTMT productivity on the horizontal axis. It was found that ground conditions affect productivity rates to the greatest extent, where installation depth was not as critical. Ground conditions may make or break a project's productivity. If unforeseen ground

conditions occur, there may be difficulties with advancing the installation, stabilizing the borehole, or maintaining accurate line and grade.

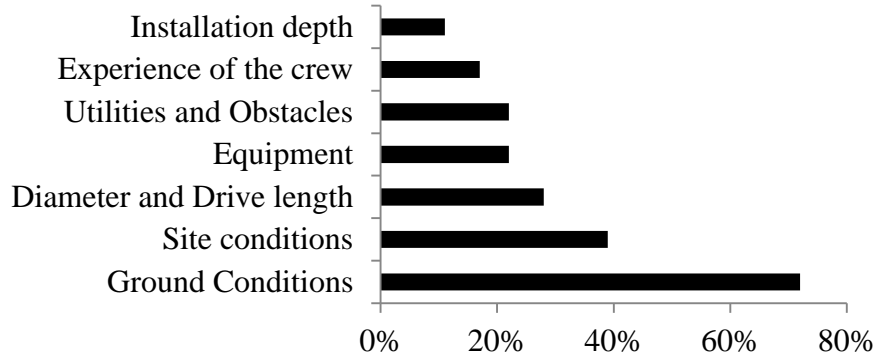


Figure 4.4 Ranking of Factors Affecting PTMT Productivity (Gottipati 2011)

The soils report for the Reid Drive Interceptor Project does not indicate highly variable soil strata to allow for proper evaluation of ground conditions on PTMT productivity, although, there were isolated sections where difficult soil conditions caused high machine pressures, as documented in the field notes. Thus, a basis for evaluation the effect of ground conditions on PTMT productivity is possible. Additionally, the effect of the other factors listed in Figure 4.4 was evaluated when the impact of the factor could be isolated from other productivity stressors. Before a just assessment of factors affecting PTMT productivity may be made, expected productivity rates and characteristics for each PTMT phase should be identified. By analyzing the trends in cycle duration frequency bar graphs and cumulative installed distance versus time graphs, insight towards the factors affecting productivity and their influence on PTMT productivity may be gained (Olson and Lueke 2013).

### 4.2.1 Phase One Productivity

Figure 4.5 represents the frequency of which the duration of all monitored pilot tube installation cycles from the three step PTMT method, drives one through five, fall into. All in all, there were 605 pilot tube cycles included in this analysis. It can be seen that cycle duration frequency is represented by an exponential distribution about the most common cycle duration bin with a more gradual decrease in occurrence frequency for the longer cycles. There were seven “fast” cycles with durations lower than 40 seconds. The infrequency of these fast cycles is due to there being a minimum amount of time required to install a pilot tube given that crew efficiency is at its maximum and installation proceeds as fast as possible. This minimum installation time is estimated to be near 40 seconds. The seven cycles installed in less than 40 seconds may be a result of odd, or difficult to interpret, thrust voltage patterns misleading the analyst into classifying a short cycle time. Thus, it is unlikely that pilot tube cycles on the Reid Drive Interceptor were quicker than 40 seconds.

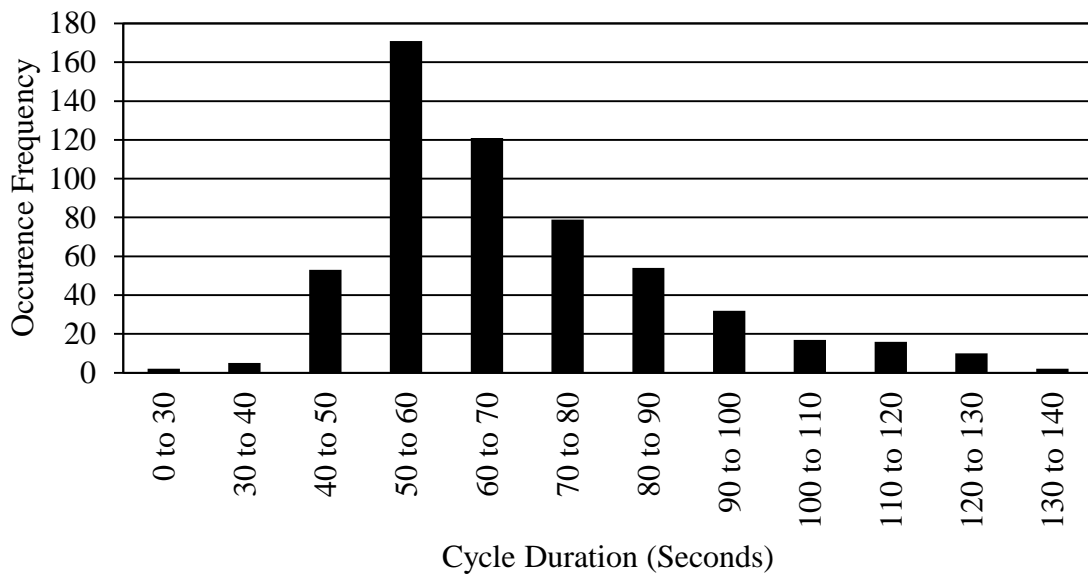


Figure 4.5 Pilot Tube Installation Cycle Duration Frequencies

Cycle duration frequencies taper in an exponential fashion from the most common duration, between 50 and 60 seconds, to longer cycles of 100 to 110 seconds. The exponential decrease in occurrence frequency is the result of more common and shorter delays, such as a laborer falling behind in his or her tasks, occurring more commonly than longer less frequent delays, such as experiencing problems with the bentonite pump. A minor delay may increase cycle time by less than 20 seconds, whereas a more substantial delay could result in cycle time increases of several minutes.

The average cycle duration was 80 seconds, but this included outlying cycles where delay caused excessive increase in cycle time. Consequently, cycles exceeding the mean plus one standard deviation, 140 seconds, have been omitted from Figure 4.5 to more accurately display cycle durations expected to occur in the field. Furthermore, these long cycle durations do not represent the true cyclical pattern of a pilot tube installation, as there was most likely a production delay caused by the need of a tool located elsewhere on the jobsite or equipment malfunction. A more adequate representation of the expected cycle time for a pilot tube installation is the median value, which was 66 seconds.

Figure 4.6 illustrates the cumulative lineal distance installed for pilot tubes from drives one through five as a function of elapsed time. Average installation rates for drives one through five are 106, 98, 139, 89, and 106 feet per hour, respectively. The average installation rate of based on the total drive footage per cumulative time to complete the drives was 102 feet per hour. This installation rate includes stoppages due to delays. If a crew were able to reduce the amount of delays occurring throughout a drive and install pilot tubes with an average cycle time equal to the median cycle time of 66 seconds, the

installation rate would increase from 102 to 136 feet per hour. This illustrates how production may be increased by 33% if construction delays are reduced to a negligible amount where there occurrence is either infrequent or the length of delay is short. Of course, a production increase of this magnitude is difficult, due to the low probability of all construction processes being completed at maximum efficiency and with zero complications. However, as the high installation rate of the third drive illustrates, production without significant delays is possible if adequate planning and preparation are completed and soil conditions, machinery operation, and other external factors go in the contractors favor.

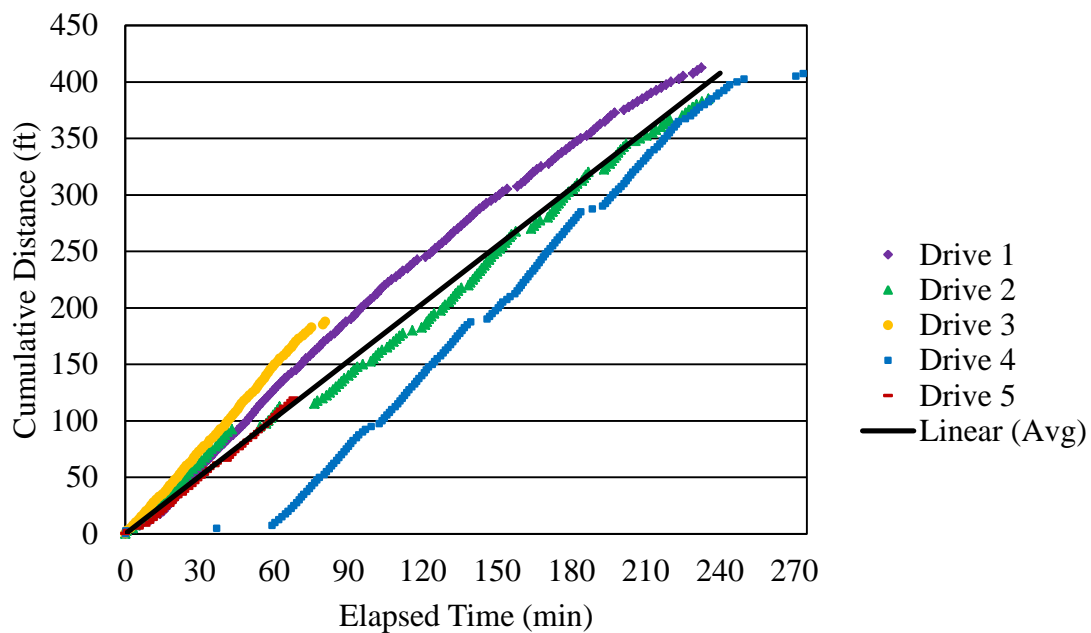


Figure 4.6 Cumulative Pilot Tube Installation Distance vs Time

From Figure 4.6 it can be seen that there was considerable delay at the beginning of the fourth drive. This may have been due to the crew retracting their rods to advance at a slightly different alignment to avoid an obstruction, or to common construction workflow delays. Delays may also be seen in drive number two between the 50 and 75



minute mark. An additional productivity trend to point out is that towards the end of each drive, the installation rate tends to decrease. This is most likely a result of the GBM operator pausing to establish communication with another crew member at the receiving pit, who is observing to see when the pilot tube protrudes into the reception shaft.

It should also be noted that there was delay on drive two when the lead pilot tube was proceeding through difficult ground conditions as noted by the field notes and seen in the high voltage outputs. The difficult ground conditions were encountered from about 30 to 90 minutes into the drive. During this period the average installation rate was 79 feet per hour. This is 19% less than the average installation rate of this drive. Although difficult to see in detail, the decreased installation rate throughout this hour is evident in Figure 4.6. In fact, the decreased installation rate throughout the difficult soil is solely a result of two cycles of which the durations were 11 and 14 minutes. The cause of the two longer cycles was not documented in the field notes, although a possible cause may be due to the operator applying lubricant without advancing the pilot tubes in an attempt to stabilize the borehole and decrease soil-pipe interface friction. Other cycles during this time period exhibited expected durations.

Another factor identified by Gottipati's survey (2011) to have an influence on productivity was drive length. Although there may be some learning effects that increase a crew's efficiency as a drive progresses, workers may tend to become fatigued towards the end of an installation, especially if they are understaffed. Additionally, increases in jacking resistance due to greater pilot tube-soil interface surface area may result in slower jacking of pilot tubes. This behavior is illustrated by the chainage versus elapsed time behavior for drive number one. Around 100 minutes into the drive the installation rate

begins to taper slowly for the remainder of the drive. It can be seen that there was not an increase in outlying or delayed cycles, but that there was merely a lengthening in the operations within the cycles. Towards the end of drives one through four it can be seen that installation rates reduced even further. This is mainly a result of increased communication between those in the jacking shaft and the reception shaft.

#### **4.2.2 Phase Two Productivity**

Casing cycle durations are much longer than those of the pilot tubes, as more time is required to excavate the borehole, clean up spoil from the reception shaft, and hook up subsequent casings for installation. Figure 4.7 shows the cycle duration frequencies of the 21-inch nominal ID 8-ft long casings from a total of 176 observations, which were completed in drives one through four. The frequency distribution is similar to that of the pilot tube cycle durations, although, the casing cycle durations exhibit slightly less variance and do not contain as many longer duration cycles. However, there is still a tendency for more long duration cycles than short duration cycles due to construction workflow delays. Also akin to the pilot tube cycles, it is unlikely that the three cycles categorized in the less than 20 minute duration bin actually were less than 20 minutes. Most likely there were irregularities in the voltage output behavior that mislead the analyst into categorizing the cycle length as less than 20 minutes. Consequently, the minimum cycle duration expected for a 21-inch nominal ID casing is between 20 and 25 minutes. Additionally, common construction workflow delays are expected to increase cycle durations from the common 25 to 30 minute range by at most 30 minutes. As the length of the delay becomes longer, the likelihood of such a delay occurring is decreased,

as illustrated by the exponential reduction in occurrence frequencies from 30 minutes onwards.

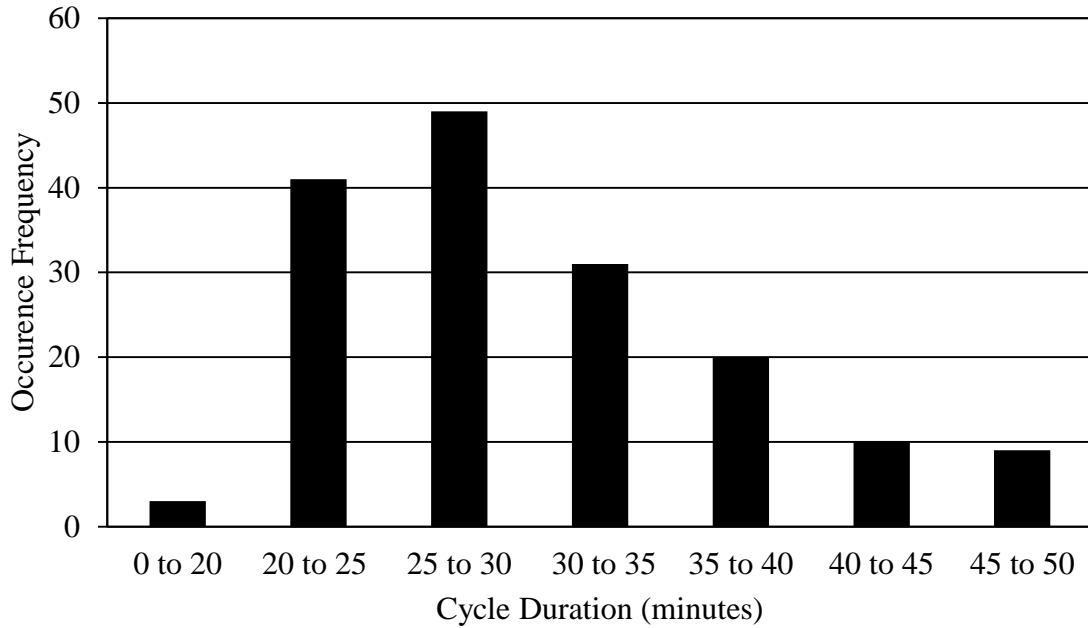


Figure 4.7 21-Inch Nominal ID Casing Installation Cycle Duration Frequencies

The average cycle duration was 33 minutes, but as with the pilot tube cycles, this included outlying cycles with excessive increase in cycle time due to delay. Resultantly, cycles with durations exceeding the bin containing the mean plus one standard deviation, 45.6 minutes, have been omitted from Figure 4.7. A more adequate representation of the expected cycle time for a 21-inch nominal ID casing installation than the average value is the median value, which was 29 minutes.

Data from drive number five included cycle behavior for 8-inch nominal ID 3.49-ft casings. A comparison between productivity of the larger diameter 8-ft casings and the smaller diameter 3.5-ft casings proves to be quite interesting, as it provides an understanding of how casing diameter and length effect productivity. Shorter casings require more casing sections to complete an installation of the same length. Accordingly,

there will be more instances where installation ceases to allow for crew members to ready the next pipe for installation. However, due to the decreased weight of the smaller casing crews can handle the casing with greater ability and less dependency on the crane operator and signal man as it is lowered into place, increasing the speed and efficiency of readying each casing for installation.

Figure 4.8 shows the cycle duration frequencies for installation of the 8-inch nominal ID 3.5-ft casings. The average cycle duration was 14.75 minutes, although this included three cycles outside the mean plus one standard deviation (24.5 minutes). Outliers were observed on the 13<sup>th</sup>, 36<sup>th</sup>, and 37<sup>th</sup> cycle and had durations of 53, 41, and 36 minutes, respectively. Field notes indicate that just after the 12<sup>th</sup> installation cycle, the muck cart, used to catch and remove spoil returns from the borehole, was struck by the GBM as it moved forward and was bent to the extent where it no longer fit in its position. Repair of the muck cart was necessary before installations could proceed, hence causing the long 53 minute 13<sup>th</sup> cycle. The 36<sup>th</sup> and 37<sup>th</sup> cycles were the last casings installed in the drive. It is believed that installation rates slowed as the lead casing approached the reception shaft, as communication between the reception shaft and jacking shaft crews increased. Upon taking an average of the cycle durations in the absence of these three outliers, the average was 12.2 minutes. This is fairly similar to the median cycle time including all cycles of 12.6 minutes. Although it is clear that most cycles were between 7.5 and 15 minutes, collection and analysis of additional data is recommended, since only one drive consisting of 37 cycles was available for analysis. Thus, a conservative cycle duration estimate may be warranted. Based on the results shown in Figure 4.8, a good

conservative cycle duration estimate for the 8-inch nominal ID 3.5-foot casings would be 12.5 to 15 minutes.

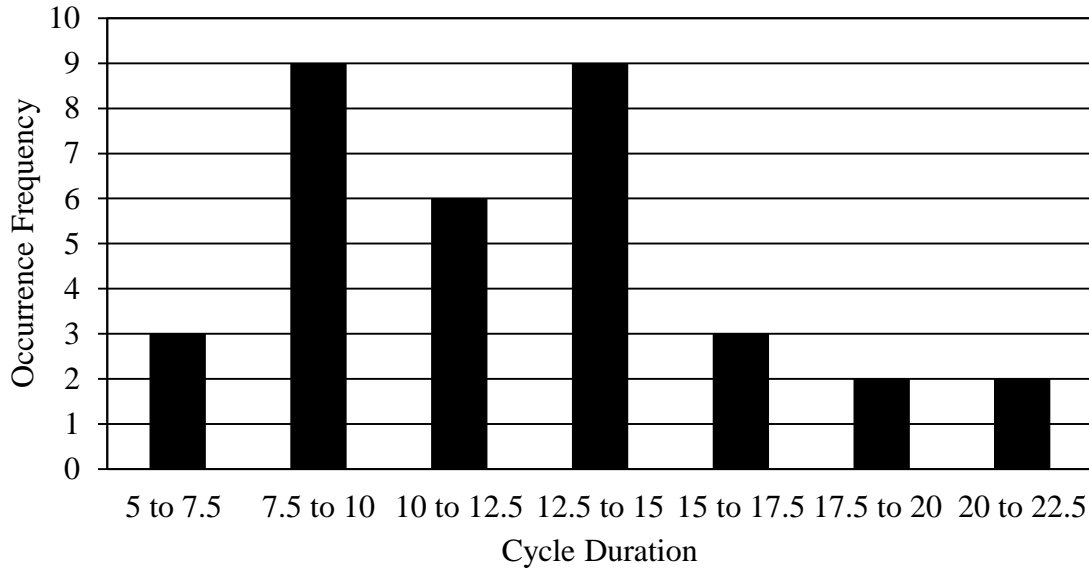


Figure 4.8 8-Inch Nominal ID Casing Installation Cycle Duration Frequencies

Figure 4.9 illustrates the cumulative linear distance installed for 21-inch and 8-inch nominal ID casings from drives one through five as a function of elapsed time. Average installation rates for the 21-inch casings of drives one through four are 13.5, 14.4, 13.6, and 16.9 feet per hour, respectively. The average installation rate based on the total drive footage per cumulative time to complete the 21-inch drives was 14.6 feet per hour. The 8-inch casing drive was installed at an average rate of 13.3 feet per hour. These installation rates include stoppages due to delays. As in the pilot tube installations, if a crew were able to reduce the amount of delays occurring throughout a drive and install 21-inch and 8-inch casings with average cycle times equal to median cycle times, 29.2 and 12.4 minutes, the installation rates would increase from 14.6 and 13.3 to 16.5 and 15.6 feet per hour, respectively. This illustrates how production may be increased by 13% and 17% for the 21-inch and 8-inch casings, respectively, if construction delays are

reduced to a negligible amount. It is not unreasonable for the median installation rates to be obtained on future installations, as drive number four exceeds the respective median rate.

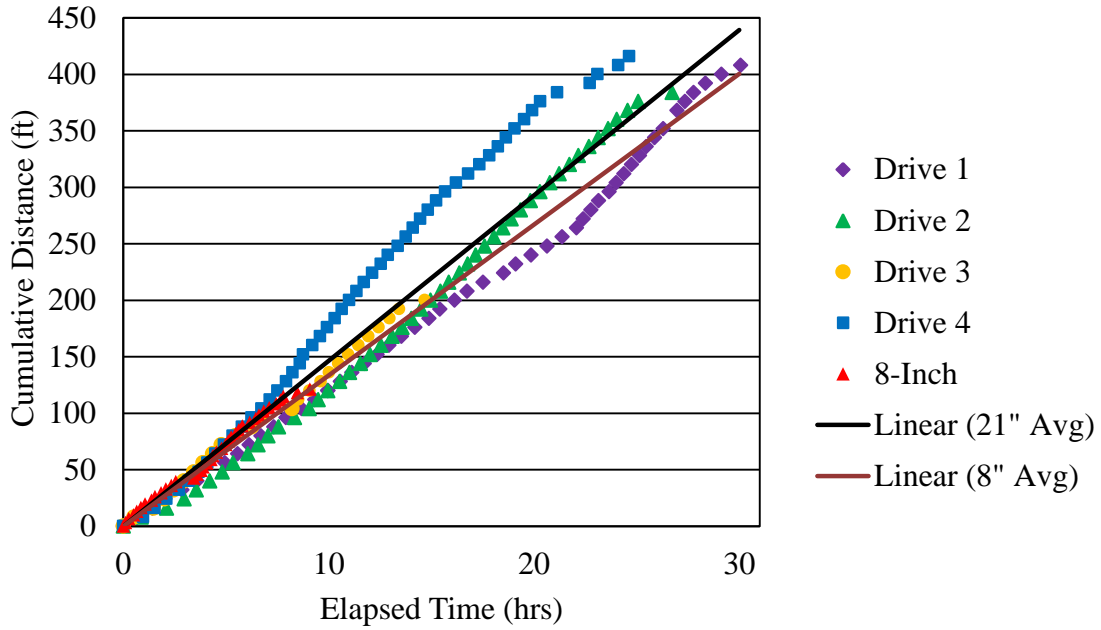


Figure 4.9 Cumulative Casing Installation Distance vs Time

#### 4.2.3 Phase Three Productivity

Product VCP installation cycle durations were between that of the pilot tubes and steel casings. The average cycle times for 21-inch and 8-inch nominal ID VCP installations were 7.5 and 3.9 minutes, respectively. An interesting aspect of the cycle duration frequency for the 21-inch VCP is that there was significant reduction in cycle times from drive numbers one to two. The average cycle times for drives one and two were 8.8 minutes and 6.3 minutes, respectively. A factor likely to contribute to the reduced cycle times from drives one to two may be efficiency gains of the crew in the reception shaft. During the second drive, completed ten days after the first, the reception shaft crew developed more efficient techniques for separating the casings once they were

fully jacked into the shaft. Casing removal is difficult, as it often takes significant prying with pry bars in the correct places to dislodge one casing from the next. Additionally, once the casings have been separated, the lead casing must be held back while the augers are disconnected. With these difficult tasks and the limited working room in the reception shafts, a significant amount of the time necessary to remove a casing depends on the techniques adopted by the crew. Figure 4.10 illustrates the cycle duration differences between the first and second drives of 21-inch VCP. It also shows how the 8-inch VCP cycles are much quicker than those of the 21-inch VCP. As described in sections 4.2.1 and 4.2.2, it should be feasible for the contractor to obtain cycle durations equal the median duration, if delays are minimized. Median cycle times for the 21-inch and 8-inch VCP installations are 6.8 and 3.0 minutes, respectively. During the second drive, the contractor was able to minimize delays and actually obtained an average cycle duration of 6.3 minutes, 30 seconds faster than the median from drives one and two.

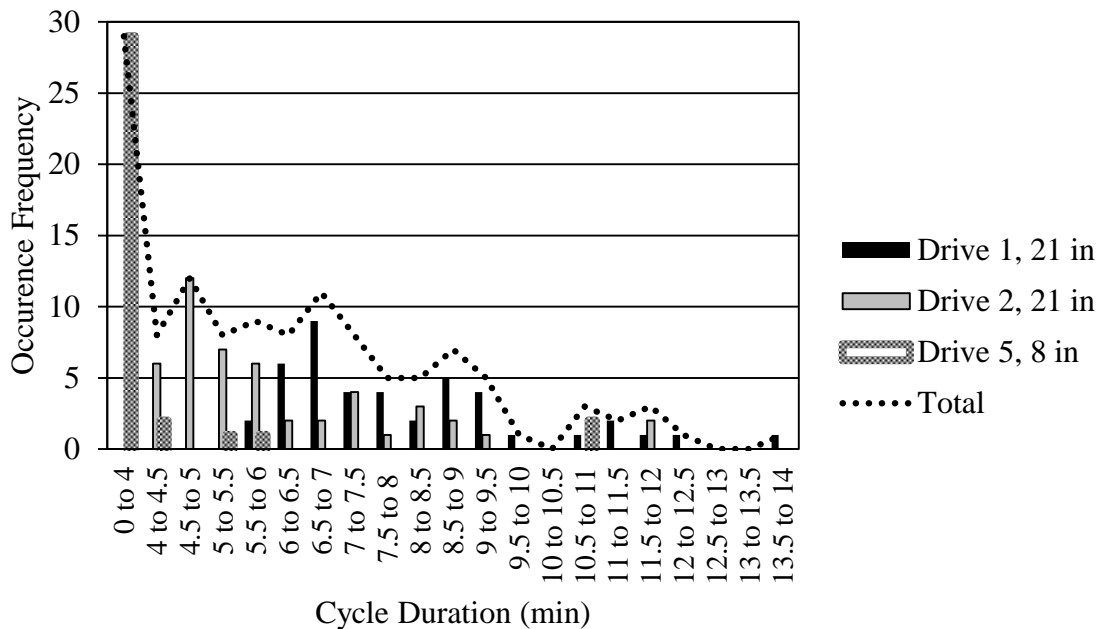


Figure 4.10 VCP Installation Cycle Duration Frequencies

Figure 4.11 illustrates the cumulative lineal distance installed for 21-inch and 8-inch nominal ID VCP from drives one, two, and five as a function of elapsed time. As described in Chapter 3 and Appendix D, monitoring of drives three and four was unsuccessful and are therefore not included in Figure 4.11. Average installation rates for the 21-inch VCPs of drives one and two are 54 and 75 feet per hour, respectively. The average installation rate of based on the total drive footage per cumulative time to complete the 21-inch drives was 63 feet per hour. The 8-inch VCP drive was installed at an average rate of 51 feet per hour. As in the pilot tube and casing installations, if a crew were able to reduce the amount of delays occurring throughout a drive and install 21-inch and 8-inch VCPs with average cycle times equal to median cycle times, 6.8 and 3.0 minutes, the installation rates would increase from 63 and 51 to 71 and 67 feet per hour, respectively. This illustrates how production may be increased by 13% and 31% for the 21-inch and 8-inch VCPs, respectively, if construction delays are reduced to a negligible amount. As with the casing installations, it is not unreasonable for the median installation rates to be reached, as drive number two exceeds the respective median rate by 4 feet per hour.



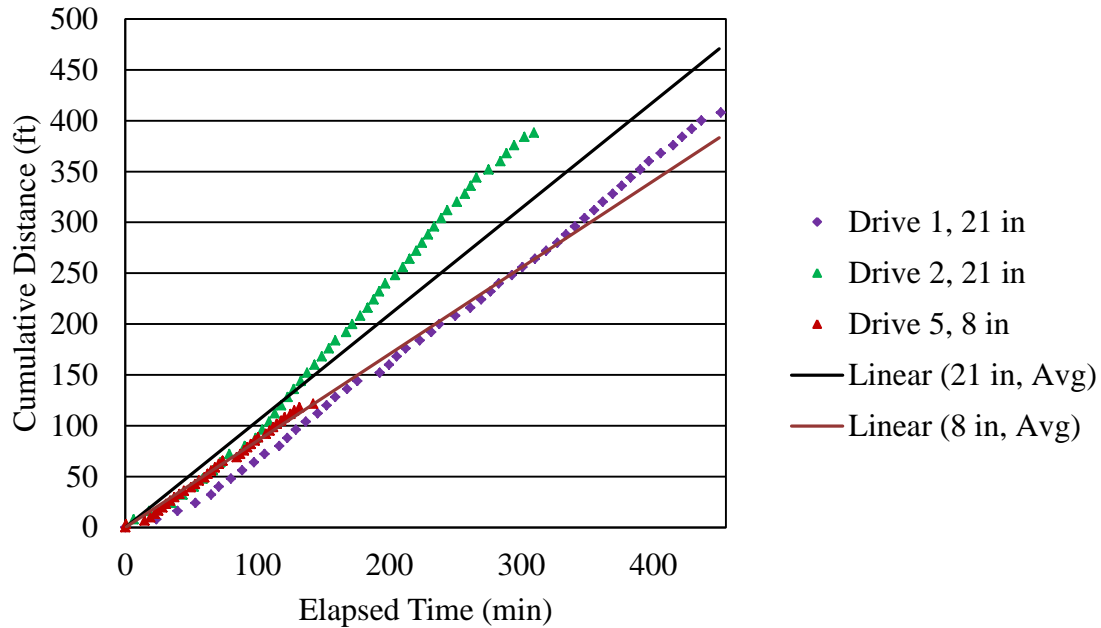


Figure 4.11 Cumulative VCP Installation Distance vs Time

### 4.3 Automatic Pattern Recognition

Manually picking through recorded data from numerous PTMT installations can be cumbersome and time consuming, even for an experienced engineer who understands what the data should look like. Furthermore, the monotony of sifting through thousands of cells of data can lead to human errors which may affect conclusions about the data's behavior. In this study, the Data Dolphin data logger was programmed to record voltage from the three pressure transducers once every three seconds. A sampling rate of this frequency results in 28,800 recorded data points, 9600 from each transducer, during an eight hour period, which is actually less than what is typically recorded during a work day as it is not uncommon for PTMT crews to work ten to twelve hour shifts. The benefit of organizing and interpreting recorded data through manual methods for use in productivity or jacking force analysis may not be worth the cost, especially if the data is to be used for proactive control of construction processes. Thus, an automated data

collection and interpretation approach can be advantageous towards providing a decreased cost to benefit ratio with quicker results. The following sections outline how an automated pattern recognition method can be used to automatically classify time series data into patterns of hydraulic pressure to detect installation cycles from all three phases of the PTMT methodology.

#### **4.3.1 Methodology**

Automated pattern recognition of time series data recorded with data loggers may be accomplished in two stages, through the use of an Artificial Neural Network (ANN) algorithm and an anomaly detection algorithm. To begin with, the pressure transducer/s responsible for recording thrust or torque hydraulics from each PTMT phase is/are identified. This is accomplished by using a “sliding window” algorithm that scans through the entire time series data set to train the algorithm and then utilizing a Back Propagation Artificial Neural Network (BP ANN) algorithm to classify which pressure transducers correspond to which phase of the PTMT methodology based on the training. Once this has been accomplished, an anomaly detection algorithm is used to further dissect the time series data and detect PTMT installation cycles and the operations within those cycles.

The first step towards using the sliding window algorithm to train the BP ANN is to define the window width and the amount of which the window is moved as it slides through the time series. Wider widths are desirable for detecting data trends on a more macro level, although a wider trend may fail to identify trends on a micro level. Consequently, the widest window was used to identify phase two, and the shortest window was used to identify phase one. The amount of the sliding step controls how

much of the data overlaps subsequent windows. Methodology for choosing the length of the sliding step is akin to that of the window width, in that longer steps are to be used in data with patterns of longer duration.

Once the window width and sliding step have been determined, the algorithm is used to calculate the median, lower quartile, upper quartile, and variance of the voltage outputs from each pressure transducer during each PTMT phase. The result is a twelve dimensional matrix that can be input into the BP ANN algorithm to predict which phase a time series sample, from a pressure transducer, represents. The BP ANN algorithm recognizes that if the variance of a given transducer's time series is small (e.g. 0.0008 volts) then the transducer was not in use for the phase of which this occurred. From this recognition, the BP ANN algorithm can predict which PTMT phase is represented by a given time series sample. To check to see if the BP ANN algorithm is running correctly, a certain proportion of the sample data needs to be reserved to test the results. Training of the BP ANN algorithm, however, requires a more abundant supply of data. Thus, 90% of the sample data was used for training purposes, and the remaining 10% was reserved for testing.

The anomaly detection algorithm is used to analyze the time series data in greater detail and in tighter time windows. Essentially, this algorithm scans the time series and looks for discontinuities in the data, or "anomalies". Based on the location of anomalies, the algorithm partitions the time series into numerous cycles, which in this case represent the installation cycles present within the PTMT phase. In this study, use of the anomaly detection algorithm was demonstrated using time series data from phase three.

Boundary conditions may be input into the anomaly detection algorithm, such as the cycle must be longer than four minutes, for more robust detection results. Figure 4.12 depicts four plots in which the entire time series, an installation cycle of typical duration, and two longer duration installation cycles for the third PTMT phase are shown. The difference between the longer and shorter cycles is usually in the duration of the pausing period, classified as operation two in Figure 4.3. There are slight differences in the durations of pushing operations, operations four and six; however, these variances are less than that of operation two, as difficult ground conditions do not decrease productivity to as great of an extent as difficulties in disassembling casing in the reception shaft.

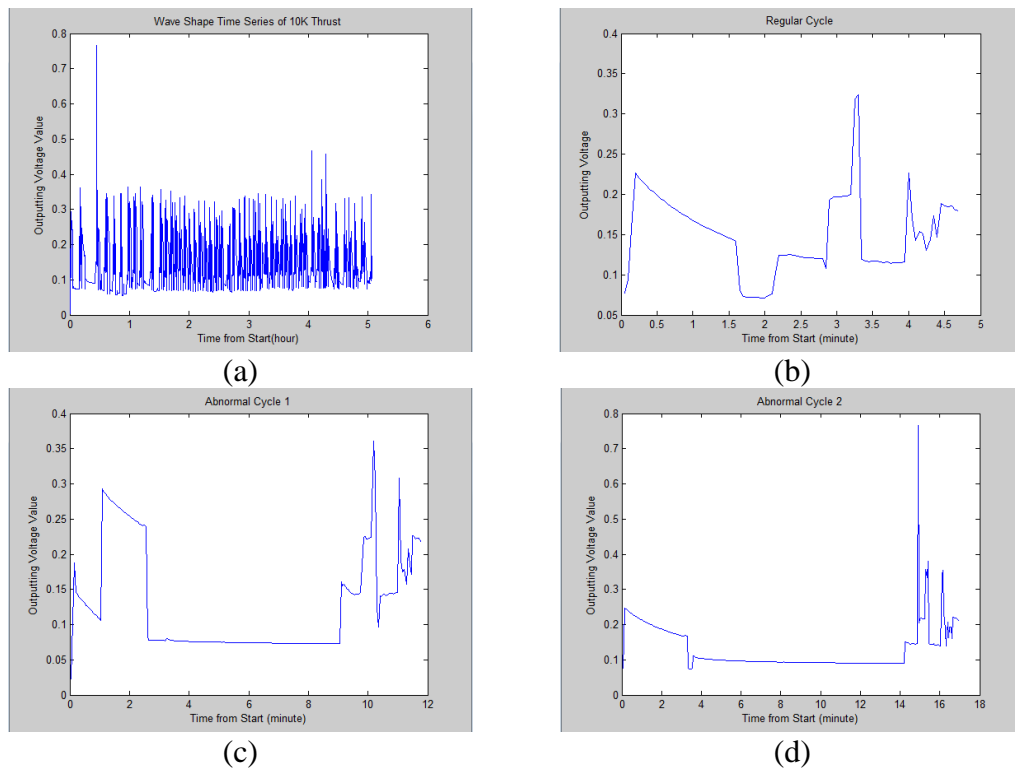


Figure 4.12 Time Series Data for Phase Three: a) Entire Time Series, b) Typical Installation Cycle, c) and d) Installation Cycles with Long Durations (Tang et al. 2013)

Varying durations of the operations within the installation cycles makes it harder for the anomaly detection algorithm to partition the time series from cycle to cycle. To

assist the algorithm with the anomaly detection, certain operations were grouped together based on the characterization of their purpose. Operation one was singled out as the “retraction” operation. The second operation also stood alone, but as the “pause” operation. Operations three through six included hooking up the pipe and pushing the first and last half of the VCP, including a period of hydraulic ram resetting in between pushes. These operations were grouped together and classified as “pushing” operations.

The anomaly detection algorithm was used for two purposes: first, to identify the phase three installation cycles within the time series, and second, to recognize the distinct operations within those installation cycles. In partitioning the time series into installation cycles, the algorithm looks for sequences of low voltage values, on the order of 0.00 to 0.008 volts. The end of these low voltage sequences are likely to be the beginning of an installation cycle. An engineer checks that the first discontinuity is indeed representative of the start of an installation cycle, the algorithm is run to check that the following low voltage sequences due in fact represent installation cycles using the boundary condition of cycle durations being longer than four minutes. When the algorithm is used to detect the operations within the installation cycles, it searches for discontinuities in a cycle’s time series where voltage values smaller than 0.12 volts jump to values larger than 0.15 volts, and visa-versa. These voltage jumps likely occur due to a switch in workflow operation between pushing, retracting, or pausing. Once the operational discontinuities are aligned with the cycle start and end discontinuities, the work flow operations may be identified and isolated from the time series data.

### 4.3.2 Results

During monitoring of the PTMT construction on the Reid Drive Interceptor Project, the day that a phase of a PTMT installation was completed was always documented. Since the phase was known, the BP ANN algorithm was used to identify which transducer was responsible for collecting data pertaining to the machine in use during any particular phase. The algorithm proved to be successful in this endeavor, with the exception of the L1 transducer.

Figure 4.13 illustrates the voltage time series data from each transducer during all three phases of the PTMT process from drive number two. It can be seen that transducer L2 is only utilized during phase one and that transducer L3 is used in phases one and two, as what was to be expected from field note documentation. L2 was responsible for thrust hydraulic monitoring during GBM operations and L3 was allocated for monitoring rotational torque hydraulics of the GBM and thrust hydraulics for the AA. Although field notes indicate that the only transducer used to monitor hydraulics in phase two was the L3 transducer and that the L1 transducer was only used for phase three monitoring, the L1 transducer was outputting active, or non-ambient, voltage values to the data logger during phase two. Reasons for the voltage output from the L1 transducer during phase two are uncertain, but complications with the L1 transducer arose as the project progressed. Whatever caused the “ghost” outputs from the L1 transducer during phase two of drive number two may have also been the reason for the complications experienced by the transducer during subsequent drives (as outlined in Appendix D).

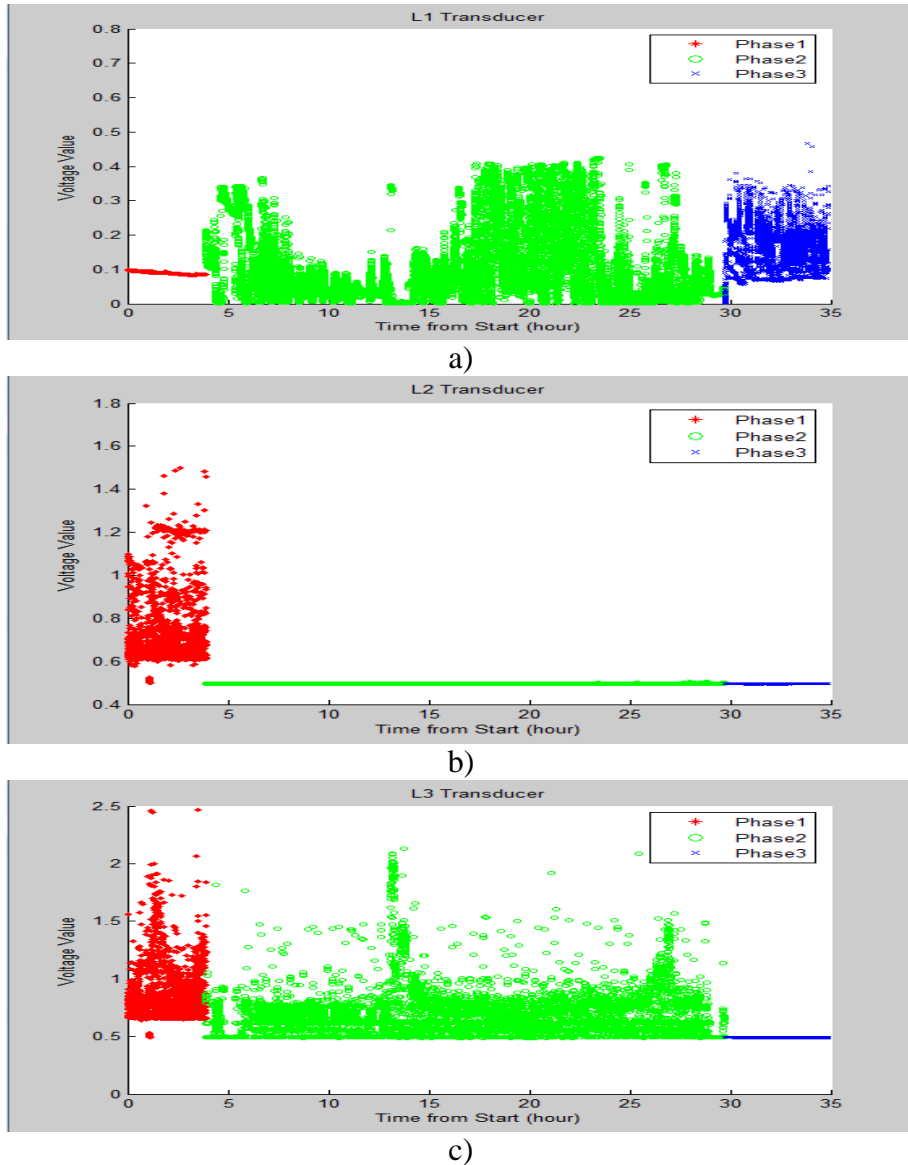


Figure 4.13 Scatter Plot of Voltage Time Series Data from All Transducers from Each PTMT Phase: a) L1, b) L2, and c) L3 Transducers (Tang et al. 2013)

The anomaly detection algorithm also proved to be successful and yield useful characteristics of the time series data. Phase three installation cycles were identified for the time series pertaining to drive number two. Manual interpretation of this drive concluded that there were 49 VCP installation cycles. The anomaly detection algorithm detected 48 discontinuities that exactly matched the predefined cycle borders. The

remaining cycle may have been missed due to the first cycle of phase three not exhibiting a retraction operation. Consequently, it is recommended to define cycles to start upon the beginning of pushing operations. Results from the algorithm can show the detected cycles and their durations (Figure 4.14), as well as statistical data such as the average minutes per cycle and degree of variance. These productivity characteristics provide contractors and engineers with the tools to identify periods of slow productivity, such as the beginning of this phase three installation, which may be attributed to needing unforeseen equipment or tools that are located elsewhere on the jobsite.

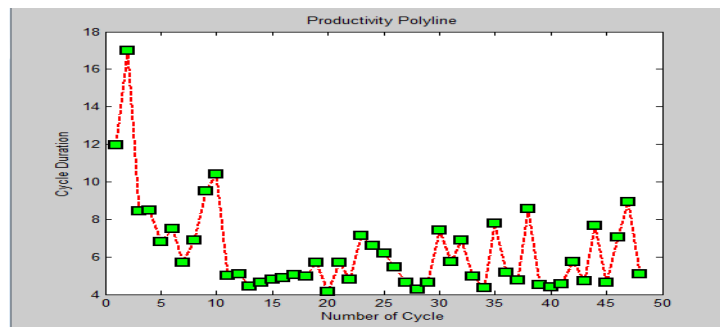


Figure 4.14 Detected Cycles and their Duration (Tang et al. 2013)

From the dissection of installation cycles and the identification of the workflow operations within, statistical behavior regarding the duration of each operation and the voltage outputs during each operation may be developed. This can allow contractors to determine why certain cycles are longer than others. Table 4.1 shows productivity results that may be obtained through the use of the operational anomaly detection algorithm. From here, it may be seen that the greatest influence to total cycle duration is the duration of the pausing period, which is greatly affected by the efficiency of the reception shaft crew in disassembling the casings. All in all, the operational portion of the anomaly



detection algorithm was able to detect all three operations (i.e. retraction, pausing, and pushing) in 81% of the detected cycles.

Table 4.1 Cycle Duration Contributing Factors (modified from Tang et al. 2013)

Cycle	Duration (minutes)			
#	Retraction	Pausing	Pushing	Total
1	2.7	6.5	2.8	12.0
2	3.3	10.9	2.9	17.0
12	0.1	2.1	2.9	5.1
19	2.2	1.7	1.8	5.7

### 4.3.3 Advantages and Limitations

Results from this analysis indicate that pattern recognition need not be completed manually, but that automatic pattern classification and anomaly detection algorithms may be used to assist engineers in organizing, classifying, and interpreting time series data from monitored PTMT installations. This significantly reduces the cost to benefit ratio of monitoring trenchless installations and analyzing the recorded data for productivity, quality control, and research purposes. Valuable information pertaining to productivity may be gained, such as statistical facets of cycle and operational durations, which may be utilized in concluding upon critical construction workflow tasks. This facet, if appropriately applied, will increase construction productivity through increased efficiency while decreasing costs associated with faster project completion and decreased use of operational resources.

The BP ANN achieved 95% accuracy in detecting the three PTMT phases. With this degree of accuracy, field notes may not be required to document which transducer is connected to which machine for which phase of the PTMT methodology. The anomaly detection algorithm was also successful. It can be used to partition time series data into

installation cycles, and further, into workflow operations within the cycles. Although, all operations may not be detected in each installation cycle due to atypical installation sequences that may occur throughout an installation, 81% of the operations were detected and allow for a sound evaluation of the impact each operation has on overall installation productivity.

Additional research on, and refinement of, the input parameters necessary to run the algorithms is warranted to further increase the quality and widespread usability of BP ANN and anomaly detection algorithms for PTMT installation data analysis. This research may include exploring window widths and sliding steps used to train the BP ANN algorithm and methods for determining threshold input values used in the anomaly detection process of discontinuities in time series data. The use of the algorithm process for interpreting time series data, at this point, still requires the expertise of an experienced engineer to specify input parameters and interpret the results. Being able to create a well-developed software package that automates input and output parameters based on a user's preferences would be the end goal. This software package may be able to take in information such as soil type, pipe diameter, and other contextual conditions and estimate PTMT productivity accordingly.

#### **4.4 Summary**

This chapter outlines how instrumentation and monitoring of PTMT jacking frames may be used to perform productivity analysis of the construction operations inherent to each PTMT phase and the cyclic operations fundamental to the installation of each pipe section. Productivity analysis may be used to increase PTMT efficiency and decrease operational costs. Analysis may be performed through manual or automatic

interpretation of the time series data. Essential to properly utilizing both techniques, is the understanding of the behavior within typical pipe section installation from each PTMT phase. With this knowledge, productivity characteristics such as installed distance versus time and the average duration to install a pipe section may be obtained. Factors affecting productivity may be quantified and comparison of how these factors affect operations within the installation of a pipe section may be explored.

## **CHAPTER 5: COMPARISON OF EMPIRICAL MODELS TO CASE STUDY**

Understanding the thrust forces involved with jacking operations is critical towards being able to properly size and select the product pipe, design the thrust reaction wall in the jacking shaft, design or select efficient jacking frames and jacks, and to select and place intermediate jacking stations (Bennett 1998). These same design aspects are also fundamental to the PTMT process, which involves jacking of pilot tubes, casing, and product pipe in three distinct phases. Empirical models have been proposed to predict thrust forces during jacking operations, as outlined in Chapter 2.

The developed models predict jacking forces for tunneling installations due to various operational parameters: lubrication of the pipe string and cutterhead, soil type and corresponding strength and behavioral characteristics, overburden pressure, water head, pipe material, pipe dimensions, and overcut (dimensions of the product pipe relative to the cutterhead). Depending on the source of information, certain installation parameters are deemed to be more influential on overall jacking stresses than others. Much of the variability between existing models occurs in calculation of the frictional component of jacking force as opposed to the face resistance at the cutterhead or leading pipe section.

It is logical that the existing predictive models used in pipe jacking may be adopted for use in determining jacking forces during PTMT operations due to the similarity in the installation processes. The following sections explore the applicability of adopting existing empirical models for this purpose. Preliminary work involves developing relationships for the recorded hydraulic pressures to jacking force, pull-back force, and rotational torque. General trends in forces and rotational torques may then be

observed in conjunction with field notes and other operational characteristics. These trends may be compared to existing models to investigate their use in predicting jacking behavior for PTMT installations. The end goal of this chapter is to recognize which operational characteristics are the most pertinent in predicting PTMT forces and to identify which equations use these characteristics in a manner most applicable to PTMT.

## **5.1 Hydraulic Pressure Correlations**

To gain valuable understanding of the forces and torques associated with PTMT installations, proper calibration of the pressure transducers and accurate translation between hydraulic pressures, forces, and rotational torques must be accomplished. With these fundamentals, one may conclude upon operational and environmental parameters that affect PTMT installation behavior. Sections 5.1.1, 5.1.2, and 5.1.3 set the framework for translating recorded hydraulic pressures to jacking forces, pull-back forces, and rotational torques for the Reid Drive Interceptor Project.

### **5.1.1 Jacking Force**

At the root of developing an appropriate relationship between hydraulic pressures in a machine's jacking rams to the resulting thrust force, lies proper calibration of the pressure transducers, as described in Chapter 3. As expected, each transducer has a distinct relationship between the pressure it is exposed to and the voltage it outputs to the Data Dolphin data logger. Furthermore, each machine utilized for the three phase PTMT methodology has a unique pressure versus thrust force relationship that needs to be identified. The ideology behind converting from hydraulic pressure to the resulting thrust is rather simple, and incorporates the surface area inside the hydraulic jacks, or rams, that the hydraulic fluid acts upon. To obtain the thrust force generated by a ram, the fluid/ram

contact area should be multiplied by the hydraulic pressure. Figure 5.1 illustrates a generic detail for jacking rams and gives insight to how hydraulics are utilized to produce force. It should be noted that the black rectangle represents the location where the shaft is fixed to the jacking frame. As hydraulic pressure increases in the piston chamber, the barrel assembly will slide along the shaft to the right with a force equal to the pressure times the inside diameter of the seal. Most jacking frames apply hydraulics in this fashion to generate thrust. Pull-back is achieved by generating greater hydraulic pressure in the area between the shaft and the barrel assembly (pink zone) than the piston chamber, resulting in the barrel assembly moving towards the left (Figure 5.1).

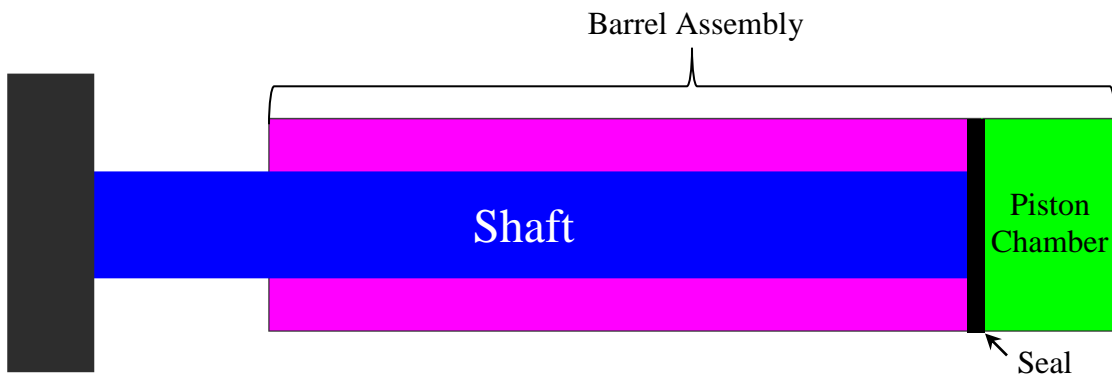


Figure 5.1 Jacking Ram General Detail

The jacking rams for the machines involved in each PTMT phase consisted of unique geometries, lending to distinct hydraulic pressure and thrust force relationships. The number of jacking rams utilized on each machine and the piston dimensions may be viewed in Table 5.1.

Table 5.1 Jacking Ram Characteristics for all Reid Drive Interceptor Jacking Frames

Jacking Frame	Phase Utilized	# of Rams	Piston I.D. (in)	Piston Area (in <sup>2</sup> )	Total Area (in <sup>2</sup> )
GBM	1	2	5	20	39
AA	2	2	9	64	127
BM Pusher	3	3	7	38	115

Multiplying recorded hydraulic pressures by the total area of the pistons for each machine enables one to graph the thrust force versus time for all installations, as illustrated by a pilot tube installation cycle in Figure 5.2. Upon linking generated thrust forces with cyclic installation operations, an unusual aspect was observed. How, during periods of machine inactivity (circled in red) is there a generated force of slightly less than 5 tons? Should not the true thrust force during this period should be zero, as the jacking rams are either stationary or extending or retracting in small amounts with little resistance? A likely reason for the non-zero thrust forces during machine inactivity may be that the hydraulic pressure between the barrel assembly and the shaft is not zero, equating to an ambient force of just less than five tons acting in the opposite direction of normal thrust operations. To account for this phenomenon, calculated thrust forces were reduced by a uniform amount to zero thrust force values during periods of machine inactivity (Figure 5.3).

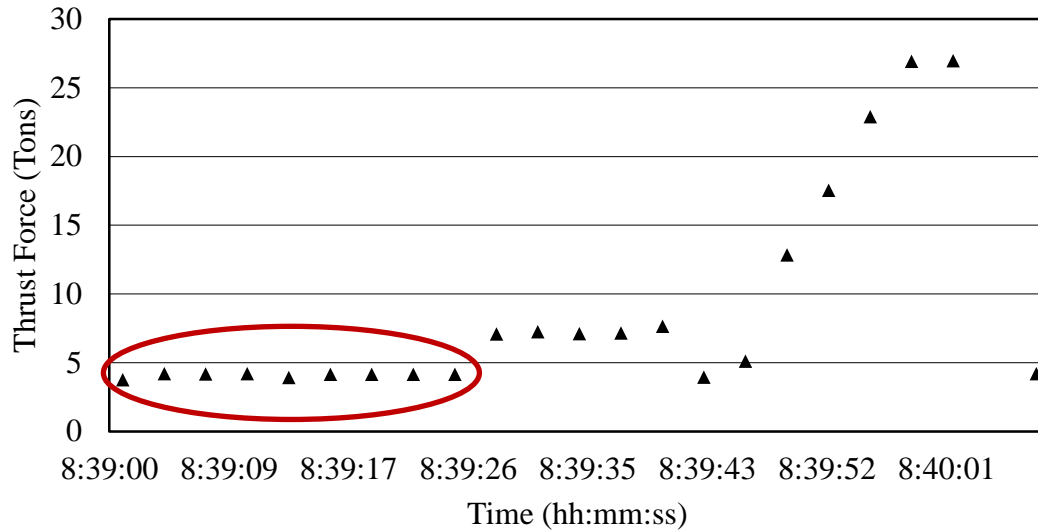


Figure 5.2 Non-Adjusted Thrust Force vs. Time for a Pilot Tube Installation Cycle

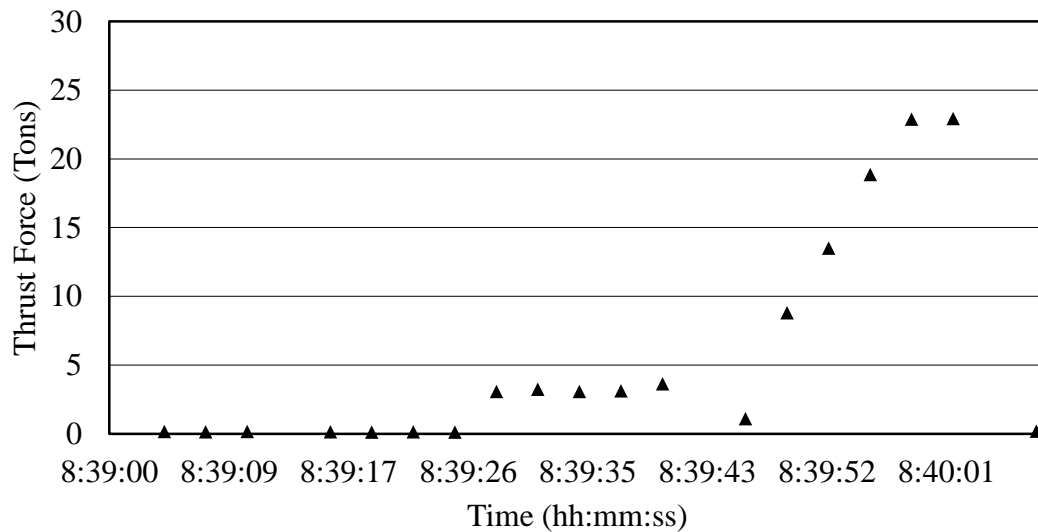


Figure 5.3 Adjusted Thrust Force vs. Time for the Figure 5.2 Pilot Tube Installation Cycle

A similar behavior was noticed with the AA. Consequently, the same approach was adopted to zero thrust force values during machine inactivity. The ambient pressure between the barrel assembly and the shaft differs depending on the machine. Thus, calculated thrust forces recorded from the AA were reduced by roughly 6 tons.



The BM pusher data also required adjustment; conversely, a uniform modification to the data was not appropriate due to the complications observed in the L1 pressure transducer (See Appendix D). Sections of consistent ambient hydraulic pressures needed to be isolated and corrected on a case by case basis. Even though picking the data apart and adjusting the pressures to result in ambient values of zero better represented actual field conditions, it was important to keep the number of isolated sections to a minimum. By doing so, the data would adequately represent the true, or logical, thrust forces produced throughout the installations while maintaining as much data authenticity as possible.

### **5.1.2 Pull-Back Force**

Pulling pipe through the borehole was not used as frequently as jacking operations. The only machine utilized for pull-back operations was the GBM, in which pulling was employed for two purposes: 1) to pull back pilot tubes allowing for a second attempt at avoiding an obstacle or location of very stiff soil, or 2) to pull back the pilot tubes, reamer, and HDPE pipe during the second phase of PT/HDD processes. The AA may be used to pull the auger string out from within installed casing to investigate conditions near the reamer, but observance of this task did not take place while recording data. The BM Pusher does not have the means to pull product pipe backwards and is incapable of pulling operations.

GBM maximum pulling force is less than its maximum jacking force due to the smaller contact area of which the hydraulic fluid acts upon to generate force. The magnitude of pull-back force under a given hydraulic pressure may be calculated by multiplying the hydraulic pressure by the contact area (Equation 5.1):

$$P_F = H_P \times \left(\frac{\pi}{4}\right)(ID_P^2 - OD_S^2) \quad (5.1)$$

where  $P_F$  = Pull-back force

$H_P$  = Hydraulic pressure

$ID_P$  = Inside diameter of the piston

$OD_S$  = Outside diameter of the shaft

As with the calculated jacking forces, calculated pull-back forces needed to be reduced to zero the forces during periods of machine inactivity. A uniform reduction of the original pull-back force by 2 tons achieved this result. The likely cause of the originally non-zero ambient pressures is akin to that which was observed with the jacking forces. Pressure inside the piston chamber creates a force that acts in the opposite direction of the pull-back force, thus necessitating the force reduction.

### 5.1.3 Rotational Torque

In addition to pulling operations, data for rotational torque was only captured during GBM operations. Rotation was accomplished in the AA through the engine and transmission, not through hydraulics. Rotation was not possible with the BM pusher, nor was it desired to apply torsion to the product pipes.

Correlations between recorded hydraulic pressures and resulting rotational torques were derived in an alternative manner to that of the jacking and pull-back forces. Linear interpolation between maximum and minimum hydraulic pressures and rotational torques for the GBM (Table 5.2) was used to develop the torque versus pressure relationship. Maximum values were obtained from the Akkerman Guided Boring Machine Technical Manual (2013), but the minimum hydraulic pressure, 0 psi, corresponding to a minimum rotational torque, 0 ft-lbs, was assumed. Upon converting pressure to rotational torque

and graphing the rotational torque versus time, it became evident that zero rotational torque corresponded to a hydraulic pressure of about 650 psi, which was observed during periods of inactivity or machine idling. Thus, the linear relationship used to convert pressures to torques was invalid, and an updated linear relationship using a minimum pressure of 650 psi corresponding to a minimum rotational torque of 0 ft-lbs needed to be applied (Table 5.2). By doing so, the proper relationship was realized and zero ft-lbs of torque was observed during periods of inactivity.

Table 5.2 Minimum and Maximum GBM Pressures and Torques

	Original Minimum	Updated Minimum	Maximum
Hydraulic Pressure (psi)	0	650	5000
Rotational Torque (ft-lbs)	0	0	10,500


## 5.2 General Trends

To begin identifying trends in forces and rotational torques, it is helpful to look at the forces and torques as they vary with time, length of drive, and the phase or drive of which they occurred. Figures illustrating time and length of drive relationships may be viewed in Appendix A. Critical installation characteristics such as the maximum observed, typical high, and typical low values were noted for each drive, as shown in Table B.2. By doing so, specific force and torque behavior representative of each PTMT or PT/HDD phase may be identified and compared (see Table B.3).

Table 5.3 ranks the various phases for PTMT and PT/HDD based on their maximum observed and typical high forces and torques. It was observed that forces and torques were the greatest during installation of 21-inch steel casings and reaming/pull-back of 4-inch HDPE product pipes, respectively. High thrust forces during jacking of 21-inch casing seem logical, as the borehole is being increased to a large extent and there

is significant casing-soil surface area for which friction may build upon. It also is reasonable that the highest torques were observed during pull-back operations, where significant torque is necessary to ream the borehole to a greater diameter.

Table 5.3 Rankings of Force and Torque Magnitudes for PTMT and PT/HDD Phases

Ranking	Force		Torque	
	Max	Typical High	Max	Typical High
Greatest	21 Casing	21 Casing	Pull Back	Pull Back
	21 VCP	21 VCP	Push PT	8 Casing
	Pull Back	Pull Back	Push PT 2	Push PT
	Push PT	8 Casing	Pull Back 2	Pull Back 2
	8 Casing	Pull Back 2	8 Casing	Push PT 2
	Pull Back 2	Push PT	N/A	N/A
	Push PT 2	Push PT 2	N/A	N/A
	Least	8 VCP	8 VCP	N/A

The smallest forces were experienced during jacking of 8-inch VCP. Rotational torques experienced during jacking of 8-inch steel casing and auguring of spoil material were relatively constant and generally were between 2000 and 4000 ft-lbs. Torques of this magnitude exceeded typical high torques of most other phases, with the exception of initial reaming operations. However, the maximum torque of 4000 ft-lbs was less than the maximum torque observed in all other phases.

There was only one monitored drive for the 8-inch casings. As such, the maximum observed torque and the typical high torque value for the 8 inch casing drive were not far apart. Maximum observed torques for other phases were representative of the most resistive conditions from several recorded drives. Since there were multiple drives of the other phases, the typical high torque value was derived from average conditions from those drives and is significantly lower than the maximum observed torque. Thus, additional monitoring of 8-inch casing installations is recommended to

draw more complete conclusions based on how the rotational torques are related to other PTMT or PT/HDD phases. However, it should be noted that thrust forces and rotational torques for drive number five were greater during installation of the casings than during installation of the pilot tubes or VCP, suggesting that if more data were collected results would show highest typical and maximum forces and torques during installation of the 8-inch casing. This behavior was also observed within the 21-inch installations.

Table B.4 identifies the drive, as defined in Table 3.2 of Chapter 3, during which the characteristics listed in Table B.3 were observed to allow for correlation to drive specific parameters such as installation depth, soil type, and other drive specific features. The following trends and observations attempt to provide insight towards which drive specific parameters have the greatest effect on thrust force, pull-back force, and rotational torque.

### **5.2.1 Installation Depth**

Installation depths for the 21-inch casings and product pipes ranged from 34 to 38-ft below grade. The lack of depth variation does not allow for proper evaluation of the effect of installation depth on the forces incurred during phases two and three of the PTMT process. Drives utilizing manhole 26.106 as a jacking shaft were of shallower depth. The 8-inch PTMT and 4-inch PT/HDD installations out of this shaft were at 26 and 25-ft of depth, respectively. Due to the approximately 10-ft depth difference between these drives and the 21-inch drives, evaluation of the effect of installation depth on pilot tube jacking forces is possible, which is a common phase of all drives.

Depth of cover did not turn out to be a factor that highly effects the thrust force or rotational torques experienced during phase one, pilot tube, operations. As one would

expect, the average high rotational torques for the deeper and shallower installations were 3375 and 2250 ft-lbs, respectively. A 40% difference in the rotational torques may indicate that installation depth has a positive correlation with installation resistance. However, upon comparing the thrust forces, a 30% difference between the higher thrust force for shallower installations and the lower thrust force for the deeper installations leads one in the opposite direction.

Drive seven, the 4-inch lateral installation out of manhole 26.100, may also provide insight to the effect of installation depth. This drive was installed at a 7% grade, resulting in a 20-ft elevation difference between the manhole and the exit pit location. The ground surface elevation at the exit location and the manhole was about the same, yet there was a valley midway through the alignment. Thrust forces observed throughout this installation did not show any sort of decrease when the lead pilot tube was under the valley and in a shallower depth of cover. On the contrary, about 100 feet into the drive, thrust forces began to rise by about 4 tons every 25-ft (Figure A.53). Rotational torque was unaffected. It is thought the thrust force increase may be due to increased tree root interference and possibly some cemented soil material.

Comparison of drives with differing depths of cover indicates that depth of cover is not a significant factor in regards to jacking resistance. Terzaghi's Arching Theory illustrates how the vertical effective stresses are decreased due to the opening of a void underneath, as is the case in phases two and three of the PTMT method. Although, phase one is a displacement method, where the soil surrounding the pilot tubes is likely in direct contact with the pilot tube, there still may be some stress reduction occurring, possibly due to the lubrication applied during installation. Further monitoring of PTMT

installations where the effect of depth is able to be isolated would provide the means to investigate this effect to a greater degree.

### **5.2.2 Soil Type**

Since jacking force is proportional to the skin friction between the soil and pipe interface and the penetration resistance at the lead face, soil type likely plays a large role in the magnitude of forces necessary to install pipelines with the PTMT methodology. Unfortunately, soil strata throughout the project was relatively consistent and was mostly composed of a silty clay of low plasticity (CL) with trace amounts of moist fine grained sand. The clay was generally reddish brown, but transitioned to a gray brown about 20-ft below grade, generally once the soil was below the ground water table. Drives five through seven, the 8-inch VCP and 4-inch HDPE laterals, were shallower and installed in stiff silty clay with standard penetration test N values of 8 to 9, whereas, the other drives were installed through a silty clay of medium stiffness with N values of 4 to 5. Elevations of the shallower and deeper drives were thought to be at, and 20-ft below, the ground water table elevation, respectively, although, their water content was not too far off, around 17% for the shallower drives and 23% for the deeper ones.

Since the drives in the stiffer and lower water content soils were either for the installation of 8-inch VCP or 4-inch HDPE laterals, and the less stiff, higher water content drives were for the installation of 21-inch VCP, the only common phase between the two sets of installations was phase one. Also, since the stiffer soils were shallower and the medium stiffness soils were deeper, comparison of the phase one forces and torques based on soil type is analogous to the assessment made to evaluate the effect of depth below grade. Thus, a complete analysis of the effect of soil type, particularly

stiffness and water content, is irresolvable based on the data collected from this project. There were, however, some installations where the operator noticed spikes in the pressure gauges of the machine and believed to be traversing through sections of “hardpan” or a cementitious soil medium.

In several instances throughout the Reid Drive Interceptor Project, the operator suspected that sections with small boulders, cobbles, or hardpan were encountered due sudden increases in the machine pressure gauge readings. Hardpan is a slang terminology commonly used by field operators to describe soil that is extremely hard and cemented together (Johnson 2013). Cementation may occur through precipitation of calcite, silica, alumina, iron oxides, or other compounds onto soil particle surfaces at interparticle contacts or in soil pores (Mitchell and Soga 2005). These compounds crystallize and often form a very hard soil structure that is more resistant to tensile and tangential stresses.

The effect of hardpan on jacking forces is unique compared to that of cobbles or boulders. Being that jacking forces are the resultant of two components, frictional resistive forces along the soil-pipe interface and penetration resistance at the lead pipe, it is possible for certain soil types to increase one component of jacking resistance while decreasing the other. Interparticle cementation results in high tensile strengths which increases borehole stability. Barla and Camusso (2013) found through numerical modeling of jacking forces through various degrees of cemented soil that as there is an exponential increase in normal stress upon reduction in the degree of cementation. As a lead pipe or pilot tube proceeds through a section of hardpan, jacking forces are likely to increase substantially as the penetration resistance drastically increases due to the



hardness of the cemented soil. Upon exiting the hard pan, jacking forces should sharply decline due to the immediate reduction in penetration resistance and the negligible amount of frictional resistance added throughout traversing through the hard pan section. Cobbles and boulders, on the other hand, are expected to cause an increase in penetration resistance as well as higher frictional forces as they continue to press against the pipeline as it is jacked through the soil.

A prime example of how hardpan can influence jacking force is seen in the second drive of the Reid Drive Interceptor Project, a 385-ft run of 21-inch mainline sewer. There were two locations along this drive where the operator suspected that hardpan was causing machine pressures to rise. As it may be seen in Figure A.13, after about 120-ft of pilot tubes had been installed jacking forces quadrupled from 4 tons to 12 tons. By about 200-ft jacking forces had reduced to 5 tons. Towards the end of the installation forces began to rise again, from 5 to 7 tons. Torque required to rotate the pilot tube string increased in a similar fashion and degree of magnitude as the jacking forces. Of course, observing pilot tube operations and analyzing thrust force data does not give insight to the reason for any jacking force increases. Examining spoil generated from phase two operations does, however, allow one to discern this cause and effect relationship.

Jacking forces prior to the first section of hardpan during phase two were near 30 tons (Figure A.16). The highest observed force during the first hardpan location was 225 tons, eight times greater than with the silty clay. Forces dropped back down to near 40 tons before increasing to around 145 tons at the second location of hardpan. Spoil material generated from the first area causing higher forces contained large amounts of

sandy clumps, watered down with lots of bentonite lubrication. This material was in contrast to the usual spoil material, a stiff putty like silty clay. Spoil from the 340-ft chainage mark contained wood fragments, sandy clumps, as well as some silty clay.

Analysis of the jacking forces during VCP jacking showed a relatively constant resistance of about 25 to 30 tons (Figure A.18). There were no signs of increased force at the hardpan locations. This is likely due to the fact that there is zero face pressure during this phase and frictional forces are limited due to the  $\frac{3}{4}$ -inch overcut between the casing and VCP diameter.

There were other drives in the Reid Drive Interceptor Project where higher forces were observed and it was thought the alignment was traversing through sections with hardpan. However, the second drive was the only one where field notes pertaining to the spoil material were taken. Field notes for drive number six, a 4-inch lateral installed with the PT/HDD method, described hardpan starting at 105-ft from the jacking shaft. Forces during pilot tube jacking rose from 4 tons to 25 tons at this location (Figure A.45). Forces upon exiting the hardpan fell to 7 tons, before rising to 20 tons at the end of the drive, where the cause of high forces was not documented.

Following pilot tube installation on the sixth drive, tooling was changed to allow for pull-back of the HDPE pipe. Pull forces followed the same trends as the pilot tube jacking. Figure A.45 illustrates HDPE pull-back forces along with pilot tube jacking forces and how changes in conditions equally influence both operations. To make comparison of the forces in regards to location easier, the length of drive is defined as the distance from the jacking shaft, where the machine was stationed. Thus, pull-back forces recorded at the beginning of pull-back operations are shown to occur at the 240-ft mark.

When pull-back operations were 40-ft from completion, the HDPE pipeline snapped and pull-forces immediately reduced from 23 to 15 tons. It is likely that pull-forces of 35 tons during the hard pan section imposed high stresses on the HDPE pipe, causing it stretch beyond elastic strain, compromising its ultimate strength. Once the reamer had been pulled through the hardpan, 110-ft chainage, pull-forces decreased to 20 tons. Forces steadily rose to 23 tons at the location of the pipe breakage. The recorded hydraulic pressures throughout this study only shed light on the forces generated from the machinery, and consequently do not directly reflect the forces experienced by the HDPE product pipe, as forces are split between the pipe and the reamer during pull-back operations. Regardless, the hardpan most likely compromised the tensile strength of the product line, which along with the slight increase in pull forces after the hardpan, may have caused the pipe to fail. Figure 5.4 shows the HDPE pipe section that was attached to the swivel; notice how close it broke to the beginning of the pipe.



Figure 5.4 Broken HDPE Pipe from Drive Six

The pipe break phenomenon occurred on at 4:30 on a Friday afternoon. By the time the pilot tubes were retracted from the borehole it was decided that retrieval of the HDPE pipe would have to wait for Monday. On Monday, crews worked with a small

closed circuit television camera to view down the HDPE line to evaluate the condition of the pipe as best as possible. Fortunately, the line looked to be in good condition until 40-ft from the jacking shaft, where the GBM stationed. Problems with the backhoe and other non-related project tasks delayed the HDPE retrieval process an additional day.

On Tuesday, a retrieval shaft was dug surrounding the location where the HDPE pipe had broken. The compromised section of the HDPE pipe was cut off to ensure installation of a quality product and to reduce chances of having another failure. Pilot tubes were jacked until the lead rod was close enough to attach the HDPE pipe with the reamer and swivel assembly. Pull-back of the HDPE product proceeded without complications or unusually high forces. There are a few interesting observations about the thrust and pull-back forces due during the HDPE retrieval process. Pilot tube jacking forces ranged from 3 to 4 tons, about 1 ton less than during the initial pilot tube jacking in the same soil location. Pull-back forces were also slightly lower; they were now 13 tons instead of 15 tons. This leads one to believe that the forces were lower due to the prior action of the pilot tube jacking and pull-back procedures creating a borehole. It is understood that the borehole may not have remained completely open, but having it open once before did contribute to lower forces in subsequent operations.

For this reason, drive number seven, another 4-inch HDPE lateral, was conducted in the following manner: jacking of pilot tubes to establish line and grade, pre-reaming of the borehole without pull-back of the product pipe to enlarge the borehole diameter, jacking of pilot tubes through the enlarged borehole to reach the exit location, and final reaming and pull-back of the HDPE product pipe. It was thought that the pre-reaming operation would result in decreased forces during pull-back of the HDPE pipe and

decrease the chances of having another pipe failure. Fortunately, the pipe failure on drive number six occurred in a location where retrieval operations were quite feasible. Alignment for drive number seven crossed through a private wood with a significant ravine in the middle. Accordingly, pipe failure during this drive would be highly detrimental to the project schedule and budget.

Pilot tube jacking forces oscillated around 4 tons for the first 100-ft of the installation, at which point they began to rise roughly 4 tons every 25-ft until they reached 22 tons by the end of the drive (Figure A.53). The 22 ton force experienced with this installation is similar to the high force of 25 tons from drive number six, although, thrust forces gradually rose to this level over a distance of 150 feet. Steady increases to jacking forces are likely due to increased frictional resistance, as opposed to penetration resistance. For this reason, and that the installation was crossing under a wood, it is believed that tree roots are the source for the force increase.

Pre-reaming forces started out at 25 tons and steadily declined to 15 tons upon entering the manhole where the GBM was stationed (Figure A.55). The 25 ton force was less than the maximum that occurred during the pipe failure; however, forces may have been higher if the swivel was trailing a continuous string of HDPE pipe. Jacking pilot tubes through the enlarged borehole went smoothly and only 3 tons was necessary to advance the pilot tubes to the exit location. There was no increase in forces upon crossing under the wood as there was with the initial piloting. Pull-back of the HDPE pipe also exhibited smaller forces than the initial pre-ream. Forces started out around 14 tons and fell to 11 tons at the completion of the pull. This resulted in a force reduction of 44% and 27% percent at the beginning and end, respectively, of the HDPE pull-back operation.

Force reductions of this magnitude provide significant benefits towards pulling back HDPE pipe in difficult ground conditions. Hence, pre-reaming is recommended when pilot tube jacking forces approach 20 tons and the PT/HDD method is to be used. An alternative to pre-reaming may include using a larger reamer, although, the benefits to this approach were not explored in this study.

### **5.2.3 Stoppages**

In addition to soil type and the presence of roots, boulders, or cobbles, stoppages play a role in increasing jacking forces. There are short cyclic stoppages, when positioning new pipes or tubes for jacking or between PTMT phases when machinery and tooling is being changed, and longer stoppages such as shutting down at the end of a work day or for the weekend. Generally speaking, as jacking operations are paused, displaced soil surrounding the borehole begins to relax and presses against the walls of the pipe. This is especially true with installations in expansive clays. Unfortunately, there was a prime example of how stoppages may be detrimental to an installation on the Reid Drive Interceptor Project that occurred before the monitoring equipment was ready for use. However, there were field notes pertaining to this drive to document the cause and affect the stoppage had on project efficiency.

Drive number one was actually a second attempt at completing a 21-inch VCP PTMT installation from manhole 26.100 to manhole 26.99B. In an effort to increase project efficiency, a second crew was enacted to originally perform this installation while the usual crew finished up work in other areas. For whatever reason, the new foreman proceed with jacking pilot tubes at a slope of positive 0.2%, when they were supposed to be installed with a negative 0.2% slope. To make matters worse, adequate lubrication was

not being applied during pilot tube jacking, consequence of the new foreman having to use an inferior and operationally temperamental bentonite pump. The incorrect grade remained unrealized until the pilot tubes were jacked into manhole 26.99B, on the Friday before the three day Memorial Day Weekend.

On Tuesday, attempts to remove the pilot tubes by pulling back into the jacking pit failed, as the tubes would not budge. Wednesday's efforts involved trying to get the pilot tube string to move by jacking from MH 26.100 towards MH 26.99B. Again, this process was futile. It was thought that the pilot tubes may be able to be pushed from MH 26.99B with the GBM while being pulled from MH 26.100 with the AA. So, on Thursday machinery was moved and prepped to begin this operation. Friday was successful in moving four pilot tubes, before it became evident that a concrete backstop was needed for the GBM to jack against. The concrete backstop was poured on Saturday morning and retrieval operations were delayed until the following Monday. By Friday the crew was able to pull out all of the stuck pilot tubes. All in all it took nine days to remove the stuck rods. Furthermore, the AA broke in the process of pulling the tubes and an alternate auger boring unit had to be brought in. Additionally, less valuable tooling was also ruined in the retrieval process. This two week setback put tremendous strain on the contractor as he was now operating on a fine line of being able to complete the project on time and for profit.

The previous scenario paves the way towards realizing the severity of what may happen after unnecessary stoppages. Evaluation of the degree to which stoppages of varying durations affect thrust forces from all PTMT and PT/HDD phases is logically the next step. In the collected data, three classes of stoppage durations could be observed:

Class One) stoppages occurring after jacking of a pipe section while retracting machinery and readying the subsequent pipe for installation, Class Two) Stoppages greater than ten minutes in which operations are halted while supplies are being gathered elsewhere on site or other from other setbacks to the installation's critical path progress, and Class Three) overnight or weekend stoppages. Class one stoppages are fundamental to all PTMT and PT/HDD processes and may be observed in plenty. Class two stoppages were sighted in each operational phase, yet occurred on a less frequent basis. Class three stoppages were only observable during jacking of 21-inch steel casing. All other phases were able to be accomplished in one day's work.

The class one stoppages were roughly less than 30 seconds, 30 seconds, 2 minutes, 5 minutes, 8 minutes, and 10 minutes for the pulling back of HDPE pipe, jacking of pilot tubes, jacking of 8-inch VCP, jacking of 21-inch VCP, jacking of 8-inch casing, and jacking of 21-inch casing, respectively. Stoppages of this duration appear to be negligible, as both force increases and decreases were observed following the period of inactivity. Class two stoppages were negligible for all phases except for jacking of 21-inch steel casing. Of the instances included within the recorded data, stoppages of 45 and 90 minutes were noticed. Ironically, the maximum thrust increase of 6 tons was observed after the 45 minute delay and a thrust decrease of 5 tons was seen after the 90 minute delay. Class three stoppages, only occurring during jacking of the 21-inch casing, ranged from 12 to 58 hours. Force increases after 12 hour stops ranged from negligible to 7 tons, while the increase in force after 58 hours was 4 tons. Of consequence to the highly variable thrust increases upon jacking delays observed in this data, a strong relationship between delay and increased thrust force could not be identified.



One correlation that could be detected was that during the jacking of a 21-inch casing, thrust forces tended to decrease. Although sometimes thrust force increased during the jacking of a casing, more often than not a decrease between 1 and 10 tons was observed. This illustrates that the friction between the soil-pipe interface is reducing from a higher static friction to a lower kinetic friction. Being that minimizing friction along the soil-pipe interface is a key component towards reducing necessary jacking forces, it is wise to progress with an installation in a manner that is as continuous as possible. Applying adequate lubrication is also a technique that should be used to help minimize frictional forces.

#### **5.2.4 Lubrication**

Lubrication aids in borehole stabilization and in decreasing the friction coefficient between the soil-pipe interface. An experiment conducted by Shou et al. (2010) involved placing various lubricants between a concrete block and soil and measuring the drag force required to move the concrete block. Depending on the lubricant, they observed friction coefficient reductions due to the lubricant ranging from 16% to 75%, with the bentonite/polymer and the plasticizer/polymer being the least and most effective, respectively. M-I SWACO's Max Bore HDD drilling fluid, which is composed of a high-yielding Wyoming bentonite, and a generic dish soap were used in conjunction to lubricate phase one and two operations on the Reid Drive Interceptor Project. Shou et al. (2010) found that bentonite reduced the friction coefficient by 23.5% in their large scale testing method. It is reasonable to assume that the addition of dish soap would reduce the friction coefficient even further.

The only phase not utilizing lubrication for the Reid Drive Interceptor Project was the jacking of VCP. During pilot tube jacking, lubrication flowed between the outer and inner walls of the tubes to the lead pilot tube, where it was expelled through a single port. Upon completing jacking of a pilot tube and before disconnecting the GBM from the pilot tube, the lubrication pump was shut off, a valve to the pilot tubes was closed, and a discharge hose was used to drain excess lubricant pressure in the line. Once a new pilot tube was hooked up, the valve supplying lubricant to the tube was opened and the lubrication pump was turned on. Lubrication during jacking of the casing was slightly more complicated and varied depending on the diameter of the casings being installed.

During the 21-inch casing installations, a 10-ft long switch over rod was utilized to connect the pilot tubes to the reamer. This rod provided added stability as well as the means of applying lubrication to the casings. Lubrication was applied from the reception shaft between the inner and outer walls of the pilot tubes. The lubrication flowed through the adapter rod, into the reamer, and out of the reamer's four prongs to the outside of the lead casing (Figure 1.3). This application was sufficient in lubricating the outside of the casings. After several casings were installed, there was enough lubricant on the outside of the casings where it began to leak into the casings and provide lubricant to the augers. Alternatively, the lubrication hose used to supply lubricant to the outside of the casings could have been fitted to the pilot tubes in a manner that supplied lubricant to the center of the lead casing. However, applying fluid to the outside of the casings and to the center of the lead casing simultaneously was not possible. Applying lubricant to the outside of the casing was thought to be the most effective, as it supplied borehole stabilization, lubrication to the soil-pipe interface, and lubrication to the auger string due to leaking

through the casing joints. Lubrication was applied continuously throughout phase two, although if spoil returns were too wet or dry the lubricant flow was reduced or increased, respectively.

Lubrication for 8-inch casing installations was applied to the exterior of the casings through the four lubrication ports located on the 8-inch reamer. Supplying lubrication to the center of the lead casing was not possible, as a different setup was used to send lubricant from the receiving shaft to the reamer. Upon completion of pilot tube installation, a sting was blown from the reception shaft to the jacking shaft through the center of the pilot tubes. Lubrication hoses were then pulled from the jacking shaft to the reception shaft. These hoses were attached to the center of the reamer, which transferred the fluid flow to the reamer's four forks. Lubrication was then controlled from crew members in the reception shaft who were in radio communication with the operator in the jacking shaft. Once a pilot tube was pushed into the reception shaft, the lubrication hoses would have to be disconnected to allow removal of that tube. The hoses would be reconnected before jacking the next casing. As in with the 21-inch jacking operation, lubrication was abundant enough to leak through the outside of the casing and lubricate the auger string in addition to the outside of the casing. The operator did not reduce lubrication flow if the spoil returns contained a large amount of lubricant, as he wanted to insure adequate lubrication to the auger string to minimize chances of it binding and becoming stuck.

Lubrication was also applied during pull-back of HDPE pipe in the PT/HDD hybrid method. As with pilot tube installation, lubrication was ejected through a single port in the lead pilot tube, on the opposite side of the reamer as the HDPE pipe. Contrary

to traditional HDD procedures where the drilling fluid is used to stabilize the borehole and return cuttings to the entrance pit, there were limited spoil returns until the last 10 to 20-ft with the PT/HDD method. As such, the lubricant mostly served to stabilize the borehole and decrease frictional resistance along the soil-pipe interface. Furthermore, the reaming process most likely displaced the soil as the borehole was being enlarged, rather than cutting it away and having it circulate through suspension to the entrance pit. For this reason, it is possible for soil displaced by the reaming head to collapse once the reamer has passed if the drilling fluid has not properly stabilized the borehole. This action would increase stresses on the trailing HDPE pipe.

Throughout the PTMT operations utilizing lubrication, the volume of lubrication applied and the bentonite to water concentration was not recorded using the data logger or any other real time monitoring device. Field notes are the only source of determining when lubrication was used, how much lubrication was applied, and the concentration of Max Bore HDD drilling fluid to water. The concentration for each lubrication application was documented as carefully as possible, but mostly consisted of observations such as two 50-pound bags were added to the bentonite tank, with an initial tank volume of 200 gallons and a final tank volume of 500 gallons. Thus, the previous tank concentration needed to be known to accurately determine the new concentration. Volume used per footage was determined by dividing the difference in bentonite tank volume from the beginning to the end of the day by the footage gained for that day. As such, lubrication quantities were a daily average and did not represent any changes in application throughout daily activities.

Table 5.4 lists the phases that used lubrication in order of greatest to least for the volume of lubricant used per 10-ft of progress. Recommended concentrations for use in clay environments are highlighted in red (MI SWACO 2013). Generally, as soil conditions become more granular, and less cohesive, one would want to increase the bentonite to water concentration. MI SWACO recommends 10 to 15 pounds per 100 gallons for clay environments, 20 to 25 pounds per 100 gallons for normal drilling, and 25 to 30 pounds per 100 gallons gravel/rock/cobble soil conditions. Concentrations, in Table 5.4, exceeding the manufacturer’s recommendations are highlighted in blue.

Table 5.4 Lubricant Volume and Concentration throughout the Reid Drive Interceptor Project

Phase	Drive	Gallons per 10 Feet	Pounds of Bentonite per 100 Gallons
8-in Casing	5	41.7	15
21-in Casing	1	37.5	33
21-in Casing	2	37.5	13
PT 1	7	18.3	25
PT	3	10.3	25
PT 2	7	8.7	21
PT	5	8.3	25
PT 1	6	7.6	19
HDPE Pull	6	7.6	19
HDPE Pull	7	3.8	21
21-in Casing	3	3.1	13
Pre-Ream	7	1.9	21
PT	1	Not Recorded	33
PT	2	Not Recorded	33
21-in Casing	4	Not Recorded	Not Recorded
PT	4	Not Recorded	Not Recorded
PT 2	6	Not Recorded	Not Recorded
HDPE Pull 2	6	Not Recorded	Not Recorded

High concentrations were used in the first and second phase of the first drive and phase one of the second drive. Reasoning for using the high concentrations was limited and was most likely a result of the laborer, myself, adopting a more is better philosophy. After several phases were completed with the high concentrations, the filter on the bentonite tank began to clog and the mixer started to malfunction. Whether this was a result of the concentration being too high or merely malfunctions in an old and well-used bentonite tank, frustrations with the bentonite system escalated, causing the crew to use a lower bentonite to water concentration, decreased lubricant application, or a combination of the two for the next several drives.

Although comparison between phase one from the first two drives and the drives where less lubrication or bentonite was used should provide insight to the lubrication effects on the Reid Drive Interceptor Project, limited effect was observed in the recorded thrust and rotational torque data. Figures A.6 and Figure A.22 show the rotational torque as it varied with drive distance for phase one of the first and third drives. Rotational torque should increase with the length of the drive as the soil-pipe interface surface area increases. This phenomenon was observed in both of these drives, although the drive utilizing a less lubricant volume at a lower bentonite to water concentration did not exhibit a larger rotational torque increase per unit length. Furthermore, comparison of thrust force versus length of drive was also inconclusive (Figures A.5 and A.21). This behavior may indicate that there are other factors, such as soil type, that influence jacking behavior to a greater extent than lubricant concentration and applied volume, that the procedures for recording lubrication quantities on this project were insufficient, or that

the lubrication applied in drive three was sufficient in stabilizing the borehole and reducing the soil-pipe friction coefficient.

There were, however, two instances throughout the Reid Drive Interceptor Project where either the hardships of ineffective lubrication were learned or the benefit of lubrication was realized. Back when the new crew was called upon to install the 21-inch VCP from manhole 26.100 to manhole 26.99B, lubrication was not adequately applied during jacking of the pilot tubes. The pilot tubes were installed at the wrong grade and retrieval operations did not commence until 3.5 days later. It ended up taking two weeks and numerous operational strategies to free the tubes from the borehole. There is little doubt that had retrieval operations been enacted immediately, the process would have been quicker and less detrimental to the project success. However, had adequate lubrication been applied during the pilot tube installation, retrieval operations likely would have been easier due to a more stable borehole with a lower soil-pipe interface coefficient of friction.

The instance of which the benefit of lubrication was realized was during the second day of jacking 21-inch casings for drive number one. Lubrication was applied during jacking of all casings except, for reasons undocumented in the field notes, lubricant was not applied during jacking of the eighth casing. Figure 5.5 shows the thrust force generated during the jacking of the seventh, eighth, ninth, and tenth casings. Best fit lines of the high forces required for their installation are shown in red. It can be seen that forces between the seventh and eighth casing were fairly consistent and ranged from 26 to 23 tons. During the ninth casing, increased friction due to the lack of lubrication was realized, and forces rose to 31 tons. By the time the tenth casing was being jacked,

lubrication, which was initiated during the jacking of the ninth casing, began to take effect and forces fell to 27 tons. It may seem peculiar that forces did not rise during the eighth pipe, when lubrication was halted, but rose during the ninth casing, when lubrication was re-instated. A likely conclusion is that during jacking of the eighth casing, most of the casings in the borehole remained lubricated. As time went on, lubrication covered less of the casing-soil interface, thus resulting in the higher forces during casing nine. It is also probable that adequate lubricant coverage along the casing-soil interface was not re-established until one casing after lubrication was re-instated, casing number ten.

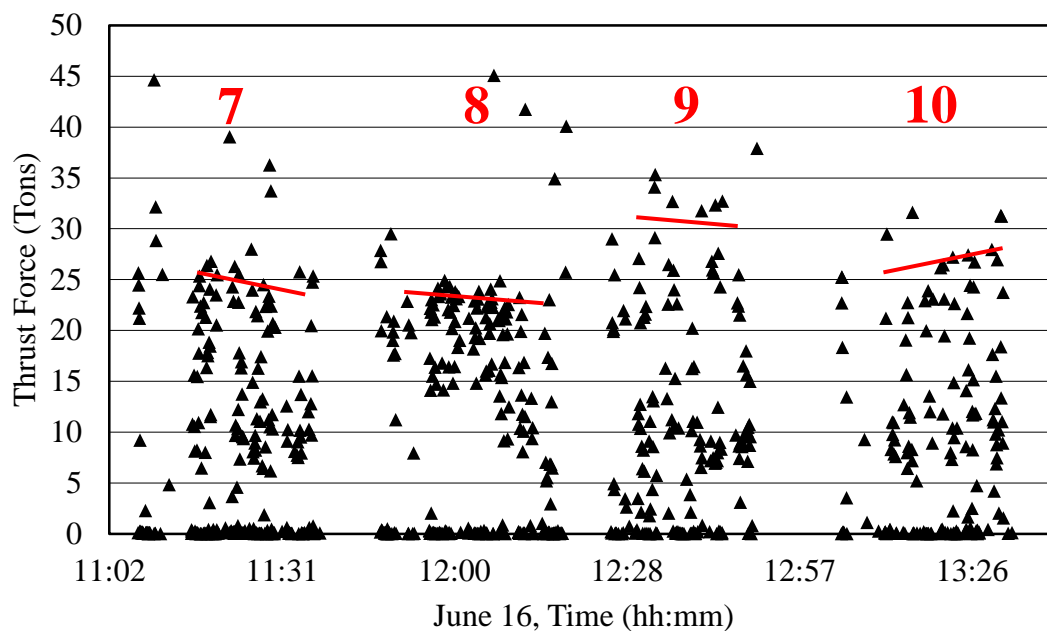


Figure 5.5 Thrust Force for Casing Numbers 7, 8, 9, and 10 for Drive One

Of course, there may have been other influences to the higher jacking forces during casing nine, although lubrication was the only one documented and able to be analyzed. If other variables affecting thrust force were in fact held constant from 11:00 am to 1:30 pm, it is evident that lubricant application plays a role in the required thrust



force. As the machine operator dictates whether or not lubrication is to be used and in what quantity and concentration, operators seemingly play a significant role in the thrust forces necessary for PTMT operations.

### **5.2.5 Operator Technique**

Project productivity and thrust forces generated during jacking installations are dependent upon an operator's experience, skillset, and preferred installation methods. Although maintaining specified line and grade is very feasible with the PTMT method, inexperienced operators may have to correct for more deviations from the intended alignment than an experienced operator. If deviations are significant enough, jacking forces will rise accordingly as pipe sections negotiate through the corrections. Inexperienced operators may also fail to appreciate the benefits of lubrication or apply lubrication in an ill-suited fashion. Furthermore, progress and thrust force characteristics are dependent on the rate and style, or pattern, of advancement.

Forward and backward movement for jacking frames is usually controlled by some sort of joy stick, or lever, located on the jacking frame. The farther the lever is pushed, the faster the machine will move, or if there is resistance, a larger force will be generated. During advancement of the casings in phase two, the usual operator on the job preferred to push the thrust lever all the way and then release it back to a neutral position in a cyclic fashion. He liked using this method of operation because it made things easier for the augers, as they essentially had a short break from capturing new material. Although the cyclic advancement procedure may have put less stress on the auger string, this method may not have been the best for minimizing forces required to jack the casings.

At about 2:55 on June 16<sup>th</sup>, circled in red on Figure 5.6, the main operator, operator one, had to leave the jobsite for a doctor's appointment at which time a less experienced operator, operator two, took over. The most noticeable change in the jacking behavior is that it took much longer for operator two to install one casing section, about one hour as opposed to 30 to 40 minutes. Operator two adopted a similar cyclic advancement style as operator one, except he did not push the lever to farthest advance position nor did he maintain advancement for as long of a duration. From the generated thrust forces it may be seen that this new technique resulted in forces that were commonly 50% lower than those from operator one, although, there were some higher forces generated occasionally. The low production of operator two caused observing crew members to suggest another operator, operator three. Operator three installed two successive casings starting at around 4:10 pm. This operator advanced the casings at a constant rate using a lever position slightly less than maximum advancement. Forces were similar to those experienced by operator one, however, there tended to be less small forces and more outlying high forces. The decrease in smaller forces may be due to the constant advancement providing a more consistent, and larger, force. The more frequent high forces may have occurred when advancement was fast or aggressive. By 5:30, operator one had returned and took over jacking the last casing shown in Figure 5.6.

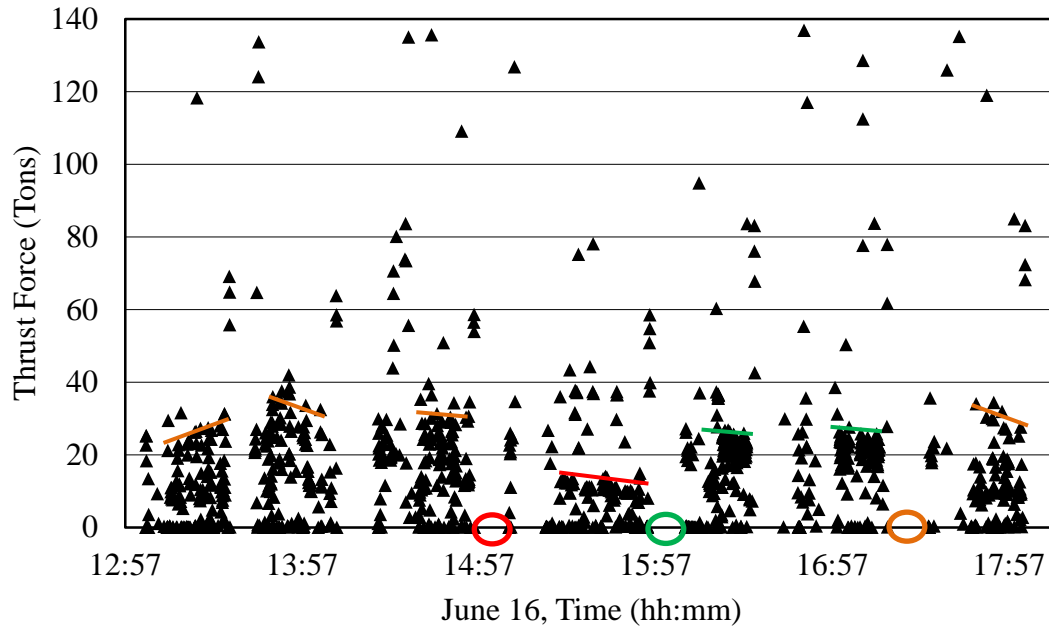


Figure 5.6 Illustration of the Dependency of Thrust Force on Operator Technique

This last example illustrates the dependency of thrust forces and jacking behavior on an operator's technique. Different techniques may result in more consistent thrust forces, smaller or larger forces, or productivity differences. It also can be seen that a slower advancement rate may lead to smaller forces, due to reduction in the face or penetration pressure needed to advance the casings. Even though slow advancement may lower thrust forces, project success also depends greatly on completing installations in a timely and efficient manner. Thus, slow advancement is not advised unless forces are approaching a critical value, such as the thrust capacity of the jacking frame or a level that would overstress the pipes or thrust block.

### 5.3 Application of Jacking Force Predictive Models

As mentioned in Chapter 2, jacking forces incurred during jacking installations are composed of two components: 1) penetration resistance at the cutterhead or leading section and 2) frictional resistance developed along the soil-pipe interface. Thrust forces

are typically the highest towards the end of a drive due to the increased soil-pipe interface area of which frictional forces act upon. The degree to which friction develops throughout an installation makes up an abundance of the uncertainty of the maximum thrust force to complete jacking installations. Numerous contributions have been made to develop predictive models as to the degree to which frictional jacking forces develop throughout an installation. The following section compares predictive models from select researchers who have developed models that are likely to be applicable to the PTMT methodology. Methodology and applicability of models from Chapman and Ichioka (1999), Bennett (1998), and Staheli (1996 and 2006) are described and compared to the data recorded from the Reid Drive Interceptor PTMT installations.

Chapman and Ichioka (1999) performed statistical analysis on data collected from ISTT's Working Group No. 3 (1994) on 398 microtunneling operations. They separated the case histories by soil type and installation method to develop predictive jacking force models for each scenario. Their models developed for auger and push-in machines should be applicable to jacking of casing and pilot tubes, respectively. Jacking of the product VCP pipes during phase three operations should mimic their auger boring equation, except their primary resistance factor should be eliminated as there is zero face resistance during this phase. The general form of their jacking force predictive model applies to slurry microtunneling installations and is represented by Equation 5.2:

$$F = f_o + \pi DPL \quad (5.2)$$

where  $F$  = Total jacking force (T)

$f_o$  = Primary resistance (T)

$D$  = Outside pipe diameter (m)

L = Jacking distance (m)

P = Frictional resistance (T/m<sup>2</sup>), see Table B.1

and

$$f_o = D_0^2 \frac{\pi}{4} P_0 \quad (5.3)$$

where  $D_0$  = Machine outside diameter (m)

$P_0$  = Face resistance (T/m<sup>2</sup>)

They found little correlation between outside diameter and face resistance for auger boring and push-in type installations in the recorded data. Therefore, they developed constants for the face resistance component of Equation 5.2 to make the predictive model applicable to cover various percentages of auger boring and push-in type installations. The following paragraphs first describe how to obtain their jacking force predictive model for push-in, phase one, and auger boring, phase two and three, installations.

Based on their collected data, a face resistance value of 200 tons/m<sup>2</sup> and 400 tons/m<sup>2</sup> should apply to 60% and 90% of push-in type installations in clay, respectively. Given the flexibility, a designer may want to conclude upon a face resistance applicable to the project at hand and choose a higher face resistance for installations in more problematic soils or when maintaining jacking force beneath the estimated jacking force used in project design is critical. They performed linear regression to develop a frictional resistance expression for push-in installations in clay soils (Equation 5.4). Thus, their jacking force predictive model for 90% of push-in type installations in clay is represented by Equation 5.5.

$$P = -2.3D + 1.7 \quad (5.4)$$

$$F = D_0^2 \frac{\pi}{4} (400 \text{ tons}/m^2) + \pi D (-2.3D + 1.7)L \quad (5.5)$$

They developed frictional and face resistance values to cover 50% and 80% of auger boring installations. In clay soil, values of 32.8 tons/m<sup>2</sup> and 50.0 tons/m<sup>2</sup> should be used for face resistance to achieve 50% and 80% coverage, respectively. Frictional resistance for 50% and 80% coverage of installations through clay soils is 0.4 tons/m<sup>2</sup> and 0.7 tons/m<sup>2</sup>. By applying these constants, their estimation of jacking force for 80% of auger boring installations may be found using Equation 5.6.

$$F = D_0^2 \frac{\pi}{4} (50 \text{ tons}/m^2) + \pi D (0.7 \text{ tons}/m^2)L \quad (5.6)$$

Additional modification to Equation 5.6 is required in order to apply them to the second and third phase of the three phase PTMT method. During phase two, the actual face resistance should be reduced as a proportion of the face resistance calculated with Equation 5.6 is non-existent due to the presence of the preceding pilot tubes. Thus, an effective area of the casing's reamer less the area of pilot tube should be used. Additionally, frictional forces transition between those computed for a full alignment of pilot tubes to a full alignment of casing. For phase three, the face resistance term should be eliminated and the frictional resistance should transition between that of the casings to that of the VCP. Applying these alterations and using the pipe dimensions indicated in Table B.5, the equations listed in Table 5.5 may be adopted for use in PTMT operations from the Reid Drive Interceptor Project.

Table 5.5 Application of Jacking Force Equations for PTMT in Clay Soil  
(based on Chapman and Ichioka 1999)

a) Pilot Tube Jacking Force (tons)

Coverage (%)	Pilot tubes
60	$2.5 + (0.49)(L)$
90	$5.1 + (0.49)(L)$

b) 21-inch Casing Jacking Force (tons)

Coverage (%)	Casings
50	$10.8 + \left[ \frac{0.81L_{Total} - 0.49L_{Total}}{L_{Total}} \right] L + 0.49L_{Total}$
80	$16.5 + \left[ \frac{1.42L_{Total} - 0.49L_{Total}}{L_{Total}} \right] L + 0.49L_{Total}$

c) 21-inch VCP Jacking Force (tons)

Coverage (%)	VCP
50	$\left[ \frac{0.77L_{Total} - 0.81L_{Total}}{L_{Total}} \right] L + 0.81L_{Total}$
80	$\left[ \frac{1.34L_{Total} - 1.42L_{Total}}{L_{Total}} \right] L + 1.42L_{Total}$

d) 8-inch Casing Jacking Force (tons)

Coverage (%)	VCP
50	$2.3 + \left[ \frac{0.36L_{Total} - 0.49L_{Total}}{L_{Total}} \right] L + 0.49L_{Total}$
80	$3.4 + \left[ \frac{0.62L_{Total} - 0.49L_{Total}}{L_{Total}} \right] L + 0.49L_{Total}$

e) 8-inch VCP Jacking Force (tons)

Coverage (%)	VCP
50	$0.36L_{Total}$
80	$0.62L_{Total}$

where  $L_{Total}$  = Total drive length (m)

$L$  = Chainage of current phase (m)

Work by Bennett (1998) involved field measurement and data collection from three microtunneling installations at the WES test facility in Vicksburg, MS. The WES test facility consisted of six different soil types with slope transitions to evaluate jacking forces in each soil type and under mixed face conditions. In addition, he reviewed case studies in sands, clays, and silts from 39 microtunneling projects. He contributes jacking resistance as the sum of the face pressure and the frictional resistance. The model he developed, Equation 5.7, predicts the frictional jacking force component as a function of the pipe's surface area, normal stresses imposed on the pipe wall, and a coefficient of friction. He applies reduction factors to account for arching effects in the soil and to establish a friction coefficient representing the soil-pipe interface behavior.

$$F_r = C_a \gamma' d_p \tan(C_f \phi_r) A_p L \quad (5.7)$$

Where  $C_a$  = Arching reduction factor

$C_f$  = Friction reduction factor

$\gamma'$  = Effective soil unit weight

$d_p$  = Pipe diameter

$\phi_r$  = Residual soil friction angle

$A_p$  = Pipe circumference

$L$  = Length of bore

Geotechnical parameters found in the geotechnical report for the Reid Drive Interceptor Project did not include the residual friction angle; however, the peak friction angle was given as 31 degrees. In order to account for the residual shear strength of the soil, which is likely to control frictional forces along the soil-pipe interface, and to appropriately apply Equation 5.7, the residual soil for the soil should be determined. A



study by Pineda-Jaimes and Colmenares-Montañez (2011) evaluated the residual and peak friction angles of a soft clay and a soft clay-concrete interface from Shelby tube samples from a lacustrine deposit in Bogotá, Columbia. To obtain the soft clay-concrete interface strengths they performed direct shear tests where a concrete surface was placed in one half of the shear box and soft clay was placed in the other half, following the ASTM D-3080 standard. Shear stresses were applied once primary consolidation had occurred, after the placement of 50, 100, and 150 kPa normal stresses. They concluded that the peak angle of soft clay-concrete interface resistance is 0.8 to 0.95 times the peak angle of soil resistance. Furthermore, they found that the residual angle of soft clay-concrete interface and the residual angle of soil resistance equaled the peak angle of soft clay-concrete interface resistance. Thus, the residual angle of soil resistance ranged from 0.8 to 0.95 times the peak angle of soil resistance. Application of their findings does not directly apply to soils in the Reid Drive Intercept, but the relationship between peak and residual soil angles of friction may be used as guideline for estimating an appropriate residual soil friction angle. Peak and residual friction angles for the Bogotá clay used in the study were seventeen and fifteen degrees.

In a paper submitted by Skempton (1985), the post-peak drop in drained shear strength was evaluated for soils with varying percentages of clay sized particles. It was found that soils with the clay fraction less than about 25% residual friction angles are similar to those of a sand or silt, with a value typically greater than 20 degrees. When the clay fraction was greater than 50%, the residual friction angle was much lower. Clay composed of Kaolinite, illite or clay mica, and montmorillonite minerals exhibited residual friction angles of 15, 10, and 5 degrees, respectively.

Due to the silty clay soil having trace amounts of fines and the absence of sieve analysis test results in the geotechnical report, a residual friction angle of 25 degrees was assumed to be representative of the soil on the Reid Drive Interceptor Project, based 80% of the 31 degree peak friction angle. Thus, Bennett's predictive model (1998) was applied with 25 degrees as the residual friction angle.

Bennett's best fit friction and arching reduction factors were utilized for this study to observe how the recorded data fit against his best predictive model. All phases of the PTMT and PT/HDD methods employed on the Reid Drive Interceptor Project were lubricated in non-dewatered soil. Drives one through four and five through seven traversed through medium stiff and stiff clays, respectively. As such, the arching and friction factors used for drives one through four were 1.5 and 1.0, respectively, and the arching and friction factors used for drives five through seven were 0.5 and 0.5, respectively. The only phase where Equation 5.7 may be directly applied is during jacking of the pilot tubes. During jacking of the casing and VCP, Equation 5.7 needs to be altered to take into account transitioning from friction due to the pilot tubes and casing to the casing and VCP, respectively. This approach is similar to that used to apply Equation 5.2 for use in PTMT installations. Equations 5.8, 5.9, and 5.10 describe the frictional forces that should develop for pilot tube and 21-inch casing and VCP installations, respectively. Equations 5.11 and 5.12 should be used for installation of 8-inch casing and VCP, respectively. Simplification processes used in developing Equations 5.8 through 5.11 are shown in Appendix C.

$$F_r = C_a \gamma' \tan(C_f \phi_r) (0.394 ft^2) L \quad (5.8)$$

$$F_r = C_a \gamma' \tan(C_f \phi_r) \left[ \left( \frac{(14.186 ft^2)L_{Total} - (0.394 ft^2)L_{Total}}{L_{Total}} \right) L + (0.394 ft^2)L_{Total} \right] \quad (5.9)$$

$$F_r = C_a \gamma' \tan(C_f \phi_r) \left[ \left( \frac{(12.566 ft^2)L_{Total} - (14.186 ft^2)L_{Total}}{L_{Total}} \right) L + (14.186 ft^2)L_{Total} \right] \quad (5.10)$$

$$F_r = C_a \gamma' \tan(C_f \phi_r) \left[ \left( \frac{(2.731 ft^2)L_{Total} - (0.394 ft^2)L_{Total}}{L_{Total}} \right) L + (0.394 ft^2)L_{Total} \right] \quad (5.11)$$

$$F_r = C_a \gamma' \tan(C_f \phi_r) (2.731 ft^2) (L_{Total}) \quad (5.12)$$

To arrive at an estimated total jacking force, face pressure needs to be added to Equations 5.8 through 5.12. Bennett (1998) states that face pressures during microtunneling operations are usually a small component of the overall jacking force. Additionally, face pressures are highly dependent on the rate of advancement and the allowable machine torque. If the torque required to excavate the borehole increases to an undesirable level, advancement is slowed, essentially decreasing the face pressure to allow for easier excavation, and vice versa. This phenomenon occurred during jacking of casing on the Reid Drive Interceptor Project, as the operator would cyclically advance, pause, advance, and pause to relieve stress on the auger string. To calculate jacking force due to face pressure, consideration as to the earth pressure, groundwater pressure, and face area should be given. Bennett refers to methodology from Weber (1981) (Equation

5.13), as reported by Stein et al. (1989), to calculate the jacking force due to face pressure for auger type excavation methods in pipe jacking. It should be noted that the coefficient of load bearing capacity,  $\lambda$ , is equivalent to the bearing capacity reduction factor and increases as  $\phi$  increases from 0.05 at  $\phi = 0^\circ$  to 0.20 at  $\phi = 25^\circ$ , to 0.75 at  $\phi = 40^\circ$ , and to 1.00 at  $\phi = 42^\circ$ . For the silty clay soil with a peak friction angle of  $31^\circ$ , from the Reid Drive Interceptor Project,  $\lambda$  is approximately 0.42.

$$F_p = \lambda \pi D t \left( c + \gamma \left( h_c + \frac{d_b}{2} \right) \tan \phi \right) \quad (5.13)$$

Where  $F_p$  = Jacking force due to face pressure

$\gamma$  = Unit weight of soil

$c$  = Cohesion

$h_c$  = Height of soil cover above pipe crown

$d_b$  = Bore diameter

$\phi$  = Peak internal angle of soil friction

$D$  = Auger screw diameter

$t$  = Cutting edge thickness

$\lambda$  = Coefficient of load bearing capacity.

Development of Equation 5.13 was spawned after it was realized that the mechanisms controlling face pressure during advancement of microtunneling machines is quite different from tip bearing during pile load tests. A pile tip creates a passive failure in the soil as it is advanced. Excavation at the face of a microtunneling machine, on the other hand, partially relieves the soil stresses and does not induce passive failure. Thus, Equation 5.13 results in a jacking force due to face pressure that is less than what would

be calculated using pile tip methodology. Jacking of pilot tubes, however, is more likely to follow pile tip methodology. Consequently, deviation from using Bennett's frictional model with Weber's face resistance model was necessary to predict jacking forces during pilot tube advancement. Chapman's face resistance methodology for push-in type installations was adopted, resulting in a face resistance of 2.5 tons and 5.1 tons for 60% and 90% coverage of pilot tube jacking, respectively.

Staheli's work (1996) involved developing an analytical model to determine the jacking forces during microtunneling operations. She describes how the face pressure during these operations is between the active and passive lateral earth pressure, as the face pressure must remain within these bounds to prevent surface settlement and heave. Resultantly, she sets the face pressure equal to an average of the active and passive lateral earth pressures. In cohesionless or permeable soils, ground water pressure was added to the average lateral earth pressure to account for the added resistance due to ground water head. In clay soils, ground water head is not likely to permeate through the soil at a fast enough rate to increase the face pressure against the front of the microtunneling shield. Therefore, in clay soils the groundwater pressure was omitted from the face pressure formula.

An average of the active and passive earth pressure will most likely accurately predict the face pressure during the second phase of PTMT, jacking of the casings. Although, the behavior of pilot tubes advancing through soil involves different mechanisms, as soil is displaced rather than excavated. Thus, the passive earth pressure is taken to represent face pressure during jacking of pilot tubes. Equations C.7 through C.10 illustrate how the Rankine active and passive effective lateral earth pressures were

obtained. Ground water pressure has been omitted as the monitored installations of this study proceed through clay soils. As previously mentioned, there is zero face pressure during phase three as the borehole has already been established.

In Staheli (2006), extensive laboratory work was conducted to establish soil-pipe residual interface friction coefficients for various pipe materials sheared against two cohesionless soils with different residual friction angles (Table 2.1). Results were interpolated and extrapolated to estimate soil-pipe interface friction coefficients for soils with residual friction angles ranging from 25 to 40 degrees. Frictional jacking force was then determined to be equal to the product of the soil-pipe interface friction and the normal force, derived from Terzaghi's Arching Theory. Thus, the frictional and total jacking force may be determined by implementing Equation 5.14 and Equation 5.15, respectively. Akin to the methodology of applying the jacking force models by Chapman and Ichioka (1999) and Bennett (1998) to model behavior intrinsic to PTMT installations, the friction jacking component from phases two and three transitions from that equated with an entire drive length of pilot tubes and casings to an entire drive of casings and VCP, respectively, when applying Equations 5.14 and 5.15.

$$JF_{frict} = \mu_{int} \frac{\gamma \cdot r \cdot \cos\left(45 + \frac{\phi_r}{2}\right)}{\tan\phi_r} \cdot \pi \cdot d \cdot l \quad (5.14)$$

where  $JF_{frict}$  = Frictional component of jacking (tons)

$\mu_{int}$  = Pipe-Soil residual interface friction coefficient (Table 2.1)

$\gamma$  = Total unit weight of the soil (tons/ft<sup>3</sup>)

$\phi_r$  = Residual friction angle of the soil (degrees)

$d$  = Pipe outside diameter (ft)

r = Pipe radius (ft)

l = Length of pipe (ft)

$$JF_{Total} = F_P \cdot \pi \cdot \frac{d^2}{4} + \mu_{int} \frac{\gamma \cdot r \cdot \cos\left(45 + \frac{\phi_r}{2}\right)}{\tan\phi_r} \cdot \pi \cdot d \cdot l \quad (5.15)$$

where  $JF_{Total}$  = Total jacking force (tons)

$F_P$  = Effective lateral earth pressure (tons/ft<sup>2</sup>)

### 5.3.1 Comparison of Select Jacking Force Predictive Models to Collected Data

The usefulness in adopting the microtunneling jacking force predictive models of Chapman and Ichioka (1999), Bennett (1998), and Staheli (2006) to predict jacking forces for the PTMT methodology varies depending on which phase of the PTMT process the model is being used to predict. One of the select predictive models may adequately predict pilot tube jacking forces while failing to capture the thrust force generating mechanisms of casing installation. Furthermore, one model may better represent the face resistance component of a PTMT phase, whereas the frictional jacking force component may be best represented by another. Accordingly, the predictive models need to be evaluated based on their face and frictional components on a phase by phase basis. Table 5.6 indicates the models that best represented each phase of the PTMT methodology. The following text describes the applicability of each model for each PTMT phase beginning with phase one, pilot tube jacking, and proceeding through phases two and three, casing and VCP installation.

Table 5.6 Most Applicable Models for Each PTMT Phase

Phase	Frictional Component	Face Component
Pilot Tube	Staheli	Chapman and Ichioka 60%
21" Casing	Staheli & Chapman and Ichioka 50%	Staheli & Chapman and Ichioka 50%
8" Casing	Bennett	Staheli
21" VCP	Staheli	N/A
8" VCP	Bennett	N/A

Figures A.57 to A.61 compare the gathered pilot tube thrust force data with the predictive models with respect to drive length for drives one through five. It was found that face resistance was most accurately predicted by Chapman and Ichioka's 60% coverage model, in which the face pressure is estimated to be 200 tons/m<sup>2</sup>. The face pressure in the medium stiff silty clay soils from drives one through four were 250, 300, 150, and 200 tons/m<sup>2</sup>, respectively, with an average of 225 tons/m<sup>2</sup>. Drive five, which mostly consisted of stiff silty clay soils, had a face pressure of 350 tons/m<sup>2</sup> and was more accurately predicted by his 90% coverage model. The face pressure predicted based on Staheli's model was consistently low. In traditional microtunneling an average of the passive and active lateral earth pressure is a valid estimate of the face pressure to be encountered during shield advancement, as the face pressure is kept within this range to prevent settlement and heave. With pilot tube jacking the soil undergoes passive failure as it is being displaced by the lead pilot tube, and therefore, the passive pressure is exceeded during pilot tube advancement. Bennett did not prescribe a specific face resistance prediction model, but like Staheli, he noted that the face pressure is generally between the active and passive lateral earth pressure for microtunneling installations. Since Chapman and Ichioka's face pressure prediction was the most applicable to this



study, his 90% and 60% face pressure predictions were used as a baseline for predicting jacking forces with Bennett's frictional model.

Staheli's predictive model for friction development throughout the length of a drive best represented the pilot tube installation behavior. Frictional jacking stresses during the pilot tube installations were low and only noticeable during drives one and two, which had frictional jacking stresses of 4.5 and 9.5 lbs/ft<sup>2</sup>, respectively. Models based on Staheli (2006), Bennett (1998), and Chapman and Ichioka (1999) predicted frictional jacking stresses of 10, 17, and 270 lbs/ft<sup>2</sup>, respectively. The low friction stresses experienced during the Reid Drive Interceptor Project's pilot tube installations may have been attributable to abundant use of lubrication.

The soil-pipe interface friction coefficient used in adopting Staheli's friction stress predictive model was 0.38, representing a steel pipe against a soil with a residual angle of friction of 25 degrees in a non-lubricated scenario. An internal angle of friction of 4 degrees is typical of Wyoming bentonite (Staheli 1996). In situations where bentonite mixes with the surrounding soil, which is likely during pilot tube jacking, the mobilized friction angle of the bentonite/soil mix can be estimated as one-third the internal angle of friction of the soil. This would result in a soil-pipe interface coefficient of tangent ( $\phi/3$ ), lowering the predicted frictional jacking stress from 10 lbs/ft<sup>2</sup> to 4 lbs/ft<sup>2</sup>.

Chapman and Ichioka's push-in predictive model was based on data from 49 microtunneling installations, which were subdivided into drives through clay and drives through sand. The lack of abundant data relating frictional jacking stresses to machine diameter in clay soil, deficient documentation regarding the use of lubrication, and the

absence of other soil parameters from the predictive model may have led to the large overestimate of the frictional jacking force required. Bennett's model takes lubrication into account through the use of his arching and friction reduction factors; however, his friction prediction slightly overestimates the collected data. If a smaller friction angle had been used, say 15 degrees, his frictional stress estimate would have been reduced from 17 to 10 lbs/ft<sup>2</sup>. Staheli's published soil-pipe interface friction coefficients did not extend to friction angles below 25 degrees. Being that 25 degrees is a reasonable estimate for the residual friction angle and for consistency of comparison between the models, Bennett and Staheli's models were fitted with a 25 degree residual friction angle.

During 21-inch casing installations, frictional stress throughout the silty clay was rather minimal, due to abundant lubrication and the ¼ inch radial overcut provided by the reamer. Jacking force increases seemed to be largely affected by the cutting head and reamer passing through more resistive soil material, which was believed to be a cemented sandy soil. Upon exiting the more resistive soil, jacking forces would decrease to a level approximately equal to what they were before entering the cemented soil. Ignoring these isolated thrust force increases, the 61 lbs/ft<sup>2</sup> frictional jacking stress predicted by Staheli was the most applicable for representing the frictional resistance of the 21-inch casings. Using a soil-pipe interface friction coefficient of tangent ( $\phi/3$ ), representative of a lubricated scenario, would have reduced the frictional jacking force from 11 lbs/ft and 407 lbs/ft to 4 lbs/ft and 157 lbs/ft for the beginning and end of the phase two PTMT process, respectively, and would have better represented the field data.

Although Staheli best predicted the frictional jacking stress for 21-inch casings, the transition from the frictional force due to a full drive length of pilot tubes to a full

drive length of casings was best represented by Chapman and Ichioka's 50% coverage model, as there was less of a difference between their pilot tube frictional jacking force and casing frictional jacking force than the other models. The Chapman and Ichioka model predicts the jacking stress to decrease from 270 lbs/ft<sup>2</sup> to 74 lbs/ft<sup>2</sup> as the drive transitions from an entire span of pilot tubes to an entire span of casings. Incorporating pipe circumference, their frictional force increases linearly from 300 lbs/ft to 496 lbs/ft from the beginning to the end of casing installation. Bennett's model based on the best fit arching and friction reduction factors for clay of medium stiffness overestimated the frictional jacking stress. Adjustment of the reduction factors to represent a stiffer and more stable borehole would have resulted in better representation of the frictional forces incurred throughout most of the installations.

Determining the correct model to represent face resistance during phase two operations was more difficult than for phase one. During phase one, the jacking force at the beginning of the installation is almost entirely due to resistance at the face, as there is limited soil-pipe interface surface area for friction to act on. In phase two, the jacking force at the beginning of jacking of the casing is representative of the face resistance to penetrate the larger diameter casing with auger flights and the friction resistance to push the pilot tubes into the reception shaft. The cumulative effect of the predicted pilot tube friction resistance and auger boring face resistance was generally over predicted by Chapman and Ichioka and under predicted by Bennett and Staheli. The high pilot tube frictional jacking stress predicted by Chapman and Ichioka allowed for a strong prediction of the starting jacking force during phase two of the 200-ft drive three. For longer drives, the high pilot tube frictional jacking stress led to an overestimate. Staheli's

prediction was most suitable for the longer drive lengths due to the smaller frictional jacking stress her model predicts for the pilot tubes. It should be noted that the face pressure model (Weber 1981) used in conjunction with Bennett's friction prediction model to predict jacking force for the PTMT methodology drastically under predicted the face pressure during casing and auger advancement. This face pressure model was derived from the shear strength of the soil at the depth of the center of the casing, the circumference of the augers, thickness of the cutting edge, and a bearing capacity factor that is based on the friction angle of the soil.

Staheli's frictional force model best represented the pilot tube behavior and thus provides a good baseline for estimating the penetration stress during casing advancement. From Figures A.62 to A.65, it can be seen that the starting jacking forces ranged from 25 to 50 tons. Staheli predicted a frictional jacking force of 2 to 3 tons for a full drive length of pilot tubes. If this is subtracted from the starting jacking forces, the force due to face resistance may be obtained. This suggests that the face resistance during phase two operations ranged from 6 to 13 tons/ft<sup>2</sup>.

A similar methodology was used to determine the face resistance during the 8-inch casing installation during drive number five. From Figure A.61 it can be seen that the thrust force required to install pilot tubes remained relatively constant throughout the length of the drive. Bennett's friction model predicted an increase of only 330 lbs from the beginning of the drive to its end, 120-ft later. Thus, the jacking force at the onset of jacking the 8-inch casings is mostly composed of face resistance at the front of the casing and auger. From Figure A.66 it can be seen that the face resistance is about 15 tons, or 26 tons/ft<sup>2</sup>.

The combination of Staheli's friction model for pilot tubes and her face pressure estimate for casing advancement best represented the thrust force at the beginning of the 8-inch casing installation. Frictional stress, again, was minimal and best represented by Bennett's model. Chapman and Ichioka's model actually predicted a decreasing frictional resistance as the length of the drive increased. The predictive model he uses to estimate frictional stress was developed statistically through observations of push-in and auger type installations. The influence of the increased diameter of the 8-inch casings on increasing frictional forces did not outweigh the decrease in frictional forces due to the alternative advancement technique. Frictional stress during auger boring installations is typically less than that of push-in installations, due to the fact that a borehole slightly larger than the OD of the casings is excavated, whereas during pilot tube advancement the soil is being displaced to make room for the incoming pilot tubes. During 21-inch casing installations, the larger diameter proved to be more influential than the alternative installation method.

Staheli's model tended to better predict thrust force during installation of the final 21-inch nominal ID VCP product, however, since her estimate of the friction force resulting from pushing a full drive length of casings was over predicted, the thrust force at the beginning of phase three was also over predicted. This over prediction was present in all of the authors' jacking force models. As the total jacking force for phase three transitions from the friction force required to push an entire drive of casings to an entire drive of VCP pipe, face pressures are non-existent. A strong comparison of the frictional forces for pushing the 25.5-in outside diameter casing to that of pushing the 24-in outside diameter VCP is not able to be confidently obtained, due to the problems experienced

with the L1 pressure transducer, as described in Appendix D. Even though a sound conclusion cannot be ascertained, it is hypothesized that the decrease in friction resistance due to the smaller pipe diameter is offset by the increased roughness of the vitrified clay over the steel, and a jacking force between 25 and 30 tons is to be expected.

When comparing recorded thrust data to the predictive models for jacking of the 8-inch VCP, jacking forces due to advancement of the casing and VCP was over predicted by Chapman and Ichioka and Staheli and slightly under predicted by Bennett. Staheli's model was the only one to account for increased frictional resistance due to the transition of the pipe material. Although this behavior was expected as the pipe string transitions from steel to VCP of a constant OD, the jacking force data did not indicate a jacking force increase from the beginning to the end of the drive. Adjustment to Staheli's interface friction coefficient to account for lubrication would have resulted in a well fit model by reducing the jacking load at the beginning to 1.8 tons, about 0.2 tons less than what was recorded. Increasing the arching and friction reduction factors used in Bennett's model to be representative of the upper bound for a stiff to hard clay as opposed to his best fit factors would yield a jacking force at the beginning of phase three of 2 tons as opposed to 1.2 tons and would fit the data very well. In this case, his model indicates that the soil consistency is on the soft side of the stiff to hard clay classification.

## **CHAPTER 6: CONCLUSIONS AND RECOMMENDATIONS**

PTMT is a trenchless technology ideal for the installation of gravity fed sewers in urban environments. Appropriate application of this technology can aid with repairing and expanding the deteriorating U.S. underground infrastructure system in an efficient and cost effective manner. Maximizing cost effectiveness is crucial, as capital investment needs over the next twenty years for wastewater and storm water pipelines alone is estimated to \$224 billion (ASCE 2013). Understanding PTMT installation behavior in terms of the factors affecting productivity and jacking forces will allow engineers, manufacturers, and contractors to fine tune the PTMT methodology to minimize costs and risks.

To gain insight towards PTMT installation behavior, jacking frames were fitted with hydraulic pressure transducers to monitor hydraulic pressures during seven distinct PTMT installations from the Reid Drive Interceptor Project in Appleton, WI. Knowledge of the jacking ram dimensional specifications enabled conversion between the recorded ram hydraulic pressures and the jacking or pull-back force output from the jacking frame. Rotational torque was able to be determined through linear interpolation between minimum and maximum jacking frame hydraulic pressures and rotational torques, as specified by the manufacturer. Recorded data was time stamped, which allowed for the data to be analyzed with respect to time, paving the way for productivity analysis.

### **6.1 Productivity Conclusions**

Identifying expected pipe installation cycle durations, average installation rates, and the factors that influence productivity for all three phases of the PTMT methodology were the objectives of this productivity analysis. Fundamental to achieving this goal was

being able to detect cyclic patterns within the time series data representative of the installation of a single pilot tube, casing, or product VCP. The typical pattern of installation cycles from each phase are detailed in Section 4.1.

Once the cycle patterns are identified for each PTMT phase, valuable information pertaining to the factors that affect productivity may be obtained through analysis of the distribution of the cycle durations. It was found that when graphing the number of cycles that occurred within specific duration intervals, most phases exhibited a skewed exponential distribution about the median cycle duration, with more cycles beyond the median duration than quicker than the median duration. The cycle duration frequency distributions for each PTMT phase may be found in Section 4.2. General cycle duration characteristics for each PTMT phase are outlined in Table 6.1.

Table 6.1 Cycle Duration Characteristics for PTMT Installations

Phase	Number of Cycles Observed	Reasonable Minimum (min)	Median (min)	Mean (min)	Mean + Standard Deviation (min)
Pilot Tube	605	0.7	1.1	1.3	2.3
8-in VCP	37	2.5	3.0	3.9	6.4
21-in VCP	95	4.0	6.8	7.5	10.6
8-in Casing	37	5.0	12.6	14.8	24.5
21-in Casing	176	20.0	29.0	33.0	45.6

Since the length of pilot tubes, casings, and product VCPs are known, installed distance with respect to time may be observed once each cycle is identified within the data stream. It was noticed that as drive length increases productivity tends to decrease. This may be attributable to fatigue or due to the increased jacking forces due to higher frictional resistance. Towards the end of all installations, there was a substantial reduction in productivity observed. As a PTMT phase approaches completion, communication



between crew members in the jacking and reception shafts increases to make sure there is appropriate clearance for the pilot tube, casing, or product VCP to be jacked into the reception shaft and to make sure it is jacked to sufficient distance.

Average installation rates for each PTMT phase are shown in Table 6.2. If delays are able to be kept to a minimum and high project efficiency can be maintained, the average installation rate should approach the median installation rate. The percent change from the average to median installation rates are also shown in Table 6.2. Greatest efficiency gains may be realized during jacking of the pilot tubes, where the added time due to delay is significant in proportion to the average cycle time. In general, as the average cycle time of a phase increases a delay of a specific duration has less of an effect on the overall efficiency. However, minimizing delays during operations with slow installation rates will result in the greatest time savings over the length of a drive.

Table 6.2 Comparison of Average and Median Installation Rates

Phase	Installation Rate (ft/hr)		% Increase	Time Saved Per 400 FT Drive (hours)
	Average	Median		
Pilot Tube	102	136	34%	1.0
21-in VCP	63	71	12%	0.7
8-in VCP	51	67	31%	1.9
21-in Casing	15	17	13%	3.2
8-in Casing	13	16	17%	4.4

Ground conditions are ranked as the highest factor that affects PTMT productivity (Gottipati 2011). Ground conditions were relatively constant throughout the Reid Drive Interceptor Project, although there were a few instances where the operator experienced high resistance to installation and hypothesized that the installation was proceeding through a section of hardpan, or cemented soil. Decreases in productivity were observed in these instances. This may have been due to a combination of the higher soil resistance

and the operator proceeding at a slightly slower rate to ensure adequate lubrication and stabilization of the borehole.

Another factor that played an influence on productivity was that of the pipe dimensions. Cycle times for the 8-in casings and VCPs were considerably shorter than those for the 21-in casings and VCPs; however, the pipes were also 4.5 feet shorter. The smaller pipes were easier to load onto the jacking frames and connect to the previously installed sections, leading to quicker and more efficient readying of the pipe for installation. On the other hand, drives with shorter pipes require more pipes to complete the installation, causing a greater proportion of cycle time being apportioned to non-advancement operations. All in all, it was found that installation rates were slower with shorter pipes, even though they were easier to ready for installation.

The largest and most well defined change in productivity was observed when comparing 21-inch VCP installation rates between the first and second drive. Phase three productivity is largely dependent on the efficiency of the reception shaft crew in dismantling and removing the casings, as jacking of the next product pipe must be stalled until the casing is removed. The veteran crew used on drive two was able to optimize their technique in dislodging the casings and augers in the reception shaft to a point where the jacking shaft crew did not have to wait to proceed with product pipe jacking. For this reason, the greater experience of the crew on drive two results in a time savings of two hours for completing a phase three installation for a drive length equal to the average length of drives one and two (398 feet).

The above analysis was completed through manual interpretation of the collected data. Automatic pattern recognition through the use of ANN, BP ANN, and anomaly

detection algorithms was explored as an alternative approach to understanding typical installation cycle behavior and productivity for each phase of the PTMT methodology. It was found that these algorithms were successful in identifying which pressure transducer was responsible for monitoring each phase, detecting the installation cycles within each phase, and pinpointing the distinct operations with the typical installation cycles. Use of the algorithms for this study was namely to demonstrate their ability in obtaining quality productivity and workflow behavioral characteristics and to present preliminary productivity results in a more time efficient manner than manual interpretation.

## **6.2 Jacking Force Conclusions**

Knowledge of how jacking forces are influenced by ground conditions and installation characteristics is essential towards reducing risks due to uncertain jacking forces, designing thrust reaction walls in the jacking shaft, and selecting appropriate product pipe specifications. The required jacking force to advance pipe sections through the soil is due to penetration resistance at the lead pipe and friction resistance developed along the soil-pipe interface. In pipe jacking and microtunneling installations, jacking resistance due to frictional development largely controls the maximum jacking force throughout a drive. Since the frictional forces are cumulative, the maximum force is observed towards the end of the drive. In this study, methodology for determining the jacking force throughout PTMT installations by instrumenting the jacking frames with hydraulic pressure transducers was explored. General trends relating factors such as pipe diameter, installation depth, soil type, stoppages, lubrication, and operator technique to jacking force were identified. Jacking force predictive models by Chapman and Ichioka

(1999), Bennett (1998), and Staheli (2006) were utilized to decipher their applicability in predicting jacking forces for the PTMT methodology.

### **6.2.1 General Trends**

Table 5.3 outlines the hierarchy of PTMT phases with regards to jacking force. Jacking of the 21-inch casings resulted in the highest forces, commonly between 35 and 60 tons. Forces were high during this phase due to the large casing circumference of which the friction acts upon and the penetration resistance due to enlarging the borehole. Maximum jacking forces during advancement of the 8-inch casings were about 15 tons. Complete isolation of the effect of pipe diameter on jacking forces between the 21-inch and 8-inch drives was not possible, as the 8-inch installation was through slightly stiffer silty clay at a shallower depth, but it is highly likely that the lower jacking force for the 8-inch pipe was due to the smaller diameter. Comparison of the 21-inch and 8-inch VCP installations produced similar results. The larger product pipes required about 35 tons, whereas the smaller product pipes required about 3 tons. Forces during jacking of the 8-inch VCP were actually the lowest of all PTMT phases, most likely due to the absence of penetration resistance.

Contrary to pipe diameter, installation depth was not strongly correlated with jacking force. This may be attributable to Terzaghi's Arching Theory. Furthermore, the stiffness of the silty clay varied between the deep and shallow installations, shadowing the influence of depth of cover.

As previously mentioned, the consistent soil borings from the Reid Drive Interceptor Project did not allow for examination of the jacking force through a wide range of soil types, nor were the borings frequent enough to identify localized sections of

more resistive soil. Thrust force variance between silty clay soils of stiff and medium consistency was insignificant. However, there were several locations where hydraulic pressure in the jacking rams substantially increased and then decreased at a short distance afterwards. These locations likely were composed of cemented soil particles, or hardpan. Drive two is a prime example of how jacking forces respond to this soil type. Another example of the effect of hardpan on jacking forces is that of drive six (PT/HDD), where high pull-back forces overstressed the HDPE pipe and caused pipe failure. Jacking force behavior throughout these drives is discussed in detail in Section 5.2.2.

Consequence to the pipe failure during drive six, drive seven (PT/HDD) was completed with a pre-reaming phase to limit pull-back forces. It was found that pull-back force reductions of 44% at the start and 27% at the end between the pre-ream and pull-back operations were realized. Actual benefits of pre-reaming are likely to be higher, as the pre-ream forces would have been higher had the reamer been trailing a continuous string of HDPE pipe.

In addition to more resistive soils, delays or stoppages during an installation can result in increased jacking forces due to relaxing of the soil around the borehole causing increased normal force against the pipe string. Soils on this project were mainly medium stiff silty clay of low plasticity, which is an ideal soil for tunneling due to its high stability and low volume change characteristics. When comparing jacking forces between delays of varying duration, slight thrust force increases were observed. However, longer durations did not always result in higher increases in thrust force. Consequently, a strong correlation between delay and increased jacking forces was not attainable. There was one instance, on the other hand, where the impact to delay was substantial and caused

significant project setback. Data logging equipment was not available to capture this behavior, although this example is discussed in detail in Section 5.2.3 based on documented field notes.

Substantial friction development throughout the length of most of the PTMT drives on the Reid Drive Interceptor Project was not observed. Adequate lubrication during phases one and two may have attributed to the minimal frictional forces. However, direct correlation between thrust forces for drives using higher concentrations of bentonite to water and a higher volume application to those with less applied lubrication of a lower concentration was not noticeable. Regardless, there were two instances where the beneficial effect of lubrication on lowering frictional forces could be observed. These examples are discussed in Section 5.2.4.

Lubricant application and attention to detail, with regards to the project specified slopes, can influence jacking forces and project productivity. These factors are highly controlled by the jacking frame operator. In addition to these factors, the rate and style of advancement adopted by the operator to jack pilot tubes, casings, or product VCPs has an influence as well. An instance where three different operators were used to install 21-inch casings highlighted the variability in productivity and jacking forces with installation technique. Detailed description of this phenomenon is discussed in Section 5.2.5. In short, consistent advancement promotes kinetic friction at the soil-pipe interface, lowering jacking forces. If difficulties with transporting spoil from the face to the jacking shaft transpire, or if jacking forces are high, a slower advancement rate may be adopted to reduce pressure at the face and ease the auguring operation.

### **6.2.2 Applicability of Existing Jacking Force Predictive Models**

Existing models from Chapman and Ichioka (1999), Bennett (1998), and Staheli (2006) were adopted for use in predicting jacking forces during each phase of the PTMT process. Since these models were developed for microtunneling and pipe jacking methodologies, alteration to their equations was necessary to capture the distinct behavior of PTMT installations. Pilot tube jacking displaces the soil, which causes the face penetration resistance to exceed the passive lateral earth pressure of the soil. Furthermore, the limited radial overcut provided by the steering head on the lead pilot tube, 0.375 inches, is generally less than the overcut provided by the tunnel boring machine used in microtunneling or pipe jacking operations. Penetration resistance during casing advancement needs to be applied to the difference in area between the casing reamer and the pilot tube, as the pilot tubes are advanced in front of the casings. Frictional resistance during casing advancement transitions between an entire drive length of pilot tubes, at the onset of installation, to an entire drive length of casings upon completion. Face resistance is non-existent during product VCP jacking as the borehole size was already enlarged to a diameter greater than the VCPs during phase two. Consequently, jacking forces experienced during phase three transition from the friction resistance of an entire drive length of casings to an entire drive length of VCPs from the beginning to the end of the phase.

Each of the selected existing models were developed based on different methodologies. Fundamentals to each model and the models' general suitability for predicting jacking forces during PTMT operations are discussed in this Chapter. Detailed methodology and applicability of the models can be found in Section 5.3.

Chapman and Ichioka's models are based off of the dimensions of the pipe, whether the soil is clay or sand, and whether slurry, auger, or push-in type microtunneling was used. They developed predictive models based on statistical analysis of an extensive database of microtunneling jacking forces to estimate the maximum jacking force expected to cover various percentages of the collected data. It was found that Chapman and Ichioka most accurately predicted the face component of jacking force during pilot tube and 21-inch casing advancement and the jacking force transition between a full drive length of pilot tubes to a full drive length of 21-inch casings during phase two.

Bennett's model was based on an extensive field experiment where the effect of soil type, lubrication, and de-watering on jacking force was able to be isolated and from review of 39 microtunneling case studies in sand, silt, and clay soils. He related the frictional jacking force to the effective unit weight of the soil, the residual angle of friction of the soil, pipe diameter, and arching and friction reduction factors to account for stress reduction due to Terzaghi's Arching Theory. Upper bound, best fit, and lower bound estimates of the friction resistance were established. He describes how jacking force due to penetration resistance is largely controlled by the torque required to excavate the borehole, but explains how face resistance is kept between the active and passive lateral earth pressure to prevent surface settlement or heave. He outlines work from Weber (1981), in which a face resistance formula was developed for auger-boring installations. When adopting Bennett's methodology for use in PTMT jacking force prediction, his frictional jacking force relationship was utilized in conjunction with face resistance methodologies from Chapman and Ichioka for phase one and Weber for phase



two. Chapman, Ichioka, and Weber's face resistance methodologies were used due to their direct application to the push-in and auger-boring methodologies. It was found that Bennett most accurately predicted the frictional component of jacking force for 8-inch casing and VCP installation.

Akin to Bennett's methodology for determining face resistance, Staheli documented how face pressures were maintained between active and passive lateral earth pressure to prevent settlement and heave. She suggested that an average of the two may be used to estimate the face pressure. This approach was utilized in phase two, where the auger-boring methodology was believed to be between the active and passive lateral earth pressure. Although during phase one, the face resistance was set equal to the passive lateral earth pressure to simulate the displacement behavior of the soil inherent to pilot tube advancement. Her frictional resistance model operates based on the residual angle of friction of the soil, the soil unit weight, pipe radius, and the coefficient of pipe-soil interface friction based on extensive laboratory testing between numerous pipe materials and sand of two different friction angles. It was found that her model best represented the face component of jacking force during phase two and the frictional component for advancement of pilot tubes and 21-inch casing and VCP.

### **6.3 Recommendations for Further Research**

To date, monitoring of PTMT operations for use in productivity and jacking force analysis has yet to be completed. This study was conducted to explore these behavioral characteristics of the PTMT methodology through means and methods that have been used to study behavior of other trenchless technologies. Data recorded for this study was entirely from seven PTMT, PTMT/Auger Boring, and PT/HDD installations from the

Reid Drive Interceptor Project in Appleton, WI. Acquiring a more extensive database with recorded installations from numerous projects with varying operational parameters would be beneficial towards determining the effect of which those parameters affect productivity and jacking force. These factors may include, but are not limited to, soil type, depth of cover, pipe diameter, lubricant type and application rate, contractor technique, and pipe material. Additional monitoring of product pipe installations is especially desired, as problems with the L1 pressure transducer for this project resulted in only two recorded drives. Ideally, further monitoring would be supplemented with detailed field notes documenting any relevant events, contractor techniques, or change in soil type. Real-time monitoring of drilling fluid application would provide the means to accurately link thrust force and productivity variation with drilling fluid use. Instrumenting a pipe during each PTMT phase, with either jacking load cells placed between pipe joints or contact stress transducers placed on the outer pipe wall, and comparing the outputs to the jacking force output of the jacking frames could provide further insight toward frictional development along the pipe string and aid in isolating penetration stresses from frictional stresses.

In addition to obtaining a more elaborate database of installation behavior, a more in depth productivity and jacking force analysis is possible. Further implementation of automatic data recognition with ANN, BP ANN, and anomaly detection algorithms to identify pipe installation behavior and perform productivity analysis can further pinpoint the factors that affect productivity and the degree of their influence. These algorithms may also be used to link thrust force data with productivity to further conclude upon the effect of high jacking forces on installation rates and crew productivity.

The scope of this study involved comparing existing predictive models developed for the microtunneling and pipe jacking methodologies to the PTMT methodology. Fundamental differences between the installation procedures of these technologies results in misrepresentation of jacking forces predicted with the existing models to those observed during PTMT. Further alteration to the existing models could be performed to better suit their applicability to the PTMT methodology.

All three jacking force models applied in this study were not directly dependent upon soil suction. Bennett's model did distinguish between dewatered and non-dewatered zones in clay and sand, although the effect of soil suction could not be directly identified as the arching and friction reduction factors were developed for dewatered non-lubricated and non-dewatered lubricated zones. In clays above the water table, large capillary stresses may develop causing the effective stress to exceed the total stress. This phenomenon is likely to increase borehole stability as the capillary stresses act like a vacuum, providing suction between the clay particles. Exploration into the effect of soil suction on jacking forces, and more specifically, the normal stress imposed on the pipe wall, may increase the precision of existing jacking force models.

With the addition of a more extensive database to isolate the effects of jacking force parameters and alteration of the existing models, jacking force predictive models for PTMT applications may be developed. Accurate and precise estimation of jacking forces along with detailed understanding of the productivity factors would allow for valuable PTMT simulation models to be created. These models could aid engineers and contractors with developing project schedules, reducing project risk, and evaluating the feasibility of PTMT methods for various proposed installations.

## REFERENCES

- Abbott, D.G. (2005). Practical Considerations in the Selection and for the Use of Microtunneling vs Other Trenchless Techniques. *Proceedings of No-Dig 2005 Conference*. NASTT. Orlando, FL.
- Allouche, E.N. (2002) Implementing Quality Control in HDD Projects—a North American Prospective. *Tunnelling and Underground Space Technology*. 16: 3-12.
- Akkerman Inc. (2013). *Guided Boring Machine (GMB) Technical Manual*. <http://www.akkerman.com/>.
- American Augers Inc. (2013). *Auger Boring Brochure*. <http://www.americanaugers.com/>.
- Ariaratnam, S.T., and Allouche, E.N. (2003) Assessment of Emerging Pulled-In-Place Pipe Products for Trenchless Applications. *Proceedings of Construction Research Congress, Winds of Change: Integration and Innovation in Construction*. Honolulu, HI.
- Ariaratnam, S.T., and Chandrasekaran, M. (2010). Development of an Innovative Free-Swimming Device for Detection of Leaks in Oil and Gas Pipelines. *Proceedings of the 2010 Construction Research Congress*. Banff, Alberta, Canada.
- Ariaratnam, S.T., and Colwell, D.A.F. (2002). Monitoring of HDPE Pipe During Horizontal Directional Drilling Installations. *Proceedings of Pipelines 2002*. ASCE. Calgary, Alberta, Canada.
- ASCE. (2013). Report Card for America’s Infrastructure. American Society of Civil Engineers. Reston, VA. <http://www.infrastructurereportcard.org/>.
- Atkinson, J.H., and Potts, D.M. (1977). Subsidence Above Shallow Tunnels in Soft Ground. *Journal of Geotechnical Engineering*. ASCE. 103.4: 303-215.
- Auld, F.A. (1982). Determination of Pipe Jacking Loads. *Proceedings of Pipe Jacking Association*. Manchester, England, UK.
- Barla, M. and Camusso, M. (2013). A Method to Design Microtunneling Installations in Randomly Cemented Alluvial Soil. *Tunnelling and Underground Space Technology*. 33: 73-81
- Baumert, M.E., and Allouche, E.N. (2002). Methods for estimating Pipe Pullback Loads for Horizontal Directional Drilling (HDD) Crossings. *Journal of Infrastructure Systems*. 8.1: 12-20.

- Baumert, M.E., and Allouche, E.N. (2003). Real-Time Monitoring for Quality Delivery of Directional Drilling Installations. *Journal of Infrastructure Systems* 9.1: 35-43.
- Bennett, D. (1998). Jacking Loads and Ground Deformations Associated with Microtunneling. Dissertation in Partial Fulfillment of the Requirements for the Degree of Doctor of Philosophy in Civil Engineering. University of Illinois at Urbana-Champaign, IL.
- Bennett, D., and Cording, E.J. (1999). Jacking Loads Associated with Microtunneling. *Proceedings of Geo-Engineering for Underground Facilities*. University of Illinois at Urbana-Champaign, Urbana, IL. 731-745.
- Boschert, J. (2007). Pilot Tube Microtunneling Explodes in the U.S. using Vitrified Clay Pipe. *Pipelines 2007*. Advances and Experiences with Trenchless Pipeline Projects. ASCE. Boston, MA.
- Carpenter, R. (2007). 9<sup>th</sup> Annual HDD Survey: Growing Pains: Maturing Market Dealing with Variety of Issues. *Underground Construction*. 1 June. 20-23.
- Chapman, D.N., and Ichioka, Y. (1999). Prediction of Jacking Forces for Microtunneling Operations. *Tunneling and Underground Space Technology*. 14.1: 31-41.
- Craig, R.N., (1983). Pipe Jacking: a State of the Art Review. *Technical Note 112*. CIRIA, London.
- Finnsson, S. (2004). TensiTrak™ - A tension Load and Drilling Fluid Pressure-Monitoring Device for Horizontal Directional Drilling Installations. *Proceedings of No-Dig 2004 Conference*. NASTT. New Orleans, LA.
- French Society for Trenchless Technology. (2004). *Microtunnelling and Horizontal Directional Drilling: Recommendations*. Project National Microtunnels. London: Hermes Science Publishing Limited.
- Gottipati, V. (2011). Pilot Tube Microtunneling: Profile of an Emerging Industry. A Thesis Presented in Partial Fulfillment of the Requirements for the Degree of Master of Science. Arizona State University, AZ.
- Haslem, R.F. (1986). Pipe Jacking Forces: From Theory to Practice. *Proceedings of Infrastructure, Renovation and Waste Control, North West Association Centenary Conference*. Institution of Civil Engineers. 173-180.
- Herzog, M. (1985). Die Pressenkräfte bei Schildvortrieb und Rohrvorpressung im Lokkergestein. *BMT*, Issue 6, 236-238 (As summarized by Stein et al. 1989).

- International Society for Trenchless Technology. (1994). Microtunnelling Jacking Forces. *Produced by Working Group No. 3 (Microtunnelling)*. ISTT Internal Report.
- Iscimen, M. (2004). Shearing Behavior of Curved Interfaces. Thesis in Partial Fulfillment of the Degree of Master of Science in Civil Engineering. Georgia Institute of Technology, GA.
- Jacobsz, S.W., Standing, J.R., and Mair, R.J. (2004). Tunneling Effects on Pile Groups in Sand. *Advances in Geotechnical Engineering: The Skempton Conference - Proceedings of a Three Day Conference on Advances in Geotechnical Engineering*. Jardine, R.J., Potts, D.M., and Higgins, K.G. (Eds.). Thomas Telford. London. 1056-1067.
- Jester, G.E. (1970). An Experimental Investigation of Soil and Structure Interaction in Cohesive Soil. *U.S. Army Engineer Waterways Experiment Station Research Report No. WES-TR-N-70-7*. Dissertation in Partial Fulfillment of the Requirements for the Degree of Doctor of Philosophy in Civil Engineering. University of Illinois at Urbana-Champaign, IL.
- Johnson, T. (2013). Experience with Trenchless Technology. *Telephone interview*. 11 Jan. 2013.
- Jung, Y.J. and Sinha, S.K. (2007) Evaluation of Trenchless Technology Methods for Municipal Infrastructure System. *Journal of Infrastructure Systems*. ASCE. June. 144 – 156.
- Laven, K., Amyot, C., Knight, M., Liew, P., Jones, C. (2007). Leak Detection on Wastewater Force mains and Siphons in North America using the Sahara<sup>®</sup> Acoustic System. *Proceedings of ASCE International Pipelines Conference*. Boston, MA.
- Lueke, J.S. and Olson, M.P. (2012). Instrumentation and Monitoring of Pilot Tube Microtunneling Installations. *Proceedings of No-Dig 2012 Conference*. NASTT. Nashville, TN.
- Lueke, J.S, Pinghe, S., and Ariaratnam, S.T. (2011). Application of Digital Photogrammetry in Trenchless Engineering. *Proceedings of International Conference on Pipelines and Trenchless Technology*. Beijing, China.
- McNulty, J.W. (1965). An Experimental Study of Arching in Sand. *U.S. Army Engineer Waterways Experiment Station Technical Report*. WES-TR-I-674. Dissertation in Partial Fulfillment of the Requirements for the Degree of Philosophy in Civil Engineering. University of Illinois at Urbana-Champaign, IL.

- Milligan, G.W.E. and Norris, P. (1993). Oxford Research in Pipe Jacking-Research Gathers Pace. *Proceedings of the 2<sup>nd</sup> International Conference on Pipe Jacking and Microtunneling*. Pipe Jacking Association. London, UK.
- Milligan, G.W.E. and Norris, P. (1999). Pipe-Soil Interaction During Pipe Jacking. *Proceedings of the Institution of Civil Engineers-Geotechnical Engineering*. 137.1: 27-44.
- Mission Clay Products. (2013). No-Dig Pilot Tube by Mission Clay Products: Sewers Without Trenches: No-Dig Pilot Tube. [www.no-dig-pipe.com](http://www.no-dig-pipe.com).
- MI SWACO. (2013). *Max Bore HDD Product Sheet*. <http://www.slb.com/services/miswaco>.
- Mitchell, J.K. and Soga, K. (2005). *Fundamentals of Soil Behavior*. 3<sup>rd</sup> ed. John Wiley & Sons, Inc.
- MMSD. (2013). Overflows. Milwaukee Metropolitan Sewerage District. <http://v3.mmsd.com/DeepTunnel.aspx>
- Norris, P. and Milligan, G.W.E. (1991). Field Instrumentation for Monitoring the Performance of Jacked Concrete Pipes. *Field Measurements in Geotechnics*. Norwegian Geotechnical Institute. Oslo, Norway. Sorum (Ed.). Balkema. Rotterdam. Volume 1.
- Olson, M.P., and Lueke, J.S. (2013). Productivity Analysis of Pilot Tube Microtunneling Installations. *Proceedings of No-Dig 2013 Conference*. NASTT. Sacramento, CA.
- Optimum Instruments. (2004). *Data Dolphin Datalogger Series Operators Manual*. Optimum Instruments Inc.
- Osumi, T. (2000). Calculating Jacking Forces for Pipe Jacking Methods. *No-Dig International Research*. October, 2000. 40-42.
- Pecora III, J.M., and Sheahan, T.C. (2004). Pipe Jacking Forces in Soft Ground Construction During Utility Installation Related to Central Artery/Tunnel Project Construction. *Civil Engineering Practice*. 19.2: 29-44.
- Pellet-Beaucour, A.L. and Kastner, R. (2002). Experimental and Analytical Study of Friction Forces during Microtunneling Operations. *Tunnelling and Underground Space Technology*. 17: 83-97.
- Pineda-Jaimes, J.A., and Colmenares-Montañez, J.E. (2011). Peak and Residual Shear Strength Parameters of Soft Clay-Concrete Interfaces. *Proceedings of Pan-Am CGS Geotechnical Conference*. Toronto, Ontario, Canada.

- Pipe Jacking Association. (1995). *An Introduction to Pipe Jacking and Microtunneling Design*. London, UK.
- Ripley, K.J. (1989) The Performance of Jacked Pipe. PhD Dissertation. University of Oxford, UK.
- Salamo, K.P. (1979). Experimentelle und theoretische Bestimmung der Pressenkräfte und der Bodenverformung beim Vortrieb eines Vorpreßrohres in rolligen Böden. Dissertation. Technische Universität Berlin. (As summarized by Stein et al. 1989).
- Scherle, M. (1977). Rohvortrieb Part 2. Bauverlag, Wiesbaden/-Berlin. (As summarized by Stein et al. 1989).
- Shou, K., Yen, J., and Liu, M. (2010). On the Frictional Property of Lubricants and its Impact on Jacking Force and Soil-Pipe Interaction of Pipe-Jacking. *Tunnelling and Underground Space Technology*. 25: 469-477.
- Skempton, A.W. (1985). Residual Strength of Clays in Landslides, Folded Strata and the Laboratory. *Géotechnique*. 35.1: 3-18.
- Sofianos, A.I., Loukas, P., and Chantzakos, Ch. (2004). Pipe jacking a sewer under Athens. *Tunnelling and Underground Space Technology*. 19: 193-203.
- Staheli, K. (1996). Development of an Analytical Model for Jacking Forces in Microtunneling. A Thesis submitted to the Faculty of Mississippi State University in Partial Fulfillment of the Requirements for the Degree of Master of Science in Civil Engineering in the Department of Civil Engineering. Mississippi State University, MS.
- Staheli, K. (2006). Jacking Force Prediction: An Interface Friction Approach Based on Pipe Surface Roughness. Dissertation in Partial Fulfillment of the Requirements for the Degree Doctor of Philosophy in the School of Civil and Environmental Engineering. Georgia Institute of Technology, GA.
- Stein, D., Möllers, K., and Bielecki, R. (1989). Microtunneling: Installation and Renewal of Non-man Size Supply and Sewerage Lines by the Trenchless Construction Methods. Ernst and Sohn. Berlin, Germany.
- Tang, P., Olson, M.P., Zhenglai, S., and Ariaratnam, S.T. (2013). Automated Monitoring of Pilot Tube Microtunneling Installations through Pattern Recognition in Time-Series Data of Hydraulic Pressure. *Proceedings of ASCE Pipelines Conference*. Worthington Renaissance Hotel, Fort Worth, TX.
- Terzaghi, K. (1943). *Theoretical Soil Mechanics*. John Wiley and Sons.



USGAO. (2013). Water Infrastructure: Approaches and Issues for Financing Drinking Water and Wastewater Infrastructure. Testimony Before the Subcommittee on Interior, Environment, and Related Agencies Committee on Appropriations House of Representatives. United States Government Accountability Office. GAO-13-451T.

Weber, W. (1981). Experimentelle Untersuchungen in rolligen Böden zur Dimensionierung von Preßbohranlagen. Dissertation. Wissenschaftlicher Bericht aus der Arbeit des Institutes für Baumaschinen und Baubetrieb der Rheinisch-Westfälisch Technischen Hochschule Aachen, RWTH Aachen. (As summarized by Stein et al. 1989).

WRF. (2013). Welcome to the Waterborne Pathogens Website. Water Research Foundation. Montana State University. <http://www.waterbornepathogens.org/>.

APPENDIX A  
SUPPLEMENTAL FIGURES

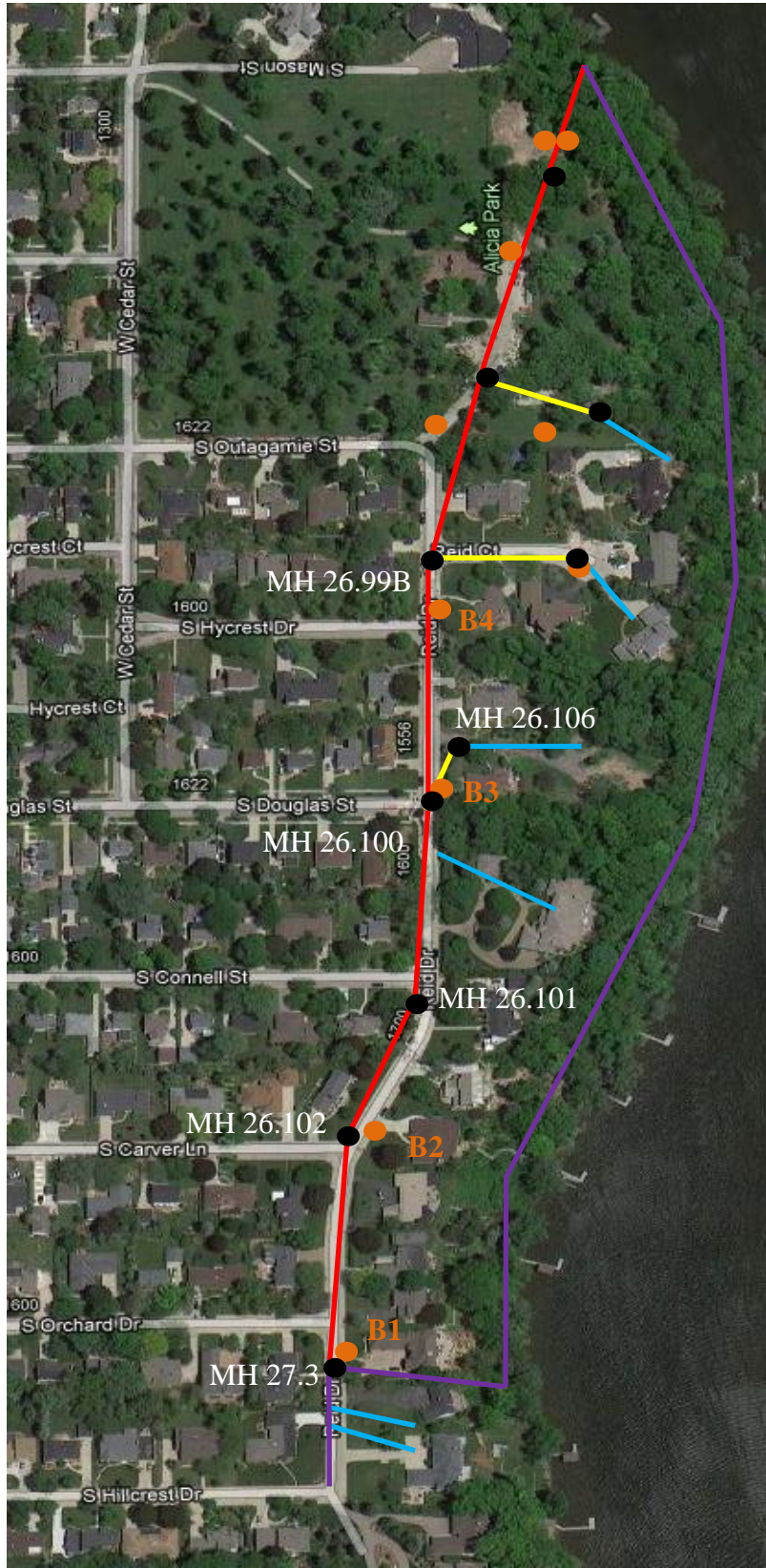


Figure A.1 Plan View of Reid Drive Interceptor Project (Only manholes and borings relevant to collected data are labeled)

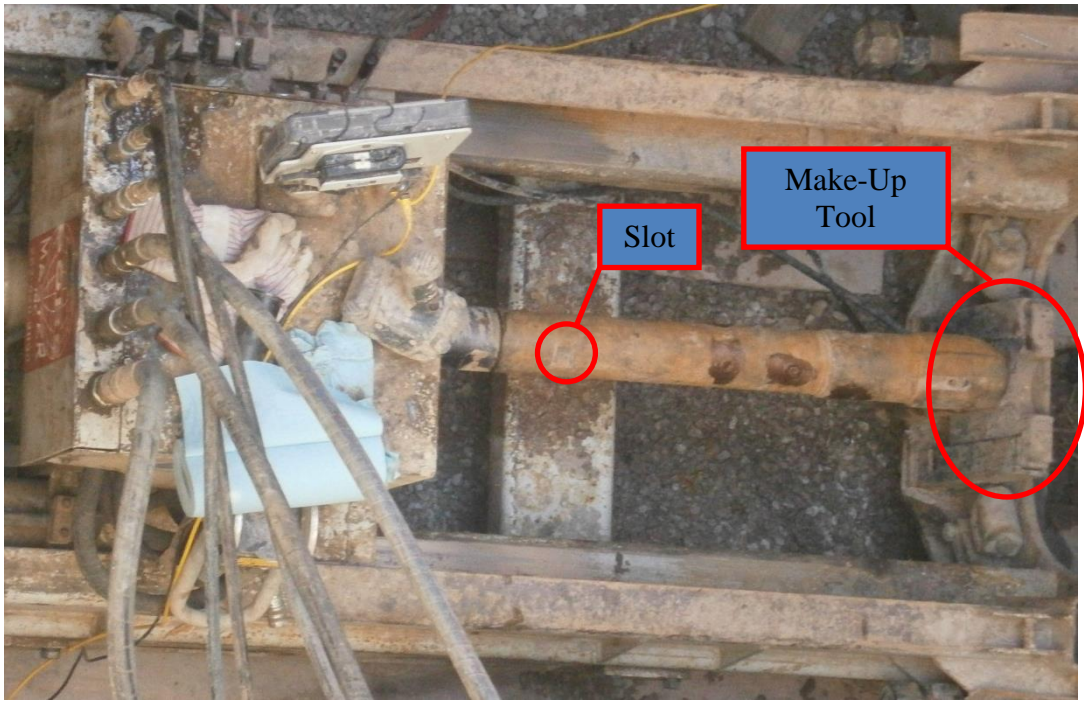


Figure A.2 Photograph of Make-Up Tool Used in Phase One Operations

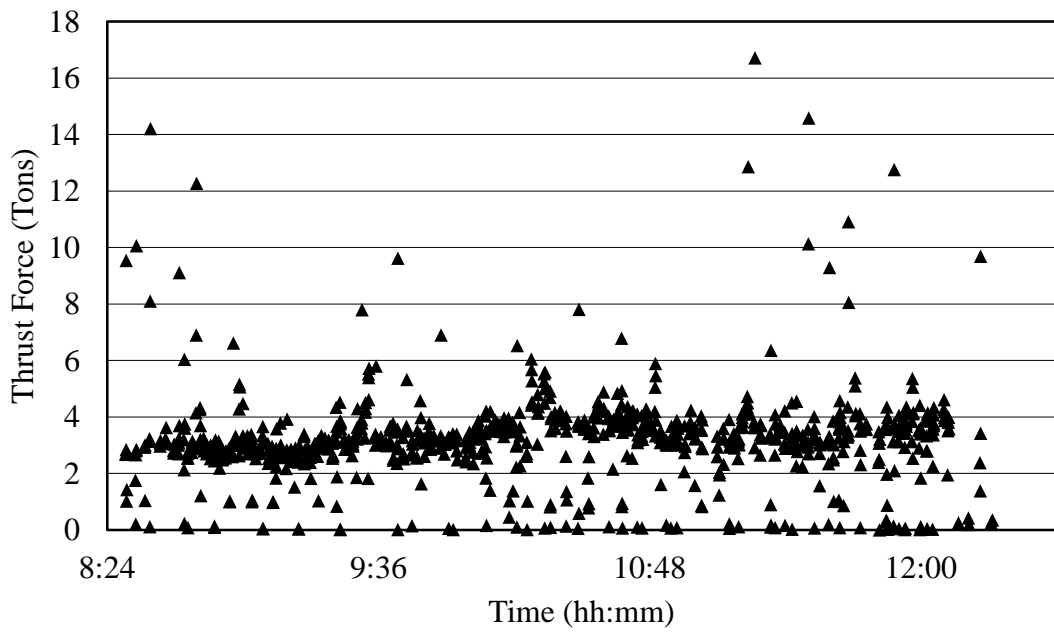


Figure A.3 Thrust Force vs. Time for Phase One of Drive One

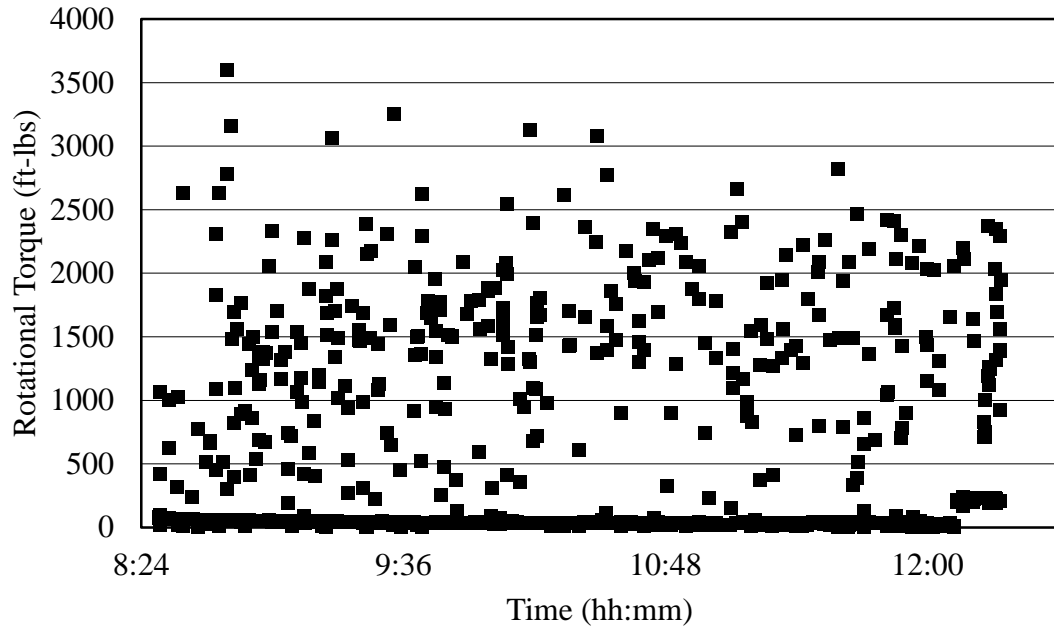


Figure A.4 Rotational Torque vs. Time for Phase One of Drive One

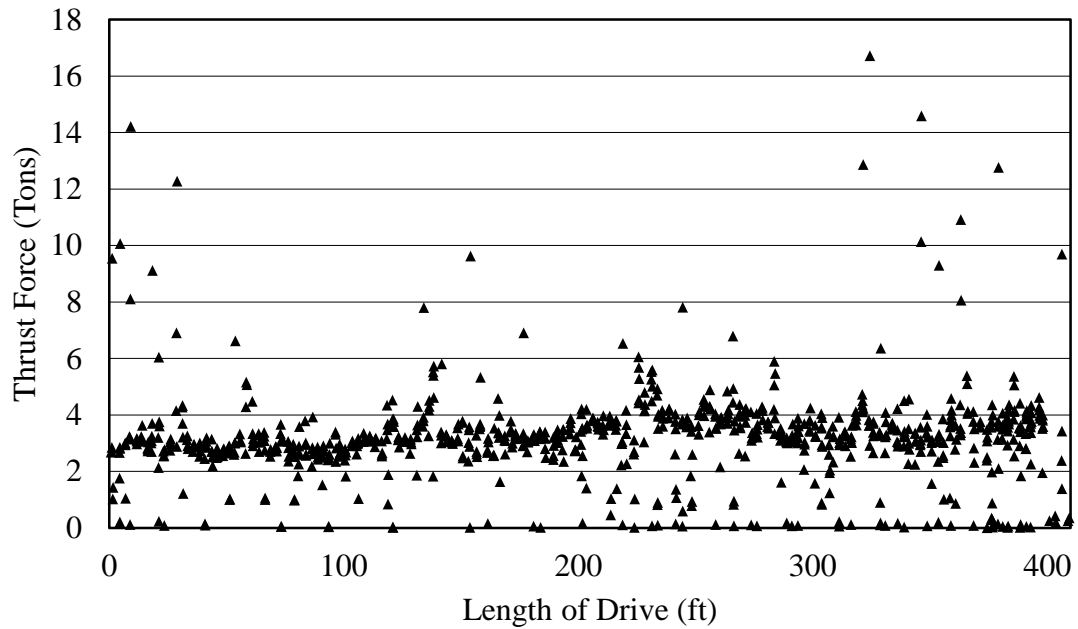


Figure A.5 Thrust Force vs. Length of Drive for Phase One of Drive One

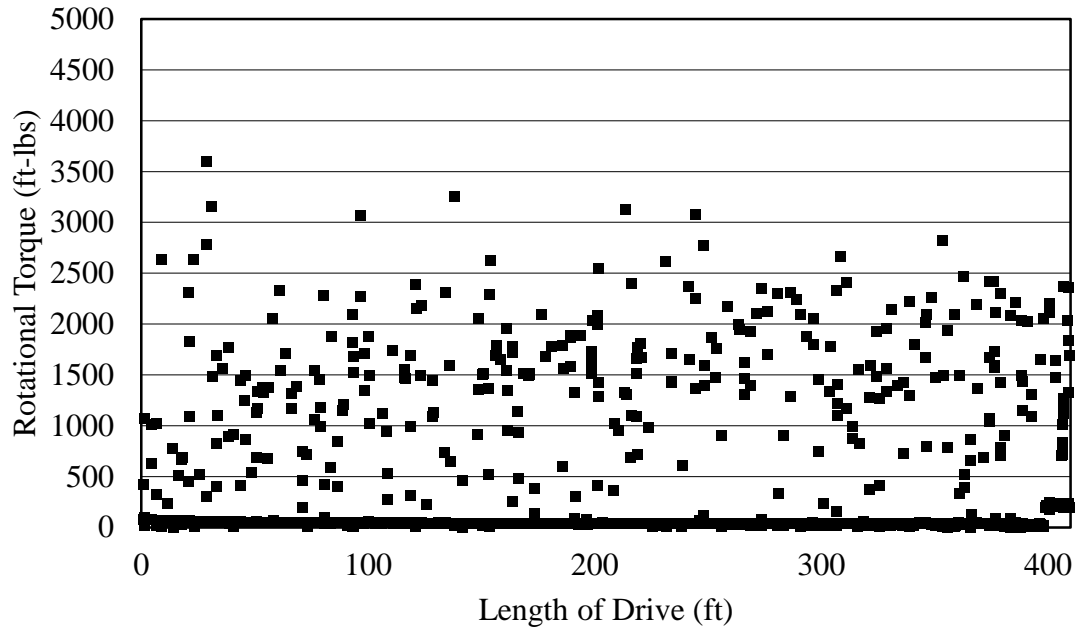
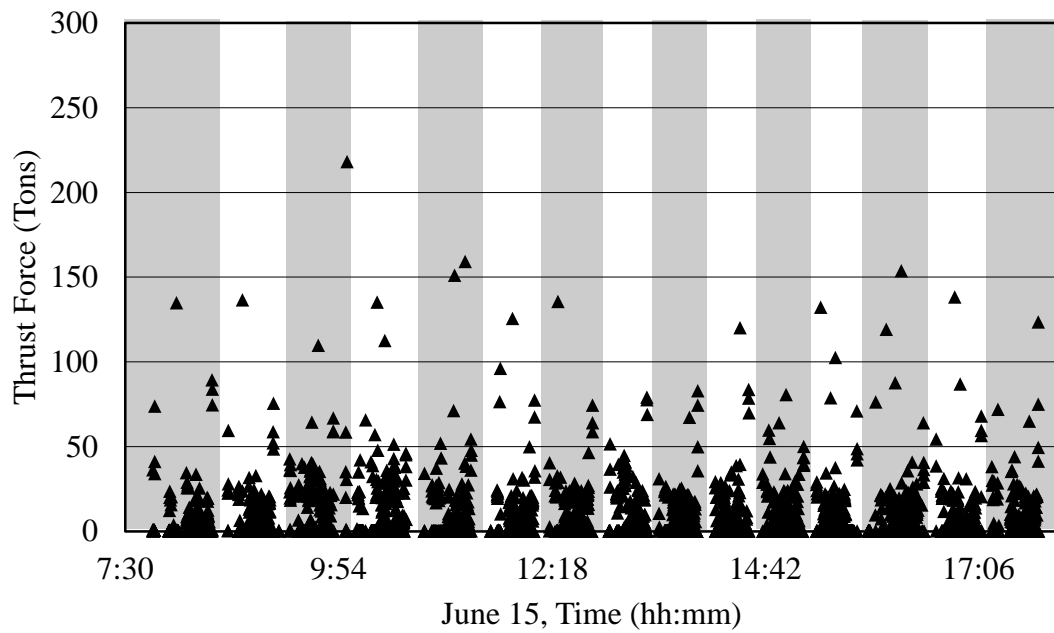
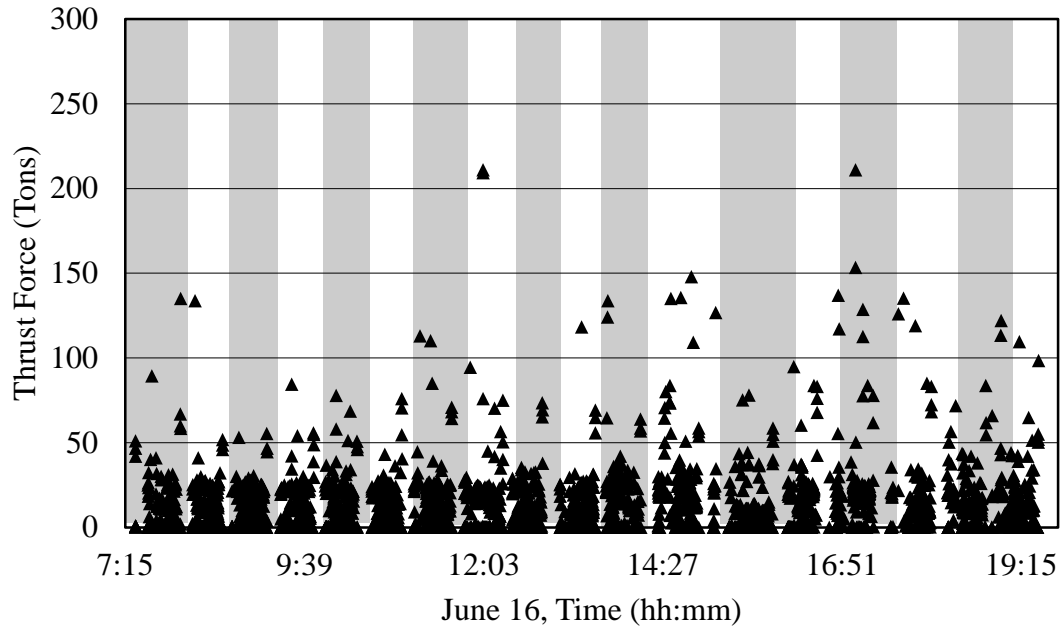


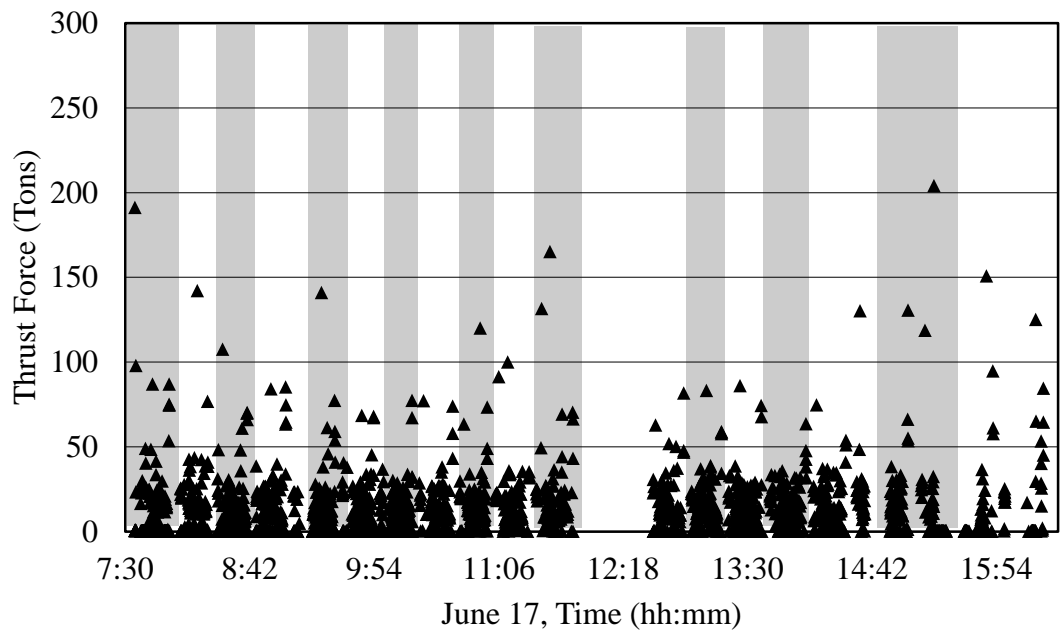
Figure A.6 Rotational Torque vs. Length of Drive for Phase One of Drive One



a) Day One, June 15<sup>th</sup>



b) Day Two, June 16<sup>th</sup>



c) Day Three, June 17<sup>th</sup>

Figure A.7 Thrust Force vs. Time for Phase Two of Drive One:  
a) Day One, b) Day Two, c) Day Three

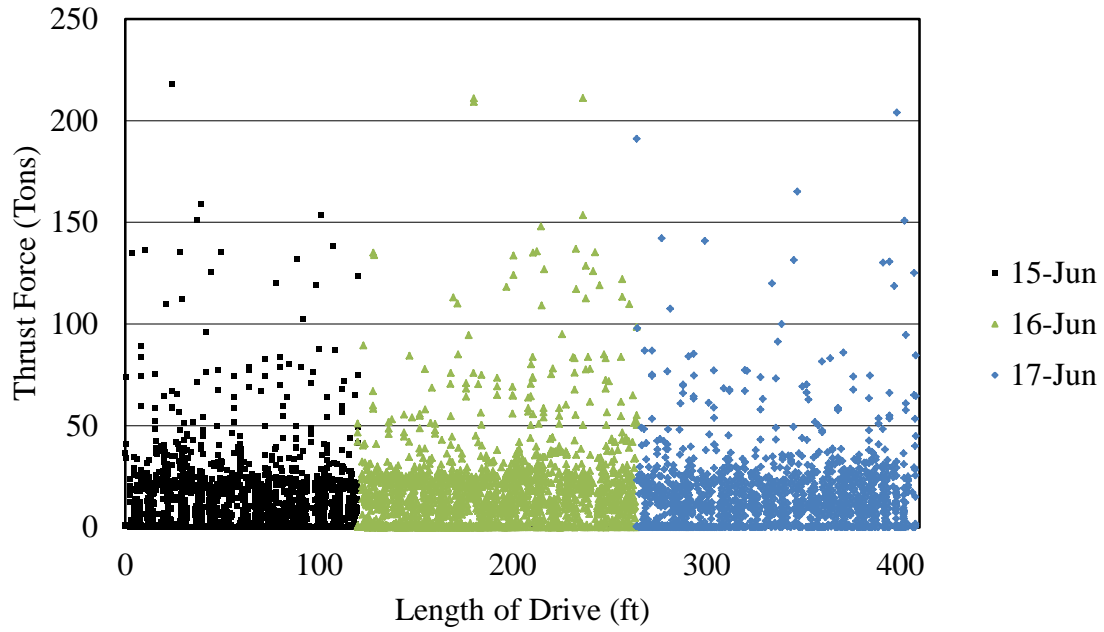


Figure A.8 Thrust Force vs. Length of Drive for Phase Two of Drive One

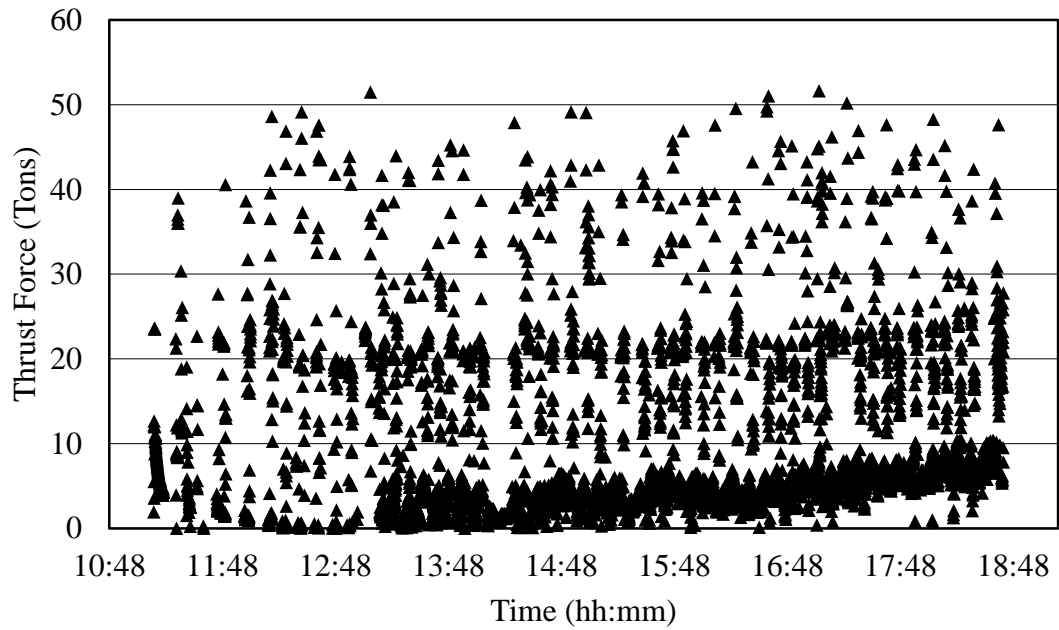


Figure A.9 Thrust Force vs. Time for Phase Three of Drive One



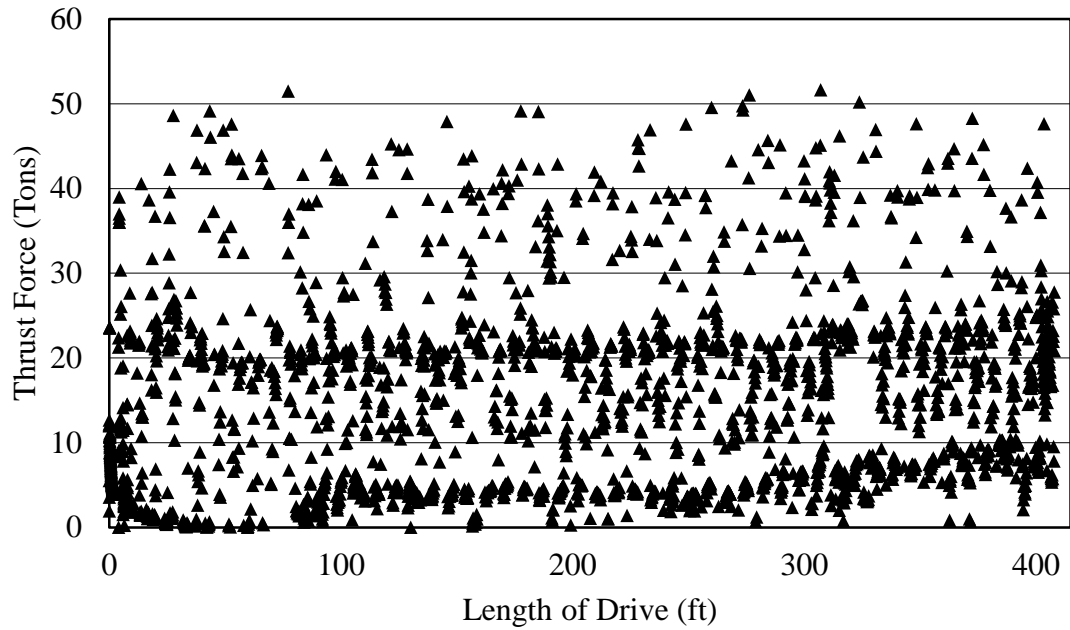


Figure A.10 Thrust Force vs. Length for Phase Three of Drive One

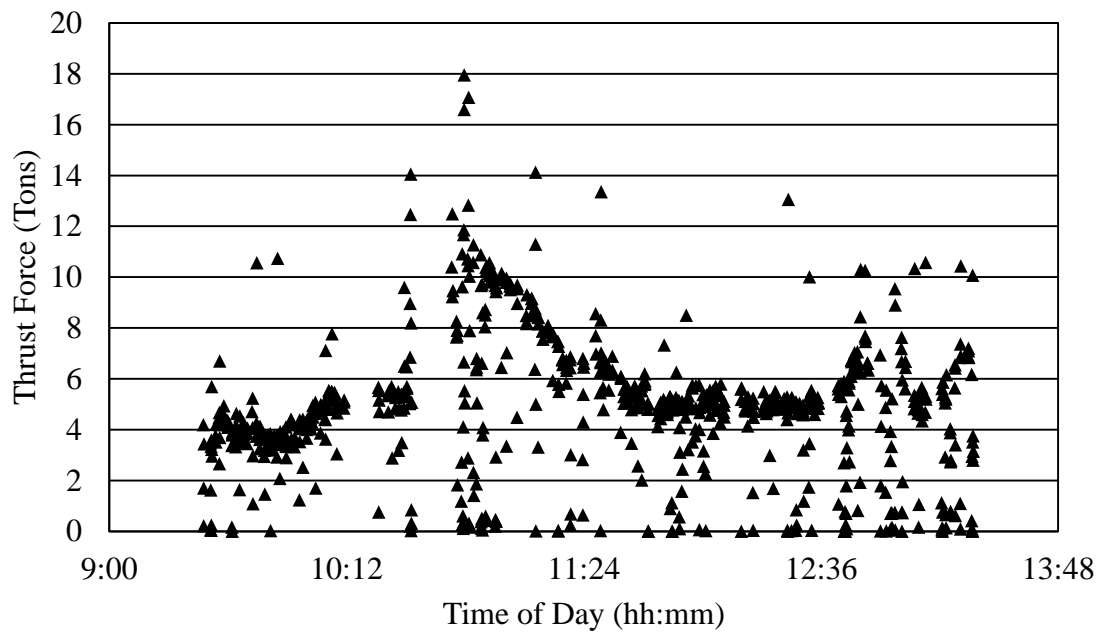


Figure A.11 Thrust Force vs. Time for Phase One of Drive Two

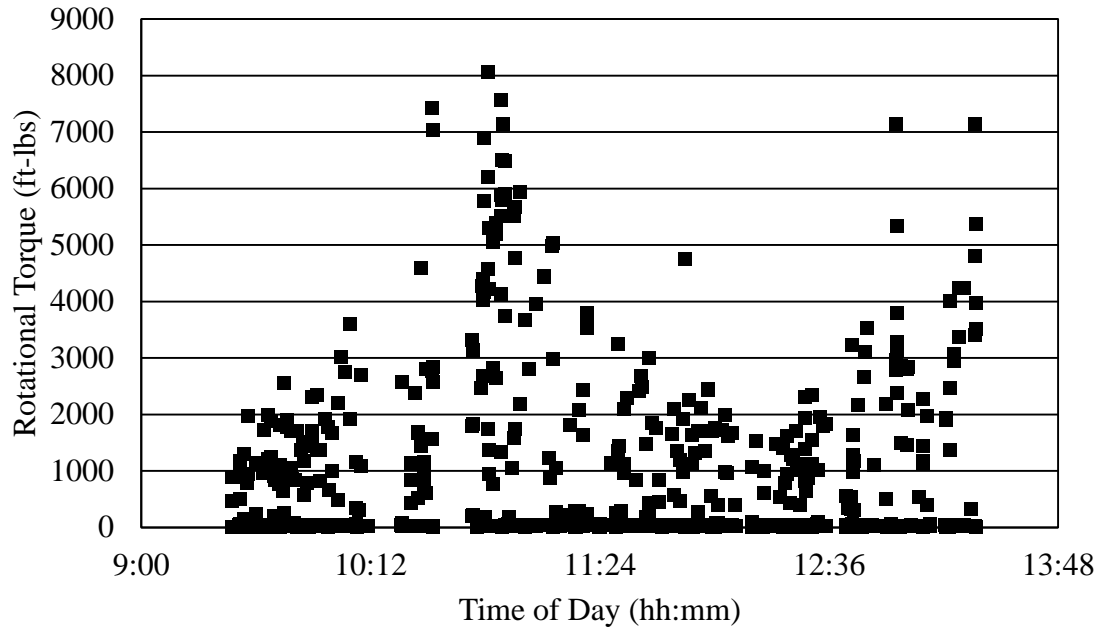


Figure A.12 Rotational Torque vs. Time for Phase One of Drive Two

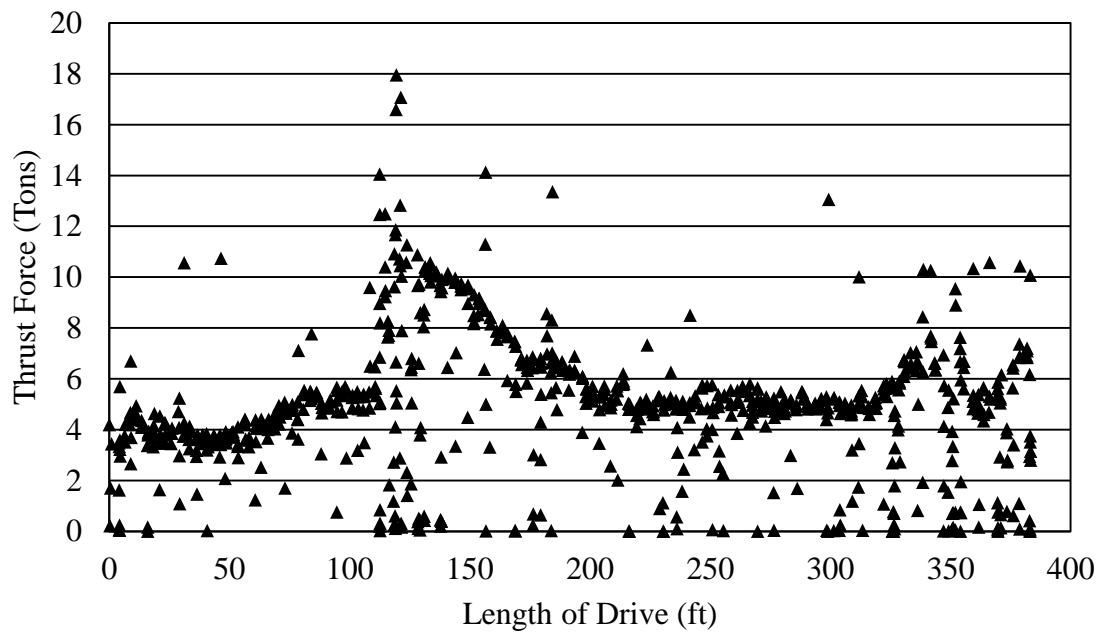


Figure A.13 Thrust Force vs. Length of Drive for Phase One of Drive Two

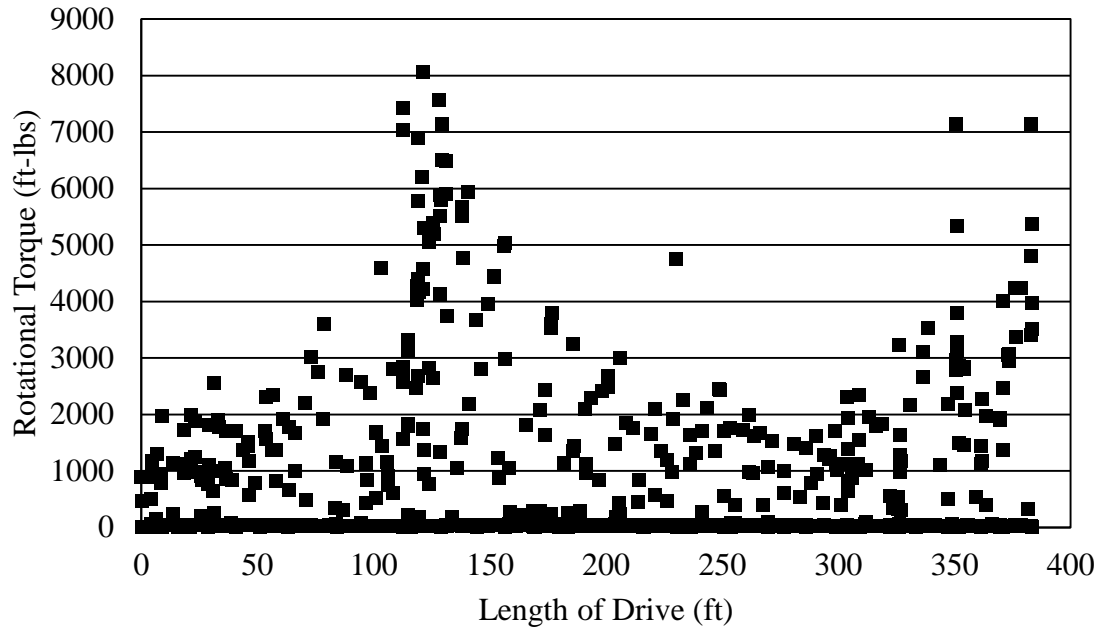
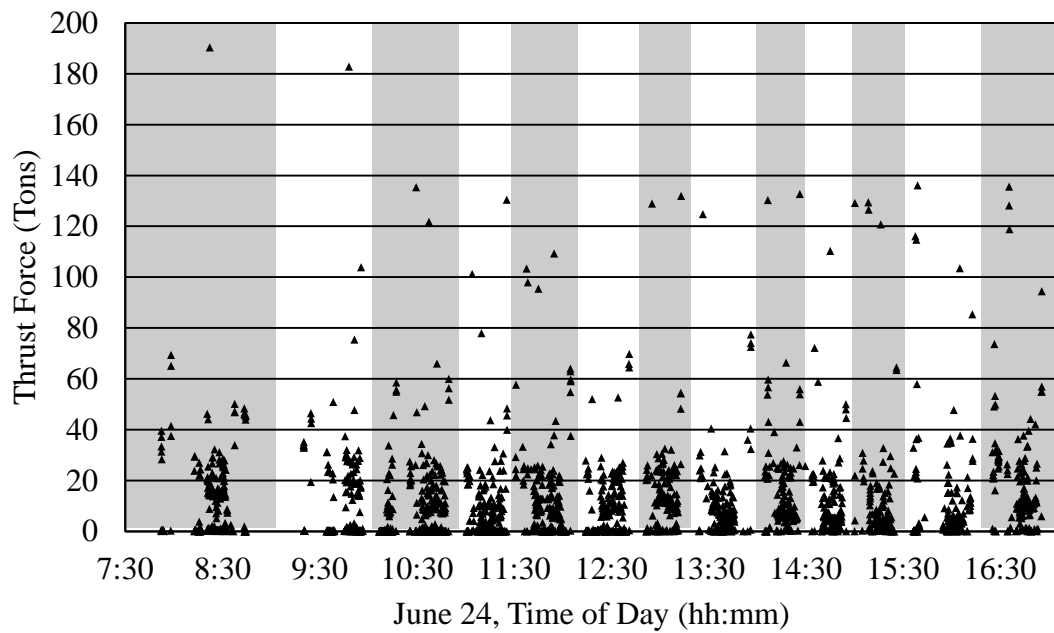
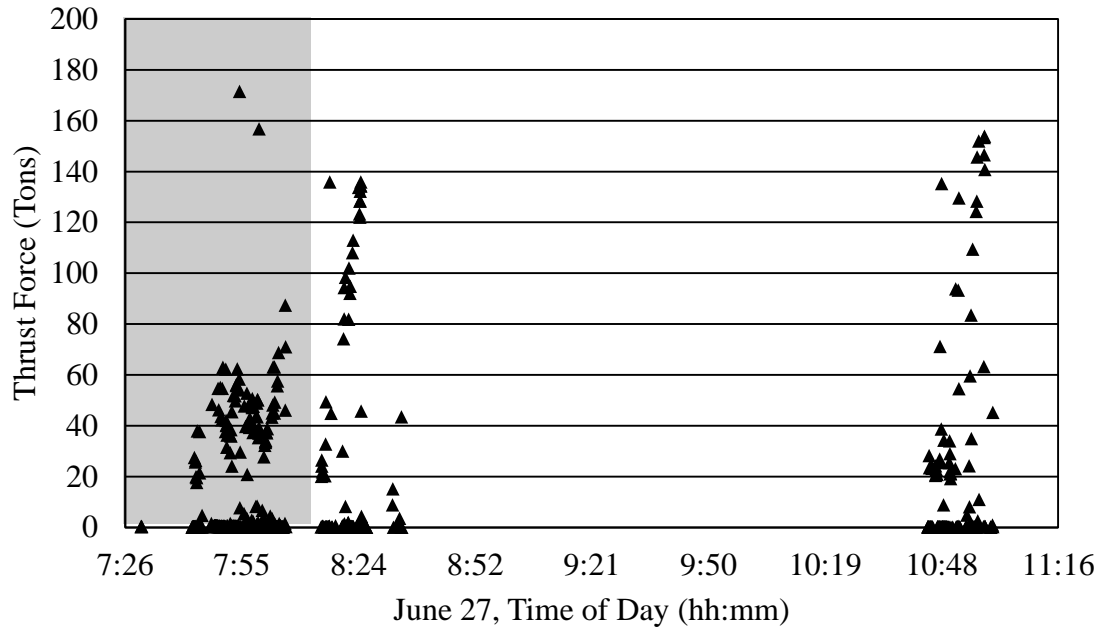


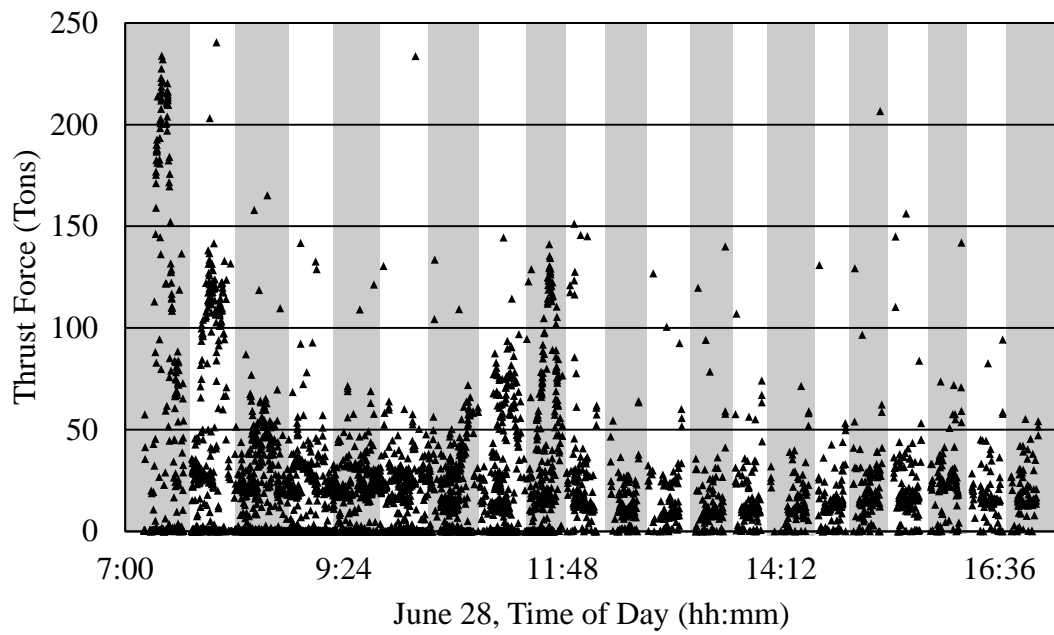
Figure A.14 Rotational Torque vs. Length of Drive for Phase One of Drive Two



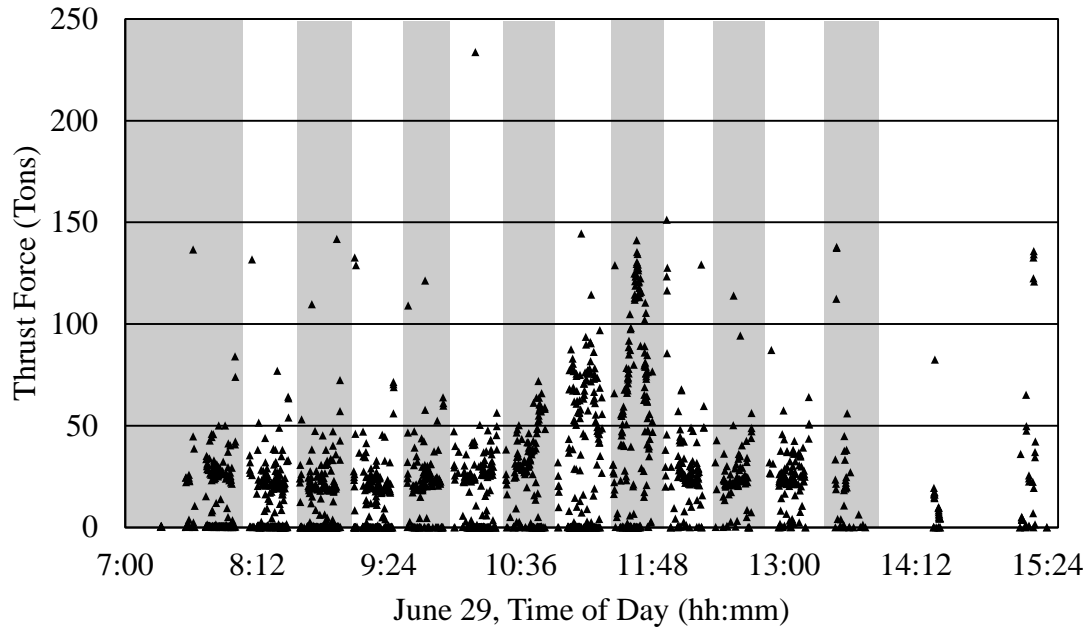
a) Day One, June 24<sup>th</sup>



b) Day Two, June 27<sup>th</sup>



c) Day Three, June 28<sup>th</sup>



d) Day Four, June 29<sup>th</sup>

Figure A.15 Thrust Force vs. Time for Phase Two of Drive Two:  
 a) Day One, b) Day Two, c) Day Three, b) Day Four

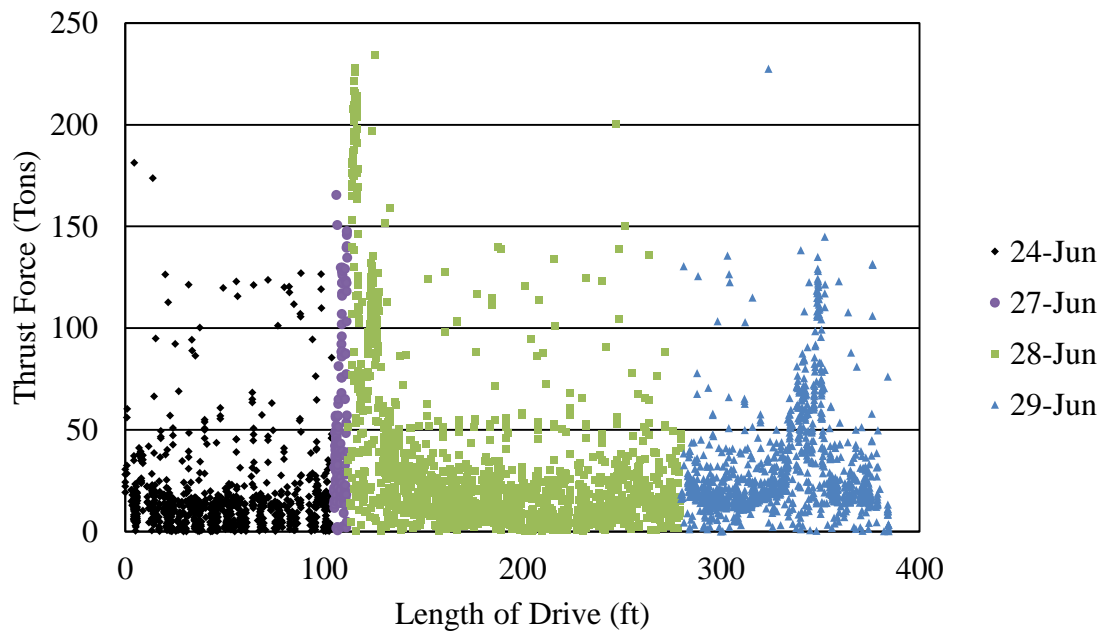


Figure A.16 Thrust Force vs. Length of Drive for Phase Two of Drive Two

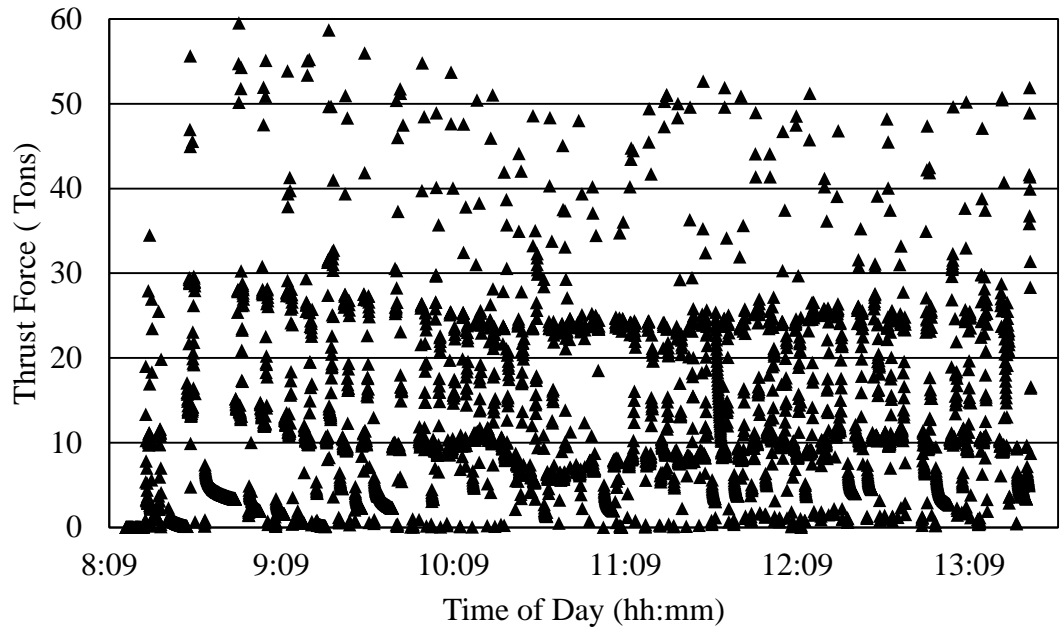


Figure A.17 Thrust Force vs. Time for Phase Three of Drive Two

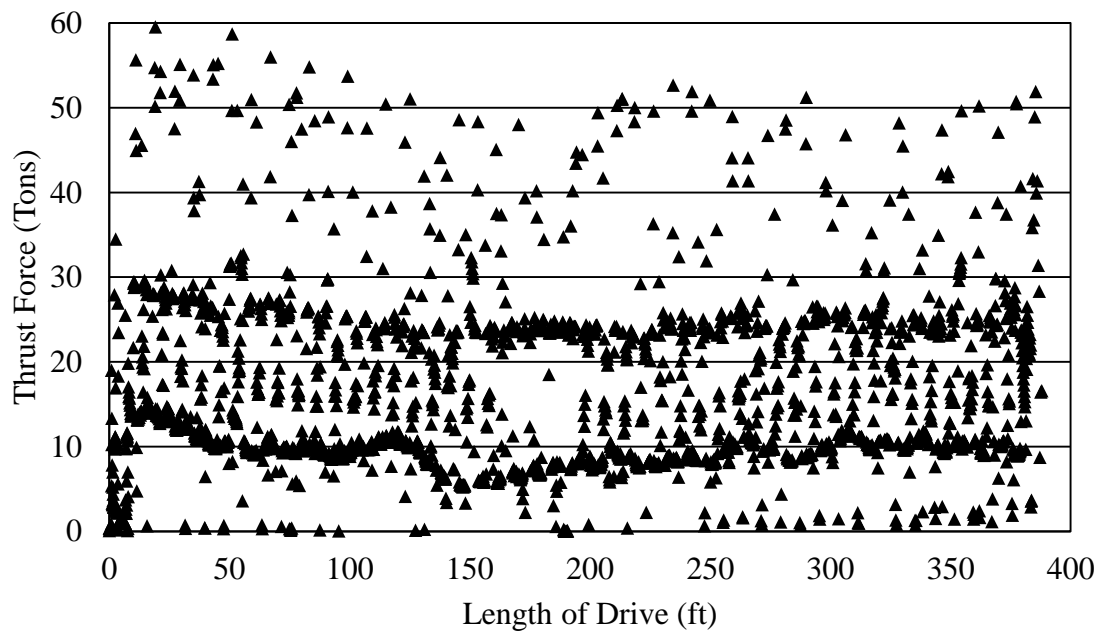


Figure A.18 Thrust Force vs. Length of Drive for Phase Three of Drive Two

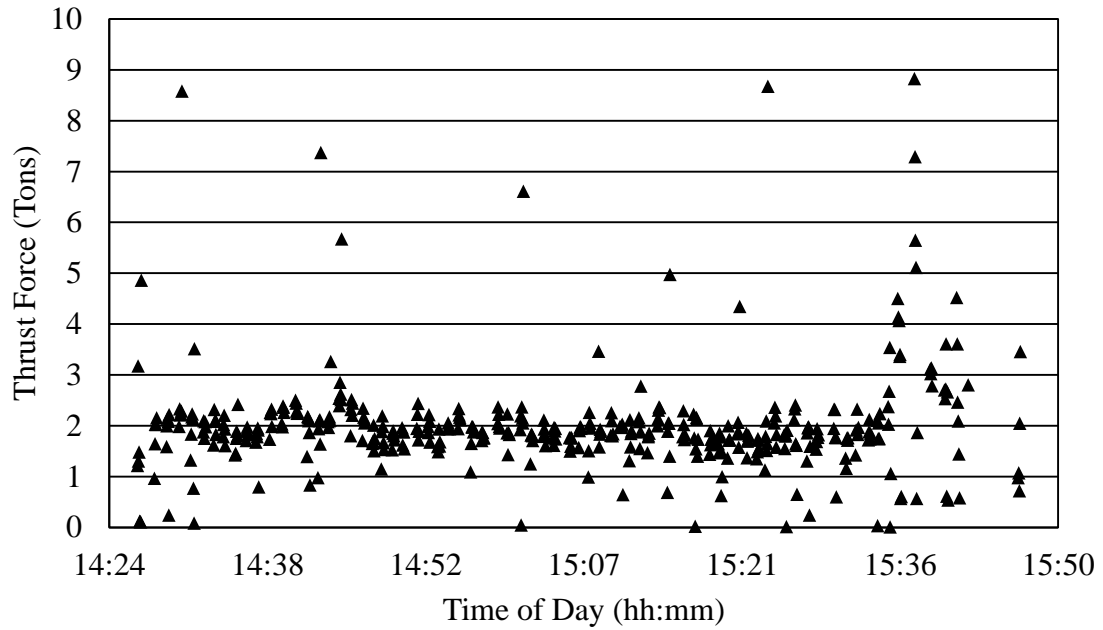


Figure A.19 Thrust Force vs. Time for Phase One of Drive Three

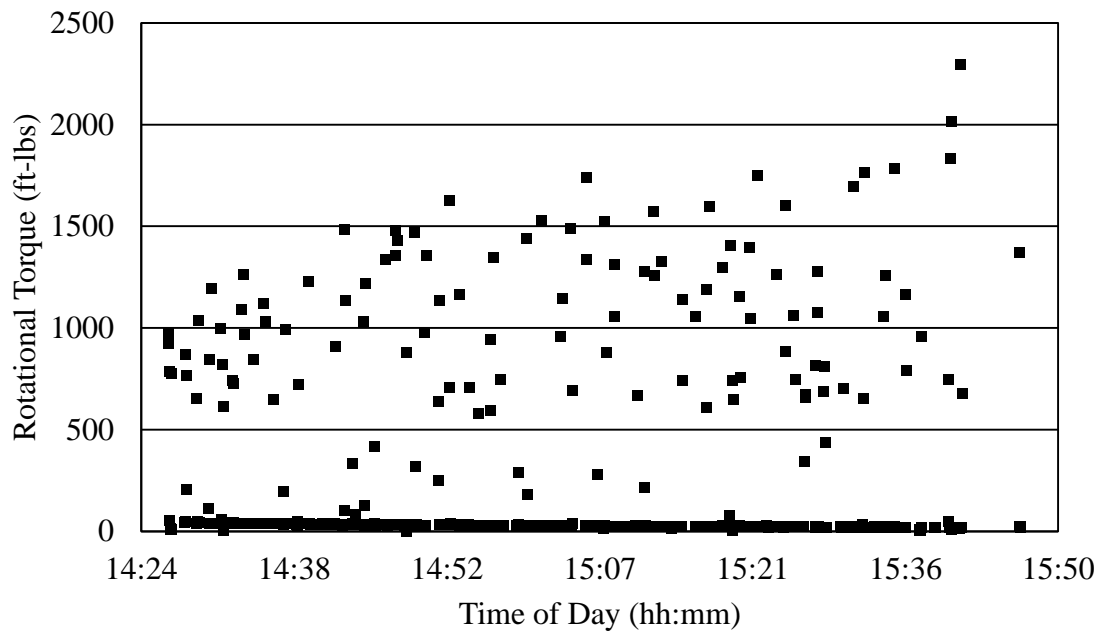


Figure A.20 Rotational Torque vs. Time for Phase One of Drive Three

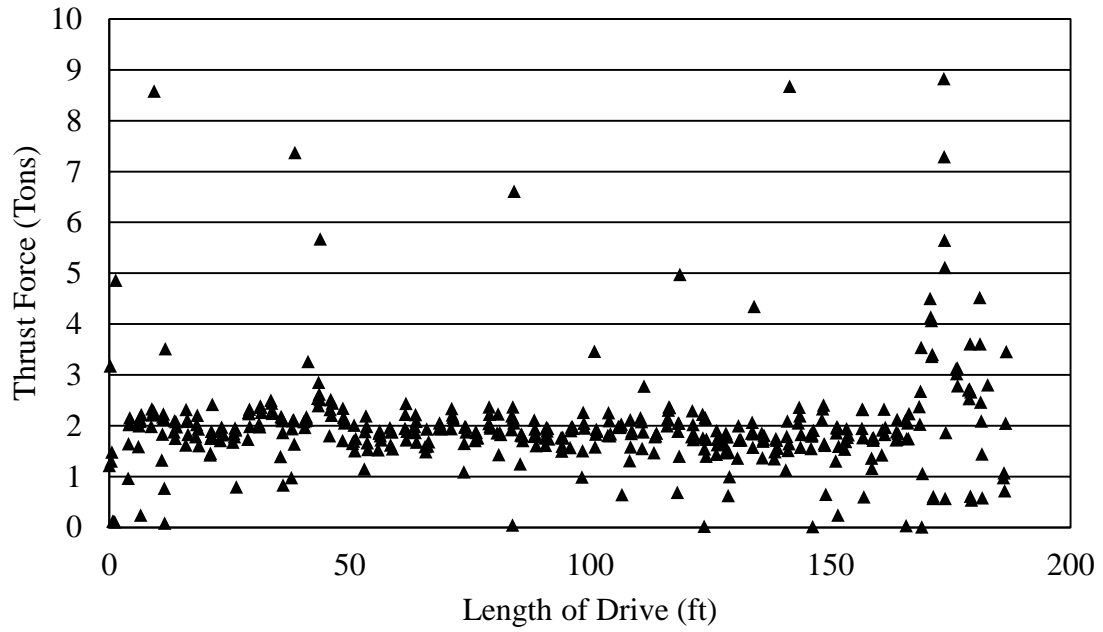


Figure A.21 Thrust Force vs. Length of Drive for Phase One of Drive Three

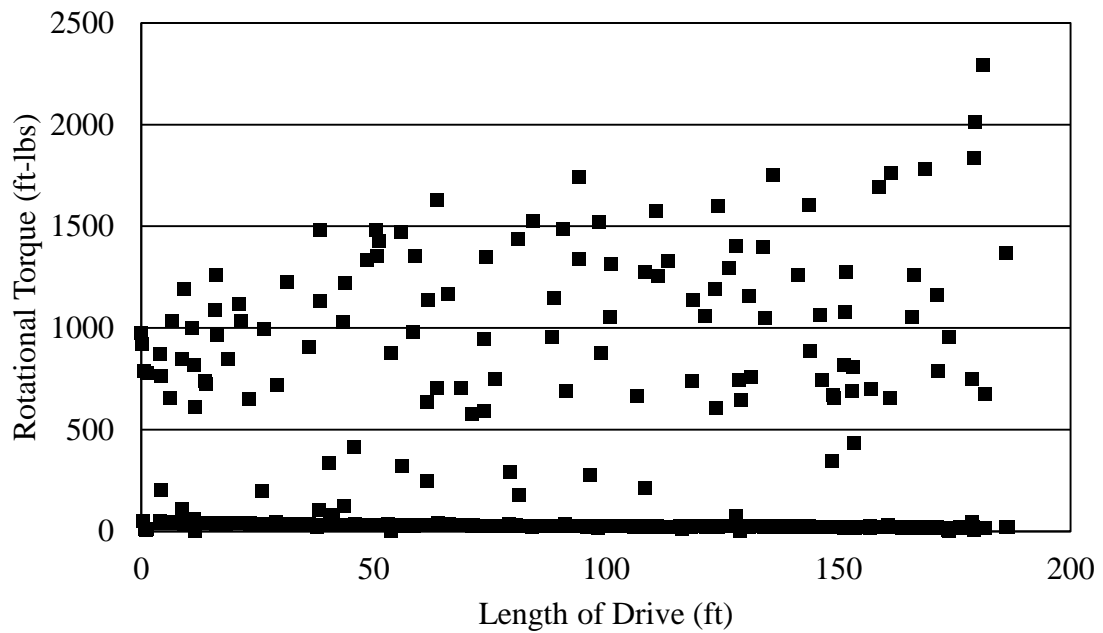
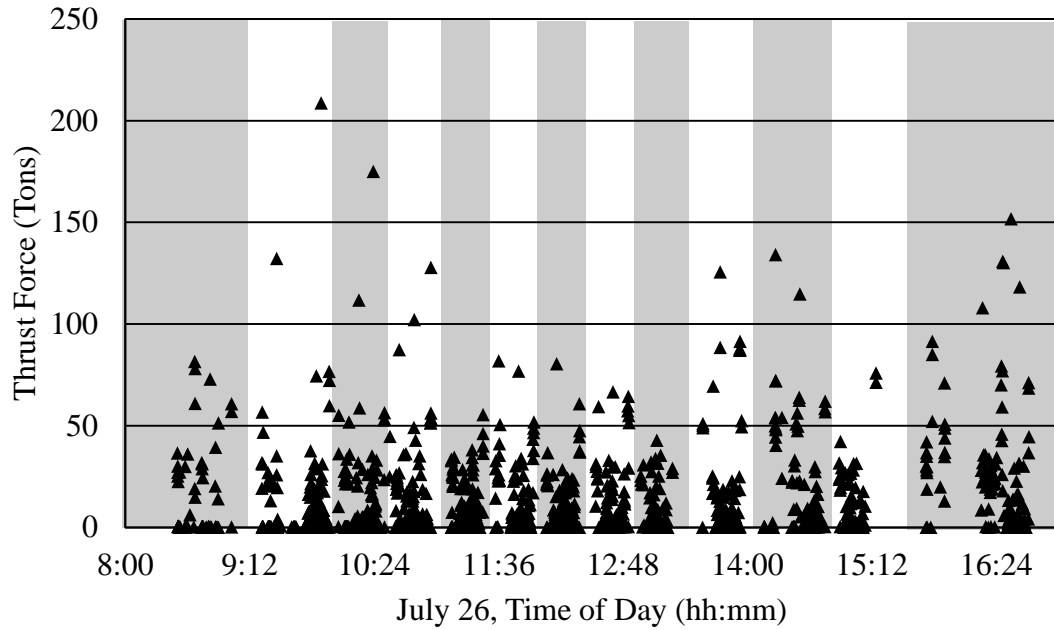
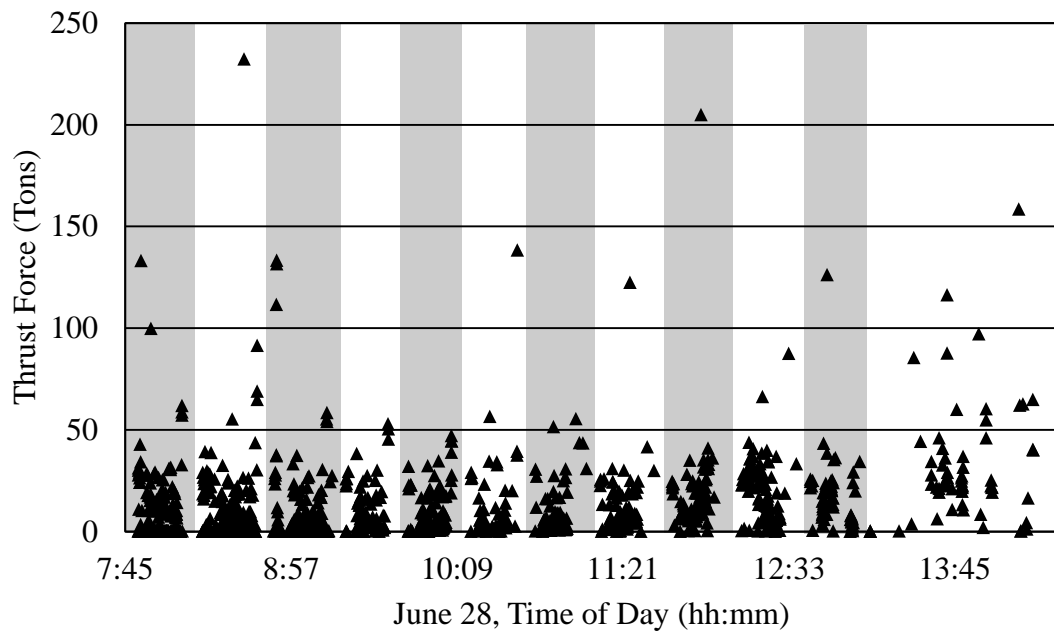


Figure A.22 Rotational Torque vs. Length of Drive for Phase One of Drive Three





a) Day One, July 26th



b) Day Two, July 28th

Figure A.23 Thrust Force vs. Time for Phase Two of Drive Three:  
a) Day One, b) Day Two

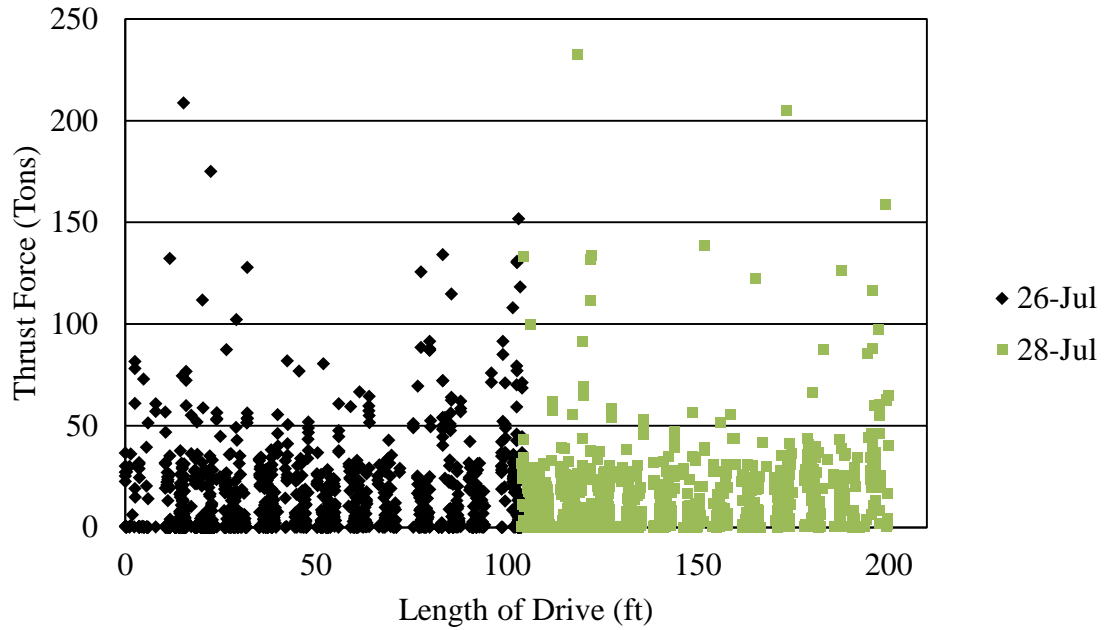


Figure A.24 Thrust Force vs. Length of Drive for Phase Two of Drive Three

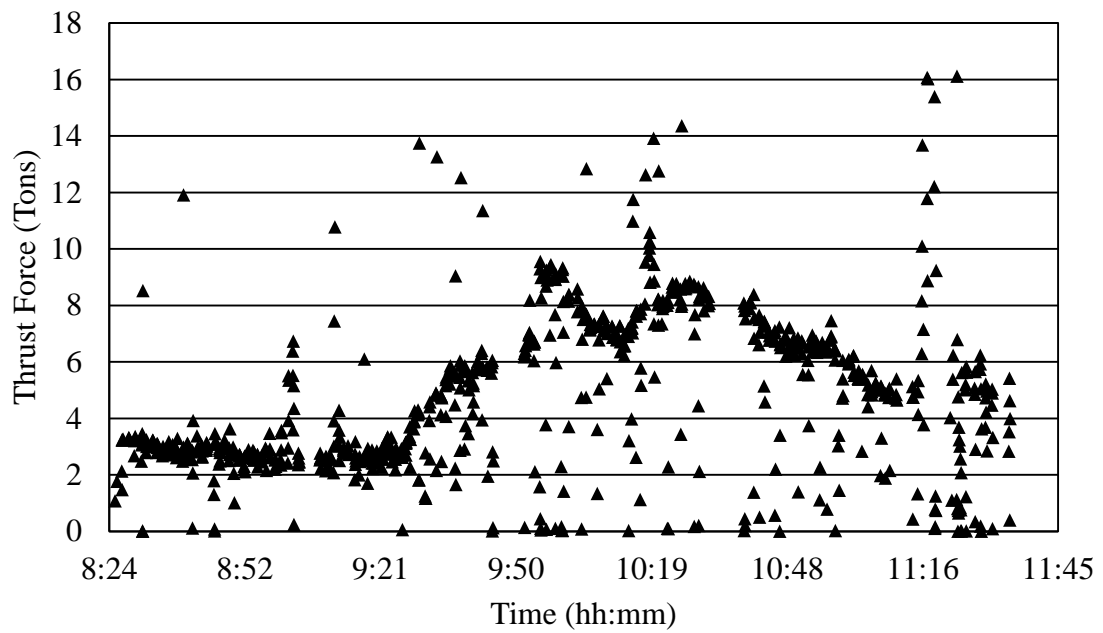


Figure A.25 Thrust Force vs. Time for Phase One of Drive Four

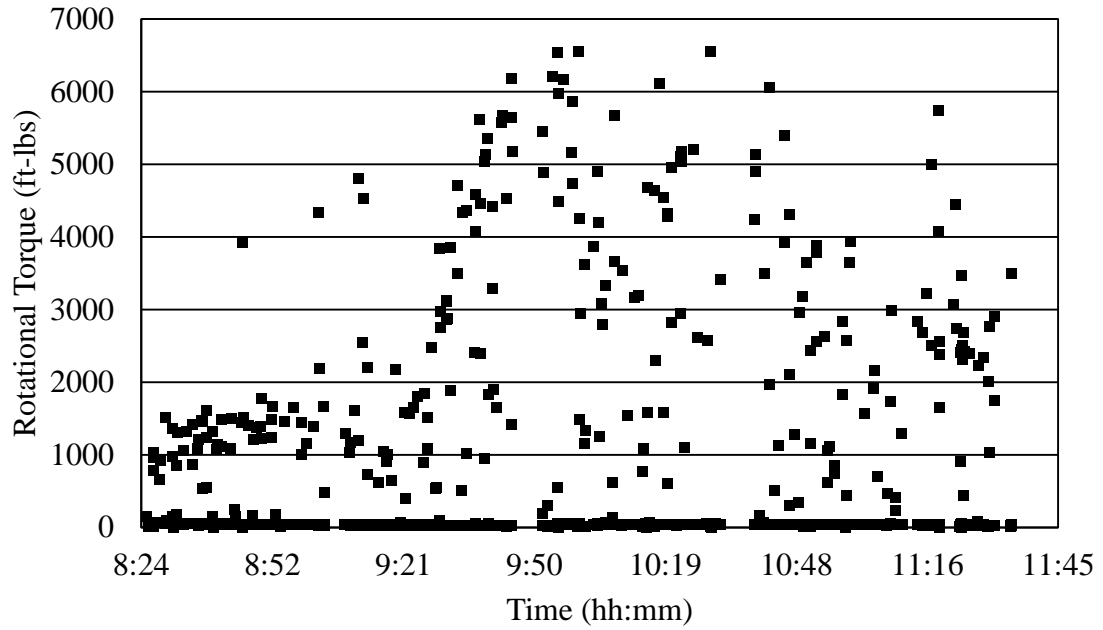


Figure A.26 Rotational Torque vs. Time for Phase One of Drive Four

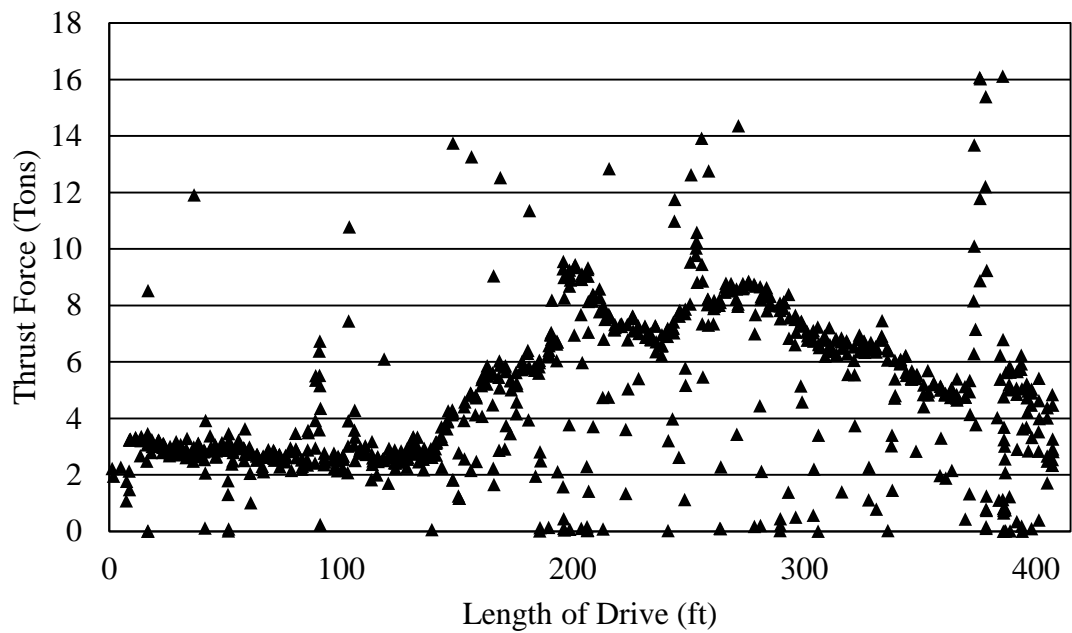


Figure A.27 Thrust Force vs. Length of Drive for Phase One of Drive Four

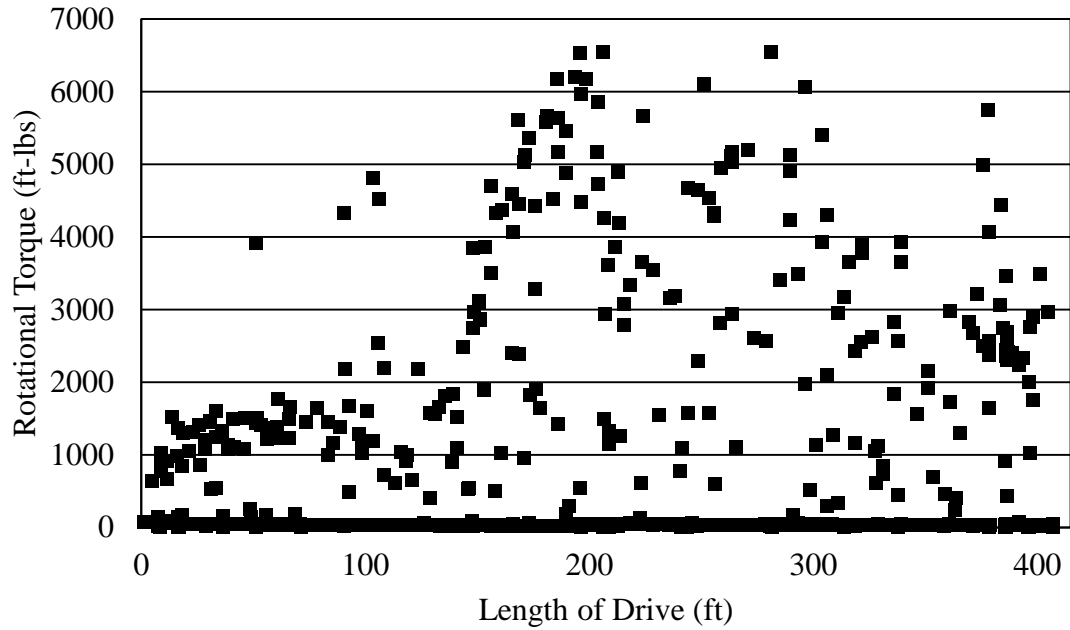
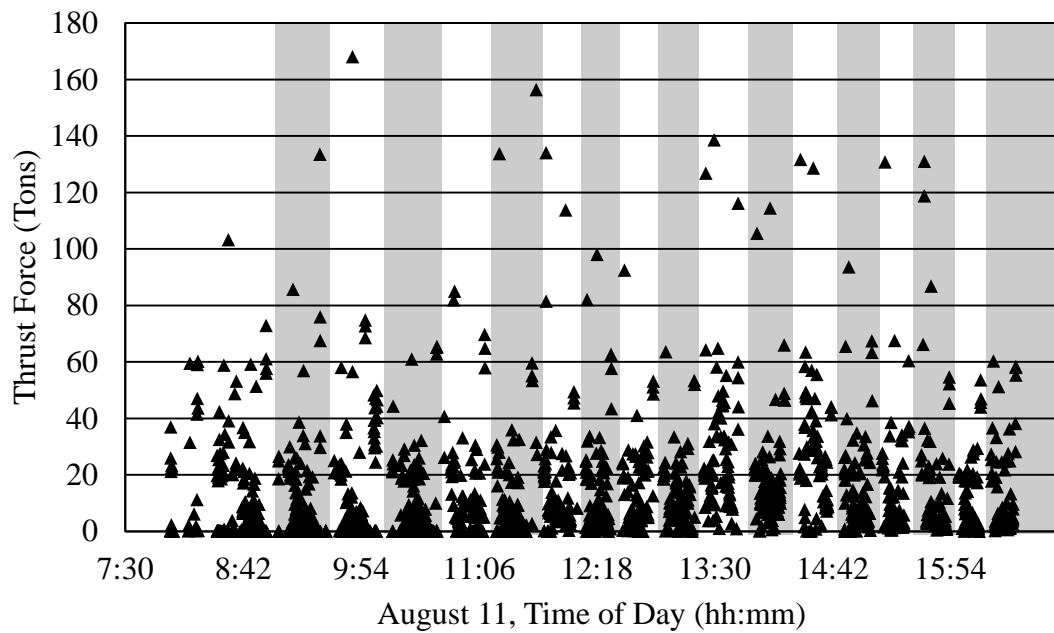
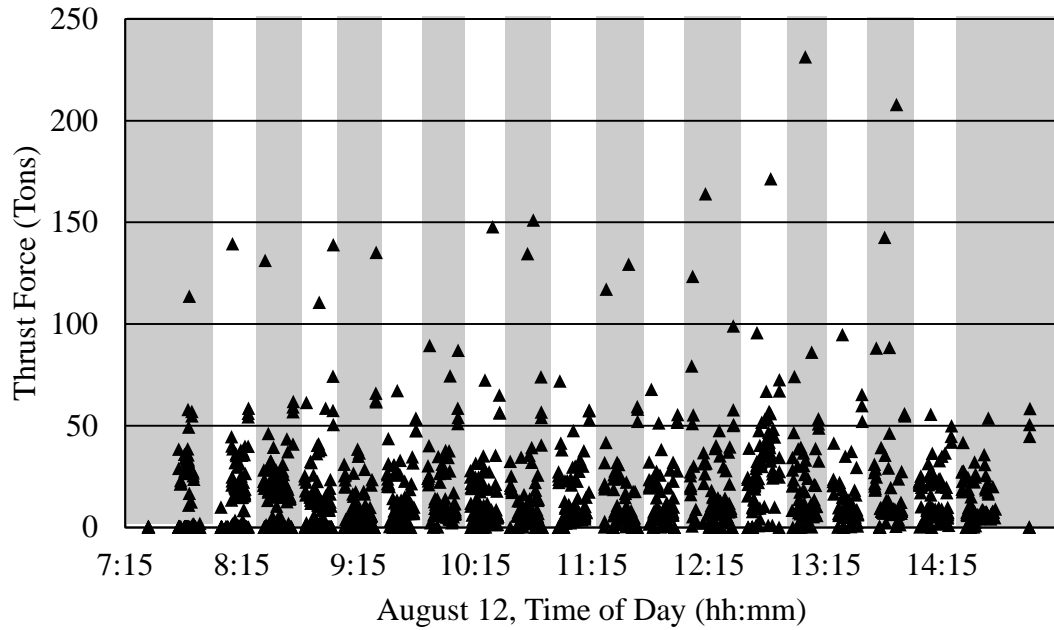


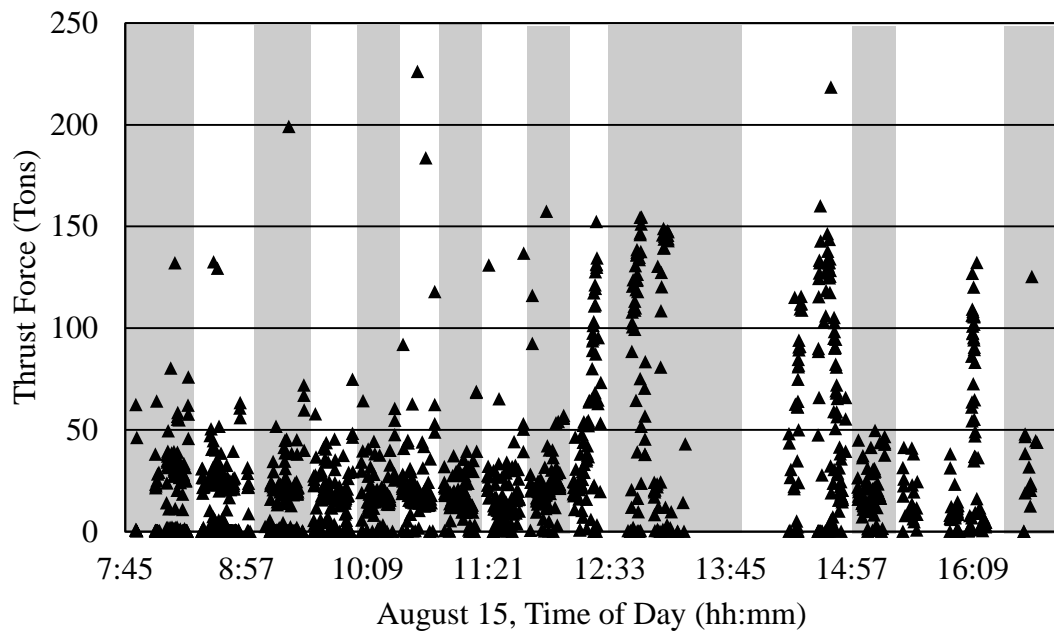
Figure A.28 Rotational Torque vs. Length of Drive for Phase One of Drive Four



a) Day One, August 11th



b) Day Two, August 12<sup>th</sup>



c) Day Three, August 15<sup>th</sup>

Figure A.29 Thrust Force vs. Time for Phase Two of Drive Four:  
a) Day One, b) Day Two, c) Day Three

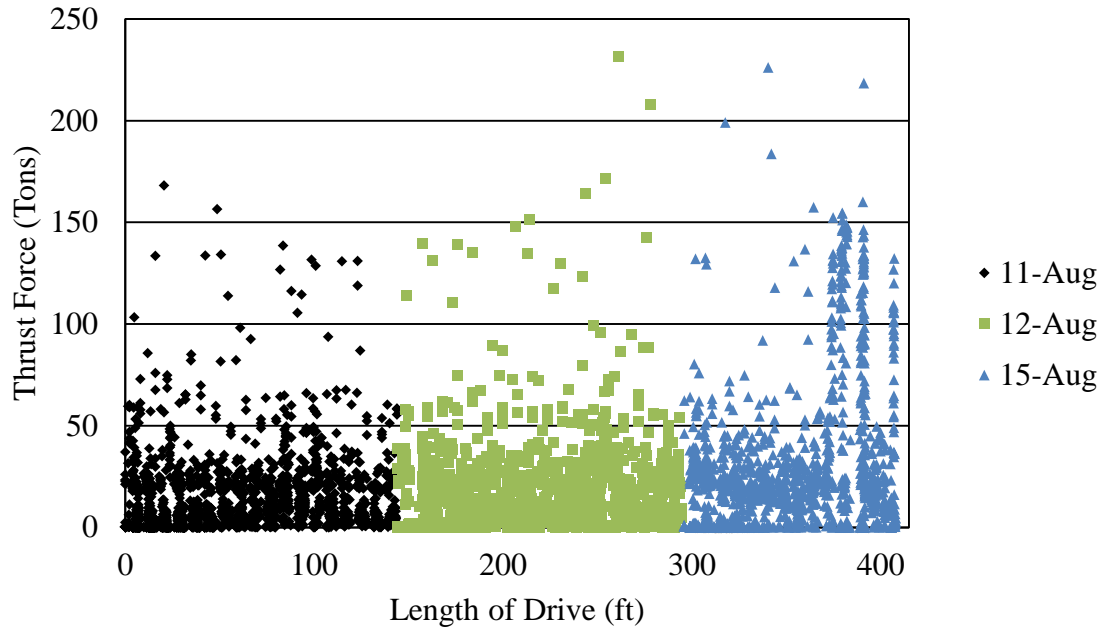


Figure A.30 Thrust Force vs. Length of Drive for Phase Two of Drive Four

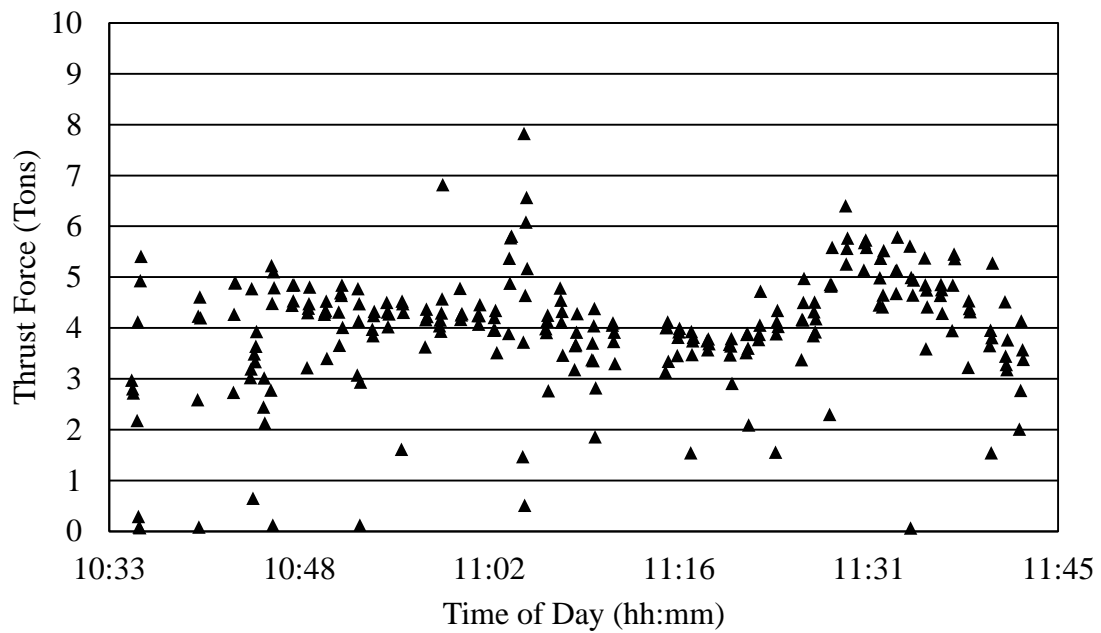


Figure A.31 Thrust Force vs. Time for Phase One of Drive Five

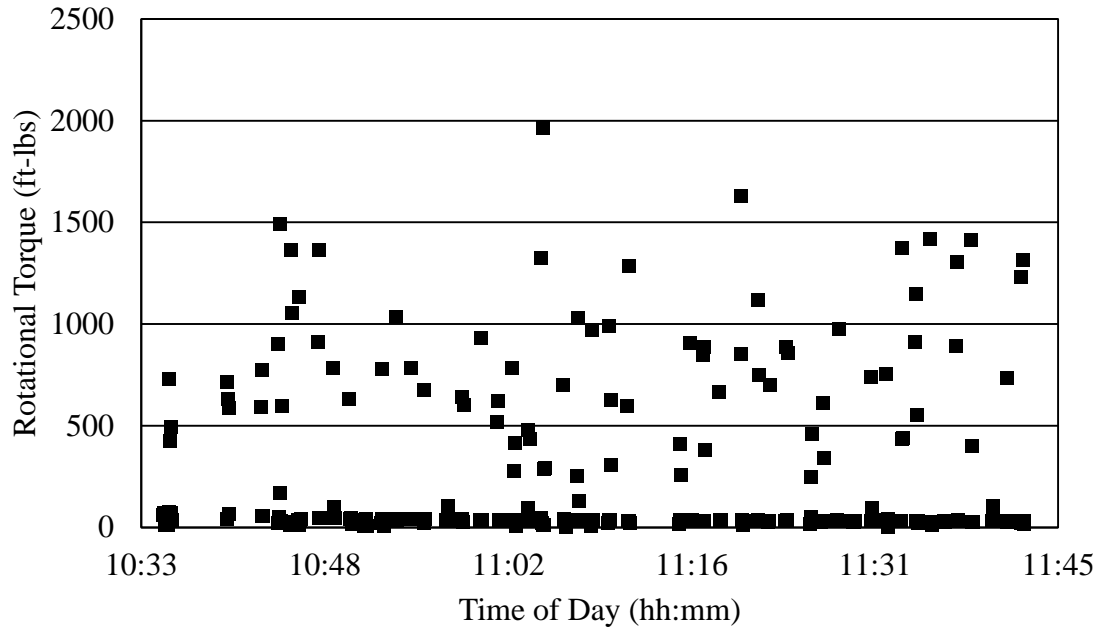


Figure A.32 Rotational Torque vs. Time for Phase One of Drive Five

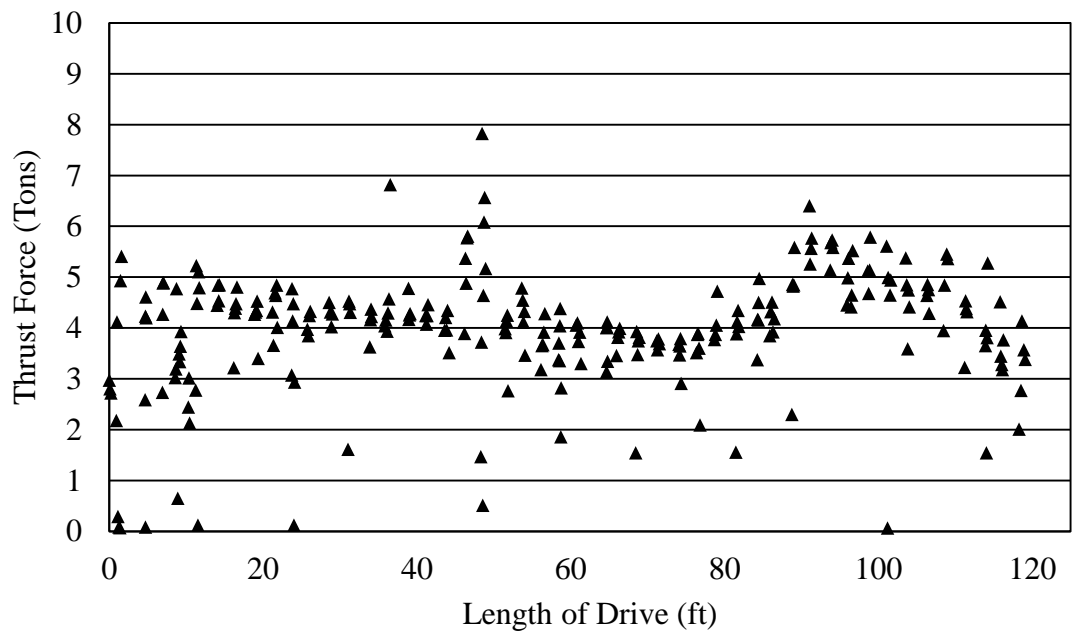


Figure A.33 Thrust Force vs. Length of Drive for Phase One of Drive Five

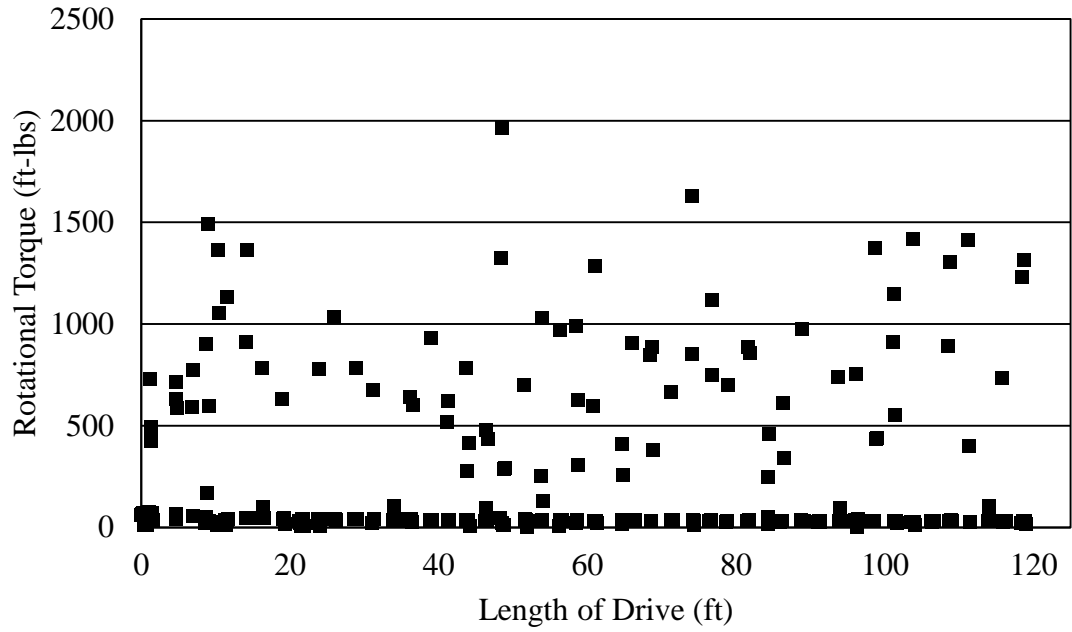


Figure A.34 Rotational Torque vs. Length of Drive for Phase One of Drive Five

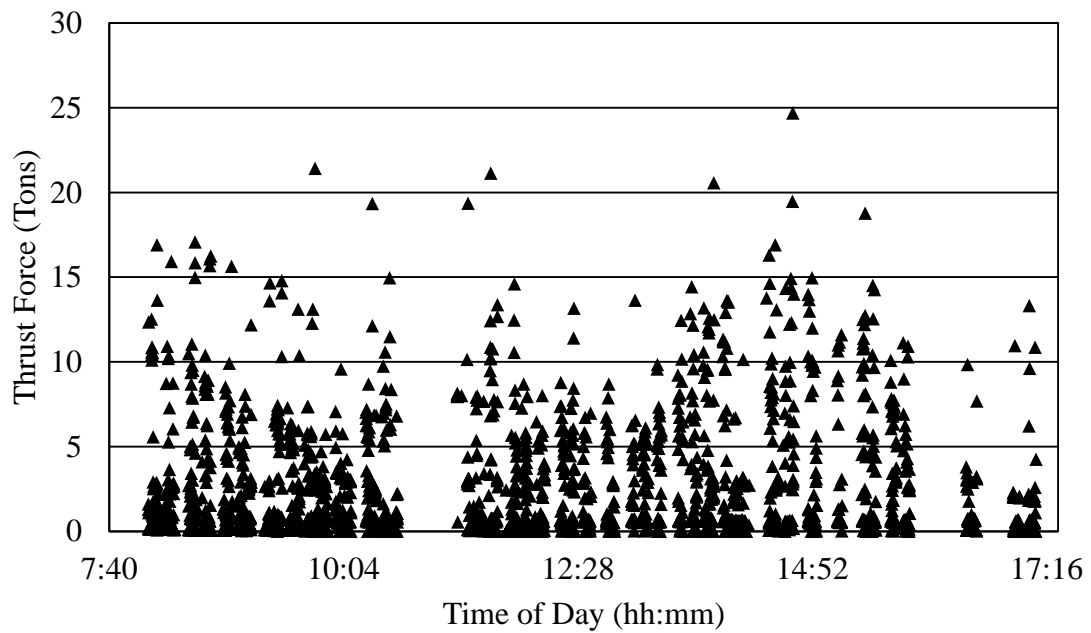


Figure A.35 Thrust Force vs. Time for Phase Two of Drive Five



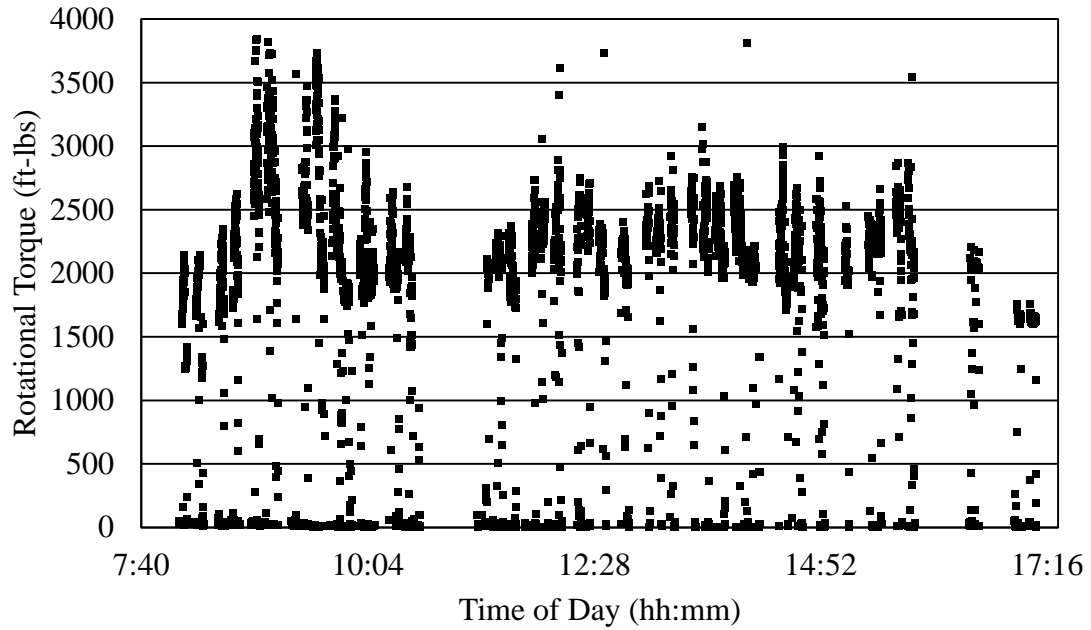


Figure A.36 Rotational Torque vs. Time for Phase Two of Drive Five

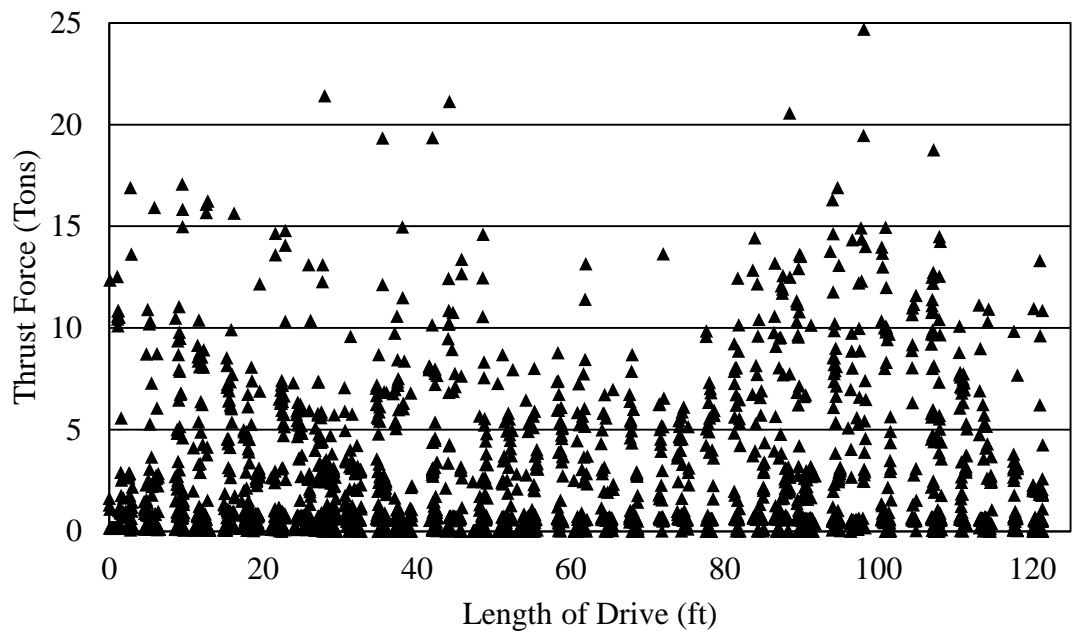


Figure A.37 Thrust Force vs. Length of Drive for Phase Two of Drive Five

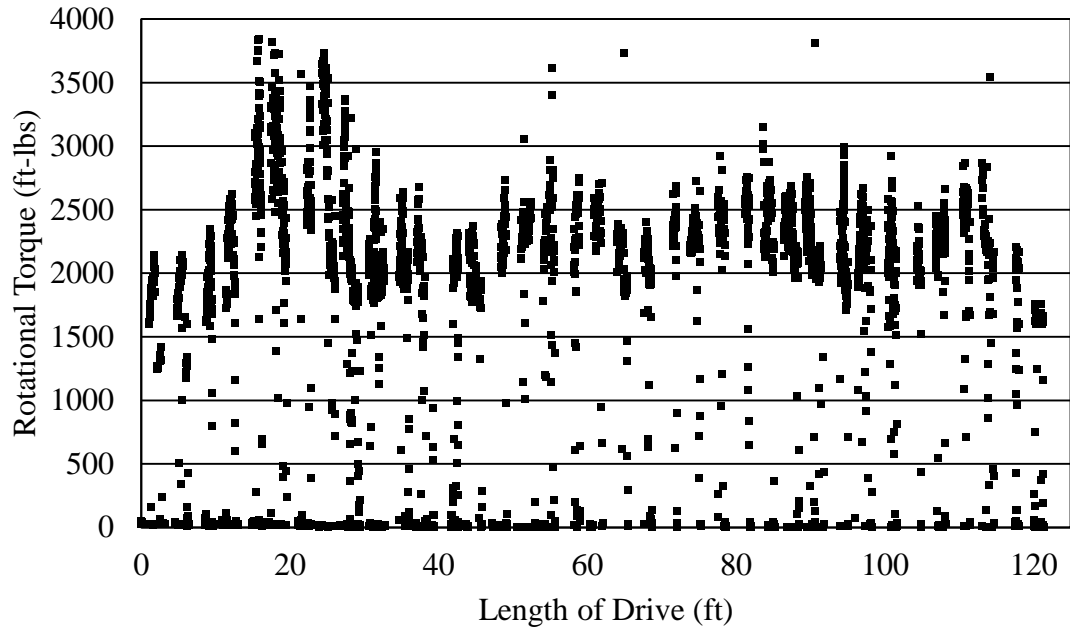


Figure A.38 Rotational Torque vs. Length of Drive for Phase Two of Drive Five

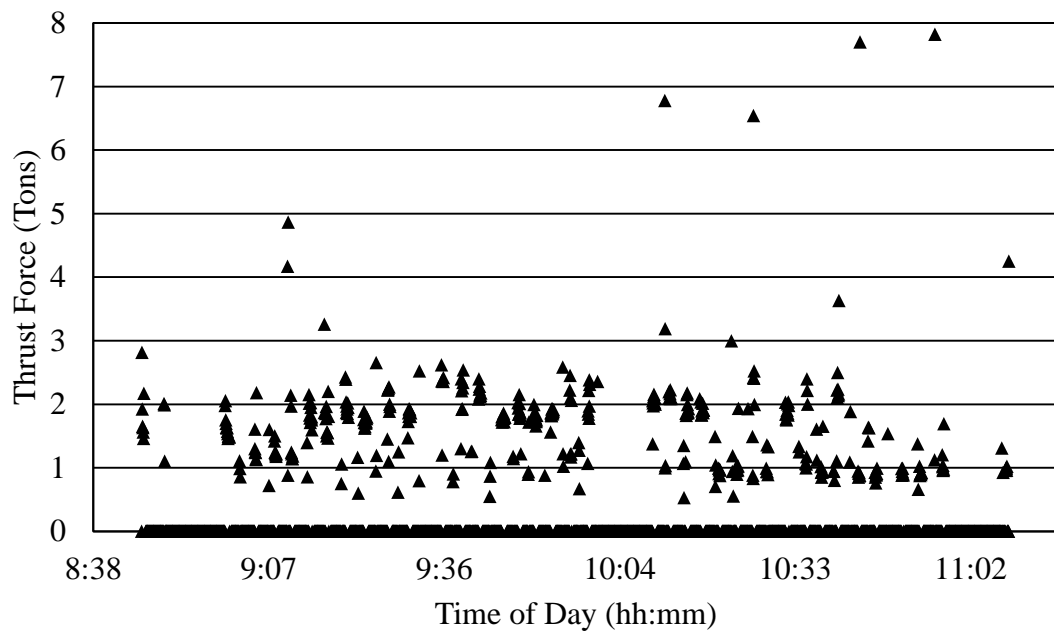


Figure A.39 Thrust Force vs. Time for Phase Three of Drive Five

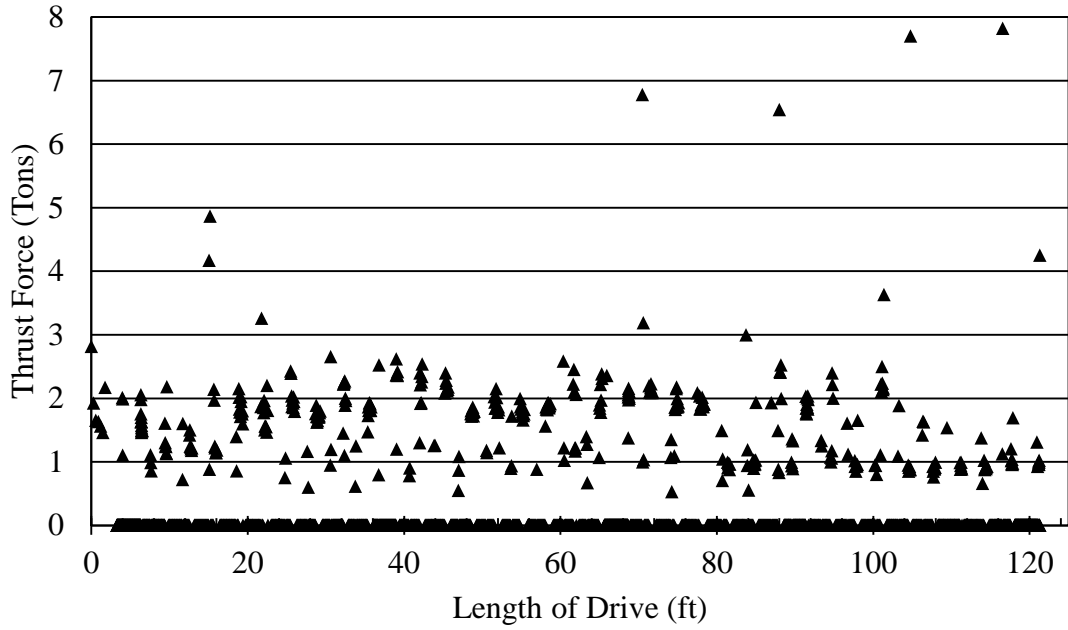


Figure A.40 Thrust Force vs. Length of Drive for Phase Three of Drive Five

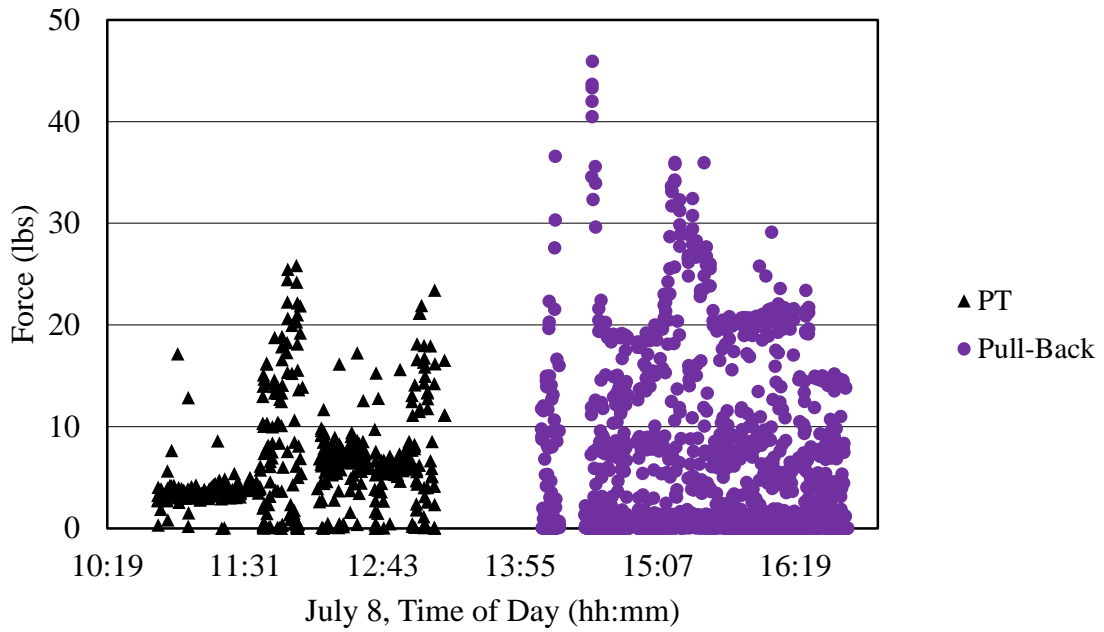


Figure A.41 July 8<sup>th</sup> Thrust and Pull Force vs. Time for Drive Six

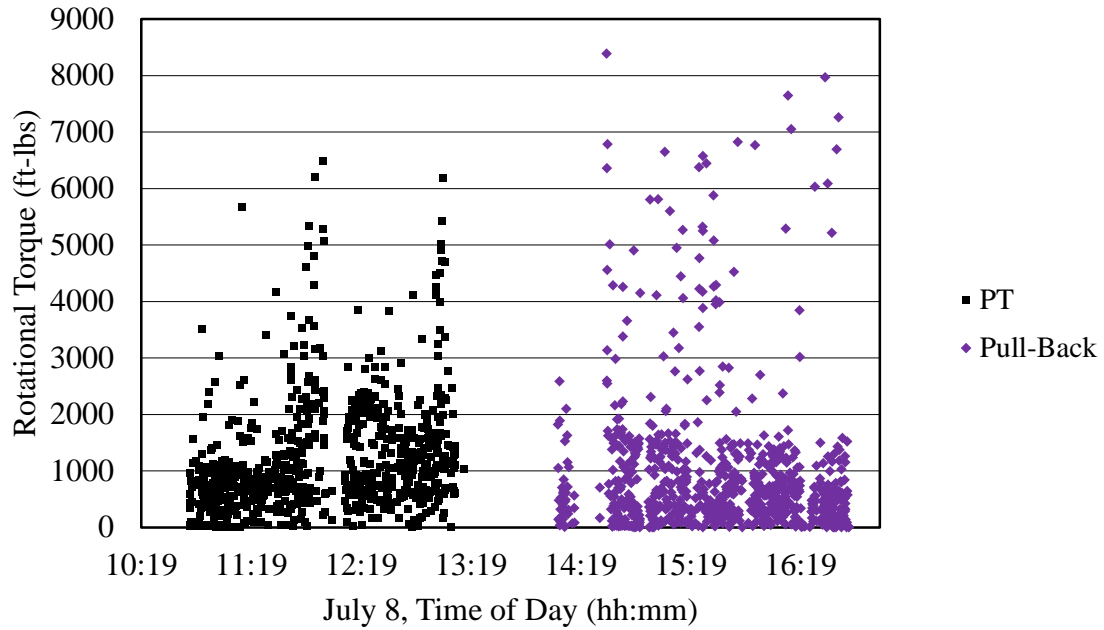


Figure A.42 July 8<sup>th</sup> Rotational Torque during PT Jacking and HDPE Pull-back vs. Time for Drive Six

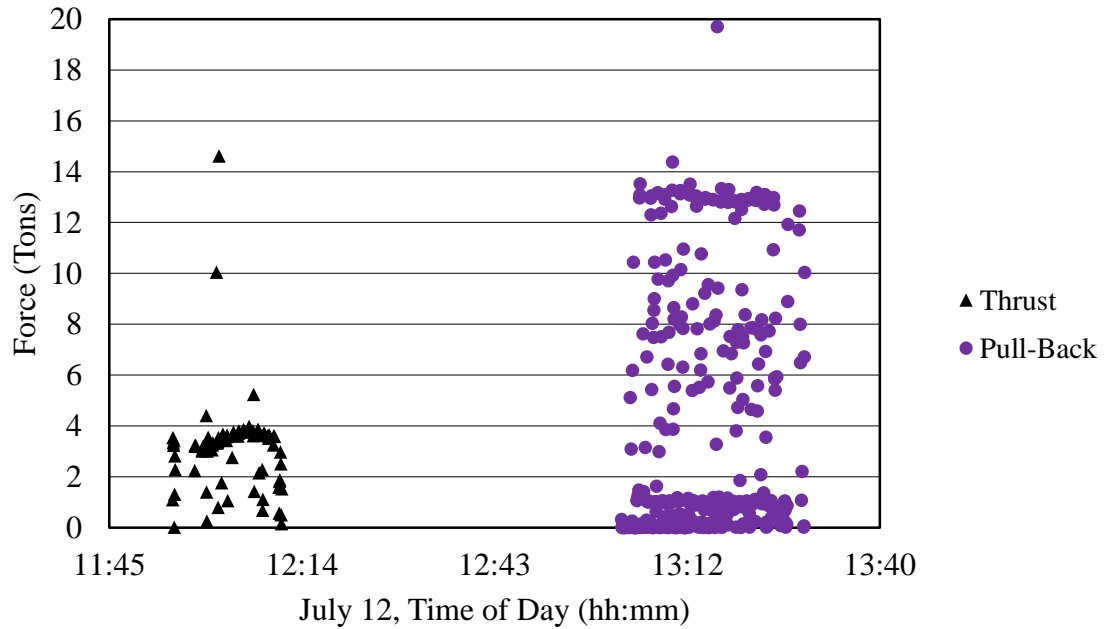


Figure A.43 July 12<sup>th</sup> Thrust and Pull Force vs. Time for Drive Six

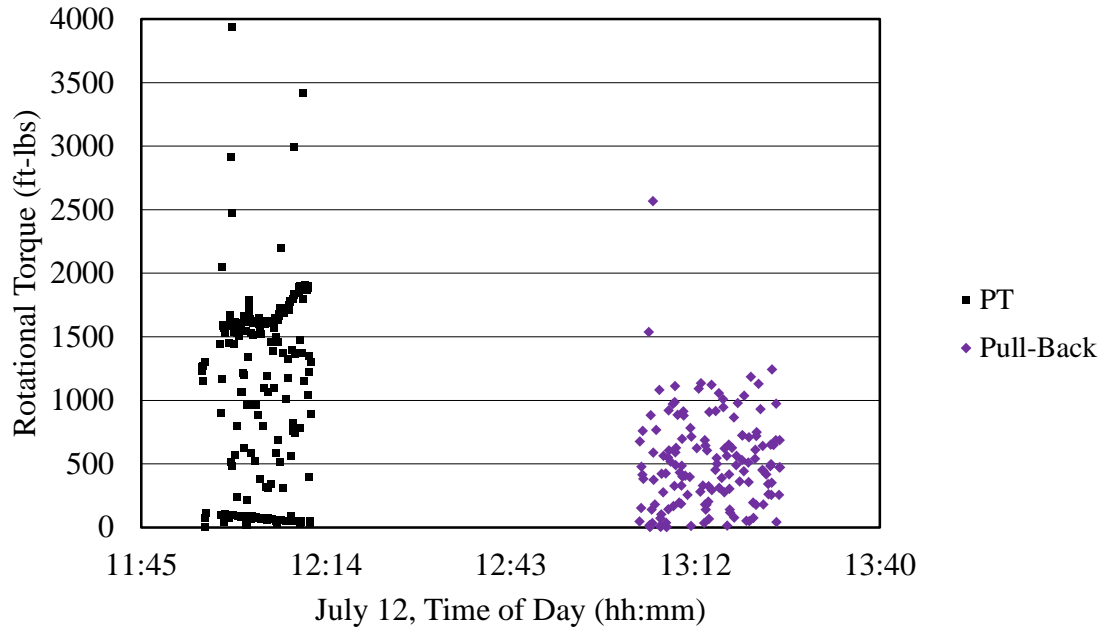


Figure A.44 July 12<sup>th</sup> Rotational Torque During PT Jacking and HDPE Pull-back vs. Time for Drive Six

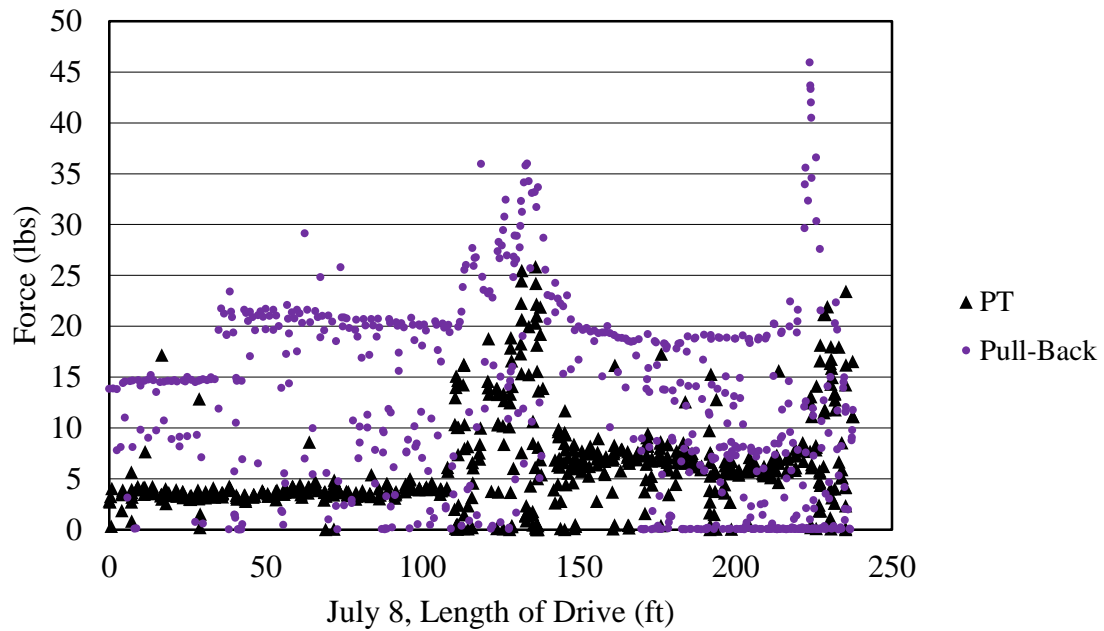


Figure A.45 July 8<sup>th</sup> Thrust and Pull Force vs. Length of Drive for Drive Six

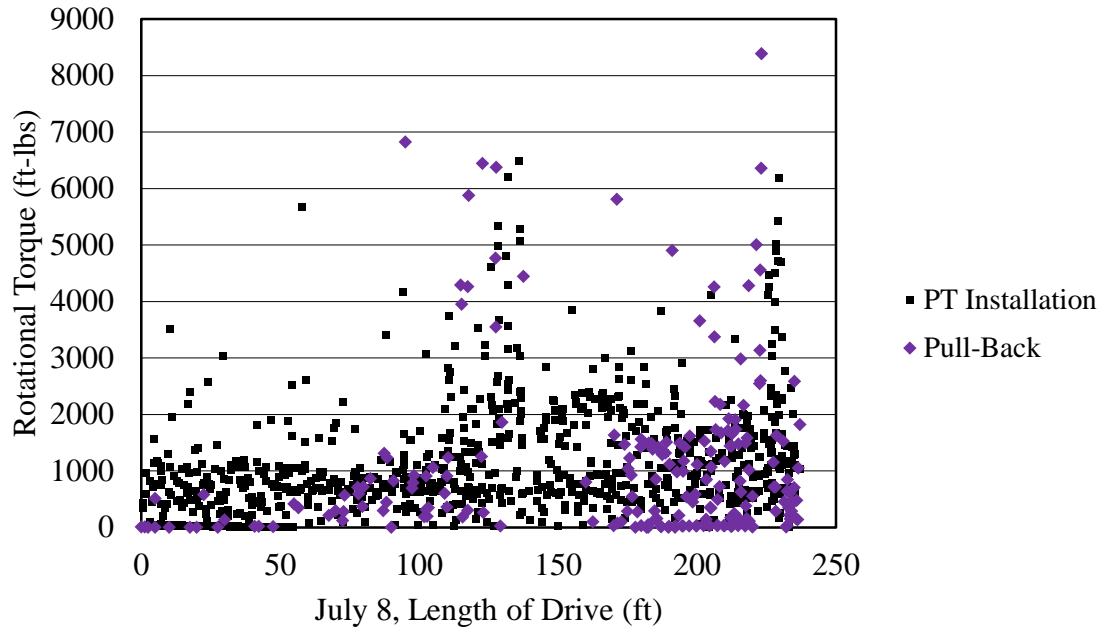


Figure A.46 July 8<sup>th</sup> Rotational Torque During PT Jacking and HDPE Pull-back vs. Length of Drive for Drive Six

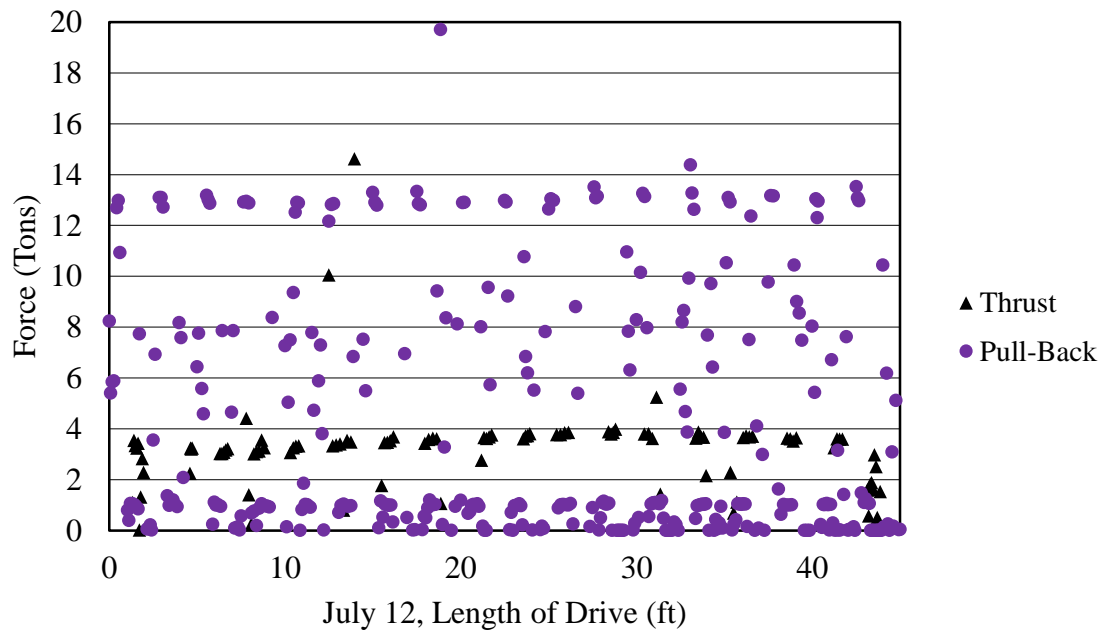


Figure A.47 July 12<sup>th</sup> Thrust and Pull Force vs. Length of Drive for Drive Six

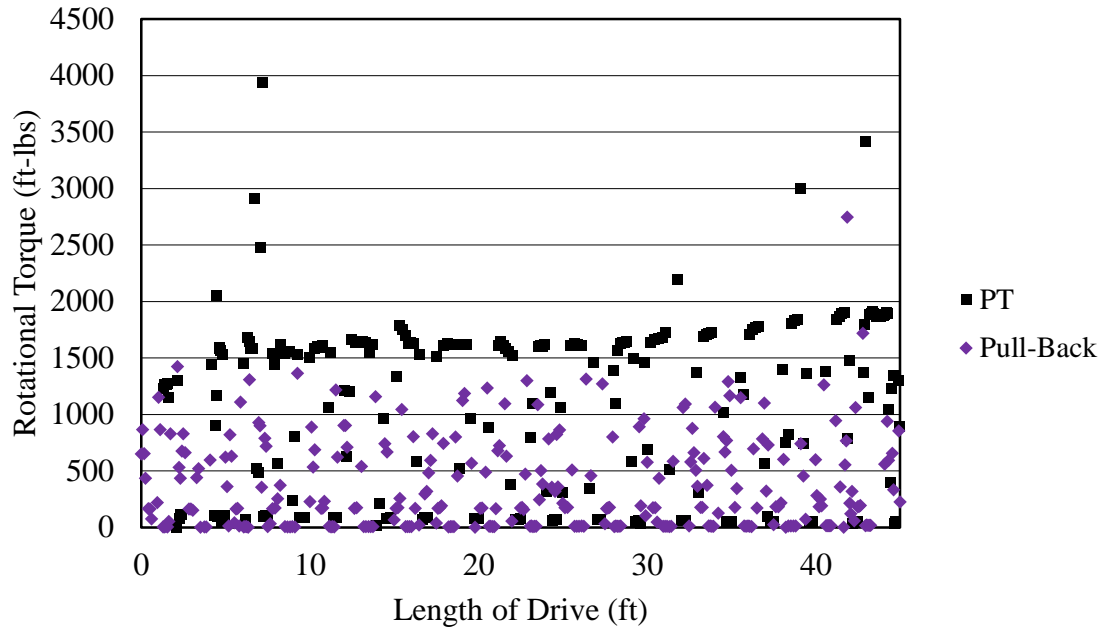


Figure A.48 July 12<sup>th</sup> Rotational Torque During PT Jacking and HDPE Pull-back vs. Length of Drive for Drive Six

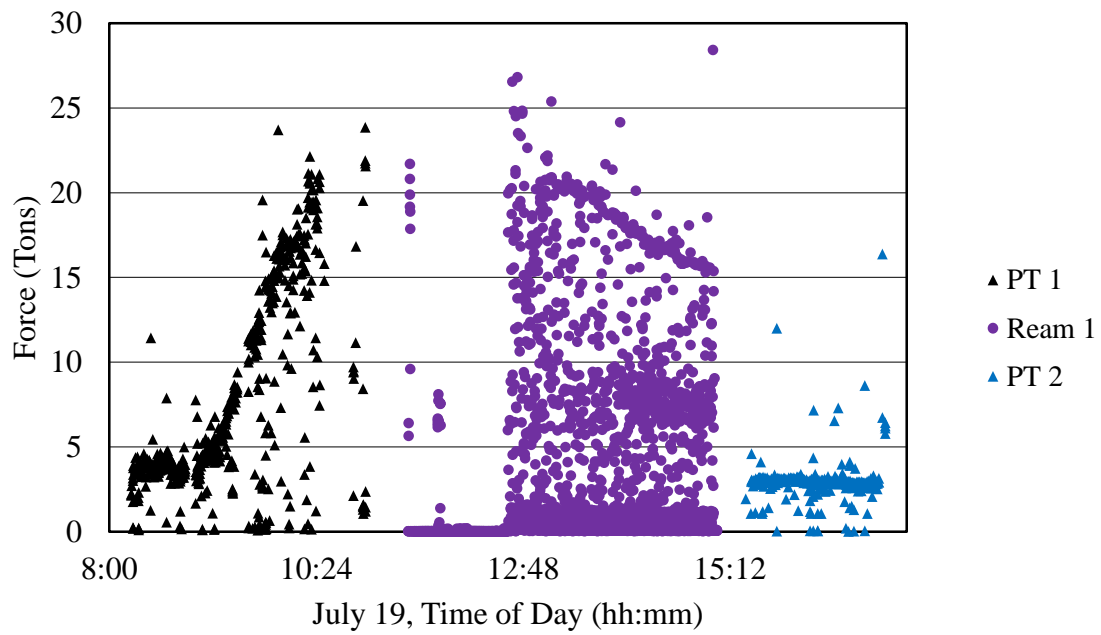


Figure A.49 July 19<sup>th</sup> Thrust and Pull Force vs. Time for Drive Seven

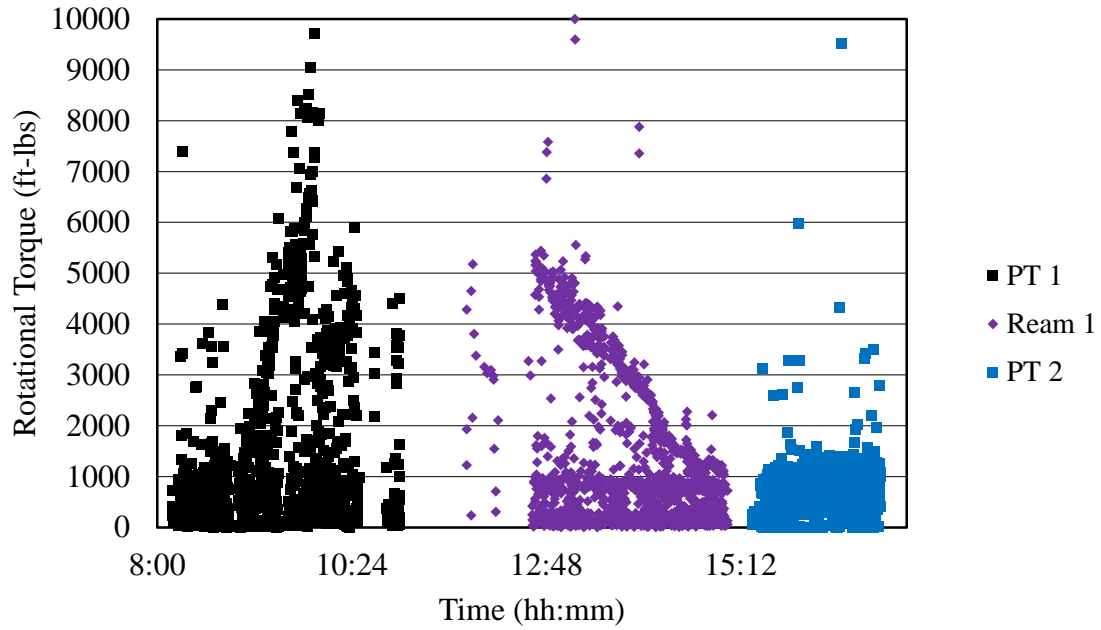


Figure A.50 July 19<sup>th</sup> Rotational Torque During PT Jacking and Pre-reaming vs. Time for Drive Seven

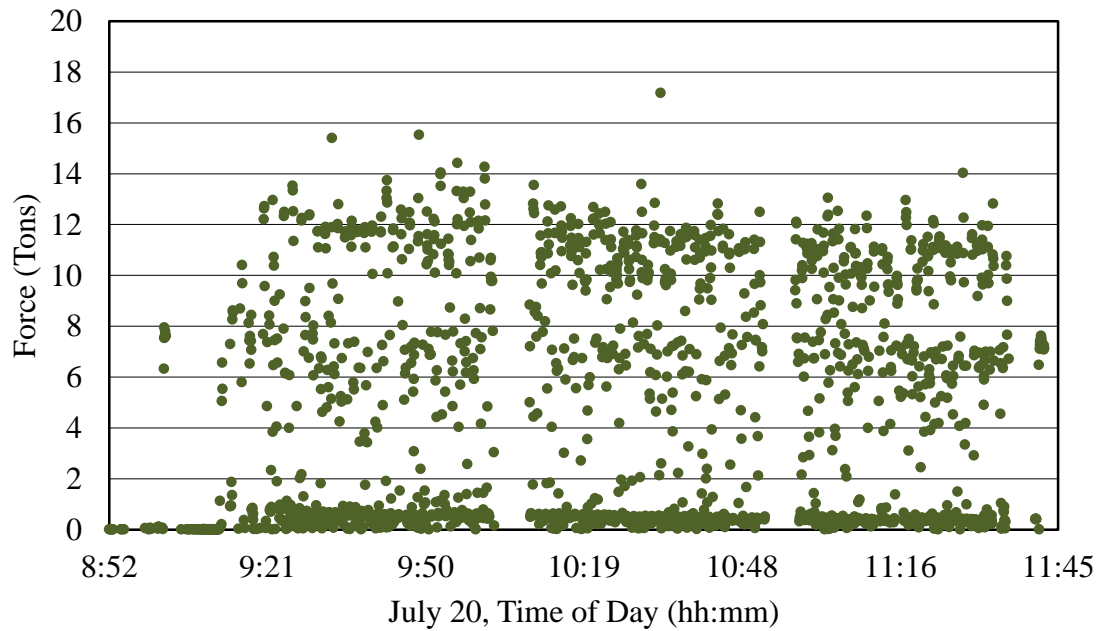


Figure A.51 July 20<sup>th</sup> HDPE Pull-back Force vs. Time for Drive Seven



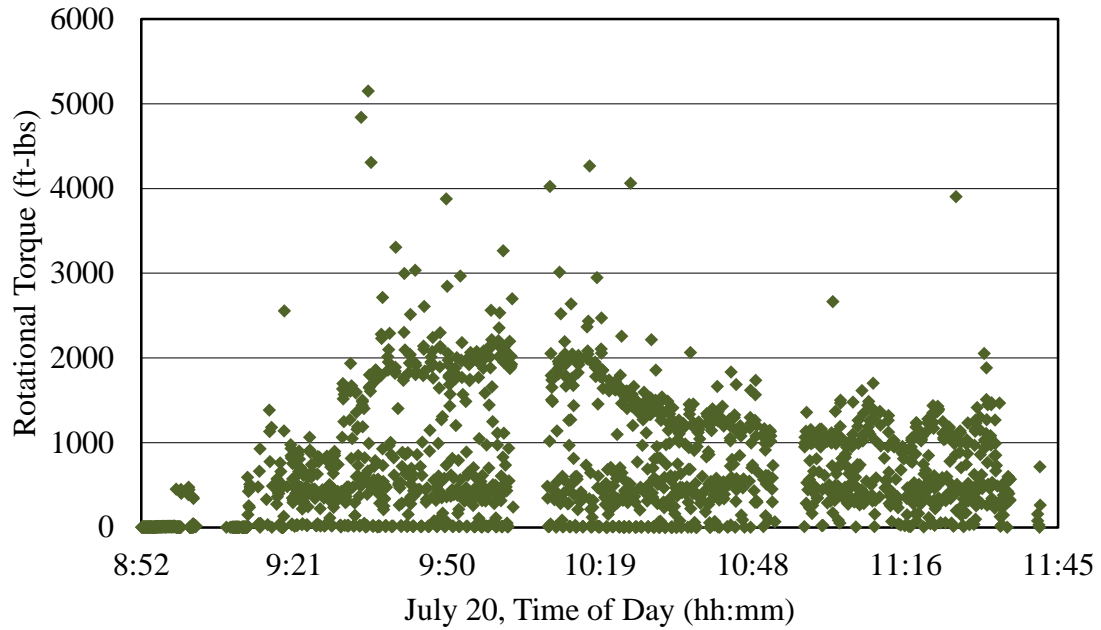


Figure A.52 July 20<sup>th</sup> Rotational Torque During HDPE Pull-back vs. Time for Drive Seven

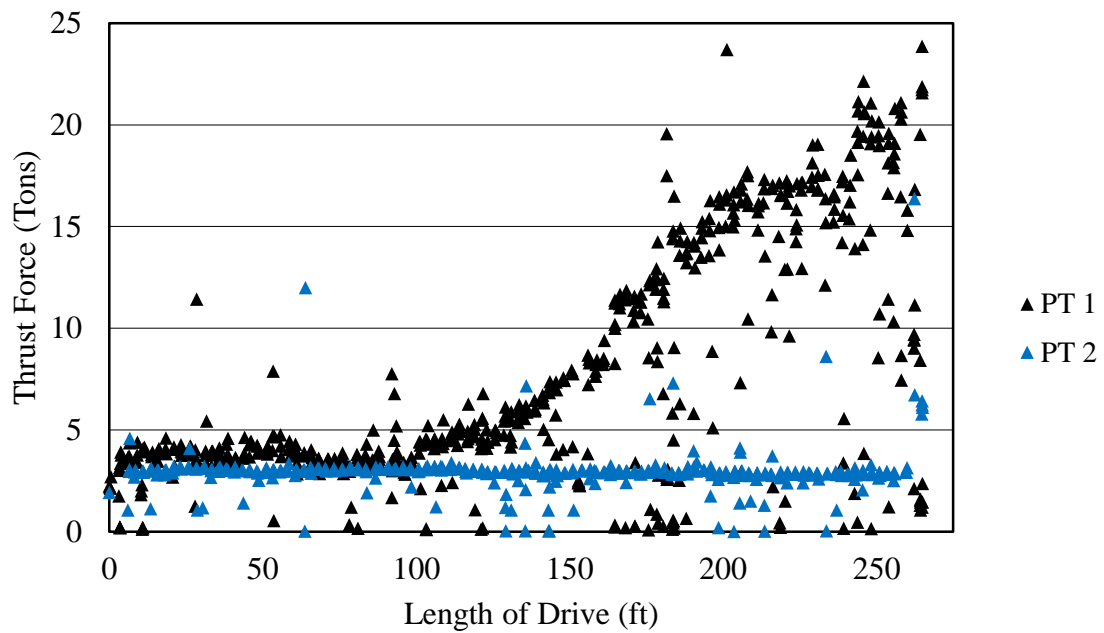


Figure A.53 Thrust Force vs. Length of Drive for Drive Seven

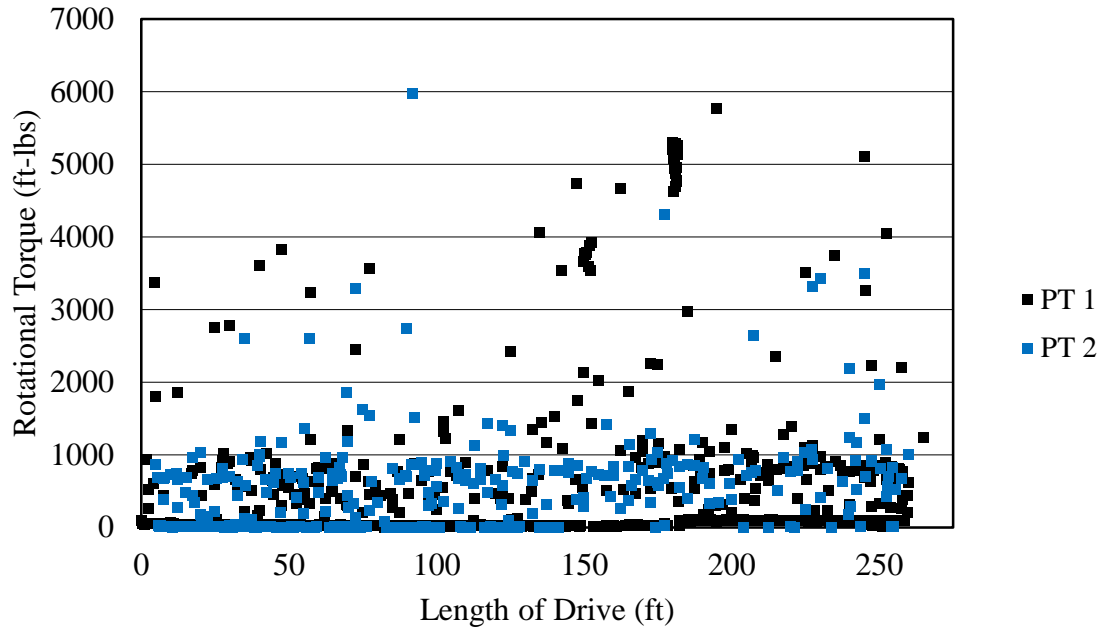


Figure A.54 Rotational Torque During PT Jacking vs. Length of Drive for Drive Seven

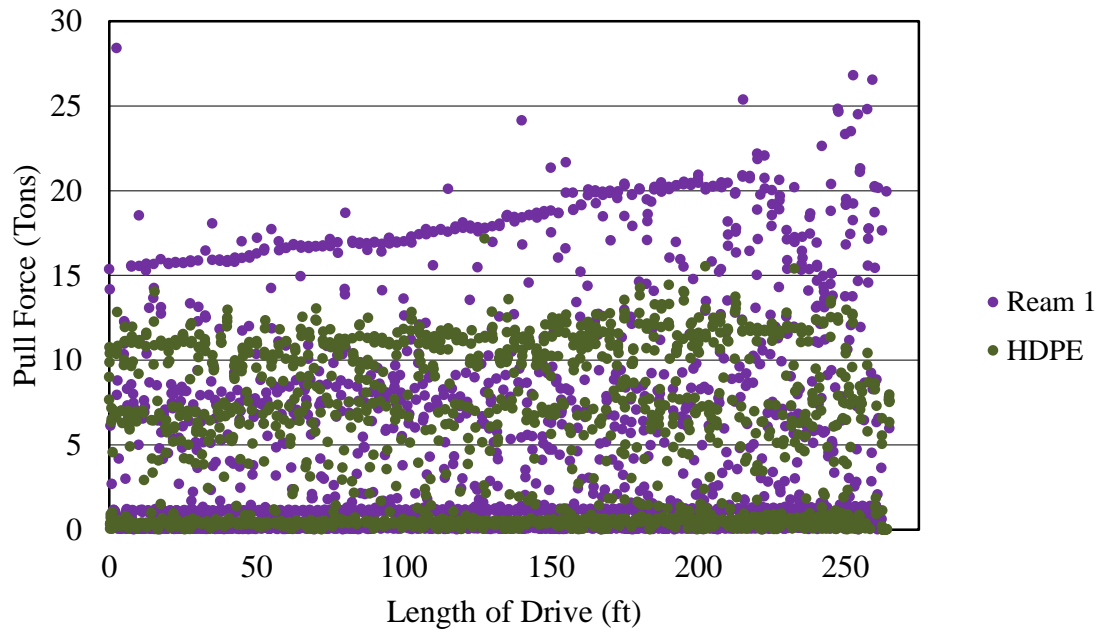


Figure A.55 Pull Force During Pre-ream and HDPE Pull-back vs. Length of Drive for Drive Seven

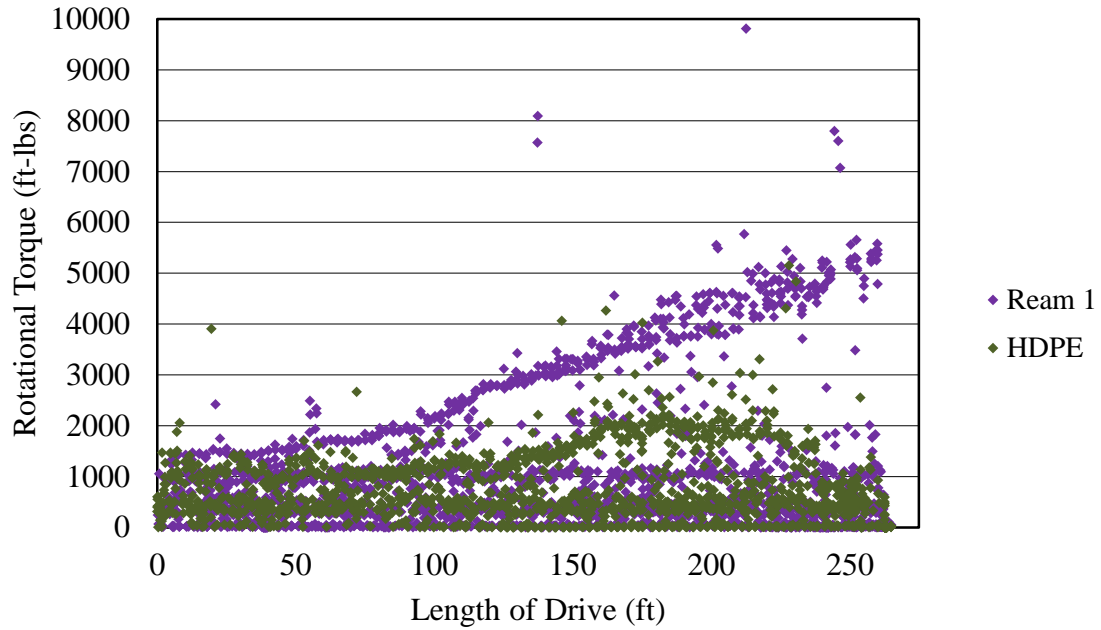


Figure A.56 Rotational Torque During Pre-ream and HDPE Pull-back vs. Length of Drive for Drive Seven

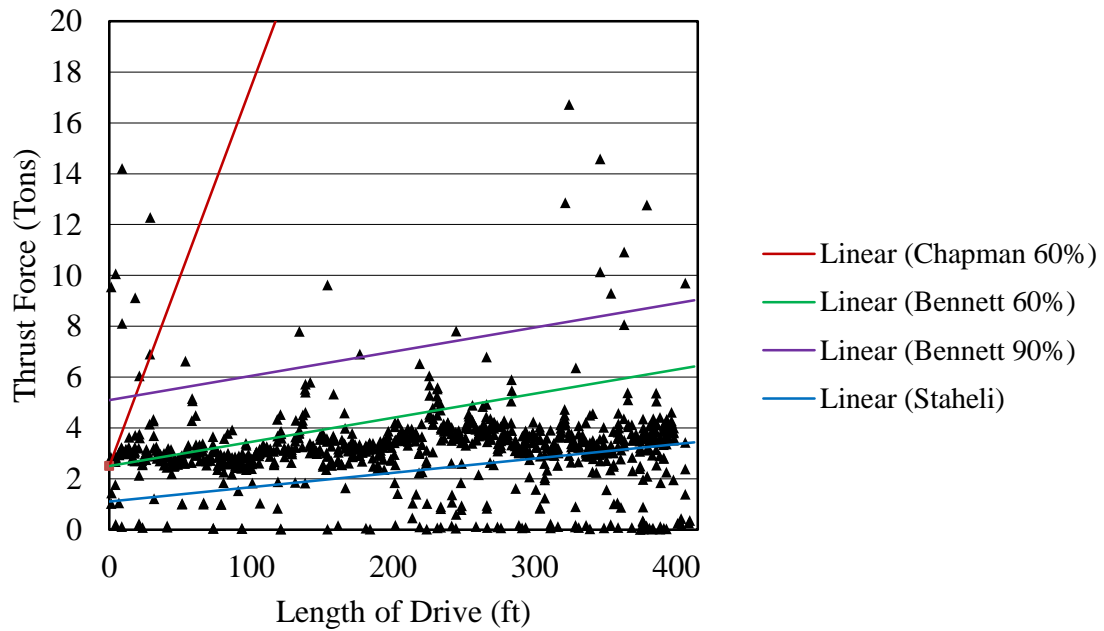


Figure A.57 Jacking Force Predictive Model Comparison: Pilot Tube, Drive One

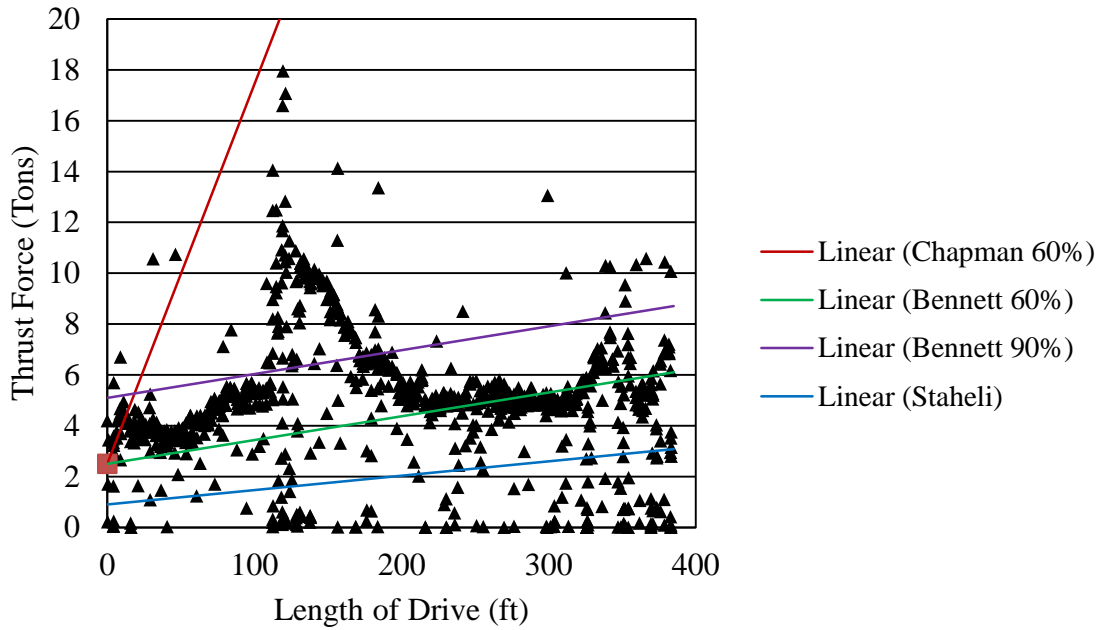


Figure A.58 Jacking Force Predictive Model Comparison: Pilot Tube, Drive Two

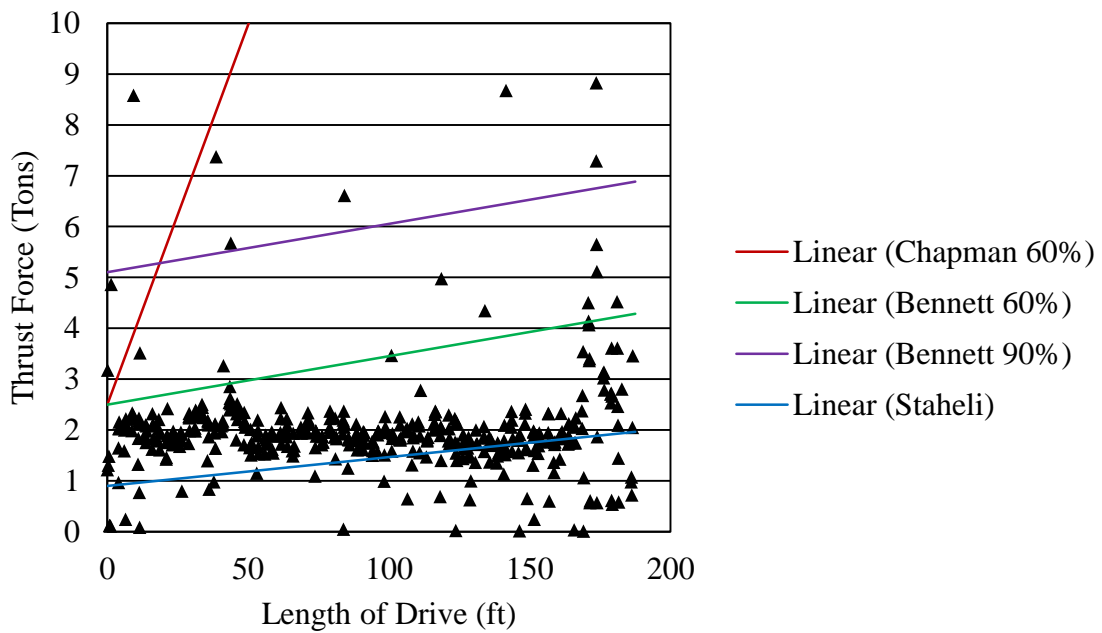


Figure A.59 Jacking Force Predictive Model Comparison: Pilot Tube, Drive Three

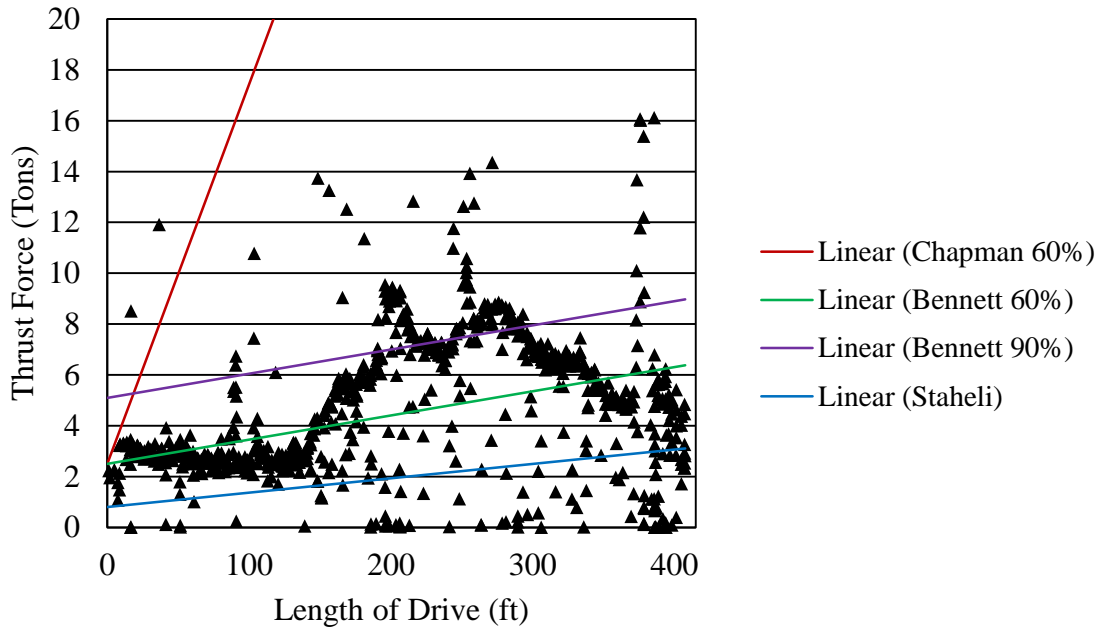


Figure A.60 Jacking Force Predictive Model Comparison: Pilot Tube, Drive Four

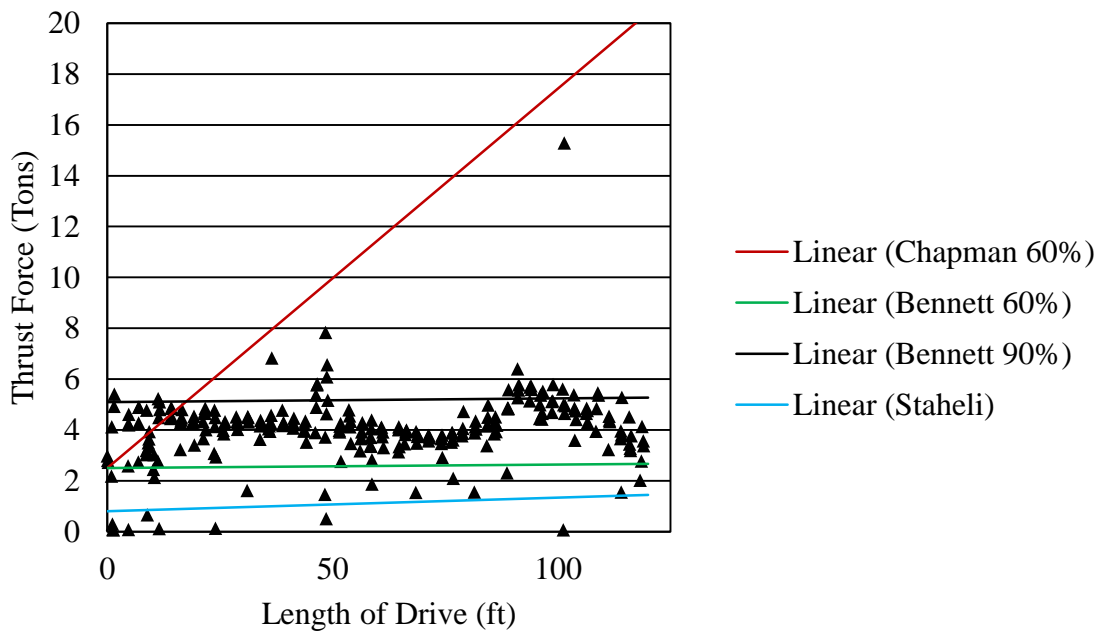


Figure A.61 Jacking Force Predictive Model Comparison: Pilot Tube, Drive Five

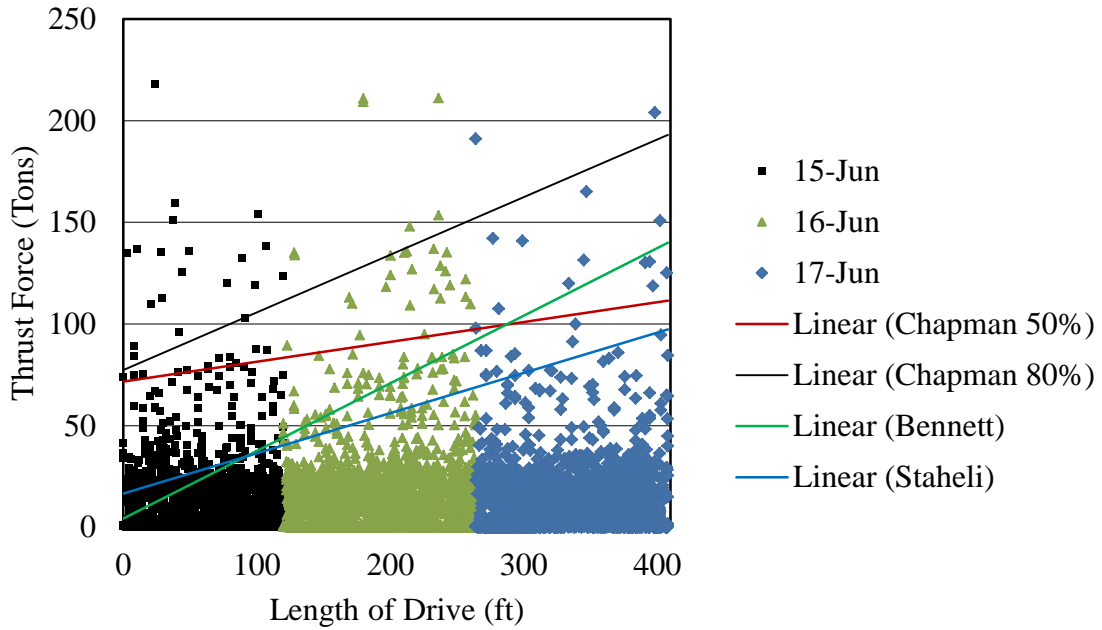


Figure A.62 Jacking Force Predictive Model Comparison: 21-Inch Casing, Drive One

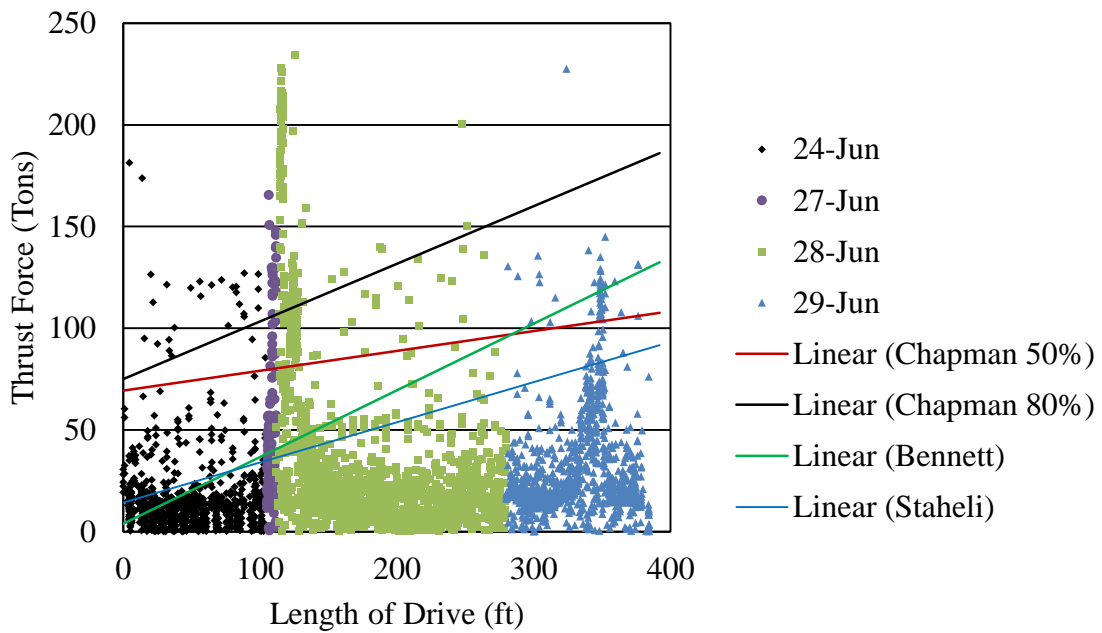


Figure A.63 Jacking Force Predictive Model Comparison: 21-Inch Casing, Drive Two

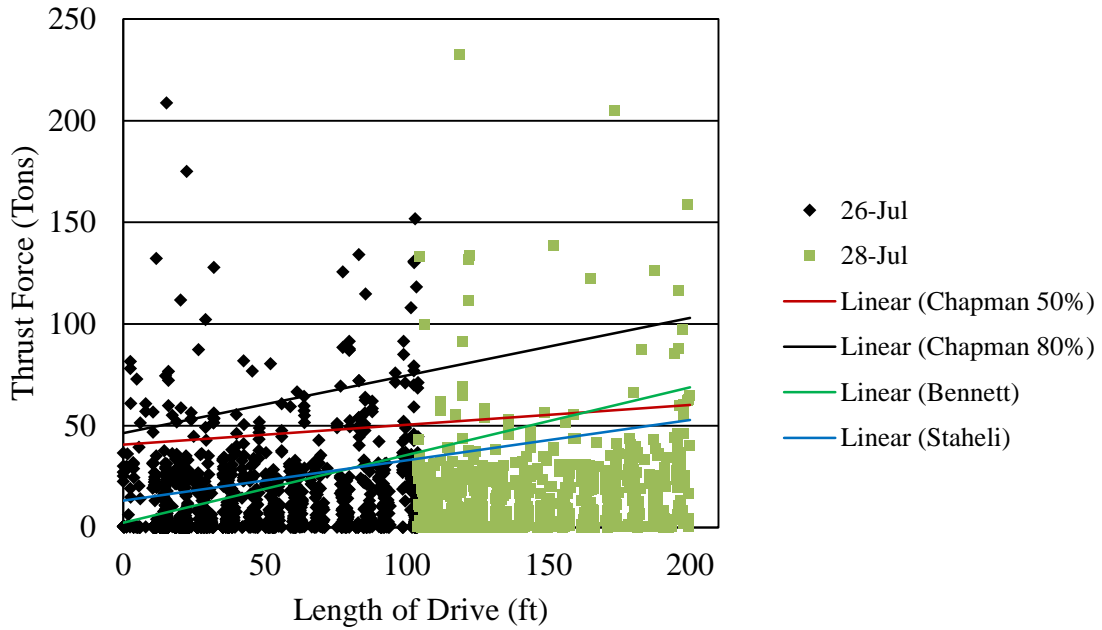


Figure A.64 Jacking Force Predictive Model Comparison: 21-Inch Casing, Drive Three

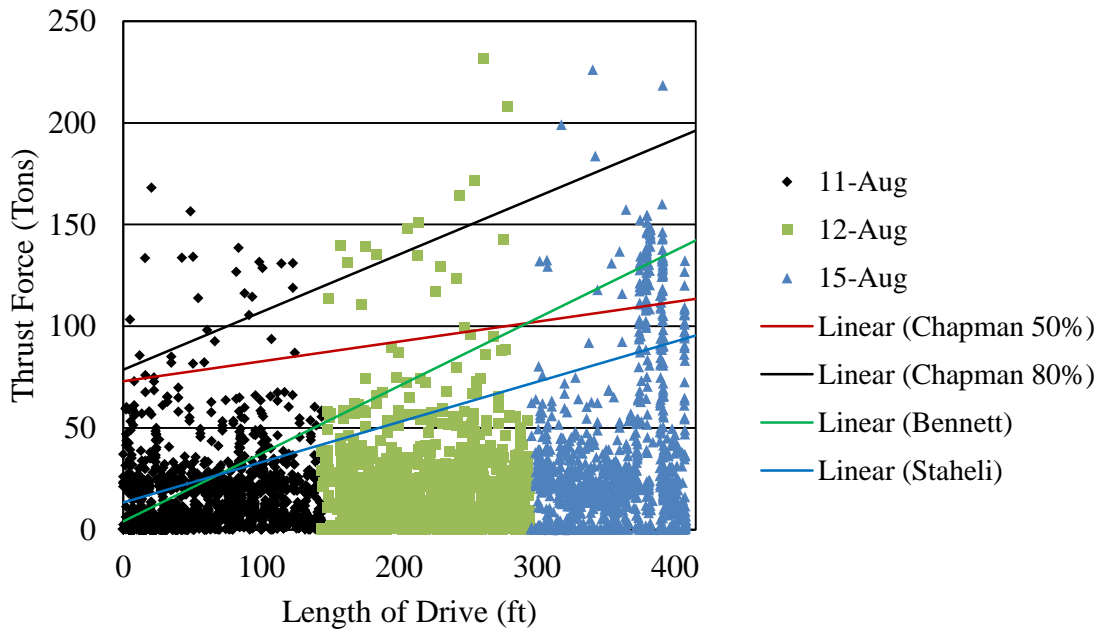


Figure A.65 Jacking Force Predictive Model Comparison: 21-Inch Casing, Drive Four

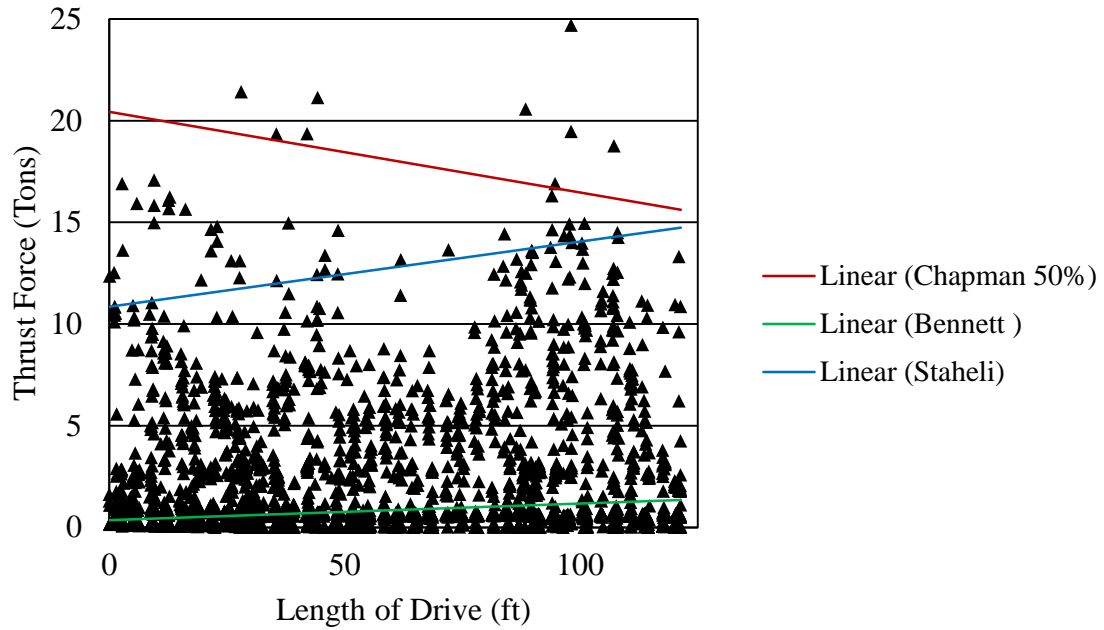


Figure A.66 Jacking Force Predictive Model Comparison: 8-Inch Casing, Drive Five

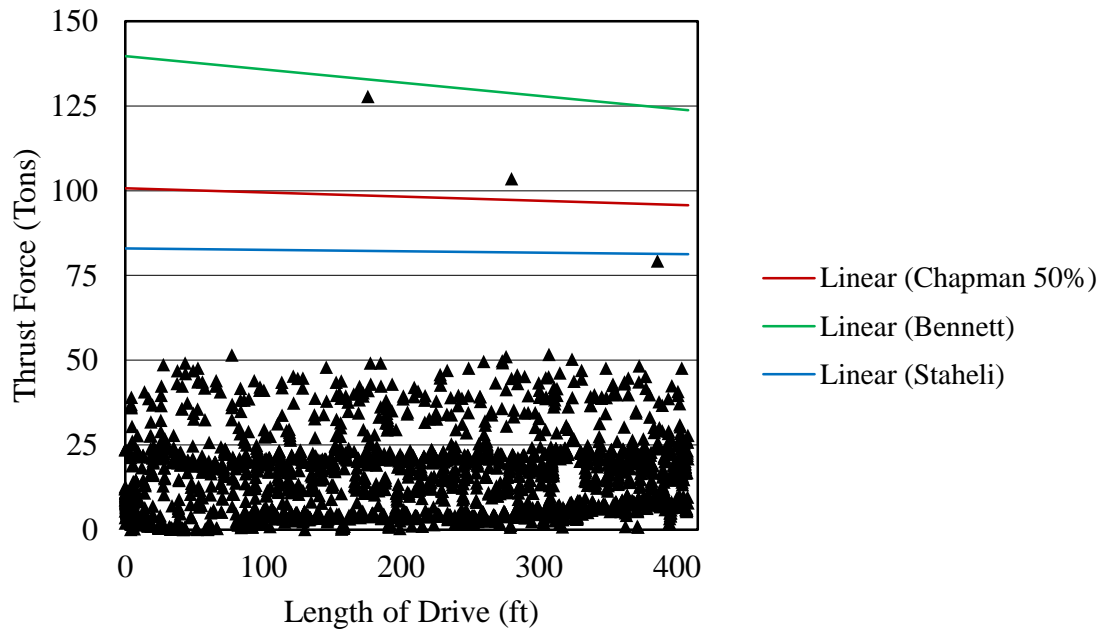


Figure A.67 Jacking Force Predictive Model Comparison: 21-Inch VCP, Drive One



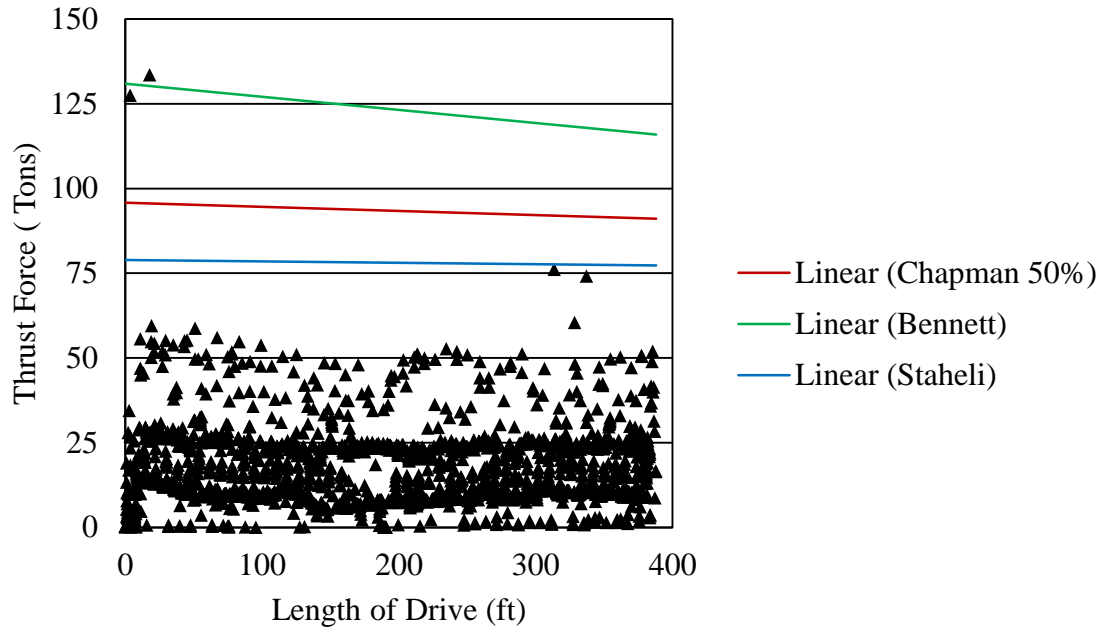


Figure A.68 Jacking Force Predictive Model Comparison: 21-Inch VCP, Drive Two

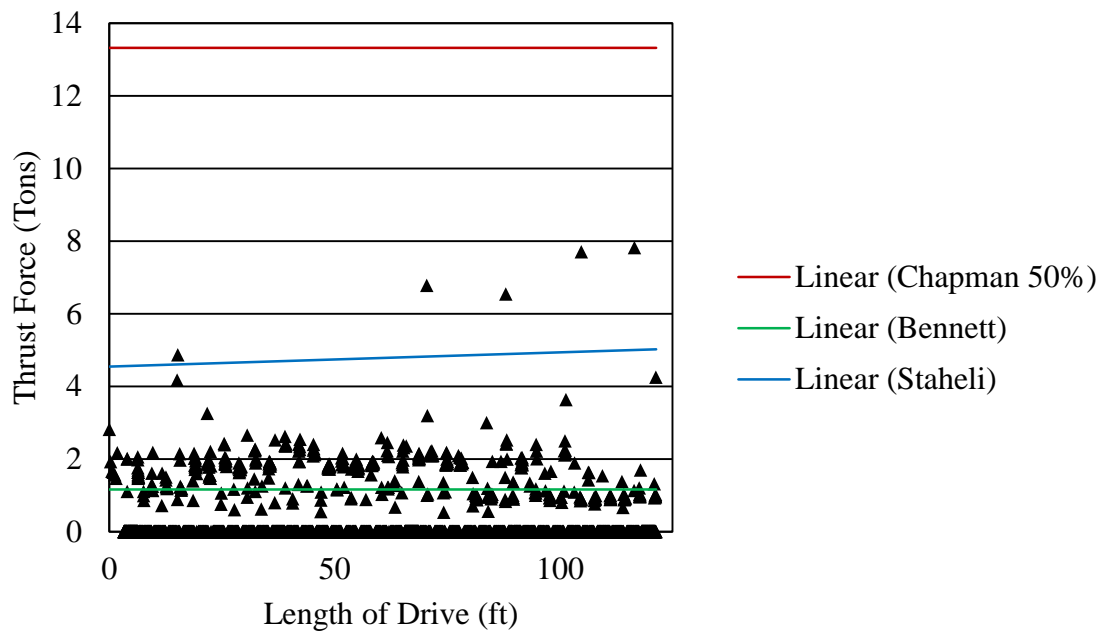


Figure A.69 Jacking Force Predictive Model Comparison: 8-Inch VCP, Drive Five

APPENDIX B  
SUPPLEMENTAL TABLES

Table B.1 Existing Models for Predicting the Frictional Component of Jacking Force  
(Modified from Staheli 2006)

Author	Frictional Component of Jacking Force (kN)	Variables and Notes
Helm (1964)	<p>Circular Cross Section: <math>\mu \cdot \gamma \cdot h \cdot \frac{K_a+1}{2}</math>                      Rectangular Cross Section: <math>\mu \cdot \gamma \cdot h \cdot \frac{K_a \cdot d_a + b_a}{b_a + d_a}</math></p>	<p><math>K_a</math> = Active earth pressure coefficient  <math>b_a</math> = External width of the microtunneling shield  <math>d_a</math> = External height or diameter of the microtunneling shield</p>
Walendky and Möncke (1970)	$\gamma \cdot h \cdot \sqrt{\frac{K_0^2 + 1}{2}} \cdot \tan \delta$	<p><math>\delta = \phi/2</math>, wall friction angle  <math>K_0</math> = At rest earth pressure coefficient  <math>H</math> = Cover depth</p>
Szentandrási (1981), Scherle (1977)	$\mu \left( H_w + \frac{d_a}{2} \cdot \frac{K_{Sch} + K_{k1} + K_{k2} + K_{So}}{4} + \frac{W_s - F_A}{4d_a} \right)$	<p><math>H_w</math> = Effective cover depth  <math>W_s</math> = Weight of pipe  <math>F_A</math> = Buoyancy</p>
Solomo (1979)	<p>Circular Cross Section: <math>\gamma \cdot \left( h + \frac{d_a}{2} \right) \cdot \sqrt{K_m} \tan \delta</math>                      Rectangular Cross Section:  <math display="block">\gamma \cdot h \cdot \mu \cdot (b_a + K_m + d_a) \cdot \frac{1 + \frac{d_a}{2h}}{b_a + d_a}</math></p>	<p>Use with very dense compacted sand.  <math>K_m</math> = Effective earth pressure coefficient</p>
Weber (1981)	<p>Circular Cross Section: <math>\mu \cdot \sqrt{p_v \cdot p_h}</math>                      Rectangular Cross Section:  <math display="block">\mu \left[ (\kappa \cdot b_a) + (K_0 \cdot d_a) + K_0 \cdot \frac{d_a^2/dh}{b_a + d_a} \right]</math></p>	<p>Slurry Boring Method  <math>\mu = 0.46</math>  <math>p_v</math> = Vertical earth pressure  <math>p_h</math> = Horizontal earth pressure</p>
Weber (1981)	$\mu \cdot E_s \cdot \frac{\Delta d_a}{d_a}$ <p>With Stiffness Modulus from Ohde:  <math display="block">E_s = \nu \cdot \left( \frac{\sigma}{\sigma_1} \right)^w</math></p>	<p>Auger Boring Method w/ Steel Pipes (318, 508, and 711 mm diameter):  <math>\nu, w</math> = Stiffness coefficients  <math>\Delta d_a</math> = Deformation dimension of the pipe string</p>

Table B.1 Continued (Modified from Staheli 2006)

Hasan (1985)	$\tan\delta \cdot \left[ \kappa_m \cdot \gamma \cdot \frac{h}{2} \cdot \left( 1 + \frac{d_a}{2} \cdot \kappa_m \cdot h \right) \right] + \frac{W}{4d_a}$				$\tan\delta$ = Coefficient of friction $\kappa_m$ = Reduction factor	
	Jacking Method	$\frac{h}{d_a}$	Overcut	No Cohesion		Cohesive
	Open Shield	$\leq 2$	N/A	$\kappa_m = 1$		$\kappa_m = 1$
		$\geq 2$	N/A	$\kappa_m = (1+\kappa)/2$		$\kappa_m = 1$
	Closed Shield	$\leq 2$	With	$\kappa_m = 1$		$\kappa_m = (1+\kappa)/2$
$\leq 2$		Without	$\kappa_m = 1$	$\kappa_m = 1$		
$\geq 2$		With	$\kappa_m = (1+\kappa)/2$	$\kappa_m = (1+\kappa)/2$		
ATV-A 161E (1990)	Circular Cross Section: $\mu \cdot \gamma \cdot h \cdot \kappa \cdot [b_a + (K_2 \cdot d_a)] + K_2 \cdot \frac{d_a^2/2h}{(b_a + d_a)}$				$\kappa = \frac{1 - e^{\tan(0.5\varphi) \cdot h/b}}{\tan(0.5\varphi) \cdot h/b}$ $b_a = \frac{2d_a}{\sqrt{3}}$	
Elbert (1990)	$0.5\mu \cdot \left[ a \cdot \gamma \cdot h + \left( \gamma \left\{ h + \frac{d_a}{2} \right\} + P_a \right) K_0 + W_s \right] \frac{10}{L_R}$				$\gamma$ = Soil density $a$ = Active load coefficient $P_0$ = Surface loads $K_0$ = At rest earth pressure coefficient $L_R$ = Pipe length	
Herzog (1996)	$\mu \cdot \gamma \cdot \left( h + \frac{d_a}{2} \right) \cdot \frac{K_0 + 1}{2}$					
Bennett (1998)	$F_r = C_a \gamma' d_p \tan(C_f \varphi_r) A_p L$				$\gamma'$ = Effective soil unit weight $d_p$ = Pipe diameter $\varphi_r$ = Residual soil friction angle $A_p$ = Pipe circumference $L$ = Length of bore	
Chapman and Ichioka (1999)	$P = a + 3.8d_a$				Statistical evaluation of 198 slurry microtunneling projects. $a = 1.53$ for clay, $2.43$ for sand, $3.43$ for sand/gravel	
Osumi (2000)	$f_0 = \beta(\pi B_c q + w)\mu' + \pi B_c C'$ $C' =$ Pipe and soil adhesion (8 kPa for $N < 10$ & 5 kPa for $N > 10$ )				$\beta$ = Jacking force reduction factor $B_c$ = Diameter of the pipe $q$ = Normal force $w$ = Pipe weight	
Paul (Stein 2005)	$\mu \cdot \left[ 2 \left( \gamma \cdot \frac{h}{d_a} + P_{VR} \right) \right] \cdot (1 + K_a) + W_s$					
Iseki (Stein 2005)	$\mu \cdot (q + W_s) + C$				$q$ = Loading vertical to pipe axis (kPa) $\mu = \tan(\varphi/2)$	

Table B.2 Overview of Forces and Torques Present on Each Drive

21 Inch Drives		Thrust Force (Tons)			Rotational Torque (ft-lbs)		
Drive	Phase	High	Typical High	Typical Low	High	Typical High	Typical Low
1	1	6	6	3	3500	2500	1500
	2	45	35	25	-	-	-
	3	50	35	22	-	-	-
2	1	13	5	3.5	8000	3000	2000
	2	225	40	16	-	-	-
	3	50	30	25	-	-	-
3	1	6	2.5	1.75	2300	2000	1000
	2	75	50	25	-	-	-
	3	-	-	-	-	-	-
4	1	10	9	3	7000	6000	1500
	2	150	60	30	-	-	-
	3	-	-	-	-	-	-
8 Inch Drive		Thrust Force (Tons)			Rotational Torque (ft-lbs)		
Drive	Phase	High	Typical High	Typical Low	High	Typical High	Typical Low
5	1	8	6	3.5	2000	1500	750
	2	25	15	7	4000	3000	1750
	3	5	2.5	1.5	-	-	-
4 Inch Laterals		Thrust or Pull Force (Tons)			Rotational Torque (ft-lbs)		
Drive	Phase	High	Typical High	Typical Low	High	Typical High	Typical Low
6	PT	25	9	4	6000	3000	1000
	Pull-Back	45	35	19	7000	2000	800
	PT2	5	4	3	2100	2100	1500
	Pull-Back 2	14.5	13	12.5	1750	1400	1100
7	PT	34	22	4	6000	1750	1000
	Pre-Ream	27	25	15	8000	5500	1500
	PT 2	6	3	3	6000	1750	1000
	Pull-Back	16	13.5	11	4500	2500	1000

Table B.3 PTMT and PT/HDD Phase Specific Force and Torque Behavior

Phase of Interest	# of Drives Used	Initial or Subsequent Pass	Force (Tons)			Torque (ft-lbs)		
			Max	Typical High	Min	Max	Typical High	Min
Pilot Tube	7	1 <sup>st</sup>	34	9	2	7000	2800	750
Pilot Tube	2	2 <sup>nd</sup>	6	4	3	6000	1950	1000
Pull Back	2	1 <sup>st</sup>	45	30	15	8000	3750	800
Pull Back	2	2 <sup>nd</sup>	16	13	11	4500	1950	1000
8" Casing	1	N/A	25	15	7	4000	3000	1750
21" Casing	4	N/A	225	46	16	N/A	N/A	N/A
8" VCP	1	N/A	5	3	1	N/A	N/A	N/A
21" VCP	2	N/A	50	33	22	N/A	N/A	N/A

Table B.4 Drives Inclusive of Maximum and Minimum Forces and Torques

Phase of Interest	Initial or Subsequent Pass	Drive #			
		Force (Tons)		Torque (ft-lbs)	
		Max	Min	Max	Min
Pilot Tubes	1 <sup>st</sup>	7	3	4	5
Pilot Tubes	2 <sup>nd</sup>	7	6 & 7	7	7
Pull Back	1 <sup>st</sup>	6	7	7	6
Pull Back	2 <sup>nd</sup>	7	7	7	7
8" Casings	N/A	5	5	5	5
21" Casings	N/A	2	2	N/A	N/A
8" VCP	N/A	5	5	N/A	N/A
21" VCP	N/A	1 & 2	1	N/A	N/A

Table B.5 Reid Drive Interceptor Project Pipe Dimensions

Pipe or Tooling	Outside Circumference (ft)	Diameter (in)		Length (ft)
		Outside	Inside	
Pilot Tube Spoon	1.31	5.0	-	-
Pilot Tubes	1.11	4.3	-	2.5
21" Reamer Assembly	6.81	26.0	-	8.0
21" Steel Casing	6.68	25.5	23.5	8.0
21" VCP	6.28	24.0	20.4	8.0
8" Reamer Assembly	3.32	12.7	-	3.5
8" Steel Casing	2.93	11.2	9.8	3.5
8" VCP	2.93	11.2	8.0	3.5
HDPE Reamer	1.57	6.0	-	-
4" HDPE	1.26	4.8	3.9	-

APPENDIX C  
SUPPLEMENTAL EQUATIONS



To determine the saturated unit weights of the soil from the dry unit weights provided in the geotechnical report, Equation C.1 was used.

$$\gamma_{sat} = \gamma_d \times (1 + w/100) \quad (C.1)$$

The simplification process for Equation 5.8 for pilot tube jacking resistance:

$$F_r = C_a \gamma' (0.354 ft) \tan(C_f \phi_r) (1.113 ft) L \quad (C.2)$$

$$F_r = C_a \gamma' \tan(C_f \phi_r) (0.394 ft^2) L \quad (5.8)$$

The simplification process for Equation 5.9 for 21-inch casing frictional jacking resistance:

$$\psi = C_a \gamma' \tan(C_f \phi_r) \quad (C.3)$$

$$F_r = \psi \left[ \left( \frac{((6.676 ft)(2.125 ft)L_{Total} - (0.394 ft^2)L_{Total})}{L_{Total}} \right) L + (0.394 ft^2)L_{Total} \right] \quad (C.4)$$

$$F_r = C_a \gamma' \tan(C_f \phi_r) \left[ \left( \frac{((14.186 ft^2)L_{Total} - (0.394 ft^2)L_{Total})}{L_{Total}} \right) L + (0.394 ft^2)L_{Total} \right] \quad (5.9)$$

The simplification process for Equation 5.10 for 21-inch VCP frictional jacking resistance:

$$F_r = \psi \left[ \left( \frac{((6.283 ft)(2.000 ft)L_{Total} - (14.186 ft^2)L_{Total})}{L_{Total}} \right) L + (14.186 ft^2)L_{Total} \right] \quad (C.5)$$

$$F_r = C_a \gamma' \tan(C_f \phi_r) \left[ \left( \frac{(12.566 ft^2)L_{Total} - (14.186 ft^2)L_{Total}}{L_{Total}} \right) L + (14.186 ft^2)L_{Total} \right] \quad (5.10)$$

The simplification process for Equation 5.11 for 8-inch casing frictional jacking resistance:

$$F_r = \psi \left[ \left( \frac{(2.929 ft)(0.932 ft)L_{Total} - (0.394 ft^2)L_{Total}}{L_{Total}} \right) L + (0.394 ft^2)L_{Total} \right] \quad (C.6)$$

$$F_r = C_a \gamma' \tan(C_f \phi_r) \left[ \left( \frac{(2.731 ft^2)L_{Total} - (0.394 ft^2)L_{Total}}{L_{Total}} \right) L + (0.394 ft^2)L_{Total} \right] \quad (5.11)$$

Methodology for determining the active and passive Rankine lateral earth pressure is shown by the following equations:

$$K_p = \tan^2(45 + \phi/2) \quad (C.7)$$

$$K_a = \tan^2(45 - \phi/2) \quad (C.8)$$

where  $K_p$  = Passive lateral earth pressure coefficient

$K_a$  = Active lateral earth pressure coefficient

$$\sigma'_a = \sigma'_0 K_a - 2c' \sqrt{K_a} \quad (C.9)$$

$$\sigma'_p = \sigma'_0 K_p + 2c' \sqrt{K_p} \quad (C.10)$$

where  $\sigma'_a$  = Active effective lateral earth pressure

$\sigma'_p$  = Passive effective lateral earth pressure

$\sigma'_0$  = Vertical effective stress

$c'$  = Effective cohesion

## APPENDIX D

### L1 PRESSURE TRANSDUCER COMPLICATIONS

The L1 transducer exhibited complications during its operation. Unfortunately, these issues remained undetected until analysis of the voltage outputs was performed, after the completion of the Reid Drive Interceptor project. The BM pusher was monitored using the L1 transducer for three 21-inch VCP installations. There was another 21-inch installation of which the Data Dolphin logging system was available and used for phase one and two. This installation took place in August, 2011, and the author of this thesis had already moved to Arizona to begin his graduate study. Workers left in charge of collecting data for this installation felt that use of the Data Dolphin for phase three recording was unnecessary due to the lack of movement on the BM pusher’s pressure gauge during previous phase three installations. In spite of the lack of activity in the pressure gauge, data from the first two monitored phase three installations indicated fluctuations in hydraulic pressure indicative of phase three operations and were useful in analysis of jacking forces and productivity. Although the data from the first two installations exhibited operational hydraulic pressure variations, peculiarities were observed with the data. Furthermore, the third monitored phase three installation did not yield usable results. Table D.1 outlines the above passage.

Table D.1 List of 21” Installations and Transducer Operational Results

Manhole Span	Date	L1 Transducer	L2 Transducer	L3 Transducer
26.100 to 26.99B	20-Jun	Monitored Useable Results	Monitored Valuable Results	Monitored Valuable Results
26.100 to 26.101	30-Jun	Monitored Useable Results	Monitored Valuable Results	Monitored Valuable Results
26.102 to 26.101	29-Jul	Monitored Poor Results	Monitored Valuable Results	Monitored Valuable Results
26.102 to 27.3	15-Aug	Not Monitored	Monitored Valuable Results	Monitored Valuable Results

In both June installations, valuable patterns in voltage output could be seen, depicting typical installation cycles for a VCP section. However, there was an instantaneous jump in voltage magnitudes during the June 20<sup>th</sup> (Figure D.1) and June 30<sup>th</sup> (Figure D.2) installations at 13:00 and 8:25, respectively. The cyclical installation pattern did not vary, but the magnitude of the maximum and minimum voltage outputs were shifted up, almost as if a second gear was being used. The foreman on the job confirmed that the second gear on the machine was never employed due to low jacking forces and the relative ease of installation. Additionally, the generator supplying power to the power pack was always operated at constant amps. This leads one to believe the reason for the voltage shift is due to malfunctions with the reducer used to scale down the voltage output from the L1 transducer to a level of which the data logger could record.

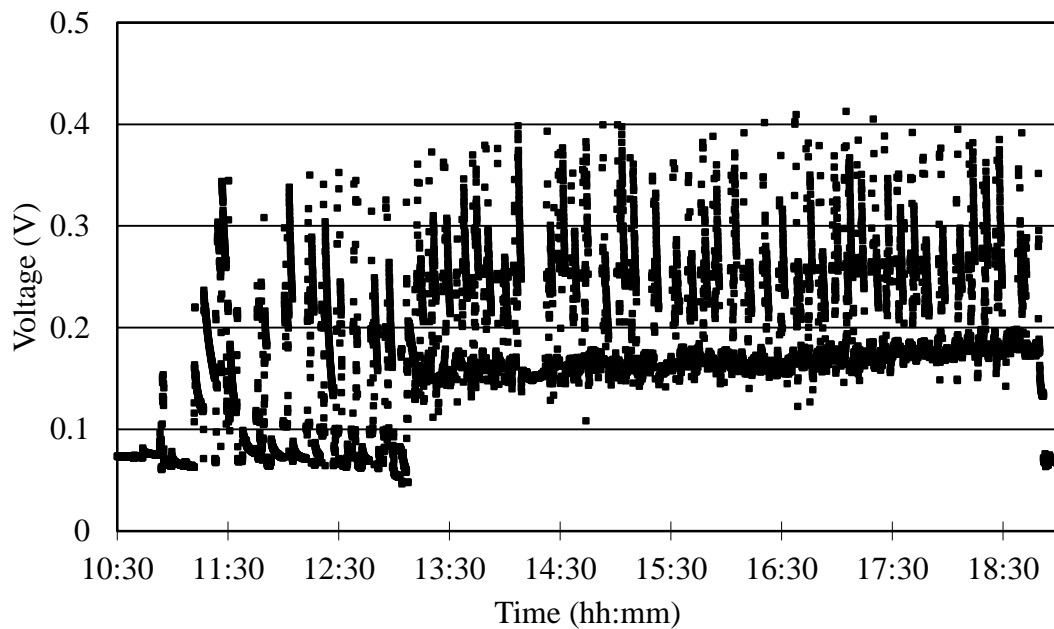


Figure D.1 Voltage vs. Time for the June 20<sup>th</sup> Installation

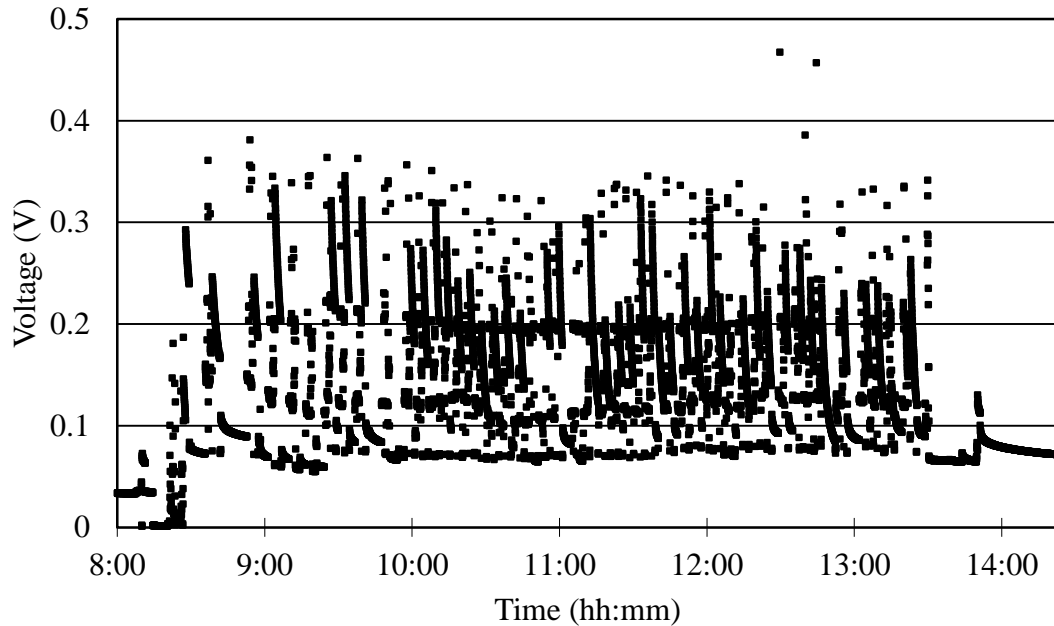


Figure D.2 Voltage vs. Time for the June 30<sup>th</sup> Installation

Besides the odd voltage shift, the bottom end voltage, or ambient voltage, varies throughout each installation. Ambient voltage for the June 20<sup>th</sup> installation experienced a negative correlation with time until the voltage shift and then experienced a steady positive correlation with time for the remainder of the day. The ambient voltage for the June 30<sup>th</sup> installation is slightly more consistent than the June 20<sup>th</sup> installation. An odd behavior that should be noted is that at 8:06, when the transducer was attached to the machine hydraulics, the ambient voltage fell from 0.034 to 0.000. This is the opposite of what one would expect, as hydraulic pressures from the machine should have caused the ambient voltage to increase.

One month passed between the last June installation and the July 29<sup>th</sup> installation, which may explain the increased irregularities in the recorded voltage. Within the first nineteen seconds of data recording, voltage outputs rose from 0.71 to 0.73. Voltage outputs of this magnitude should be indicative of the maximum outputs expected during a

phase three installation, as realized from the two June installations, yet the transducer was not even hooked up to the BM pusher at this time. Upon fixing the transducer to the BM Pusher, voltage outputs remained at 0.73 and did not vary for the remainder of the day, despite operation of the machine during the installation.

These oddities posed the need to investigate further into the behavior of the L1 transducer. It was thought that viewing the mean, median, mode, maximum, and minimum voltage outputs for the transducer throughout the summer would provide an understanding of the transducer's atypical behavior (Figure D.3).

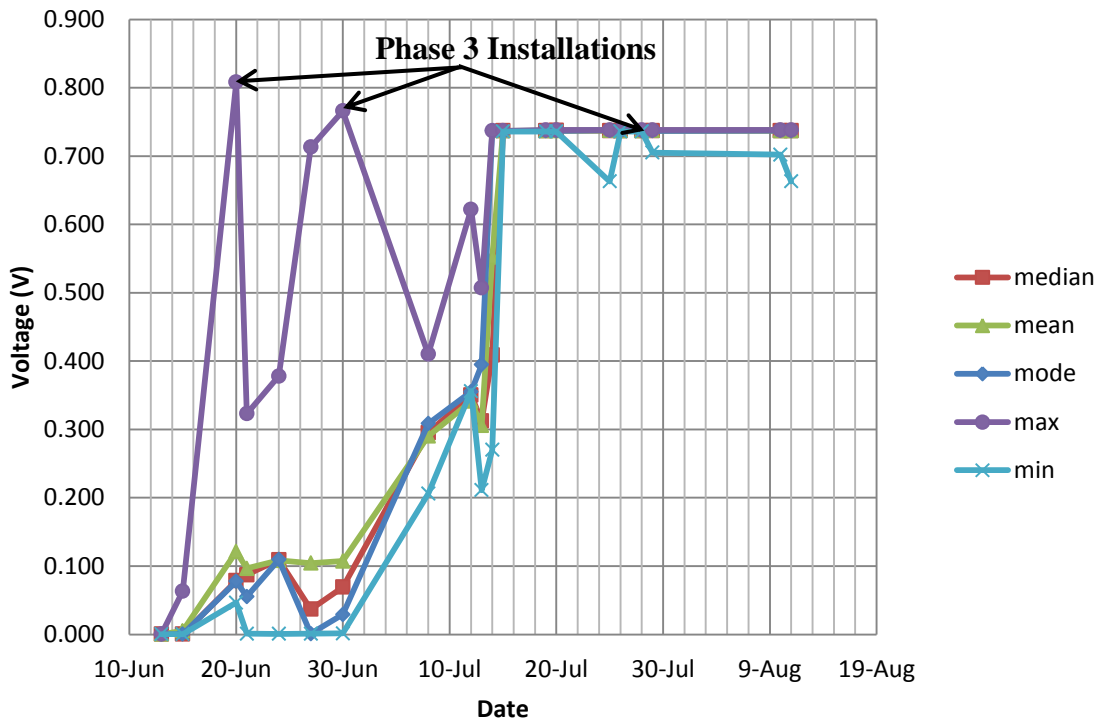


Figure D.3 Voltage Outputs for the L1 Transducer Throughout Summer

It can be seen that minimum voltage values fluctuated erratically in the beginning and began to stabilize around 0.7 volts around mid-July. This indicates malfunctioning in either the transducer or reducer and the need for recalibration or repair. Furthermore, it was noticed that even when the L1 transducer was not being used to capture phase three

operations, voltage outputs varied, almost as if the transducer was exposed to hydraulic pressures. Through in-depth field observations, it is known that the L1 transducer was only fixed to equipment hydraulic lines during phase three operations. Thus, voltage outputs from the L1 transducer during phases one and two should have been constant.

Investigation into the behavior of the other transducers, L2 and L3, was carried out to identify whether the variation in voltage outputs for L1 during periods of non-operation were unique. Figure D.4 illustrates the behavior of the L3 transducer in a similar fashion as Figure D.3 does for transducer L1. It should be noted that during periods of non-operation, voltage outputs do not vary and equal a constant 0.5 volts, corresponding to zero hydraulic pressure. This is what is to be expected. Transducer L2 exhibits similar results.

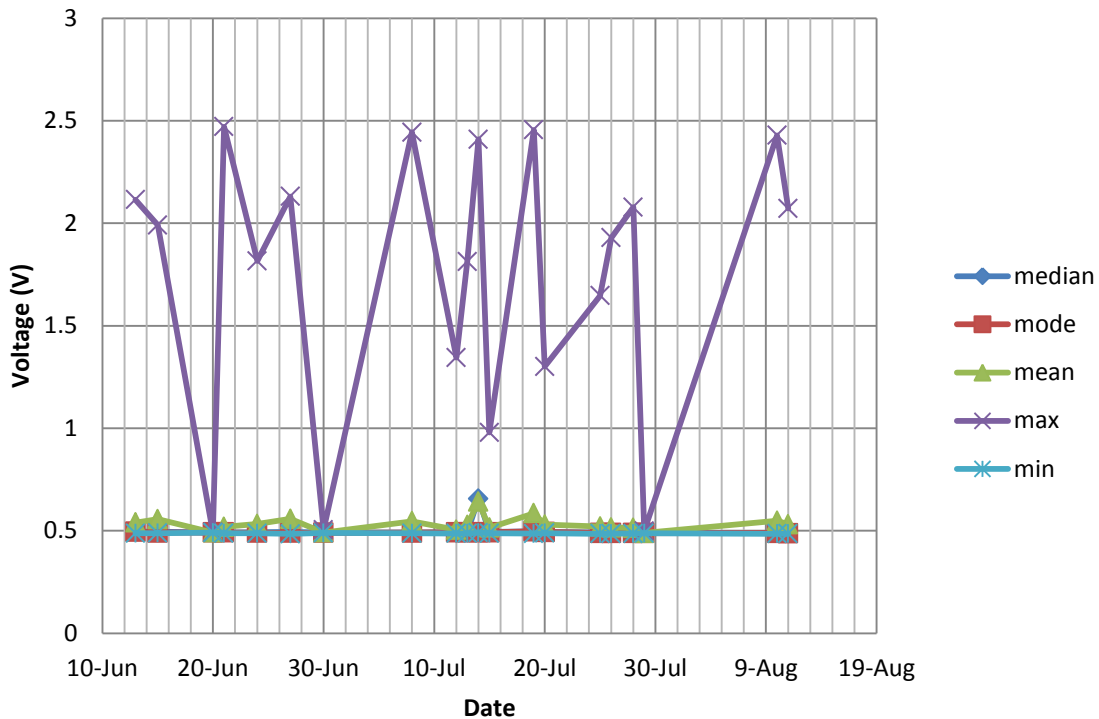


Figure D.4 Voltage Outputs for the L3 Transducer Throughout Summer



In November of 2012, communication was established with the Data Dolphin and the user's computer. The status of the Data Dolphin was loaded onto the computer and it was observed that voltage outputs for the L1 transducer remained near 0.73 volts. This provided further evidence of malfunctioning in either the L1 transducer or its reducer. Due to the irregularities in the recorded voltage in transducer L1 throughout the summer, recorded data for the July 29<sup>th</sup> installation is invalid. Recorded data for the June 20<sup>th</sup> and June 30<sup>th</sup> installation exhibit certain behavioral patterns expected of product VCP installation and may be used in jacking force and productivity analysis. However, modifications to the base, or ambient, voltage corresponding to zero thrust force must be made, as detailed in Chapter 5.